NSF/CEE-83214

PB84-127919

UNIVERSITY OF SOUTHERN CALIFORNIA

DEPARTMENT OF MECHANICAL ENGINEERING
OHE 430 • LOS ANGELES, CALIFORNIA 90089-1453

STRONG MOTION EFFECTS DUE TO SEISMIC WAVES IN DIPPING LAYERS

M. Dravinski

A Report on Research Conducted Under
a Grant form the National Science Foundation

STRONG MOTION EFFECTS DUE TO SEISMIC WAVES IN DIPPING LAYERS

by

M. Dravinski

Department of Mechanical Engineering

University of Southern California, Los Angeles, CA 90089-1453

A Report on Research Conducted Under a Grant

from the National Science Foundation

September, 1983

REPORT DOCUMENTATION PAGE	1. REPORT NO. NSF/CEE-83214	2.	3. Recipient's Accession No. PB84 127919
4. Title and Subtitle: Strong Motion Effects Due to Seismic Waves in Dipping Layers			5. Report Date: September 1983
7. Author(s): M. Dravinski			8. Performing Organization Rept. No.
9. Performing Organization Name and Address: University of Southern California, Department of Mechanical Engineering, Los Angeles, CA 90089-1453			10. Project/Task/Work Unit No.
			11. Contract(C) or Grant(G) No. (C) (G) CEE8119696
12. Sponsoring Organization Name and Address: Directorate for Engineering (ENG), National Science Foundation, 1800 G Street, N.W., Washington, DC 20550			13. Type of Report & Period Covered
			14.

15. Supplementary Notes

16. Abstract (Limit: 200 words)

Six papers are presented. The first investigates the antiplane strain model for scattering of plane SH waves by dipping layers of arbitrary shape. The indirect boundary method is utilized and shown to provide very good results for a wide range of frequencies. The second paper reports on a study of steady state wave motion for diffraction of plane P, SV, and Rayleigh waves by dipping layers of arbitrary shape. The third paper discusses the use of an indirect boundary integral equation approach to examine amplification of motion caused by diffraction and scattering of a plane harmonic SH-wave by a layered medium in the Los Angeles basin. Paper four reports on the effect of inclusion shape upon ground motion and paper five examines ground motion amplification due to elastic inclusions in a half-space. The final paper addresses the amplification of P, SV, and Rayleigh waves by two alluvial valleys.

17. Document Analysis a. Descriptors

Earthquakes
Boundaries
Seismic waves
Amplification
Boundary layer
Steady state
Inclusions
Plane waves
Diffraction
Harmonic analysis
Mathematical models

b. Identifiers/Open-Ended Terms

Ground motion
Los Angeles (California)
Rayleigh waves

M. Dravinski, /PI

c. COSATI Field/Group

18. Availability Statement: NTIS

19. Security Class (This Report)

20. Security Class (This Page)

21. No. of Pages: 216

22. Price

TABLE OF CONTENTS

INTRODUCTION

This report contains a summary of the research effort conducted under a grant CEE-8119696 from the National Science Foundation. The report consists of six chapters: the first three address the problem of strong ground motion due to the dipping layers and the remaining three deal with the topics indirectly related to the main theme of the grant which were completed, in part or entirely, due to support from the grant.

Each chapter of the report is s self contained paper. Presentation style varies from chapter to chapter according to the requirements of the journals where the papers have been submitted for publication. Names of the journals where the papers were published are indicated at the first page of each of the chapters.

Part of the research results in this paper were presented at two conferences: 19th Annual Meeting of the Society of Engineering Science (October, 1982 at University of Missouri - Rolla) and Annual Meeting of the Seismological Society of America (May, 1983 in Sal Lake City).

SCATTERING OF PLANE HARMONIC SH-WAVE BY DIPPING LAYERS OF ARBITRARY SHAPE*

By M. Dravinski

Abstract

The antiplane strain model for scattering of plane SH waves by dipping layers of arbitrary shape is investigated by using the indirect boundary integral method. The dipping layers are of finite length perfectly bonded together. The material of the layers is assumed to be homogeneous, linearly elastic, and isotropic.

Presented numerical results incorporate variation in the number of layers, the angle of incidence, the frequency of the incident wave, the material properties, and the shape of the layers.

*To appear in the Bulletin of Seismological Society of America, October, 1983

Introduction

Soil amplification problems are usually solved by two methods: 1. numerical methods, and 2. analytical methods. Each of these has limitations. The analytical methods are applied mainly to linear, isotropic and homogeneous materials and simple geometries. The numerical methods, on the other hand, are often inapplicable to problems of interest in geophysics and earthquake engineering. Namely, the most commonly used numerical methods, finite differences and finite elements require a computational grid which fills the solution domain of the problem under consideration. This reduces the effectiveness of these methods for geotechnical problems which involve large dimensions.

For many problems it is possible to construct a surface integral representation of the solution. Corresponding integral equations involve only the boundary and initial values (and possibly the interior sources). The boundary value problem is thus formulated in terms of boundary values and the solution at interior points need not be considered in order to solve the integral equations (Cole et al., 1978). Once the integral equations are solved, the solution at any interior point can be determined through the original integral representation. Therefore, the main advantage of the boundary integral methods (BIM's) lie in the fact that only the boundary of the body is being discretized thus reducing the number of unknown variables significantly in comparison to the finite element and finite difference procedures. In addition, the problem of filling the space with a three dimensional grid is eliminated.

Indirect BIM used in this paper to study steady-state wave motion in dipping layers originates in the works of Kupradze (1963), Copley (1967) and Oshaki (1973). Application of the method to wave propagation problems

in geophisics and earthquake engineering is due to Sanchez-Sesma and Rosenblueth (1979), Sanchez-Sesma and Esquivel (1979), Apsel (1979), Dravinski (1982) and Wong (1982).

Observation from some recent earthquakes (Sozen et al., 1968, Jennings, 1971) indicated that the area of intense damage can be highly localized. Esteva (1977) established that the intensity of strong ground motion may change greatly within a short distance. Subsequent investigations (e.g., Boore, 1973) reinforced a belief that the inhomogeniety of the soil and surface (subsurface) irregularities are probably the main cause of localized amplification effects. Recent investigations by the author (1982) demonstrated the possibility of very large amplification effects due to single dipping layer (valley) in a half-space when subjected to different incident waves. Variation of the surface motion proved to be very sensitive upon a number of parameters, such as, frequency and angle of incidence of the incoming wave, material properties of the half-space and inclusion, geometry of the inclusion, location of the observation station at the surface of the half-space, etc. However, the role of additional layers upon the surface motion remained open. By including several layers into consideration it is possible to examine how they influence the resulting surface motion and thus determine if it is necessary to incorporate the presence of additional dipping layers in more realistic models.

Statement of Problem

Geometry of the problem is depicted by Fig. 1. The finite number of dipping layers of arbitrary shape* are bonded together to form a layered half-space. Denoting the spatial domain for the layers by D_j, $j = 0, 1, 2, \ldots, R$, it follows then that the half-space is given as the union of all domains, i.e., $D_0, D_1, \ldots, D_R$ are referred to as the half-space layer, the first layer, ..., and the R-th layer, respectively. Interfaces between the layers are denoted by C_i, $i = 1, 2, \ldots, R$. Perfect bonding along the interfaces is understood. The material of the layers is assumed to be linearly elastic, homogeneous and isotropic.

The problem model is of the antiplane-strain type, i.e., the layered half-space extends to infinity perpendicularly to the plane of the drawing and the motion of the elastic medium takes place along the z-axis only. In the absence of body forces, the steady-state wave motion is governed by

$$(\nabla^2 + k_j^2)\, w_j(x,y,\omega) = 0 \; ; \; j = 0,1,2,\ldots,R \; ; \; \nabla^2 \equiv \frac{\partial^2}{\partial x^2} + \frac{\partial^2}{\partial y^2} \qquad (1)$$

where k denotes the wave number, ω represents the circular frequency, and w is the only nonzero component of displacement vector acting along the z-axis. Subscript j in (1) refers to layer D_j, $j=0, 1, 2, \ldots, R$.

The boundary condition along the surface of the half-space is specified by

$$\frac{\partial w_j}{\partial y} = 0 \; ; \text{ at } y=0 \; ; \; j=0,1,2,\ldots,R. \qquad (2)$$

For the sake of subsequent simplification an antiplane-strain elstodynamic state vector $\underset{\sim}{z}_j^T(\underset{\sim}{r})$ is introduced (Wheeler and Sternberg, 1968)

---

*Interfaces between the layers are assumed to be sufficiently smooth with no sharp corners being present.

$$\underset{\sim}{s}_j^T(\underset{\sim}{r}) \equiv [w(\underset{\sim}{r}),\ \sigma_{nz}(\underset{\sim}{r})]_j;\ \underset{\sim}{r} \in C \in D_j,\ j=0,1,\ldots,R \tag{3}$$

where one says that $\underset{\sim}{s}_j$ is an elastodynamic state vector for domain D_j with the displacement field w, and the stress field σ_{nz}, associated with the sheer modulus μ_j, the shear wave speed β_j, along some surface C with unit normal vector $\underset{\sim}{n}$. The superscript T in equation (3) denotes the transpose.

Perfect bonding between the layers requires continuity of displacement and stress field along the interfaces C_j, $j=1,2,\ldots,R$ what in terms of elastodynamic state vector $\underset{\sim}{s}$ can be written as

$$\underset{\sim}{s}_{j-1}(\underset{\sim}{r}) = \underset{\sim}{s}_j(\underset{\sim}{r})\ ;\ \underset{\sim}{r} \in C_j\ ;\ j=1,2,\ldots,R. \tag{4}$$

Incident plane SH-wave is assumed of the form

$$w^{inc} = \exp[-ik_o(x \sin\theta_o - y \cos\theta_o) + i\omega t];\ i \equiv \sqrt{-1} \tag{5}$$

where the angle of incidence θ_0 has been defined by Fig. 1. For briefness, the factor $\exp(i\omega t)$ is omitted throughout the analysis.

Solution of Problem

As the incident wave, arriving from the depth of the half-space layer D_0, strikes interface C_1, it is partially reflected "back" into the half-space layer and partially transmitted "forward" into the layer D_1 (see Fig. 1). The wave field inside the first layer partially reflects "back" into D_1 and it is partially transmitted into domains D_0 and D_2 along interfaces C_1 and C_2. This process continues as the wave field propagates throughout the layered medium. Therefore, the total wave field in the half-space is specified by

$$w_o = w^{ff} + w_o^s\ ;\ \underset{\sim}{r} \in D_0 \tag{6}$$

$$w_j = w_j^s\ ;\ \underset{\sim}{r} \in D_j\ ;\ j=1,2,\ldots,R, \tag{7}$$

where the superscripts s and ff denote the scattered and free-wave-field, respectively. If the scattered wave field is expressed in terms of single layer potentials (Ursell, 1973) it follows then

$$w_o^s(\underline{r}) = \int_{C_1^-} q_o(\underline{r}_o)\, G_o(\underline{r},\underline{r}_o)\, d\underline{r}_o \quad ; \quad \underline{r} \in D_o \tag{8a}$$

$$w_j^s(\underline{r}) = \int_{C_j^+} p_j(\underline{r}_o)\, G_j(\underline{r},\underline{r}_o)\, d\underline{r}_o + \int_{C_{j+1}^-} q_j(\underline{r}_o)\, G_j(\underline{r},\underline{r}_o)\, d\underline{r}_o ; \; \underline{r} \in D_j ; \quad j=1,2,\ldots,R-1 \tag{8b}$$

$$w_R^s(\underline{r}) = \int_{C_R^+} p_R(\underline{r}_o)\, G_R(\underline{r},\underline{r}_o)\, d\underline{r}_o \quad ; \quad \underline{r} \in D_R, \tag{8c}$$

where q_j and p_j, $j=0,1,2,\ldots,R$ are the unknown density functions. The functions G_j, $j=0,1,2,\ldots,R$ are the Green's function for the line load in the half-space, and they satisfy the following equations

$$(\nabla^2 + k_j^2)\, G_j(\underline{r},\underline{r}_o) = -\delta(|\underline{r} - \underline{r}_o|) \quad ; \quad j=0,1,2,\ldots,R \tag{9a}$$

$$\left.\frac{\partial G_j}{\partial y}\right|_{y=0} = 0 , \tag{9b}$$

where $\delta(\cdot)$ represents the Dirac delta-function. The Green's functions are then given explicitly by (Miklowitz, 1978)

$$G_j(\underline{r},\underline{r}_o) = \frac{i}{4}\left\{H_o^{(2)}(k_j\sigma_1) + H_o^{(2)}(k_j\sigma_2)\right\} \; ; \; j=0,1,2,\ldots,R \tag{10a}$$

$$\sigma_1 = \left((x - x_o)^2 + (y - y_o)^2\right)^{\frac{1}{2}} \tag{10b}$$

$$\sigma_2 = \left((x - x_o)^2 + (y + y_o)^2\right)^{\frac{1}{2}}, \tag{10c}$$

with $H_o^{(2)}(\cdot)$ being the Hankel function of the second kind and of order zero.

Surfaces C_j^+ and C_j^-, j=1,2,...,R are defined inside and outside of the corresponding interface C_j (Kupradze, 1963). Namely, each interface C_j, j=1,2,...,R can be viewed as the location of sources which "form" reflected and transmitted wave fields as the incoming wave strikes the interface. For the sake of simplification, it is proposed to place those sources slightly inside (outside) of the interface. Thus, for any interface C_j, j=1,2,...,R, C_j^- and C_j^+ denote the "inner" and "outer" source surface, respectively. The principal advantage of this procedure is the elimination of singularities in the kernels of integrals in equations 8a-8c as $\underset{\sim}{r}_o$ approaches $\underset{\sim}{r}$. Thus a need to analytically handle integrable singularities of the Green's functions present in the single layer potentials is avoided. This method is frequently referred to as Kupradze's method (Christiansen, 1976; Fairweather and Johnston, 1982) since it has been originally proposed by Kupradze (1963). It has been successfully applied to problems of geophysics by a number of researchers (e.g., Sanchez-Sesma and Rosenblueth, 1979; Sanchez-Sesma and Esquivel, 1979; Apsel, 1979; Wong, 1982; and Dravinski, 1982). This approach appears very attractive but it is not without difficulties of its own. Namely, the location of the source surfaces must be chosen carefully to obtain accurate results. For this reason an extensive testing of Kupradze's method has been done for the type of problems investigated in this paper (Wong, 1982; Dravinski, 1982). Summary of these investigations is presented in the part of the paper dealing with numerical accuracy of results.

If one assumes the scattered wave field in terms of discrete line sources, i.e., the density functions of the following form

$$q_{j-1}(\underset{\sim}{r}) = a_{m_j}^{j-1}\,\delta(|\underset{\sim}{r} - \underset{\sim}{r}_{m_j}|)\ ;\ j=1,2,\ldots,R\ ;\ m_j=1,2,\ldots,M_j\ ;\ \underset{\sim}{r}_{m_j} \in C_j^- \qquad (11a)$$

$$p_j(\underset{\sim}{r}) = b_{\ell_j}^{j}\,\delta(|\underset{\sim}{r} - \underset{\sim}{r}_{\ell_j}|)\ ;\ \ell_j=1,2,\ldots,L_j\ ;\ \underset{\sim}{r}_{\ell_j} \in C_j^+; \qquad (11b)$$

then the scattered wave field becomes

$$w_o^s(\underline{r}) = a_{m_1}^o G_o(\underline{r},\underline{r}_{m_1}) \; ; \; m_1=1,2,\ldots,M_1 \; ; \; \underline{r}_{m_1} \in C_1^- \tag{12a}$$

$$w_i^s(\underline{r}) = b_{\ell_i}^i G_i(\underline{r},\underline{r}_{\ell_i}) + a_{m_{i+1}}^i G_i(\underline{r},\underline{r}_{m_{i+1}}) ;$$

$$i=1,2,\ldots,R-1$$
$$\ell_i=1,2,\ldots,L_i$$
$$m_i=1,2,\ldots,M_i$$
$$\underline{r}_{\ell_i} \in C_i^+$$
$$\underline{r}_{m_i} \in C_i^- \tag{12b}$$

$$w_R^s(\underline{r}) = b_{\ell_R}^R G_R(\underline{r},\underline{r}_{\ell_R}) \; ; \; \underline{r}_{\ell_R} \in C_R^+, \tag{12c}$$

where summation over repeated subscripts is invoked. The summation convention is suppressed for repeated indices if one index is a superscript and the other is a subscript. Subscript indexes, such as ℓ_i and m_i, should be viewed as simple indexes ℓ and m, respectively.

For example, equation (12c) implies $w_R^s = b_1^R G_R(\underline{r},\underline{r}_1) + b_2^R G_R(\underline{r},\underline{r}_2) + \ldots + b_{L_R}^R G_R(\underline{r},\underline{r}_{L_R})$, etc.

Source intensities $a_{m_j}^{j-1}$ and $b_{\ell_j}^j$, $j=1,2,\ldots,R$, $m_j=1,2,\ldots,M_j$, $\ell_j=1,2,\ldots,L_j$ in equations (11a,b) are evaluated through the use of continuity conditions specified by equation (4). Choosing N_j "observation" points (along each interface C_j, $j=1,2,\ldots,R$) to evaluate equation (4), the source intensities in least-square-sense are determined to be

$$[a_1^o \ldots a_{M_1}^o \, b_1^1 \ldots b_{L_1}^1 \, a_1^1 \ldots a_{M_2}^1 \, b_1^2 \ldots b_{L_2}^2 \ldots b_1^R \ldots b_{L_R}^R]^T = (\underline{G}^* \underline{G})^{-1} \underline{G}^* \underline{f}, \tag{13}$$

where matrices $\underline{G}$ and $\underline{f}$ are given in Appendix A. Superscripts T and * denote transpose and transpose complex conjugate, respectively. Physically, $\underline{G}$ contains the Green's functions evaluated at different source and observation points while $\underline{f}$ incorporates information about the incident (free) - field

along the interface C_1. Substitution of the source intensities determined by equation (13) into equations (12a,b,c) and then into equations (6) and (7) implies the total displacement field throughout the elastic medium. Evaluation of the response in time domain can be accomplished then by means of the Fourier synthesis.

Evaluation of Results

Throughout the numerical evaluation of the results all variables are presented in dimensionless form. For that purpose the wave velocity β_o and shear modulus μ_o are chosen to be unity; distances are normalized with respect to the half-width of the first layer; and surface displacement amplitude is presented normalized with respect to the amplitude of the surface free-field motion. Dimensionless frequency Ω is introduced as the ratio of the total width of the first dipping layer and the wavelength of the incident wave field. Numerical results are presented for single, two, and three layer models.

Since interfaces C_j, $j=1,2,3$ are of arbitrary shape, they are assumed to be specified in terms of the discrete set of points through which a normalized B-spline approximation is determined. This procedure permits the construction of efficient algorithm applicable to a wide range of interface shapes. For more information on this topic the reader is referred to the report by the author (Dravinski, 1983) in which a complete computer code is presented and explained in detail.

Single-Layer-Model

Displacement fields throughout the elastic medium for a dipping layer in a half-space follows from equations (12a,b,c), (6) and (7) to be

$$w_o(\underline{r}) = w^{ff}(\underline{r}) + a^o_{m_1} G_o(\underline{r},\underline{r}_{m_1}) \; ; \; \underline{r}_{m_1} \in C_1^- \; ; \; m_1=1,2,\ldots,M_1 \qquad (14a)$$

$$w_1(\underline{r}) = b^1_{\ell_1} G_1(\underline{r},\underline{r}_{\ell_1}) \; ; \; \underline{r}_{\ell_1} \in C_1^+ \; ; \; \ell_1=1,2,\ldots,L, \qquad (14b)$$

where the coefficients $a^o_{m_1}$ and $b^1_{\ell_1}$ are formally given by equation (13). Numerical results pertinent to the single dipping layer are used for testing purposes since the exact solutions for certain shapes of dipping layers are

available in the literature.

Figure 2 depicts the normalized surface displacement amplitude atop a half-space with the semi-elliptical dipping layer subjected to a plane harmonic SH-wave. The results are in complete agreement with the exact solution-results given by Wong and Trifunac (1974).

It is evident from Fig. 2 that the presence of a dipping layer (inclusion) may cause very large strong ground motion amplification effects.

Two-Layer-Model

For this model the surface displacement field is given explicitly by

$$w_o(\underline{r}) = w^{ff}(\underline{r}) + a^o_{m_1} G_o(\underline{r},\underline{r}_{m_1}) \quad ; \quad \underline{r}_{m_1} \in C_1^- \; ; \; m_1=1,2,\ldots,M_1 \tag{15a}$$

$$w_1(\underline{r}) = b^1_{\ell_1} G(\underline{r},\underline{r}_{\ell_1}) + a^1_{m_2} G_1(\underline{r},\underline{r}_{m_2}) \; ; \; \underline{r}_{\ell_1} \in C_1^+ \; ; \; \underline{r}_{m_2} \in C_2^-;$$

$$\ell_1=1,2,\ldots,L_1 \; ; \; m_2=1,2,\ldots,M_2 \tag{15b}$$

$$w_2(r) = b^2_{\ell_2} G_2(r,r_{\ell_2}) \; ; \; r_{\ell_2} \in C_2^+ \; ; \; \ell_2=1,2,\ldots,L_2 \tag{15c}$$

with coefficients a's and b's specified by equation (13).

Surface motion for the two-layer-model is shown by Fig. 3. The frequency of incident field and geometry of the first layer are the same as in the case of the single-layer-model discussed initially. Still, the overall surface motic amplification effect shown by Fig. 3 is smaller than that shown by Fig. 2. This difference arises due to different contrast in material properties between the half-space layer and the first dipping layer in the two models considered. Reduction of maximum embedment depth further reduced the surface amplification effects as shown by Fig. 4. If the frequency of the incoming wave is doubled the surface response atop two dipping layers is shown by Fig. 5. Comparison of Figs. 4 and 5 indicates an increase of ground motion amplification effect with the increase of frequency. However,

similar effects may be achieved by introducing more contrasting materials for layers, as shown by Fig. 6. Combination of higher frequency of incident waves and high contrast in material properties may lead locally to a drastic increase in surface strong ground motion amplification effects as illustrated by Fig. 7. It is interesting to observe from the results of Figs. 2-7 that as the sensitivity of surface motion to the presence of subsurface inhomogeniaty increases, the dependence of surface motion upon the angle of incidence becomes more pronounced. Overall maximum of surface motion is observed for horizontally incident waves.

Three-Layer-Model

The surface displacement field for three dipping layers follows from equations (12a,b,c), (6) and (7) to be

$$w_o(\underset{\sim}{r}) = w^{ff}(\underset{\sim}{r}) + a^o_{m_1} G_o(\underset{\sim}{r},\underset{\sim}{r}_{m_1}) \; ; \; m_1=1,2,\ldots,M_1; \; \underset{\sim}{r}_{m_1} \in C_1^- \tag{16a}$$

$$w_1(r) = b^1_{\ell_1} G_1(r,r_{\ell_1}) + a^1_{m_2} G_1(r,r_{m_2}) \; ; \; \ell_1=1,2,\ldots,L_1$$
$$\underset{\sim}{r}_{\ell_1} \in C_1^+$$
$$m_2=1,2,\ldots,M_2$$
$$\underset{\sim}{r}_{m_2} \in C_2^- \tag{16b}$$

$$w_2(\underset{\sim}{r}) = b^2_{\ell_2} G_2(\underset{\sim}{r},\underset{\sim}{r}_{\ell_2}) + a^2_{m_3} G_2(\underset{\sim}{r},\underset{\sim}{r}_{m_3}) \; ; \; \ell_2=1,2,\ldots,L_2$$
$$\underset{\sim}{r}_{\ell_2} \in C_2^+$$
$$m_3=1,2,\ldots,M_3$$
$$\underset{\sim}{r}_{m_3} \in C_3^- \tag{16c}$$

$$w_3(\underset{\sim}{r}) = b^3_{\ell_3} G_3(\underset{\sim}{r},\underset{\sim}{r}_{\ell_3}) \; ; \; \ell_3=1,2,\ldots,L_3; \; \underset{\sim}{r}_{\ell_3} \in C_3^+, \tag{16d}$$

where coefficients a's and b's are defined by equation (13).

For frequency $\Omega = 0.75$ and higher contrast in material properties of the dipping layers and the half-space layer, the surface displacement pattern is presented by Fig. 8. A very large local amplitude can be observed. There is a substantial difference in the peak amplitude of the surface motion for various angles of incidence with the largest (the smallest) being observed for horizontal (vertical) incidence. Reduction in the contrast of material properties for half-space layer and dipping layers resulted in a surface motion of considerably lower amplitude, less sensitive upon the angle of incidence, as shown by Fig. 9. An increase in the frequency of the incident wave produced opposite effects: maximum amplitude of surface motion increased in value and sensitivity of strong ground motion upon the angle of incidence appears more pronounced (see Fig. 10).

From the presented results it follows that amplification of surface motion due to subsurface inhomogeneities depends upon the number of physical parameters of the problem model under consideration. This is to be expected if one views the motion of elastic medium as a result of interference of incident and scattered waves. This interference may be constructive or destructive, thus implying locally amplification or reduction of surface motion. Parameters which affect this interference will affect the resulting motion as well.

Results of surface motion for a more general type of layers is depicted by Fig. 11 and Fig. 12 for positive and negative angles of incidence, respectively. Evidently, surface motion is significantly affected by the presence of dipping layers. Surface motion amplification depends strongly upon the location of the observation point on the surface of the half-space and the angle of incidence of the incoming wave. A higher value for the ratio of the width

versus the depth of the first dipping layer is chosen simply to illustrate appreciable surface ground motion at a rather low frequency and thus reduce the amount of required computations.

Actual alluvial basins for which the proposed method of solution is formally applicable still contain many particular details to be accounted for, therefore corresponding results will be reported separately.

On Numerical Evaluation of Results

Extensive testing of the indirect boundary integral method used in this work has been done using the known exact solutions available in literature (Dravinski, 1982). These results can be summarized as follows: a) The method provides very good results for a wide range of frequencies. An increase in the frequency of the incident wave required an increase in the number of sources (which represent the scattered wave fields) in order to maintain the same accuracy; b) It was determined that source surfaces (C_j^+ and C_j^-) should not be placed in the immediate vicinity of the corresponding interface C_j. A good choice of source surfaces appears to be the one in which they "follow" in shape interface C_j.

Thus, "inner" and "outer" source surfaces (C_j and C_j^+, j=1,2,...,R) are obtained through the scaling of interface C_j by numbers smaller and larger than 1, respectively. In this paper, the scaling factors are chosen to be 0.8 and 1.2. Throughout the numerical evaluation of results, the number of "observation" points along each interface C_j is chosen to be N_j=20, j=1,2,...,P. The number of source points along corresponding surfaces C_j^- and C_j^+ is chosen to be $M_j = L_j = 10$, j=1,2,...,R. The choice of these parameters is made based upon the analysis of the single layer model for which the exact solution is available (Wong and Trifunac, 1974). Therefore, calculations corresponding to multiple dipping layers are checked in the following manner: The material properties of all dipping layers are assumed to be the same and the shape of the first dipping layer is chosen

to be a semi-elliptical one. In all cases the exact results of Wong and Trifunac (1974), shown by Fig. 2, are recovered.

For the case when no exact solution is available, one may check the numerical convergence of the results by increasing the number of "observation" points (N_j, j=1,2,...,R in equations A1-A4) along the interfaces C_j and the number of sources (M_j and L_j in equations 12a-12c) until the resulting displacement field does not change with their increase (Wong, 1982).

Although the proposed technique is applicable to a very general class of problems involving dipping layers, models with many irregular layers will require a substantial memory size of the digital computer. Since the discretization procedure takes place along the interfaces only, this restriction is far less severe than in the solution procedures which involve finite element or finite difference approach.

Summary and Conclusions

Scattering of plane harmonic SH-wave by dipping layers of arbitrary shape is studied by using the indirect boundary integral method. The displacement field is evaluated throughout the elastic medium so that the continuity conditions along the interfaces between the layers are satisfied in mean-square-sense. It is shown that the presence of dipping layers may cause very large amplification of surface ground motion. The presented results indicate that surface displacement amplification depends upon the number of parameters, such as: the location of the observation point at the surface of the half-space, the geometry and material properties of the layers, angle of incidence, the frequency of the incoming wave. Change in any of these parameters may change significantly the surface response pattern.

Although approximate in nature, the proposed method allows study of the class of problems for which no analytical or numerical solutions are available in literature at present time.

Acknowledgement

The author expresses appreciation to M. Modest for providing him with a computer program for curve fitting using the B-spline technique.

This research has been supported by a grant (CEE-81-19696) from the National Science Foundation.

Appendix A

By choosing N_j observation points along interface C_j, $j=1,2,\ldots R$, M_j sources along C_j^- and L_j sources along C_j^+, matrix $\underset{\sim}{G}$ in equation (13) is of the order $2(N_1 + N_2 + \ldots + N_R) \times (M_1 + L_1 + \ldots M_R + L_R)$ and it is specified by

$$\underset{\sim}{G} = \begin{bmatrix} \underset{\sim}{S}^0_{N_1M_1} & -\underset{\sim}{S}^1_{N_1L_1} & -\underset{\sim}{S}^1_{N_1M_2} & \underset{\sim}{0} & \underset{\sim}{0} & \underset{\sim}{0} & \underset{\sim}{0} & & \underset{\sim}{0} & \underset{\sim}{0} \\ \underset{\sim}{0} & \underset{\sim}{S}^1_{N_2L_1} & \underset{\sim}{S}^1_{N_2M_2} & -\underset{\sim}{S}^2_{N_2L_2} & -\underset{\sim}{S}^2_{N_2M_3} & \underset{\sim}{0} & \underset{\sim}{0} & & \underset{\sim}{0} & \underset{\sim}{0} \\ \underset{\sim}{0} & \underset{\sim}{0} & \underset{\sim}{0} & \underset{\sim}{S}^2_{N_3L_2} & \underset{\sim}{S}^2_{N_3M_3} & -\underset{\sim}{S}^3_{N_3L_3} & -\underset{\sim}{S}^3_{N_3M_4} & \ldots & \underset{\sim}{0} & \underset{\sim}{0} \\ \vdots & & & \vdots & \vdots & \vdots & \vdots & & & \\ \underset{\sim}{0} & \underset{\sim}{0} & & \underset{\sim}{0} & \underset{\sim}{0} & \underset{\sim}{0} & \underset{\sim}{0} & \underset{\sim}{S}^{R-1}_{N_RL_{R-1}} & \underset{\sim}{S}^{R-1}_{N_RM_R} & -\underset{\sim}{S}^{R}_{N_RL_R} \end{bmatrix} \tag{A1}$$

where matrices $\underset{\sim}{S}^i_{N_jM_j}$ of order $2N_j \times M_j$ are defined by

$$\underset{\sim}{S}^i_{N_jM_j} \equiv [\underset{\sim}{s}_i(\underset{\sim}{r}_{n_j}, \underset{\sim}{r}_{m_j})] \; ; \; \underset{\sim}{r}_{n_j} \in C_j \; ; \; n_j=1,2,\ldots,N_j$$
$$\underset{\sim}{r}_{m_j} \in C_j^- \; ; \; m_j=1,2,\ldots,M_j. \tag{A2}$$

and matrices $\underset{\sim}{S}^i_{N_jL_j}$ of order $2N_j \times L_j$ are specified through

$$\underset{\sim}{S}^i_{N_jL_j} \equiv [\underset{\sim}{s}_i(\underset{\sim}{r}_{n_j}, \underset{\sim}{r}_{\ell_j})] \; ; \; \underset{\sim}{r}_{n_j} \in C_j \; ; \; n_j=1,2,\ldots,N_j$$
$$\underset{\sim}{r}_{\ell_j} \in C_j^+ \; ; \; \ell_j=1,2,\ldots,L_j. \tag{A3}$$

The elastodynamic Green's state $\underset{\sim}{s}_i(\underset{\sim}{r}, \underset{\sim}{r}_o)$ is defined as an elastodynamic state vector at $\underset{\sim}{r}$ due to line source at $\underset{\sim}{r}_o$.

Vector $\underset{\sim}{f}$ in equation (13) is of the order $2(N_1 + \ldots + N_R) \times 1$ and it is defined by

$$\underset{\sim}{f} = \begin{bmatrix} \underset{\sim}{s}_o^{ff}(\underset{\sim}{r}_1) \\ \underset{\sim}{s}_o^{ff}(\underset{\sim}{r}_2) \\ \vdots \\ \underset{\sim}{s}_o^{ff}(\underset{\sim}{r}_{N_1}) \\ \underset{\sim}{0} \end{bmatrix} \quad ; \quad \underset{\sim}{r}_1, \ldots, \underset{\sim}{r}_{N_1} \in C_1. \tag{A4}$$

References

Apsel, R. J. (1979). "Dynamic Green's Functions for Layered Media and Applications to Boundary Value Problems", Ph.D. Thesis, U. C. San Diego.

Boore, D. M. (1973). "The Effect of Simple Topography on Seismic Waves: Implications for the Accelerations Recorded at Pacoima Dam, San Fernando Valley, California", Bull. Seism. Soc. Am. 62, 1608-1619.

Christiansen, S. (1976). "On Kupradze's Functional Equations for Plane Harmonic Problems", Function Theoretic Methods In Differential Equations, R. P. Gilbert and R. J. Weinacht (Eds.), Pitman Publishing, London, pp. 205-243.

Cole, D. M., D. D. Kosloff, and J. B. Minster (1978). "A Numerical Boundary Integral Equation Method for Elastodynamics. I", Bull. Seism. Soc. Am. 68, 1331-1357

Copley, L. A. (1967). "Integral Equation Method for Radiation from Vibrating Surfaces", J. Acoust. Soc. Am. 41, 807-816.

Dravinski, M. (1983). "Computer Program for Scattering of Plane Harmonic SH Wave by Dipping Layers of Arbitrary Shape", Dept. Mech. Engr. Report No. 01, Univ. of Southern California, Los Angeles, California (in preparation).

Dravinski, M. (1982). "Influence of Interface Depth upon Strong Ground Motion", Bull. Seism. Soc. Am. 72, 597-614.

Esteva, L. (1977). "Microzoning: Models and Reality", Proc. World Conf. Earthquake Engr., 6th, New Delhi.

Fairweather, G. and R. L. Johnston (1982). "The Method of Fundamental Solutions for Problems in Potential Theory", Treatment of Integral Equations by Numerical Methods, C. T. H. Baker and G. F. Miller (Eds.), Academic Press, New York, pp. 349-360.

Kupradze, V. D. (1963). Dynamical Problems in Elasticity, p. 86, North Holland Publishing Co., Amsterdam.

Miklowitz, J. 1978). The Theory of Elastic Waves and Waveguides, North Holland, Amsterdam.

Oshaki, Y. (1973). "On movements of a Rigid Body in Semi-Infinite Elastic Medium", Proc. Japanese Earthquake Engineering Symposium, Tokyo, Japan.

Sanchez-Sesma, F. J. and E. Rosenblueth (1979). "Ground Motions at Canyons of Arbitrary Shapes under Incident SH Waves", Earthquake Eng. Struct. Dyn. 7, 441-450.

Sanchez-Sesma, F. J. and J. A. Esquivel (1979). "Ground Motion on Alluvial Valley Under the Incident Plane SH Waves", Bull. Seism. Soc. Am. 69, 1107-1120.

Sozen, M. A., P. C. Jennings, R. B. Matthiesen, G. W. Housner and N. M. Newmark (1968). "Engineering Report on the Caracas Earthquake of 29 July, 1967", Nat. Acad. Sci., Washington, DC.

Ursell, F. (1973). "On the Exterior Problem of Acoustics", Proc. Cambridge Phil. Soc. 74, 117-125.

Wheeler, L. T. and E. Sternberg (1968). "Some Theorems in Classical Elastodynamics", Arch. Rat. Mech. Anal. 31, 51-90.

Wong, H. L. (1982). "Diffraction of P, SV, and Rayleigh Waves by Surface Topographies", Bull. Seism. Soc. Am. 72, 1167-1184.

Wong, H. L. R. D. Trifunac (1974). "Surface Motion of Semi-Eliptical Alluvial Valley for Incident Plane SH Waves", Bull. Seism. Soc. Am. 64, 1389-1408.

Figure Captions

Figure 1 Problem geometry

Figure 2 Surface displacement amplitude for single dipping layer. ($\Omega = 0.5$, $\mu_1 = 0.167$, $\beta_1 = 0.5$).

Figure 3 Surface displacement amplitude for two dipping layers. ($\Omega = 0.5$, $\mu_1 = 0.6$, $\beta_1 = 0.8$, $\mu_2 = 0.3$, $\beta_2 = 0.6$).

Figure 4 Surface displacement amplitude for two dipping layers. ($\Omega = 0.5$, $\mu_1 = 0.6$, $\beta_1 = 0.8$, $\mu_2 = 0.3$, $\beta_2 = 0.6$).

Figure 5 Surface displacement amplitude for two dipping layers. ($\Omega = 1$, $\mu_1 = 0.6$, $\beta_1 = 0.8$, $\mu_2 = 0.3$, $\beta_2 = 0.6$).

Figure 6 Surface displacement amplitude for two dipping layers. ($\Omega = 0.5$, $\mu_1 = 0.3$, $\beta_1 = 0.6$, $\mu_2 = 0.1$, $\beta_2 = 0.4$)

Figure 7 Surface displacement amplitude for two dipping layers. ($\Omega = 1$, $\mu_1 = 0.1$, $\beta_1 = 0.4$, $\mu_2 = 0.02$, $\beta_2 = 0.2$).

Figure 8 Surface displacement amplitude for three dipping layers. ($\Omega = 0.75$, $\mu_1 = 0.3$, $\beta_1 = 0.6$, $\mu_2 = 0.1$, $\beta_2 = 0.4$, $\mu_3 = 0.02$ $\beta_3 = 0.2$)

Figure 9 Surface displacement amplitude for three dipping layers. ($\Omega = 0.75$, $\mu_1 = 0.6$, $\beta_1 = 0.8$, $\mu_2 = 0.3$, $\beta_2 = 0.6$, $\mu_3 = 0.1$, $\beta_3 = 0.4$)

Figure 10 Surface displacement amplitude for three dipping layers. ($\Omega = 1.5$, $\mu_1 = 0.6$, $\beta_1 = 0.8$, $\mu_2 = 0.3$, $\beta_2 = 0.6$, $\mu_3 = 0.1$, $\beta_3 = 0.4$)

Figure 11 Surface displacement amplitude for three dipping layers of arbitrary shape. ($\Omega = 0.75$, $\mu_1 = 0.6$, $\beta_1 = 0.8$, $\mu_2 = 0.3$, $\beta_2 = 0.6$, $\mu_3 = 0.1$, $\beta_3 = 0.4$)

Figure 12 Surface displacement amplitude for three dipping layers of arbitrary shape. ($\Omega = 0.75$, $\mu_1 = 0.6$, $\beta_1 = 0.8$, $\mu_2 = 0.3$, $\beta_2 = 0.6$, $\mu_3 = 0.1$, $\beta_3 = 0.4$).

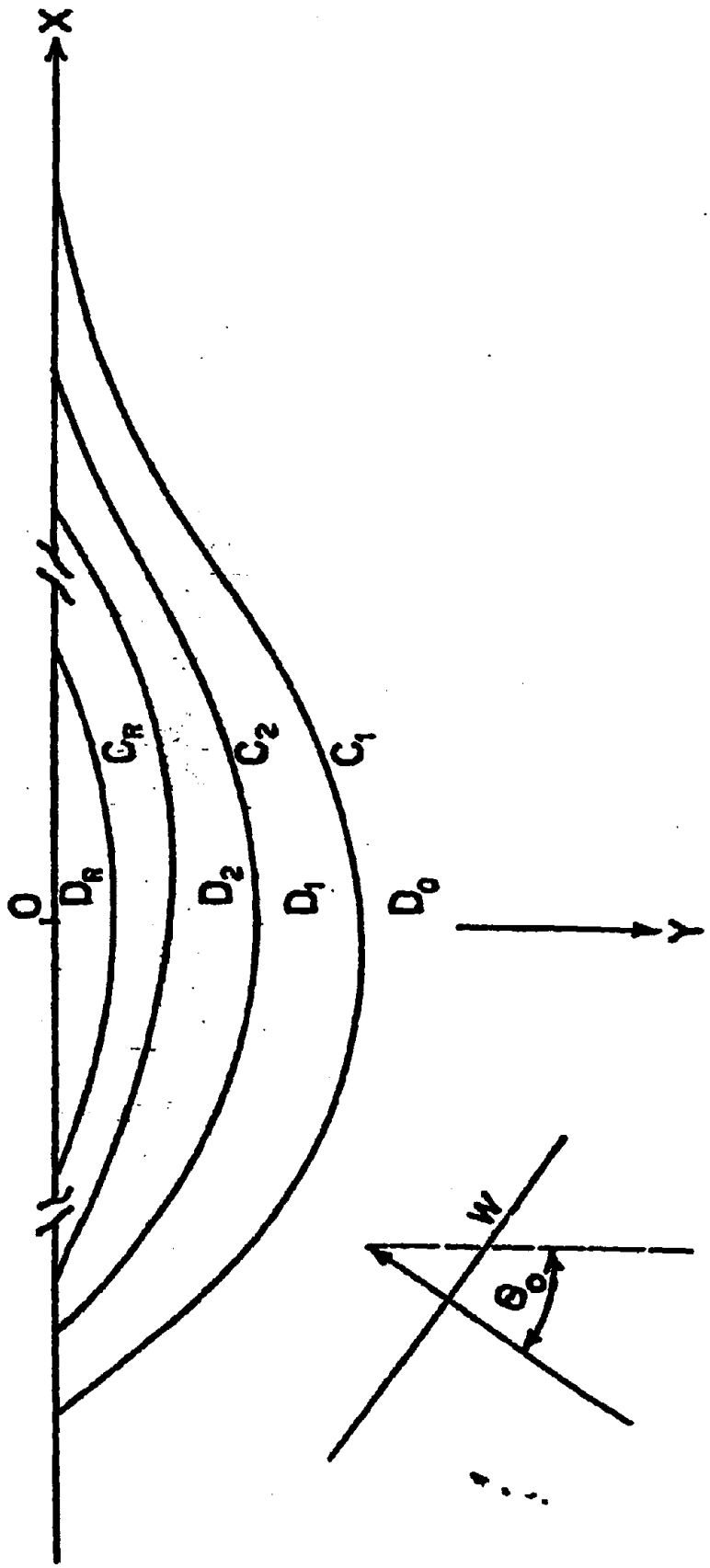

Fig. 1

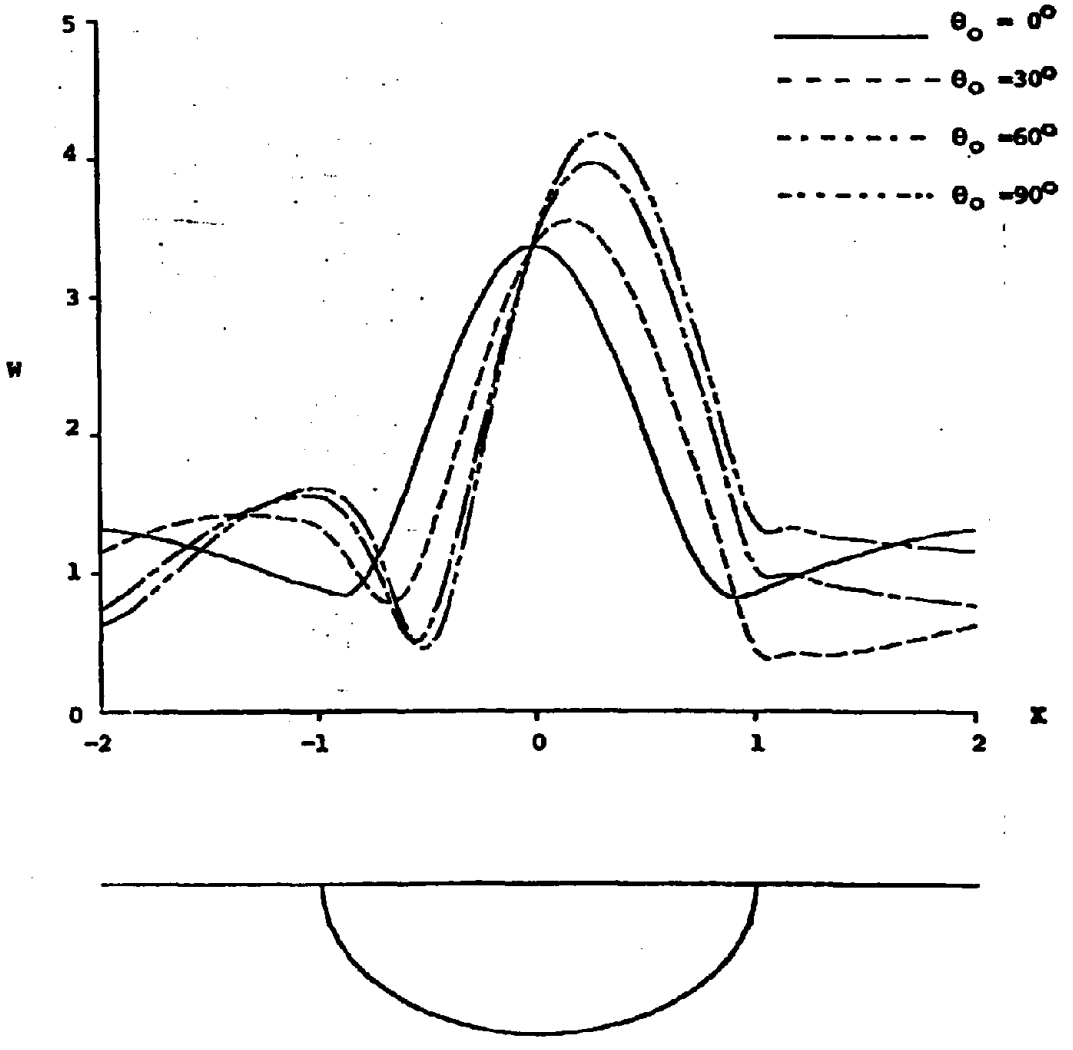

Fig. 2

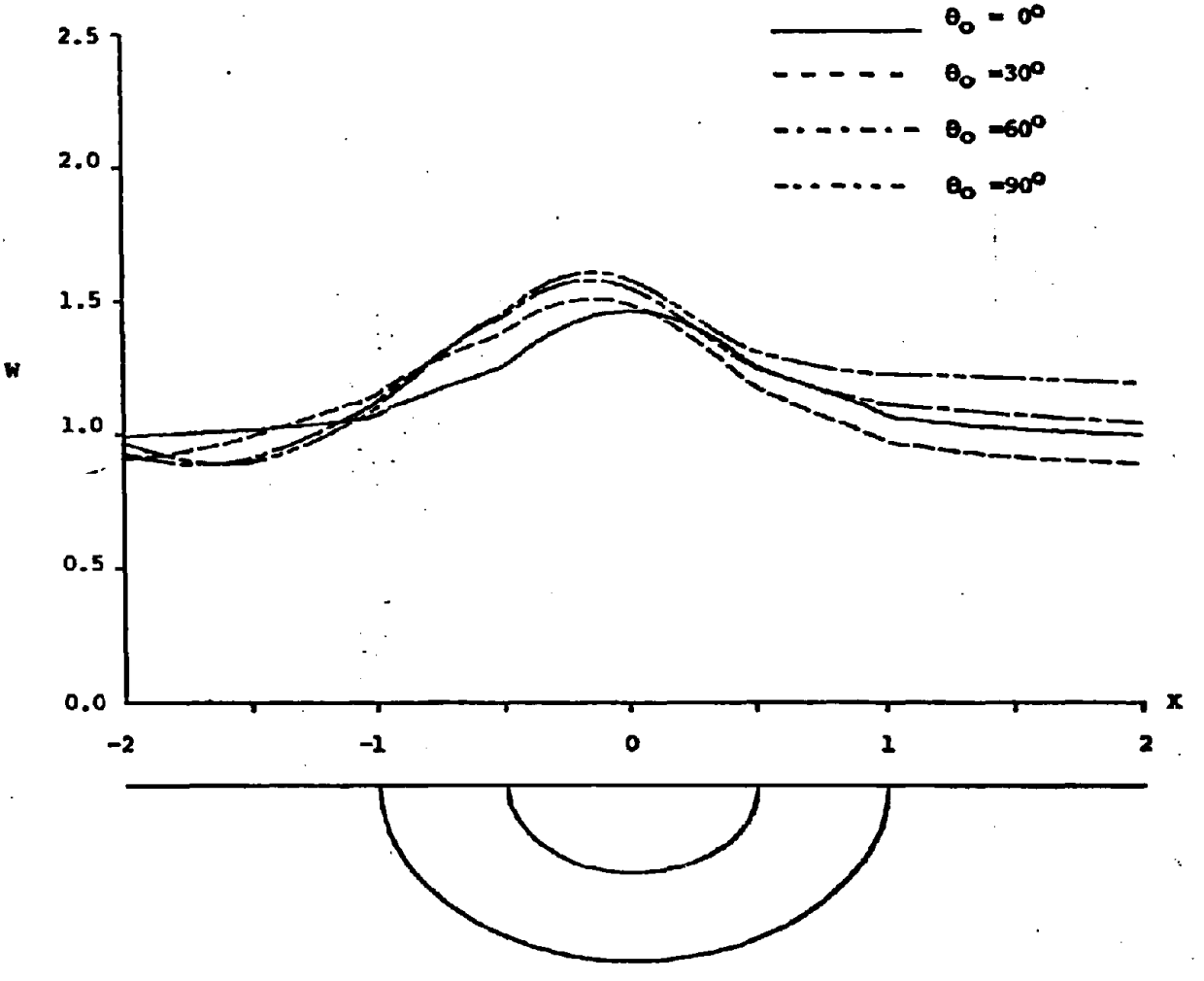
$\theta_o = 0^o$
$\theta_o = 30^o$
$\theta_o = 60^o$
$\theta_o = 90^o$
W
2.5
2.0
1.5
1.0
0.5
0.0
X
-2
-1
0
1
2

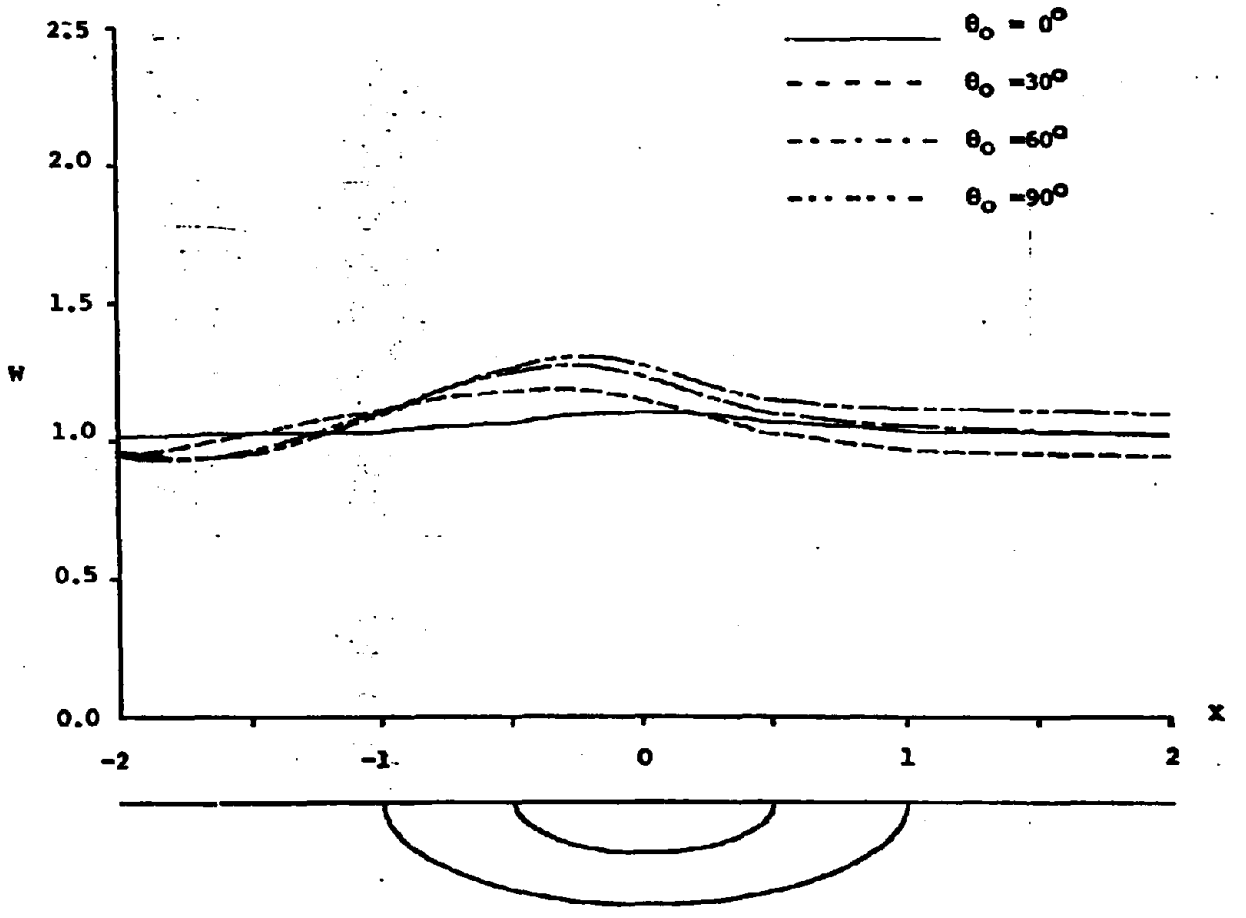
$\theta_o = 0^o$
$\theta_o = 30^o$
$\theta_o = 60^o$
$\theta_o = 90^o$
2.5
2.0
1.5
1.0
0.5
0.0
W
-2
-1
0
1
2
X

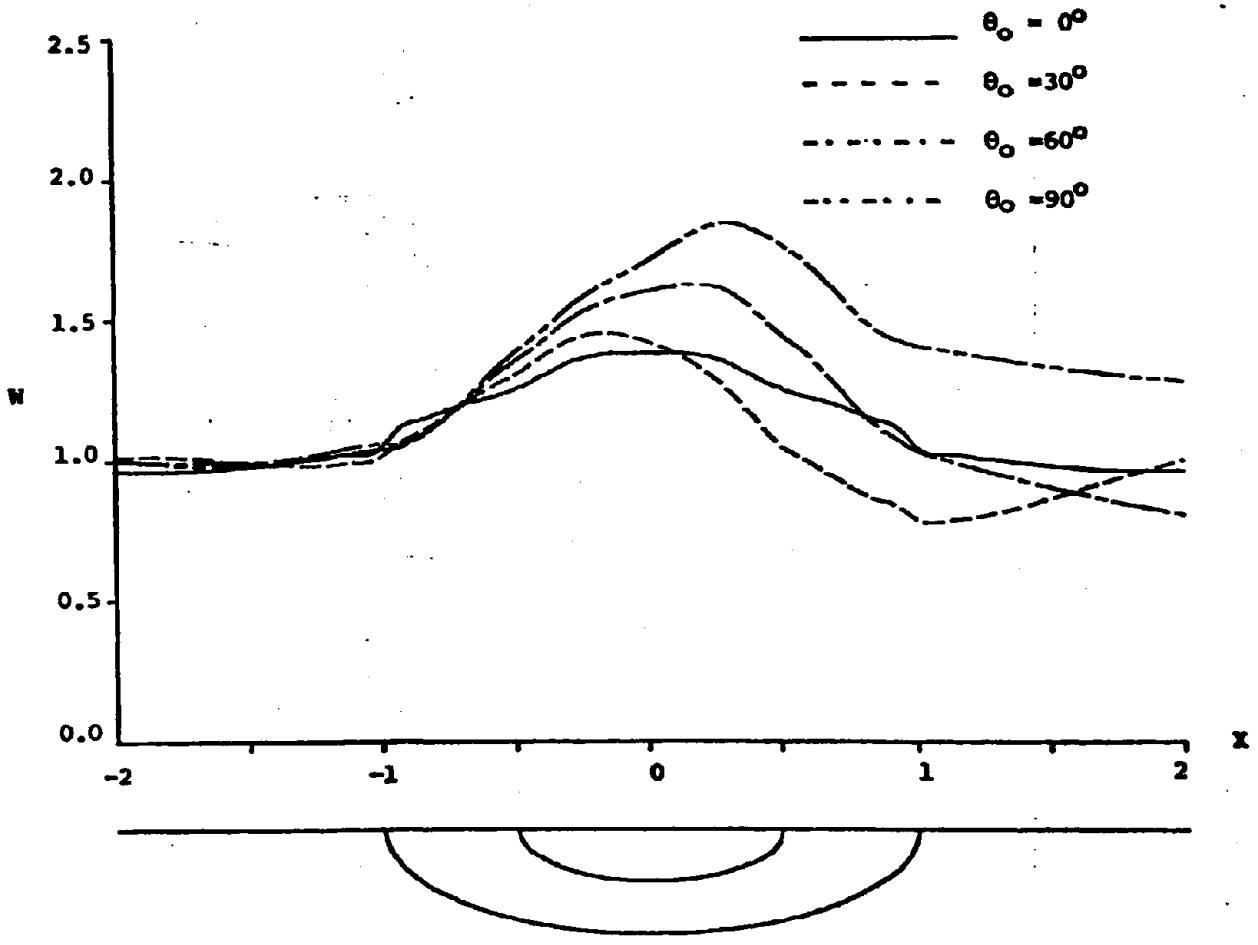
$\theta_o = 0^o$
$\theta_o = 30^o$
$\theta_o = 60^o$
$\theta_o = 90^o$
2.5
2.0
1.5
1.0
0.5
0.0
W
-2
-1
0
1
2
X

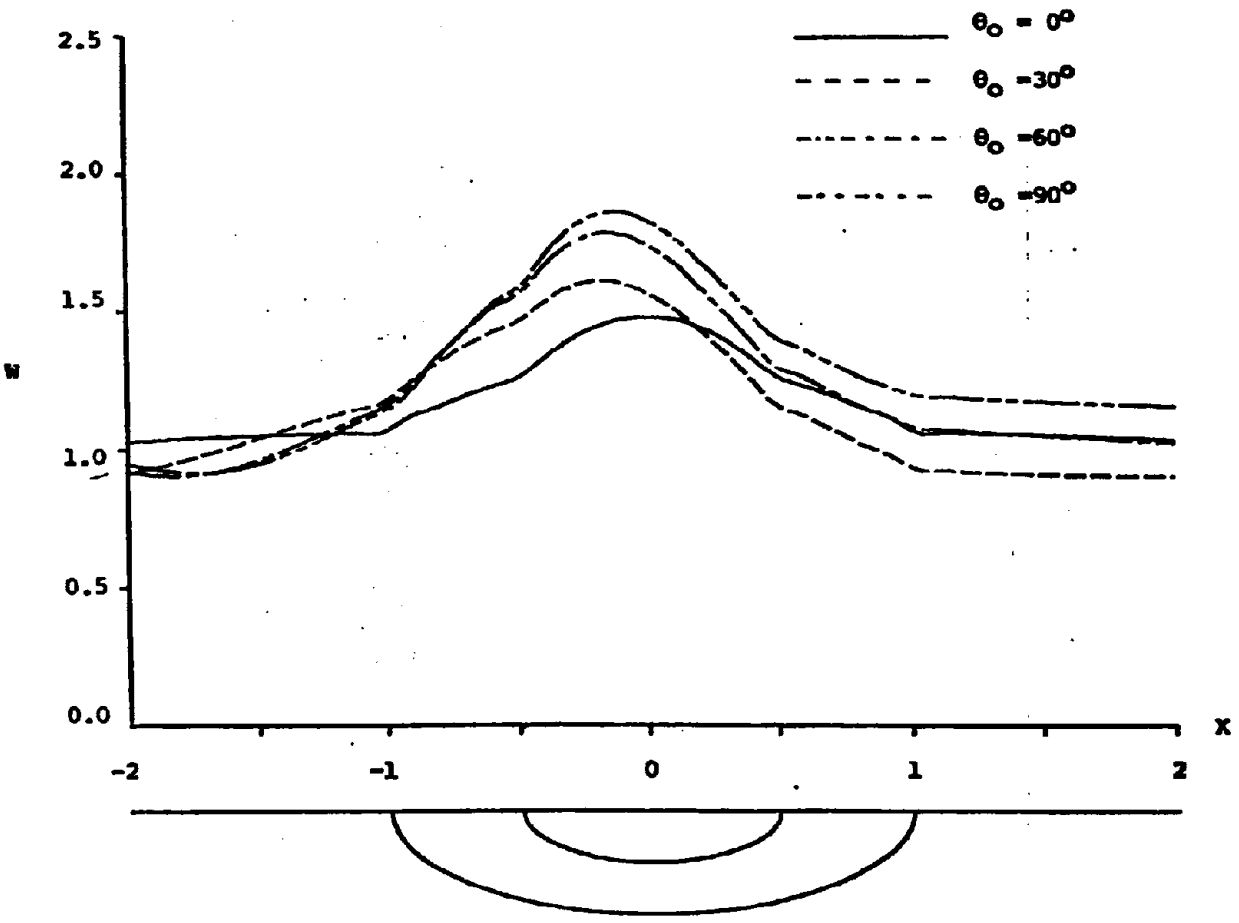
$\theta_o = 0^o$
$\theta_o = -30^o$
$\theta_o = -60^o$
$\theta_o = -90^o$
2.5
2.0
1.5
1.0
0.5
0.0
w
x
-2
-1
0
1
2

Fig. 6

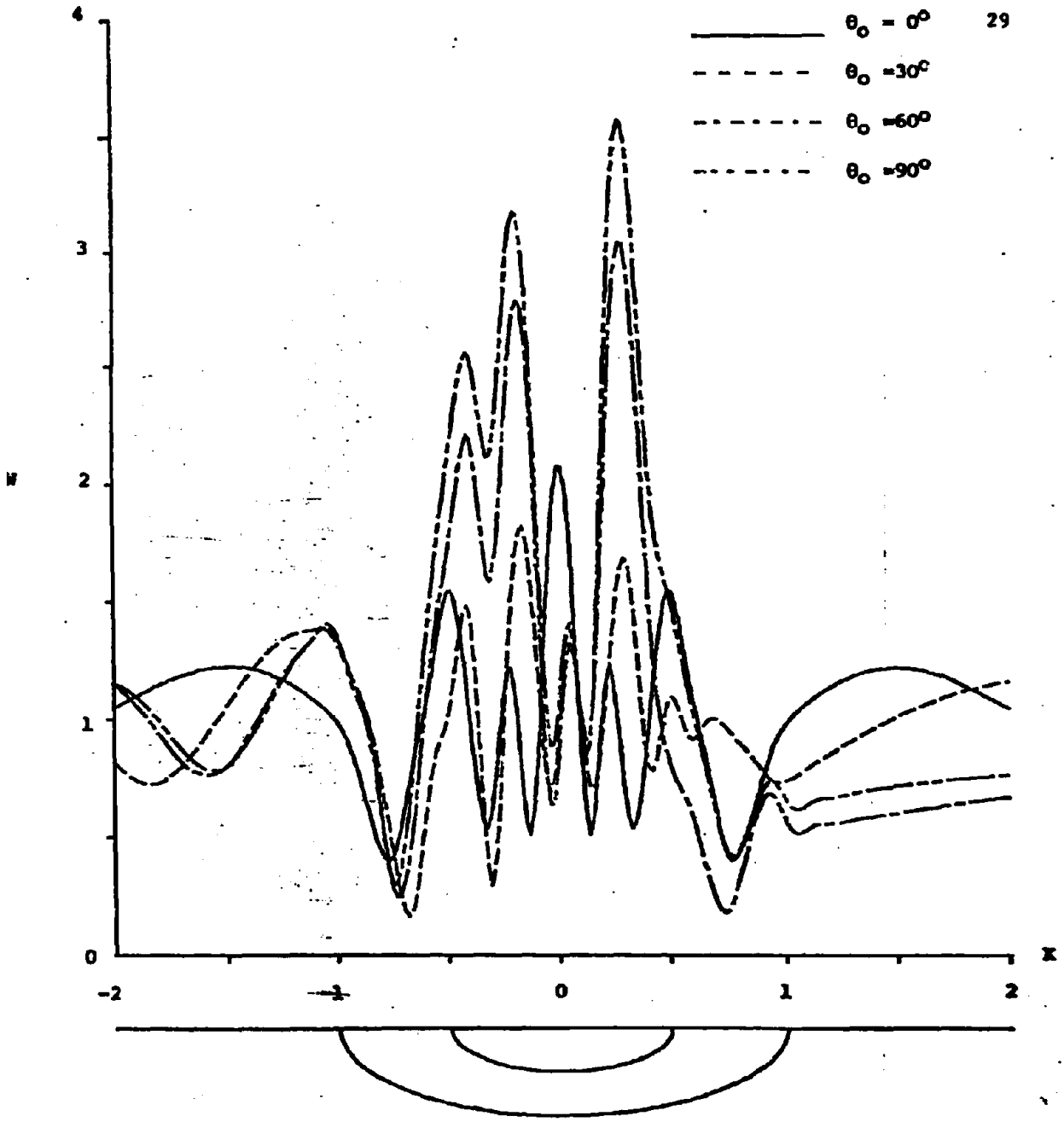
θo = 0°
θo =30°
θo =60°
θo =90°
W
X
4
3
2
1
0
-2
-1
0
1
2

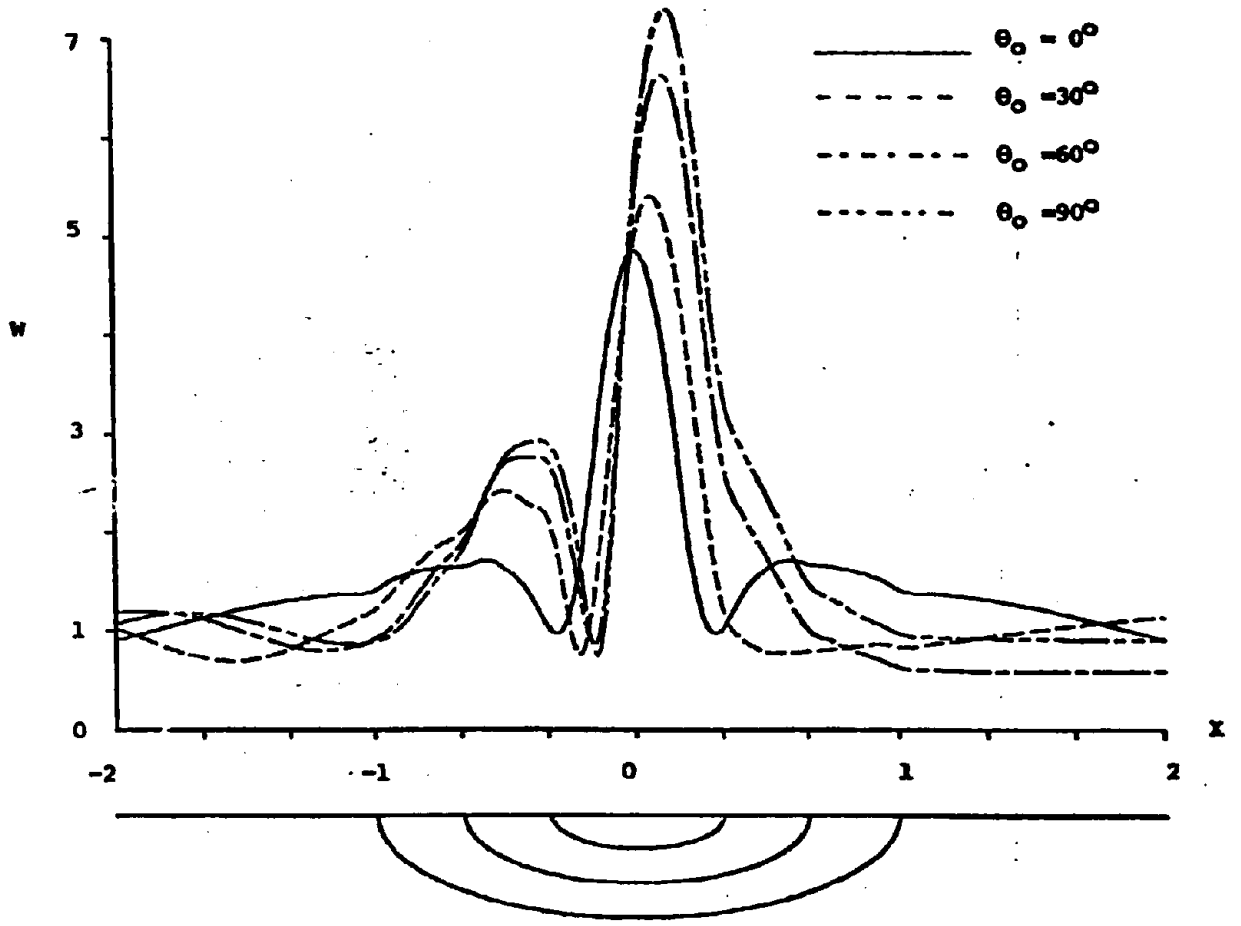
7
5
3
1
0
W
-2
-1
0
1
2
X
θ_o = 0°
θ_o =30°
θ_o =60°
θ_o =90°

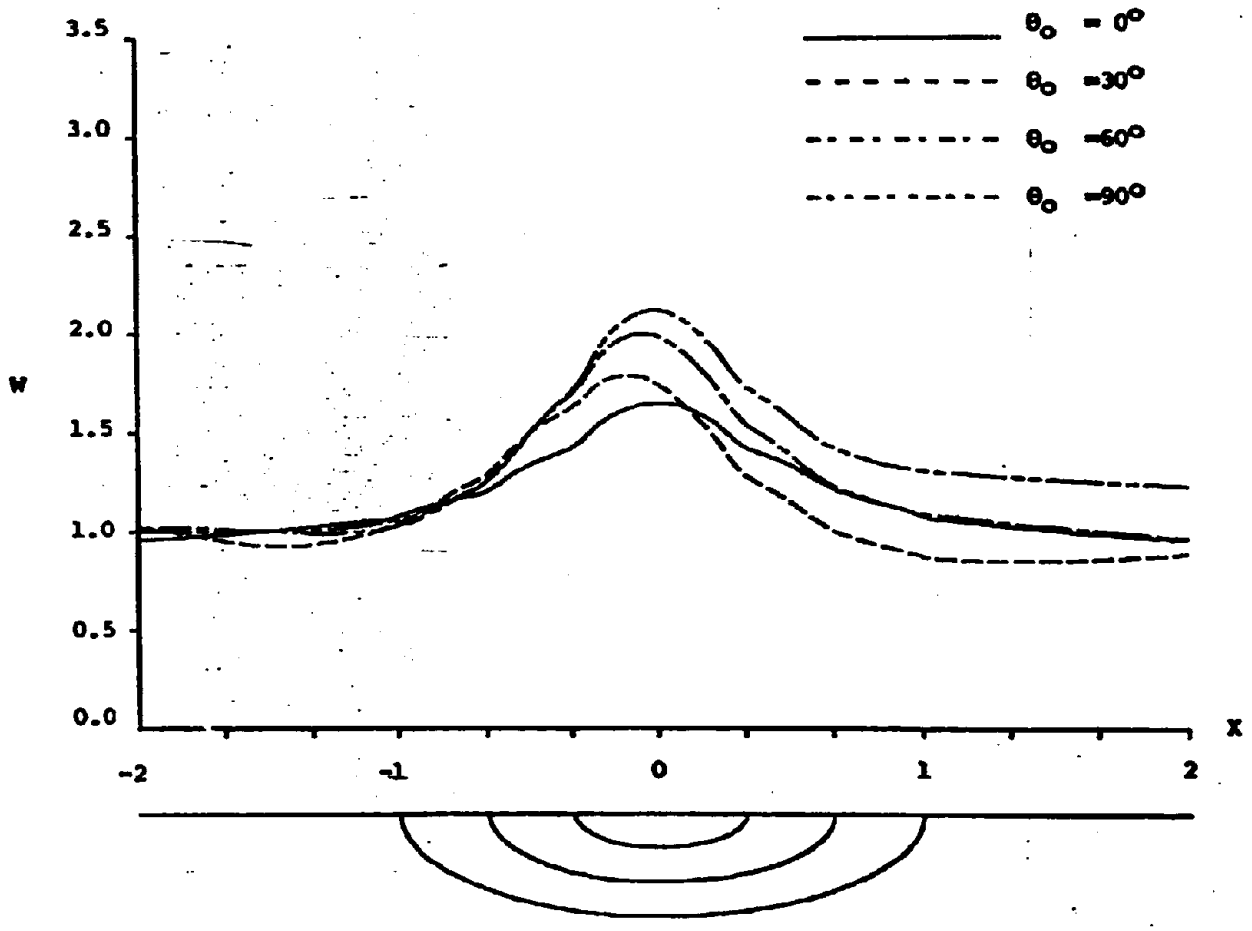
θ_o = 0°
θ_o =30°
θ_o =60°
θ_o =90°
3.5
3.0
2.5
2.0
1.5
1.0
0.5
0.0
W
-2
-1
0
1
2
X

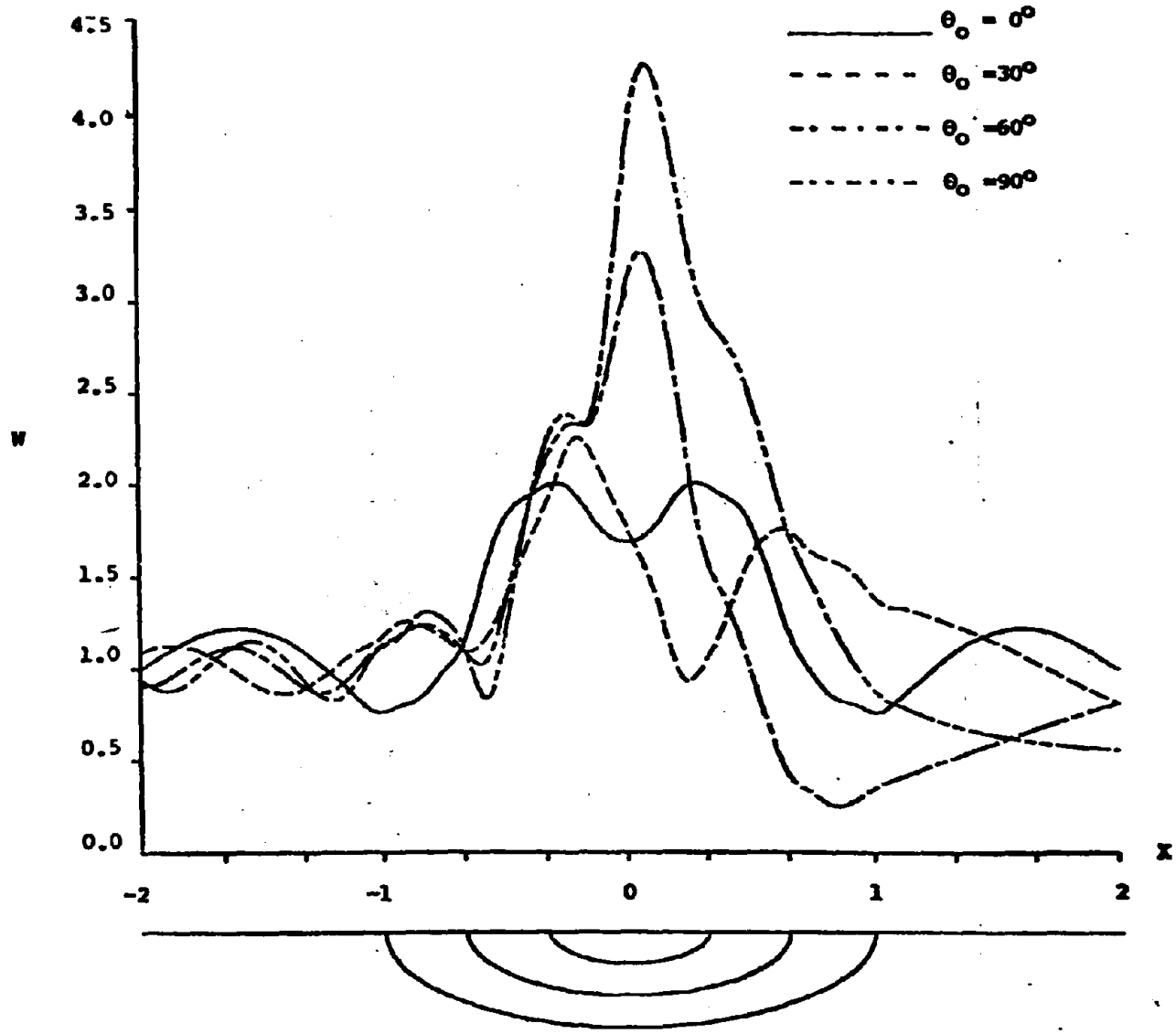
θ_o = 0°
θ_o =30°
θ_o =60°
θ_o =90°
W
X
4.5
4.0
3.5
3.0
2.5
2.0
1.5
1.0
0.5
0.0
-2
-1
0
1
2

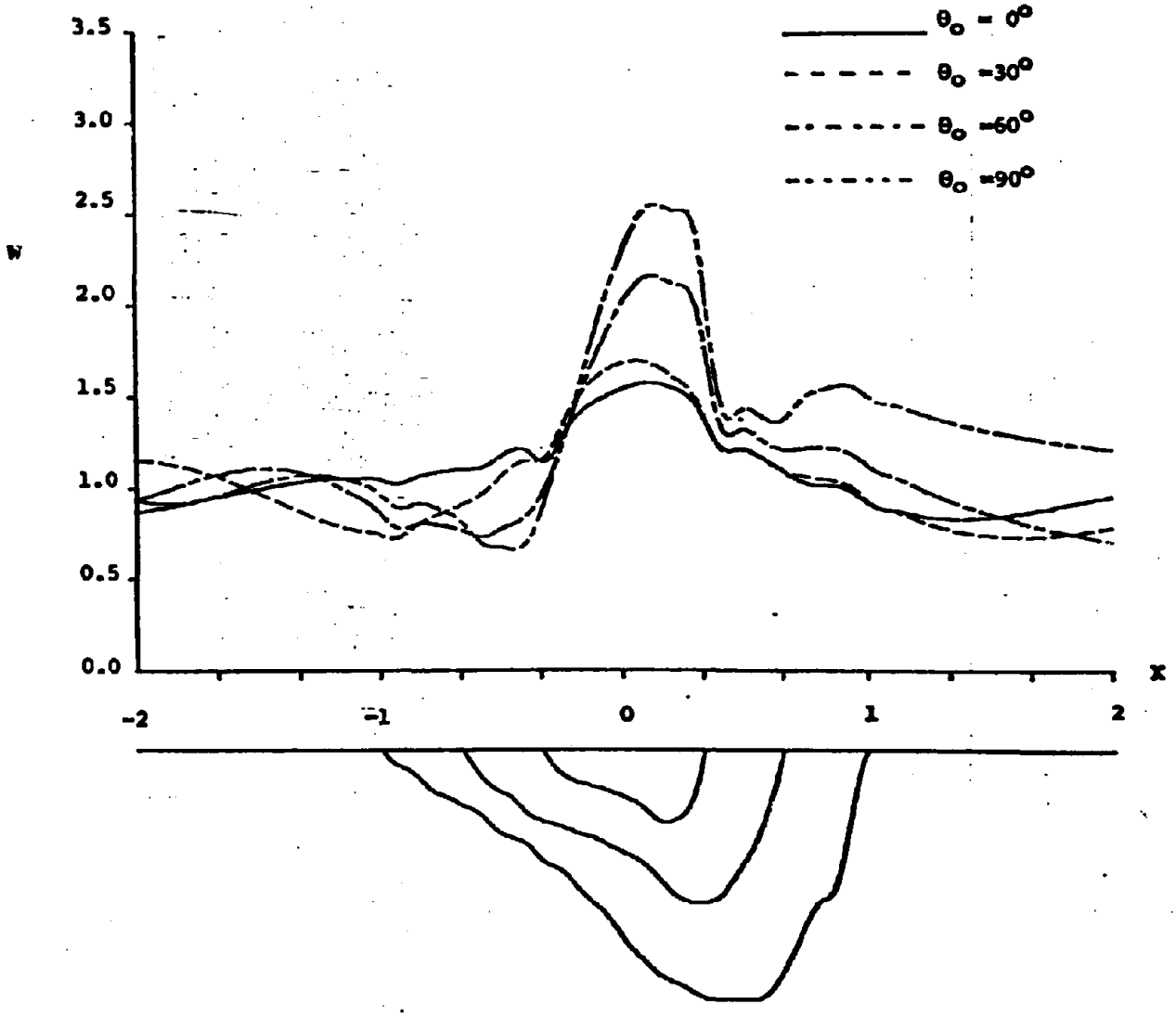
$\theta_o = 0^o$
$\theta_o = 30^o$
$\theta_o = 60^o$
$\theta_o = 90^o$
w
x
3.5
3.0
2.5
2.0
1.5
1.0
0.5
0.0
-2
-1
0
1
2

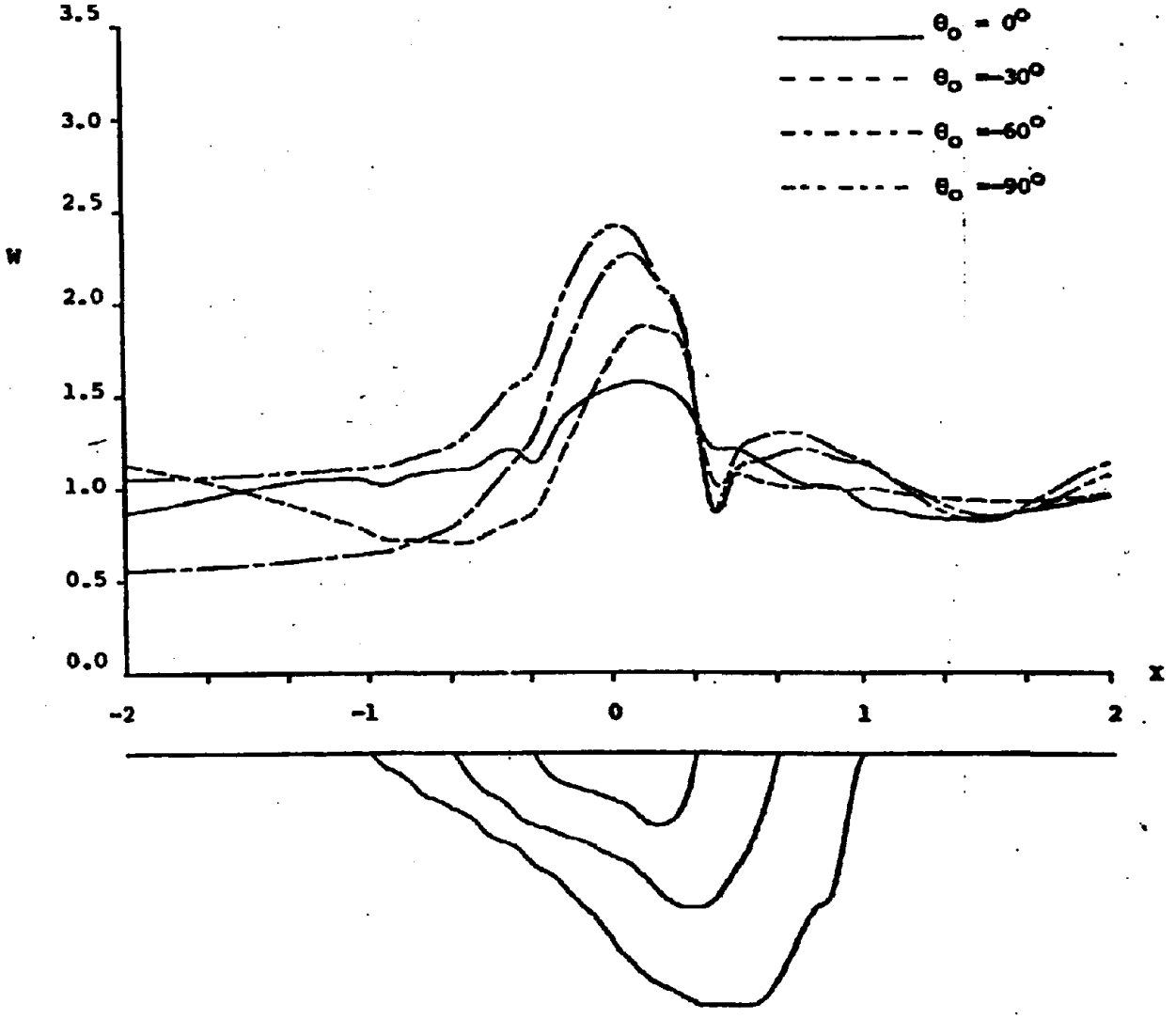
3.5
3.0
2.5
2.0
1.5
1.0
0.5
0.0
W
-2
-1
0
1
2
X
$\theta_o = 0°$
$\theta_o = -30°$
$\theta_o = -60°$
$\theta_o = -90°$

Strong Ground Motion Amplification by Dipping Layers: Plane Strain Model *

M. Dravinski

Abstract

Steady state wave motion for diffraction of plane P, SV, and Rayleigh waves by dipping layers of arbitrary shape is investigated by employing an indirect boundary integral equation method. The layers are of finite length perfectly bonded together. The material of the layers is assumed to be homogeneous, linearly elastic, and isotropic.

Presented numerical results demonstrate that the surface strong ground motion amplification effects depend upon a number of parameters: (i) frequency of the indicent wave, (ii) contrast in material properties between the layers, (iii) angle of incidence (for P and SV waves), and (iv) location of observation point. It is shown that the presence of dipping layers may cause locally large amplification or reduction of the surface ground motion when compared with corresponding free-field motion.

---

* Submitted for publication.

Introduction

In a recent paper (Dravinski, 1983) the antiplane strain model for scattering of plane harmonic SH waves by dipping layers of arbitrary shape was investigated by using an indirect boundary integral equation method (BIEM). In the present paper, the method has been extended to the plane strain model.

Strong ground motion amplification of elastic waves by dipping layers appears to be of considerable importance since a number of alluvial basins involve this type of subsurface irregularities. For example, Yerkes et al. (1965) showed that the geological structure of the Los Angeles basin incorporates several subsurface dipping layers of finite length. Complex geometry of the layers precludes construction of closed form analytical solutions and one has to rely upon the convenient numerical approach for evaluation of the results. The most commonly used numerical methods, finite elements and finite differences, require a computational grid to fill the solution domain of the problem under consideration. Consequently, these procedures do not appear to be very effective for geotechnical problems which involve large dimensions.

For many problems of interest it is possible to construct a surface integral representation of the solution. Corresponding integral equations involve only the boundary and initial values (and possibly interior sources). Once the integral equations are solved, the solution at any interior point can be determined through the original integral representation (Cruse and Rizzo, 1968; Cole et al., 1978). Since only the boundary of the model is being discretized, the number of unknown variables is greatly reduced in comparison to the finite element or finite difference procedures. A detailed review of the literature pertinent to the BIEM's is given by Brebbia (1981) and it will not be repeated here.

Basic ideas of the indirect BIEM used in the present paper originates in the works of

Kupradze (1963), Copley (1967) and Oshaki (1973). Extension of the method to wave propagation problems in geophysics and earthquake engineering is due to Sanchez-Sesma and Rosenblueth (1979), Sanchez-Sesma and Esquivel (1979), Apsel (1979), Dravinski (1982a,b,c) and Wong (1982).

Statement of Problem

Geometry of the problem is depicted by Fig. 1. The finite number (R) of dipping layers of arbitrary shape are perfectly bonded together to form a layered half-space. Interfaces between the layers are assumed to be sufficiently smooth with no sharp corners being present. Spatial domain of the half-space is denoted by D_o and that of the layers by D_j, j=1,2,...,R. Interfaces between the layers are denoted by C_i, i=1,2,...,R. The layers are assumed to be linearly elastic, homogeneous and isotropic.

The problem model is assumed to be of the plane strain type, i.e., the layered half-space extends to infinity perpendicularly to the plane of the drawing and the motion of the medium takes place in the x,y-plane only. The plane motion of the elastic media is described by a displacement vector $\underline{u}_j^T=(u_j,v_j)$, j=0,1,2,...,R, where u and v represent displacement components along the x and y-axis, respectively and superscript T denotes the transpose. The displacement field is related to the displacement potentials through

$$u_j = \frac{\partial \phi_j}{\partial x} + \frac{\partial \psi_j}{\partial y} \quad ; \quad v_j = \frac{\partial \phi_j}{\partial y} - \frac{\partial \psi_j}{\partial x} \quad , \quad j=0,1,\ldots,R, \tag{1}$$

where ϕ and ψ denote dilatational and equivoluminal displacement potential, respectively. Throughout the paper, the subscript 0 refers to half-space, while the subscripts 1,2,...,R refer to the layers of domain $D_1,D_2,\ldots,D_R$, respectively. The displacement potentials satisfy the equations of motion (Miklowitz, 1978)

$$\nabla^2 \begin{bmatrix} \phi_j \\ \psi_j \end{bmatrix} + \begin{bmatrix} h_j^2 \phi_j \\ k_j^2 \psi_j \end{bmatrix} = \underline{0} \quad ; \quad j=0,1,2,\ldots,R \quad , \quad \nabla^2 \equiv \frac{\partial^2}{\partial x^2} + \frac{\partial^2}{\partial y^2} \, , \tag{2}$$

where h and k represent the wave numbers associated with dilatational and equivoluminal waves, respectively. Throughout the analysis factor $\exp(i\omega t)$ is understood, where ω represents the circular frequency. Components of the stress tensor are related to the displacement potentials through (Miklowitz, 1978)

$$\sigma_{xx}/\mu = -k^2\phi - 2\frac{\partial^2\phi}{\partial y^2} + 2\frac{\partial^2\psi}{\partial x\partial y} \tag{3a}$$

$$\sigma_{xy}/\mu = -k^2\psi + 2\frac{\partial^2\phi}{\partial x\partial y} - 2\frac{\partial^2\psi}{\partial x^2} \tag{3b}$$

$$\sigma_{yy}/\mu = -k^2\phi - 2\frac{\partial^2\phi}{\partial x^2} - 2\frac{\partial^2\psi}{\partial x\partial y}, \tag{3c}$$

where μ denotes the shear modulus and the subscript j=0,1,2,...,R is omitted for simplification. Boundary conditions are specified by

$$\sigma_{xyj} = 0 \qquad y = 0 \text{ and } \underset{\sim}{r} \in D_j,\ j=0,1,2,\ldots,R \tag{4a}$$

$$\sigma_{yyj} = 0. \tag{4b}$$

Usual radiation conditions should be satisfied for scattered waves at infinity (Miklowitz, 1978).

At this point it is convient to introduce an elastodynamic state vector $\underset{\sim}{s}(r)$ according to (Wheeler and Sternberg, 1968)

$$\underset{\sim}{s}_j^T(\underset{\sim}{r}) \equiv \left[u(\underset{\sim}{r}),\ v(\underset{\sim}{r}),\ \sigma_{nn}(\underset{\sim}{r}),\ \sigma_{nt}(\underset{\sim}{r})\right]_j,\ \underset{\sim}{r} \in C \in D_j,\ j=0,1,2,\ldots,R, \tag{5}$$

where one says that $\underset{\sim}{s}_j$ is an elastodynamic state vector for domain D_j with the displacement field u and v, and the stress field σ_{nn} and σ_{nt}, associated with the shear modulus μ_j, the dilatational wave speed c_{dj}, and the shear wave speed c_{sj}, along the same surface C with the unit normal and tangent vectors $\underset{\sim}{n}$ and $\underset{\sim}{t}$, respectively. Superscript T in equation (5) denotes the transpose.

Perfect bonding between the layers (requires continuity of displacement and stress field along the interfaces C_j,j=1,2,...,R) in terms of elastodynamic state vectors can be expressed as

$$\underset{\sim}{s}_{j-1}(\underset{\sim}{r}) = \underset{\sim}{s}_j(\underset{\sim}{r}),\ \underset{\sim}{r} \in C_j,\ j=1,2,\ldots,R. \tag{6}$$

The incident P-wave is specified by

$$\phi^{inc} = \frac{i}{h_o} \exp\left[-ih_0(x \sin\theta_o - y \cos\theta_o)\right], \tag{7a}$$

where $i = \sqrt{-1}$, and θ_o represents the angle of incidence. The incident SV-wave is defined through

$$\psi^{inc} = -\frac{i}{k_o} \exp\left[-ik_0(x \sin\theta_o - y \cos\theta_o)\right] \tag{7b}$$

and the incident Rayleigh wave is chosen of the form

$$u^{inc} = \exp(-i\kappa_o x)\left[\exp(-b_d y) - \frac{1}{2}\left(2 - \frac{c_o^2}{c_{so}^2}\right)\exp(-b_s y)\right] \tag{7c}$$

$$v^{inc} = i\kappa_o \exp(-i\kappa_o x)\left[-\frac{b_s}{2}\exp(-b_d y) + \frac{1}{2b_s}\left(2 - \frac{c_o^2}{c_{so}^2}\right)\exp(-b_s y)\right] \tag{7d}$$

$$b_d = \kappa_o\left(1 - \frac{c_o^2}{c_{do}^2}\right)^{\frac{1}{2}}\ ;\ b_s = \kappa_o\left(1 - \frac{c_o^2}{c_{so}^2}\right)^{\frac{1}{2}} \tag{7e}$$

where c_o and κ_o denote the Raleigh wave velocity and the corresponding wave number, respectively. Particular forms of the incident field are chosen so that the free components u^{ff} and v^{ff} of the displacement vector u^{ff} along the surface of the half-space turn out to be the real numbers. All the results of the displacement field are presented normalized with respect to the $(|u^{ff}|^2 + |v^{ff}|^2)^{\frac{1}{2}}$.

Solution of Problem

The total displacement field in the half-space and the dipping layers is specified by

$$\underset{\sim}{u}_o = \underset{\sim}{u}^{ff} + \underset{\sim}{u}_o^s \ ;\ \underset{\sim}{x} \in D_o \tag{8a}$$

$$\underset{\sim}{u}_j = \underset{\sim}{u}_j^s \ ;\ \underset{\sim}{x} \in D_j;\ j=1,2,\ldots,R, \tag{8b}$$

where the superscripts ff and s denote the free and scattered wave field, respectively and $\underset{\sim}{u}^T$ denotes the displacement vector (u,v). Assuming the scattered displacement potentials

in terms of single layer potentials it follows then

$$\phi_o^s(\underline{r}) = \int_{C_1^-} q_o(\underline{r}_o)\phi_o(\underline{r};\underline{r}_o)d\underline{r}_o \quad ; \quad \underline{r} \in D_o \tag{9a}$$

$$\phi_j^s(\underline{r}) = \int_{C_j^+} p_j(\underline{r}_o)\phi_j(\underline{r};\underline{r}_o)d\underline{r}_o + \int_{C_{j+1}^-} q_j(\underline{r})\phi_j(\underline{r};\underline{r}_o)d\underline{r}_o \quad ; \quad \underline{r} \in D_j; \quad j=1,2,\ldots,R-1 \tag{9b}$$

$$\phi_R^s(\underline{r}) = \int_{C_R^+} p_R(\underline{r}_o)\phi_R(\underline{r};\underline{r}_o)d\underline{r}_o \quad ; \quad \underline{r} \in D_R \tag{9c}$$

$$\psi_o^s(\underline{r}) = \int_{C_1^-} \bar{q}_o(\underline{r}_o)\psi_o(\underline{r};\underline{r}_o)d\underline{r}_0 \quad ; \quad \underline{r} \in D_o \tag{9d}$$

$$\psi_j^s(\underline{r}) = \int_{C_j^+} \bar{p}_j(\underline{r}_o)\psi_j(\underline{r};\underline{r}_o)d\underline{r}_o + \int_{C_{j+1}^-} \bar{q}_j(\underline{r})\psi_j(\underline{r};\underline{r}_o)d\underline{r}_o \; ; \; \underline{r} \in D_j \; ; \quad j=1,2,\ldots,R-1 \tag{9e}$$

$$\psi_R^s(\underline{r}) = \int_{C_R^+} \bar{p}_R(\underline{r}_o)\psi_R(\underline{r};\underline{r}_o)d\underline{r}_o \quad ; \quad \underline{r} \in D_R, \tag{9f}$$

where p_j, q_j, $\bar{p}_j$ and $\bar{q}_j$, j=0,1,2,...,R are the unknown density functions. The functions $\phi_j(\underline{r};\underline{r}_o)$ and $\psi_j(\underline{r};\underline{r}_o)$, j=0,1,2,...,R are the Green's functions corresponding to dilatational and equivoluminal line load in the half-space. The Green's functions satisfy the following equations

$$\nabla^2 \begin{bmatrix} \phi_j(\underline{r};\underline{r}_o) \\ \psi_j(\underline{r};\underline{r}_o) \end{bmatrix} + \begin{bmatrix} k_j^2\phi_j(\underline{r};\underline{r}_o) \\ k_j^2\psi_j(\underline{r};\underline{r}_o) \end{bmatrix} = -\underline{1}\delta(|\underline{r}-\underline{r}_o|); \; j=0,1,2,\ldots,R \tag{10a}$$

with appropriate boundary conditions

$$\sigma_{xy\,j}(\underline{r};\underline{r}_o) = 0 \quad \text{at } y = 0 \; ; \; \underline{r} \in D_j \; ; \; j=0,1,2,\ldots,R \; , \tag{10b}$$

$$\sigma_{yy\,j}(\underline{r};\underline{r}_o) = 0 \tag{10c}$$

where $\underline{1}^T \equiv (1, 1)$ and $\delta(\cdot)$ is the Dirac's delta function. For an explicit solution for the Green's functions the reader is referred to the paper by Lamb (1906).

Introduction of auxiliary surfaces C_j^+ and C_j^-, j=1,2,...,R in the integral representation for the scattered wave field (equations (9a-f)) is the fundamental characteristic of the BIEM used in the present paper. Surfaces C_j^- and C_j^+ are defined inside and outside of the corresponding interface C_j, respectively (Kupradze, 1963). This eliminates the singularities in the kernels of the integrals in equations (9a-f) as $\underline{r}_o$ approaches $\underline{r}$. Therefore, the need to analytically handle integrable singularities of the Green's functions present in the single layer potentials is avoided (see Pao and Mow, 1973). This BIEM has been successfully applied to the problems of geophysics by a number of researchers, e.g., Sanchez-Sesma and Rosenblueth, 1979; Sanchez-Sesma and Esquivel, 1979; Apsel, 1979; Wong, 1982; and Dravinski, 1982a,b,c). Although introduction of the auxiliary surfaces simplifies numerical procedure considerably, the method is not without difficulties of its own (Fairweather and Johnston, 1982), since the auxiliary surfaces C_j^+ and C_j^-, j=1,2,...,R must be chosen carefully to obtain accurate results. More on this is presented in the part of the paper dealing with numerical accuracy of the results.

As the incident wave strikes the first interface C_1 the wave is partially reflected back into the half-space D_o and it is partially transmitted into the first dipping layer D_1 (see Fig. 1). Reflection and transmission of the scattered wave field in the first layer takes place along the interfaces C_1 and C_2. A similar process can be observed for subsequent layers as well. Therefore, one can view each interface C_j, j=1,2,...,R as the location of sources which "form" the scattered wave field throughout the layered medium. If the scattered wave field is expressed in terms of discrete line sources the density functions in equations (9a-f) are of the following form

$$q_{j-1}(\underline{r}) = a_{m_j}^{j-1}\delta(|\underline{r}-\underline{r}_{m_j}|) \; ; \; j=1,2,\ldots,R \; ; \; m_j=1,2,\ldots,M_j \; ; \; \underline{r}_{m_j} \in C_j^- \qquad (11a)$$

$$\bar{q}_{j-1}(\underline{r}) = \bar{a}_{m_j}^{j-1}\delta(|\underline{r}-\underline{r}_{m_j}|) \; ; \qquad (11b)$$

$$p_j(\underline{r}) = b^j_{\ell_j}\,\delta(|\underline{r}-\underline{r}_{\ell_j}|)\ ;\ \ell_j=1,2,\ldots,L_j\ ;\ \underline{r}_{\ell_j}\in C_j^+ \tag{11c}$$

$$\bar{p}_j(\underline{r}) = \bar{b}^j_{\ell_j}\,\delta(|\underline{r}-\underline{r}_{\ell_j}|), \tag{11d}$$

where summation over repeated indices is understood. Subscripted indices, such as m_j or ℓ_j should be viewed as simple indexes m and ℓ, respectively. Thus, for example equation (11a) implies $q_o(\underline{r})=a^0_1\,\delta(|\underline{r}-\underline{r}_1|)+a^0_2\delta(|\underline{r}-\underline{r}_2|)+\ldots+a^0_{M_1}\,\delta(|\underline{r}-\underline{r}_{M_1}|)$, etc. Substituting equations (11a–d) into equation (9a–f) leads to the scattered wave field

$$\phi^s_o(\underline{r}) = a^o_{m_1}\,\phi_o(\underline{r};\underline{r}_{m_1})\ ;\ \underline{r}\in D_o\ ;\ \underline{r}_{m_1}\in C_1^-\ ;\ m_1=1,2,\ldots,M_1 \tag{12a}$$

$$\psi^s_o(\underline{r}) = \bar{a}^o_{m_1}\,\psi_o(\underline{r};\underline{r}_{m_1})\ ; \tag{12b}$$

$$\phi^s_i(\underline{r}) = b^i_{\ell_i}\,\phi_i(\underline{r};\underline{r}_{\ell_i}) + a^i_{m_{i+1}}\,\phi_i(\underline{r};\underline{r}_{m_{i+1}})\ ;\ \underline{r}\in D_i\ ;\ \begin{array}{l} i=1,2,\ldots,R-1\\ \ell_i=1,2,\ldots,L_i\\ m_i=1,2,\ldots,M_i\\ \underline{r}_{\ell_i}\in C_i^+\\ \underline{r}_{m_i}\in C_i^-\end{array} \tag{12c}$$

$$\psi^s_i(\underline{r}) = \bar{b}^i_{\ell_i}\,\psi_i(\underline{r};\underline{r}_{\ell_i}) + \bar{a}^i_{m_{i+1}}\,\psi_i(\underline{r};\underline{r}_{m_{i+1}}) \tag{12d}$$

$$\phi^s_R(\underline{r}) = b^R_{\ell_R}\,\phi_R(\underline{r};\underline{r}_{\ell_R})\ ;\ \underline{r}\in D_R\ ;\ \ell_R=1,2,\ldots,L_R \tag{12e}$$

$$\psi^s_R(\underline{r}) = \bar{b}^R_{\ell_R}\,\psi_R(\underline{r};\underline{r}_{\ell_R}), \tag{12f}$$

where the summation over repeated indices is suppressed if one index is a superscript and the other one is a subscript. For example, equation (12e) implies

$\phi^s_R = b^R_1\phi_R(\underline{r};\underline{r}_1)+b^R_2\phi_R(\underline{r};\underline{r}_2)+\ldots+b^R_{L_R}\phi_R(\underline{r};\underline{r}_{L_R})$, etc.

The unknown source intensities $a^{j-1}_{m_j}$, $\bar{a}^{j-1}_{m_j}$, $b^j_{\ell_j}$, and $\bar{b}^j_{\ell_j}$ $j=1,2,\ldots,R$, $m_j=1,2,\ldots,M_j$; $\ell_j=1,2,\ldots,L_j$ are determined through the use of the continuity conditions specified by equation (6). By choosing N_j collocation points (along each interface C_j, $j=1,2,\ldots,R$) to evaluate equation (6) the source intensities are determined in the least square sense, i.e.

$$\left[a_1^0 \cdots a_{M_1}^0 \; \bar{a}_1^0 \cdots \bar{a}_{M_1}^0 \; b_1^1 \cdots b_{L_1}^1 \; \bar{b}_1^1 \cdots \bar{b}_{L_1}^1 \cdots a_1^{R-1} \cdots a_{M_{R-1}}^{R-1} \; \bar{a}_1^{R-1} \cdots \bar{a}_{M_{R-1}}^{R-1} \; b_1^R \cdots b_{L_R}^R \; \bar{b}_1^R \cdots \bar{b}_{L_R}^R\right]^T$$

$$= (\underline{G}^* \underline{G})^{-1} \underline{G}^* \underline{f}, \qquad (13)$$

where the matrices a and f are given in the Appendix and the superscript * denotes the transpose complex conjugate.

Evaluation of Results

Throughout the numerical evaluation of the results all variables are presented in dimensionless form. For that purpose the shear wave velocity c_{so} and shear modulus μ_o are chosen to be unity; distances are normalized with respect to the half width of the first layer and surface displacement amplitude at each point is presented normalized with respect to the corresponding amplitude of the surface free-field motion, i.e., $(|u^{ff}|^2 + |v^{ff}|^2)^2$. Dimensionless frequency Ω is introduced as the ratio of the total width of the first dipping layer and the wavelength of the incident wave field.

Single-Layer-Model

Scattered wave field for a single dipping layer embedded in a half-space as specified by equations (12a-f) follows to be

$$\phi_o^s(\underset{\sim}{r}) = a_{m_1}^o \phi_o(\underset{\sim}{r};\underset{\sim}{r}_{m_1}) \quad ; \quad \underset{\sim}{r} \in D_o \quad ; \quad \underset{\sim}{r}_{m_1} \in C_1^- \quad ; \quad m_1=1,\ldots,M_1 \tag{14a}$$

$$\psi_o^s(\underset{\sim}{r}) = \bar{a}_{m_1}^o \psi_o(\underset{\sim}{r};\underset{\sim}{r}_{m_1}) \tag{14b}$$

$$\phi_1^s(\underset{\sim}{r}) = b_{\ell_1}^1 \phi_1(\underset{\sim}{r};\underset{\sim}{r}_{\ell_1}) \quad ; \quad \underset{\sim}{r} \in D_1 \quad ; \quad \underset{\sim}{r}_{\ell_1} \in C_1^+ \quad ; \quad \ell_1=1,\ldots,L_1 \tag{14c}$$

$$\psi_1^s(\underset{\sim}{r}) = \bar{b}_{\ell_1}^1 \psi_1(\underset{\sim}{r};\underset{\sim}{r}_{\ell_1}), \tag{14d}$$

where the coefficients $a_{m_1}^o$, $\bar{a}_{m_1}^o$, $b_{\ell_1}^1$, and $\bar{b}_{\ell_1}^1$ are formally given by equation (13). Substitution of equations (14a-d) into equation (1) and then into equations (8a,b) leads to the displacement field throughout the elastic medium for appropriate incident wave field (P, SV, or Rayleigh wave). Figs. 2-4 depict the normalized surface displacement amplitude atop the half-space with a semi-elliptical dipping layer subjected to different cases of P, SV, and Rayleigh waves for dimensionless frequency $\Omega=1$. It is evident from the results of Figs. 2-4 that the presence of the dipping layer may cause significant ground motion amplification (reduction) at the surface of the half-space when compared with the surface

response in the absence of the irregularity, i.e., free-field motion. Furthermore, for incident P and SV wave surface motion appears to be very sensitive upon the angle of incidence. Detailed discussion of the single layer response can be found elsewhere (Dravinski, 1982).

Two-Layer-Model

For two dipping layers embedded in an elastic half-space scattered wave field follows from equations (12a-f) to be

$$\phi_o^s(\underset{\sim}{x}) = a^o_{m_1}\phi_{(1)}(\underset{\sim}{x};\underset{\sim}{x}_{m_1}) \quad ; \quad \underset{\sim}{x} \in D_o \; ; \; \underset{\sim}{x}_{m_1} \in C_1^- \; ; \; m_1=1,2,\ldots,M_1 \tag{15a}$$

$$\psi_o^s(\underset{\sim}{x}) = \bar{a}^o_{m_1}\psi(\underset{\sim}{x};\underset{\sim}{x}_{m_1}) \tag{15b}$$

$$\phi_1^s(\underset{\sim}{x}) = b^1_{\ell_1}\phi_1(\underset{\sim}{x};\underset{\sim}{x}_{\ell_1}) + a^1_{m_2}\phi_1(\underset{\sim}{x};\underset{\sim}{x}_{m_2}) \; ; \; \underset{\sim}{x} \in D_1 \; ; \; \underset{\sim}{x}_{m_2} \in C_2^- \; ; \; \underset{\sim}{x}_{\ell_1} \in C_1^+ \quad m_2=1,2,\ldots,M_2 \; ; \; \ell_1=1,2,\ldots,L_1 \tag{15c}$$

$$\psi_1^s(x) = \bar{b}^1_{\ell_1}\psi_1(\underset{\sim}{x};\underset{\sim}{x}_{\ell_1}) + \bar{a}^1_{m_2}\psi_1(\underset{\sim}{x};\underset{\sim}{x}_{m_2}) \tag{15d}$$

$$\phi_2^s(\underset{\sim}{x}) = b^2_{\ell_2}\phi_2(\underset{\sim}{x};\underset{\sim}{x}_{\ell_2}) \; ; \; \underset{\sim}{x} \in D_2 \; ; \; \underset{\sim}{x}_{\ell_2} \in C_2^+ \; ; \; \ell_2=1,2,\ldots,L_2 \tag{15e}$$

$$\psi_2^s(\underset{\sim}{x}) = \bar{b}^2_{\ell_2}\psi_2(\underset{\sim}{x};\underset{\sim}{x}_{\ell_2}) \tag{15f}$$

where the source intensities $a^o_{m_1}$, $\bar{a}^o_{m_1}$, $b^1_{\ell_1}$, $\bar{b}^1_{\ell_1}$, etc. are known through equation (13). Again, summation over repeated indices is understood. Substitution of equations (15a-f) into equation (1) provides the scattered displacement field while the use of equations (8a,b) for a particular type of incident wave implies total displacement field throughout the elastic medium.

For different angles of incidence (for P and SV waves) and for Rayleigh waves the normalized surface displacement amplitude for the two layers model is shown by Figs. 5-7. A fairly high contrast in the material properties between the layers is assumed with dimensionless frequency =1. It follows from the results presented by Figs. 5-7 that

layering in the model creates substantial ground motion amplification effects. Clearly, the response at the surface of the half space appears to depend upon the type and angle of incidence of the incident wave as well as the location of the observation point at the surface of the half-space. Comparison of Figs. 2-4 with Figs. 5-7 indicate that the presence of the additional dipping layer D_2 caused a considerable change in the surface displacement amplification pattern atop the layers and less change atop the surface of the half-space D_o. This suggests that dipping layering may be of great importance in the evaluation of the possible strong ground motion for different alluvial basins during an actual earthquake.

The change in the frequency of the incident wave to Ω=0.5 resulted in the surface displacement field shown by Figs. 8-10. Evidently, surface displacement amplification is very sensitive upon the frequency of the incident wave for all three types of waves.

So far, the following parameters in the problem have been varied: the type of incident wave, the angle of incidence, the frequency of the incoming wave and the number of layers. Results of Figs. 11-13 correspond to the surface response for less contrast in the material properties between the layers and at frequency Ω=1. It is apparent from the results of Figs. 5-7 and Figs. 11-13 that the contrast in the material properties of the layers is of major importance for the resulting surface ground motion.

Therefore, presented results indicate the following: (i) the presence of dipping layers may cause very large amplification (reduction) of the surface ground motion; (ii) ground motion amplification appears to be very sensitive upon the number of parameters such as: the type of incident wave, the angle of incidence, the frequency of the incoming wave, the number of layers, the material properties of the layers and the location of the observation point at the surface of the half-space. This can be explained in terms of interaction of the incident and the scattered waves. The two may interact constructively

or destructively at an observation station, thus resulting in corresponding amplification or reduction of the surface ground motion. Parameters which affect the two wave fields may influence that interaction and thus affect the surface ground motion. Consequently, it appears from the presented results that the strong ground amplification at a given site would be very difficult to specify by a simple parameter. Instead, it should incorporate several of them in order to account for strong ground motion amplification at the site more precisely.

On Numerical Evaluation of Results

Extensive testing of the indirect BIEM used in this paper is required in order to obtain accurate results. While the testing of the method for the antiplane strain problems is simple due to the abundance of problems for which the exact solution is available, for the subsurface inclusions in a half-space and the plane strain model situation is quite opposite. Even for very simple geometries of elastic inclusion in the half-space the author is not aware at the present time of any closed form analytical solution dealing with steady state motion caused by diffraction of P, SV_z or Rayleigh wave.

Previous testing of the method for full-space problem models, for which the exact solution exists, indicated very similar behaviour of the BIEM solutions in the plane strain model as in the case of the antiplane strain model (Dravinski 1982a,b). These conclusions can be summarized as follows: a) The method provides very good results for a wide range of frequencies. Increase in the frequency of the incident wave field requires an increase in the number of sources and collocation points in order to maintain the same accuracy; b) Source surfaces C_j^{+-} should not be placed in the immediate vicinity of the interface C_j. A good choice of the source surfaces appears to be the one in which they "follow" in shape interface C_j. Therefore, the surfaces C_j^- and C_j^+ in the present paper are chosen by scaling the interface C_j by factors 0.5 and 1.5 respectively.

Error analysis of the method (Dravinski, 1982; Wong, 1982) suggested a procedure for checking the numerical results. It was observed that convergence of the results in the test problems has been achieved when the increase in the number of collocation and source points did not produce any change in the resulting displacement field. This procedure has been used in the present work to determine the number of sources at which to evaluate the surface displacement field.

Summary and Conclusions

Amplification of plane harmonic P, SV, and Rayleigh waves by dipping layers of arbitrary shape embedded into an elastic half-space is investigated by using an indirect boundary integral equation approach. The problem has been investigated within the framework of the linear theory of elasticity. The displacement field is evaluated for the arbitrary number of layers throughout the elastic medium so that the continuity of the stress and displacement field between the layers is satisfied in the mean-square-sense.

Numerical results indicate the following: (i) dipping layers may cause locally very large amplification (reduction) of the surface ground motion; (ii) amplification pattern of the motion depends upon the number of parameters present in the problem such as the type of incident wave, the angle of incidence, frequency, the material properties of the layers, the number of layers, and the location of the observation point at the surface of the half-space. Change of any of the parameters may cause substantial change in the strong ground motion atop the surface of the half-space.

Acknoweledgement

This research has been supported by a grant CEE-81-19696 from the National Science Foundation.

References

Apsel, R. J. (1979). "Dynamic Green's Functions for Layered Media and Applications to Boundary Value Problems", Ph.D. Thesis, U. C. San Diego.

Brebbia, C. A. (1981). "Introductory Remarks", Boundary Element Methods, Proceedings of the Third International Seminar, Irvine, California, July 1981, Editor C. A. Brebbia, CML Publications, Springer-Verlag, New York.

Cole, D. M., D. D. Kosloff, and J. B. Minster (1978). "A Numberical Boundary Integral Equation Method for Elastodynamics. I", Bull. Seism. Amer., 68, 1331-1357.

Copley, L. A. (1967). "Integral Equation Method for Radiation from Vibrating Surfaces", J. Acoust. Soc. Am., 41, 807-816.

Cruise, T. A. and F. J. Rizzo (1968). "A Direct Formulation and Numerical Solution of the General Transient Elastodynamic Problem. I", J. Math. Anal. Applic., 22, 224-259.

Dravinski, M. (1982a). "Scattering of Elastic Waves by an Alluvial Valley", J. Eng. Mech. Division, ASCE, 108, 1-17.

Dravinski, M. (1982b). "Scattering of SH-Waves by Subsurface Topography", J. Eng. Mech. Division, ASCE, 108, 19-31.

Dravinski, M. (1982c). "Influence of Interface Depth Upon Strong Ground Motion", Bull. Seism. Soc. Amer., 72, 597-614.

Dravinski, M. (1983). "Scattering of Plane Harmonic SH-Wave by Dipping Layers of Arbitrary Shape", Bull. Seism. Soc. Amer. 73,

Fairweather, G. and R. L. Johnston (1982). "The Method of Fundamental Solutions for Problems in Potential Theory", Treatment of Integral Equations by Numerical Methods, C. T. H. Baker and G. F. Miller (Eds.) Academic Press, New York, 349-360.

Kupradze, V. P. (1963). "Dynamical Problems in Elasticity", Progress in Solid Mechanics, Vol. 3, Editors I. N.

Sneddon and R. Hill, North Holland, Amsterdam.

Lamb, M. (1906). "On Propagation of Tremors Over the Surface of an Elastic Solid", Phil. Trans. Roy. Soc. London, Series A, 203, 1-42.

Miklowitz, J. (1978). The Theory of Elastic Waves and Waveguides, North Holland, Amsterdam.

Oshaki, Y. (1973). "On Movements of a Rigid Body in Semi-Infinite Elastic Medium", Proc. Japanese Earthquake Engineering Symposium, Tokyo, Japan.

Pao, Y. H. and C. C. Mow (1973). Diffraction of Elastic Waves and Dynamic Stress Concentration, Crane & Russak, New York, 165-171.

Sanchez-Sesma, F. Y. and J. A. Esquivel (1979). "Ground Motion on Alluvial Valley Under Incident Plane SH Waves", Bull. Seism. Soc. Amer., 69, 1107-1120.

Sanchez-Sesma, F. Y. and E. Rosenblueth (1979). "Ground Motions at Canyons of Arbitrary Shapes Under Incident SH Waves", Earthquake Eng. Struct. Dyn., 7, 441-450.

Wheeler, L. T. and E. Sternberg (1968). "Some Theorems in classical Elastodynamics", Arch. Rat. Mech. Anal., 31, 51-90.

Wong, H. L. (1982). "Diffraction of P, SV, and Rayleigh Waves by Surface Topographies", Bull. Seism. Soc. Am., 72, 1167-1184.

Yerkes, R. F., T. M. McCulloh, J. E. Schoellhamer, and J. G. Vedder (1965). "Geology of the Los Angeles Basin California - An Introduction", Geological Survey Professional Paper, 420-A.

Appendix

In order to specify the matrices $\underset{\sim}{G}$ and and $\underline{f}$ in equation (13) it is convenient to define the following quantities:

Dilatational and shear elastodynamic Green's state vector

$$\underset{\sim}{s}^{d}(\underset{\sim}{r};\underset{\sim}{r}_o) \equiv \begin{bmatrix} u^{d}(\underset{\sim}{r};\underset{\sim}{r}_o) \\ v^{d}(\underset{\sim}{r};\underset{\sim}{r}_o) \\ \sigma^{d}_{nn}(\underset{\sim}{r};\underset{\sim}{r}_o) \\ \sigma^{d}_{nt}(\underset{\sim}{r};\underset{\sim}{r}_o) \end{bmatrix}; \quad \underset{\sim}{s}^{s}(\underset{\sim}{r};\underset{\sim}{r}_o) \equiv \begin{bmatrix} u^{s}(\underset{\sim}{r};\underset{\sim}{r}_o) \\ v^{s}(\underset{\sim}{r};\underset{\sim}{r}_o) \\ \sigma^{s}_{nn}(\underset{\sim}{r};\underset{\sim}{r}_o) \\ \sigma^{s}_{nt}(\underset{\sim}{r};\underset{\sim}{r}_o) \end{bmatrix} \tag{A1}$$

where superscript d(s) denotes dilatational (shear) line load at $\underset{\sim}{r} = \underset{\sim}{r}_o$. It should be emphasized that due to coupling caused by the stress free boundary conditions (eqs. (10a,b)) dilatational lineload at $\underset{\sim}{r}_o$ results in dilatational as well as shear wave field (see Lamb, 1906). Therefore, components of the displacement field $u^{d}(\underset{\sim}{r};\underset{\sim}{r}_o)$ and $v^{d}(\underset{\sim}{r};\underset{\sim}{r}_o)$ in equation (A1) contain contribution from both types of waves. A similar situation occurs for a shear line load at $\underset{\sim}{r}_o$ and corresponding displacement (and stress) field.

Elastodynamic Green's state matrix for domain D_k, k=1,2,...,R of the order $4N_i \times 2M_i$ is defined by

$$\underset{\sim}{S}^{k}_{N_i M_j} \equiv \left[\underset{\sim}{s}^{d}(\underset{\sim}{r}_{n_i};\underset{\sim}{r}_{m_j}), \underset{\sim}{s}^{s}(\underset{\sim}{r}_{n_i};\underset{\sim}{r}_{m_j}) \right] ; \quad \begin{matrix} \underset{\sim}{r}_{n_i} \in C_i ; n_i = 1,2,\ldots,N_i \\ \underset{\sim}{r}_{m_j} \in C_j ; m_j = 1,2,\ldots,M_j \end{matrix} \tag{A2}$$

Similarly

$$\underset{\sim}{S}^{k}_{N_i L_j} \equiv \left[\underset{\sim}{s}^{d}(\underset{\sim}{r}_{n_i};\underset{\sim}{r}_{\ell_j}), \underset{\sim}{s}^{s}(\underset{\sim}{r}_{n_i};\underset{\sim}{r}_{\ell_j}) \right] ; \quad \begin{matrix} \underset{\sim}{r}_{n_i} \in C_i ; n_i = 1,2,\ldots,N_i \\ \underset{\sim}{r}_{\ell_j} \in C^{+}_j ; \ell_j = 1,2,\ldots,L_j \end{matrix} \tag{A3}$$

Then the matrices $\underset{\sim}{G}$ and $\underline{f}$ in equation (13) are defined by

$$\underset{\sim}{G} \equiv \begin{bmatrix} \underset{\sim}{S}^{0}_{N_1 M_1} & -\underset{\sim}{S}^{1}_{N_1 L_1} & -\underset{\sim}{S}^{1}_{N_1 M_2} & \underset{\sim}{0} & \underset{\sim}{0} & \underset{\sim}{0} & \underset{\sim}{0} & \cdots & \underset{\sim}{0} & \underset{\sim}{0} & \underset{\sim}{0} \\ \underset{\sim}{0} & \underset{\sim}{S}^{1}_{N_2 L_1} & \underset{\sim}{S}^{1}_{N_2 M_2} & -\underset{\sim}{S}^{2}_{N_2 L_2} & -\underset{\sim}{S}^{2}_{N_2 M_3} & \underset{\sim}{0} & \underset{\sim}{0} & \cdots & \underset{\sim}{0} & \underset{\sim}{0} & \underset{\sim}{0} \\ \underset{\sim}{0} & \underset{\sim}{0} & \underset{\sim}{0} & \underset{\sim}{S}^{2}_{N_3 L_2} & \underset{\sim}{S}^{2}_{N_3 M_3} & -\underset{\sim}{S}^{3}_{N_3 L_3} & -\underset{\sim}{S}^{3}_{N_3 M_4} & \cdots & \underset{\sim}{0} & \underset{\sim}{0} & \underset{\sim}{0} \\ \vdots & & & & & & \vdots & & \vdots & \vdots & \vdots \\ \underset{\sim}{0} & \cdots & & & & & \cdots \ \underset{\sim}{0} \ \cdots & & \underset{\sim}{S}^{R-1}_{N_R L_{R-1}} & \underset{\sim}{S}^{R-1}_{N_R M_R} & -\underset{\sim}{S}^{R}_{N_R L_R} \end{bmatrix} \tag{A4}$$

$$\underset{\sim}{f} \equiv \begin{bmatrix} -\underset{\sim}{s}^{ff}(\underset{\sim}{r}_1) \\ \vdots \\ -\underset{\sim}{s}^{ff}(\underset{\sim}{r}_{N_1}) \\ \underline{0} \end{bmatrix}, \tag{A5}$$

where the matrix $\underline{G}$ is of the order $4(N_1+\ldots+N_R)$ x $2(M_1+L_1+\ldots+M_R+L_R)$ and the matrix $\underline{f}$ is of the order $4(N_1+\ldots+N_R)$ x 1.

Figure Captions

Fig. 1 Model Geometry

Fig. 2 Surface Displacement Amplitude Spectra for Single Semielliptical Dipping Layer (with the Principal Axis A_1 and B_1)
(a) Incident P-wave: θ_o=10°
(b) Incident P-wave: θ_o=30°
(c) Incident P-wave: θ_o=60°
(If not stated differently Ω=1, N_1=16, M_1=L_1=8, μ_o=1, c_{so}=1, c_{do}=1, μ_1=0.1, c_{s1}=0.5, c_{d1}=1, A_1=2, B_1=1.4)

Fig. 3 Surface Displacement amplitude Spectra for Single Semielliptical Dipping Layer
(a) Incident P-wave: θ_o = 80°
(b) Incident SV-wave: θ_o = 10°
(c) Incident SV-wave: θ_o = 30°

Fig. 4 Surface Displacement Amplitude Spectra for Single Semielliptical Dipping Layer
(a) Incident SV-wave: θ_o = 60°
(b) Incident SV-wave: θ_o = 80°
(c) Incident Rayleigh wave.

Fig. 5 Surface Displacement Amplitude Spectra for Two Semielliptical Dipping Layers (with the principal axis A_1, 3_1, A_2, and B_2)
(a) Incident P-wave: θ_o = 10°
(b) Incident P-wave: θ_o = 30°
(c) Incident P-wave: θ_o = 60°
(If not stated differently Ω=1, N_1=N_2=16, M_1=L_1=M_2=L_2=8, μ_o=1, c_{so}=1, c_{do}=2, μ_1=0.1, c_{s1}=0.5, c_{d1}=1, μ_2=0.01, c_{s2}=0.25, c_{d2}=0.5, A_1=2, B_1=1.4, A_2=1, B_2=0.7).

Fig. 6 Surface Displacement Amplitude Spectra for Two Semielliptical Dipping Layers
(a) Incident P-wave: θ_o = 80°
(b) Incident SV-wave: θ_o = 10°
(c) Incident SV-wave: θ_o = 30°

Fig. 7 Surface Displacement Amplitude Spectra for Two Semielliptical Dipping Layers
(a) Incident SV-wave: θ_o = 60°
(b) Incident SV-wave: θ_o = 80°

(c) Incident Rayleigh wave

Fig. 8 Surface Displacement Amplitude Spectra for Two Semielliptical Dipping Layers
(a) Incident P-wave: $\theta_o = 10°$
(b) Incident P-wave: $\theta_o = 30°$
(c) Incident P-wave: $\theta_o = 60°$
(Ω=0.5)

Fig. 9 Surface Displacement Amplitude Spectra for Two Semielliptical Dipping Layers
(a) Incident P-wave: $\theta_o = 80°$
(b) Incident SV-wave: $\theta_o = 10°$
(c) Incident SV-wave: $\theta_o = 30°$
(Ω=0.5)

Fig. 10 Surface Displacement Amplitude Spectra for Two Semielliptical Dipping Layers
(a) Incident SV-wave: $\theta_o = 60°$
(b) Incident SV-wave: $\theta_o = 80°$
(c) Incident Rayleigh wave
(Ω=0.5)

Fig. 11 Surface Displacement Amplitude Spectra for Two Semielliptical Dipping Layers
(a) Incident P-wave: $\theta_o = 10°$
(b) Incident P-wave: $\theta_o = 30°$
(c) Incident P-wave: $\theta_o = 60°$
(Ω=1, μ_1=0.6, c_{s1}=0.8, c_{d1}=1.6, μ_2=0.3, c_{s2}=0.6, c_{d2}=1.2)

Fig. 12 Surface Displacement Amplitude Spectra for Two Semielliptical Dipping Layers
(a) Incident P-wave: $\theta_o = 80°$
(b) Incident SV-wave: $\theta_o = 10°$
(c) Incident SV-wave: $\theta_o = 30°$
(Ω=1, μ_1=0.6, c_{s1}=0.8, c_{d1}=1.6, μ_2=0.3, c_{s2}=0.6, c_{d2}=1.2)

Fig. 13 Surface Displacement Amplitude Spectra for Two Semielliptical Dipping Layers.
(a) Incident SV-wave: $\theta_o = 60°$
(b) Incident SV-wave: $\theta_o = 80°$
(c) Incident Rayleigh wave
(Ω=1, μ_1=0.6, c_{s1}=0.8, c_{d1}=1.6, μ_2=0.3, c_{s2}=0.6, c_{d2}=1.2)

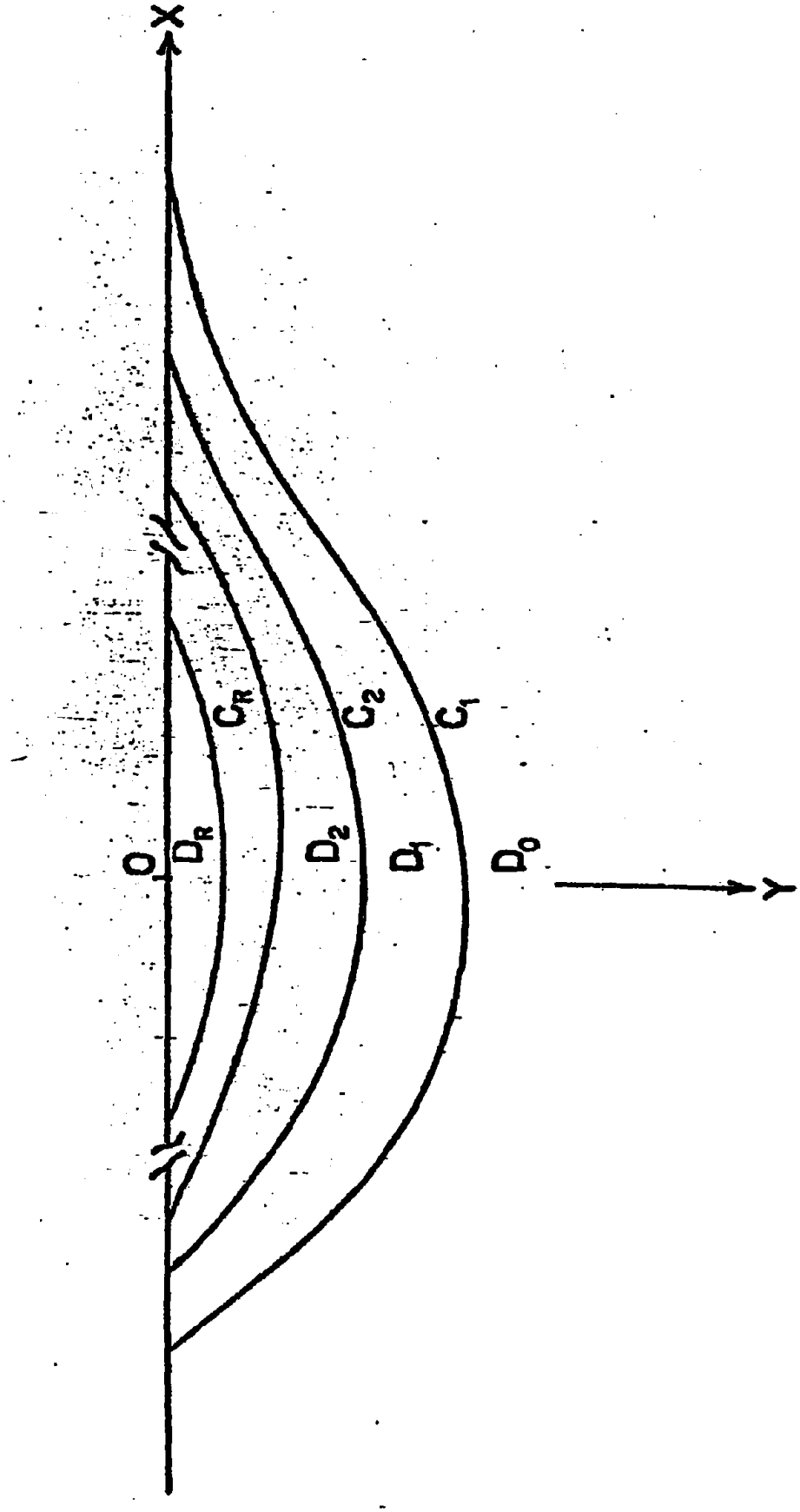

Fig. 1

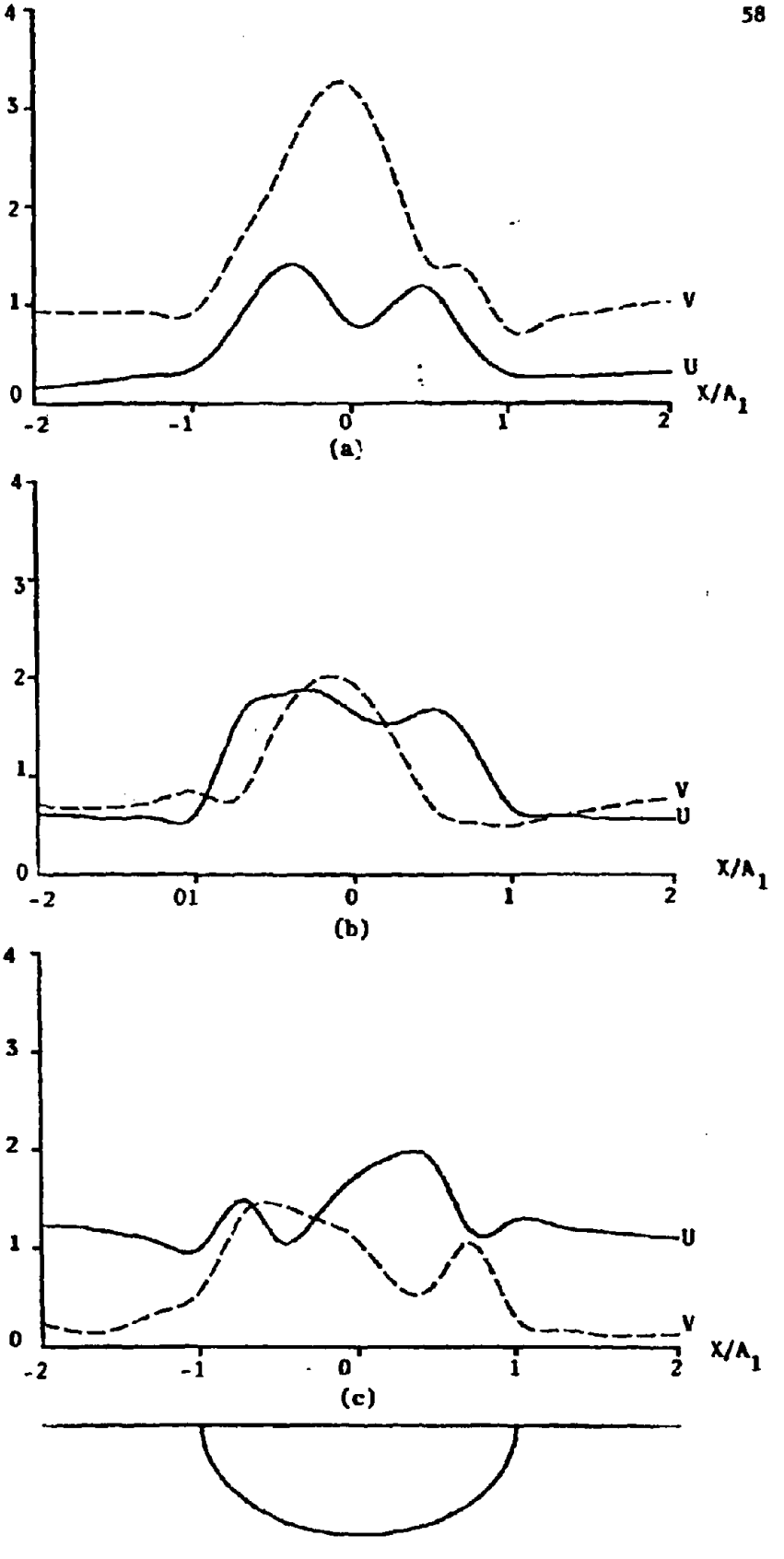
4
3
2
1
0
V
U
X/A1
-2
-1
0
1
2
(a)
4
3
2
1
0
V
U
X/A1
-2
01
0
1
2
(b)
4
3
2
1
0
U
V
X/A1
-2
-1
0
1
2
(c)

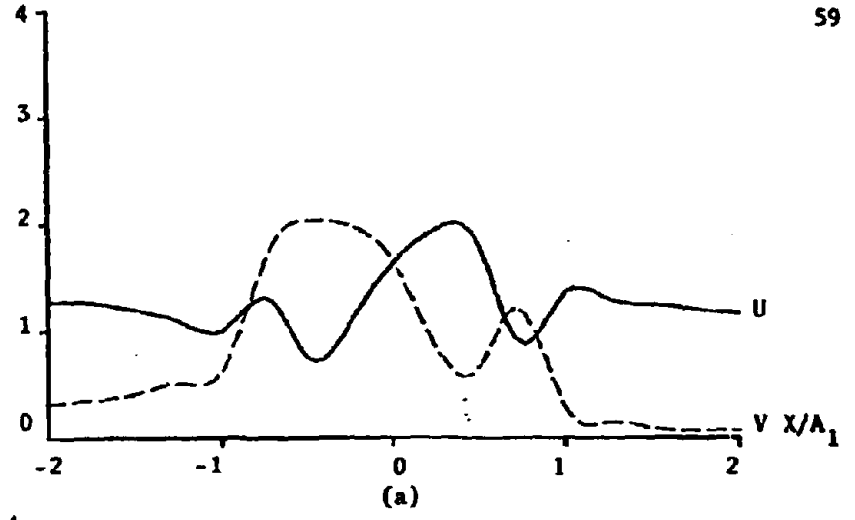

(a)

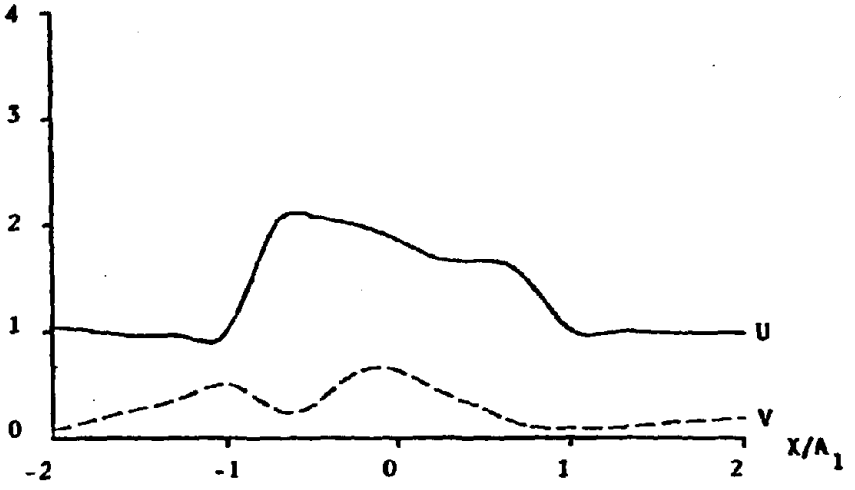

(b)

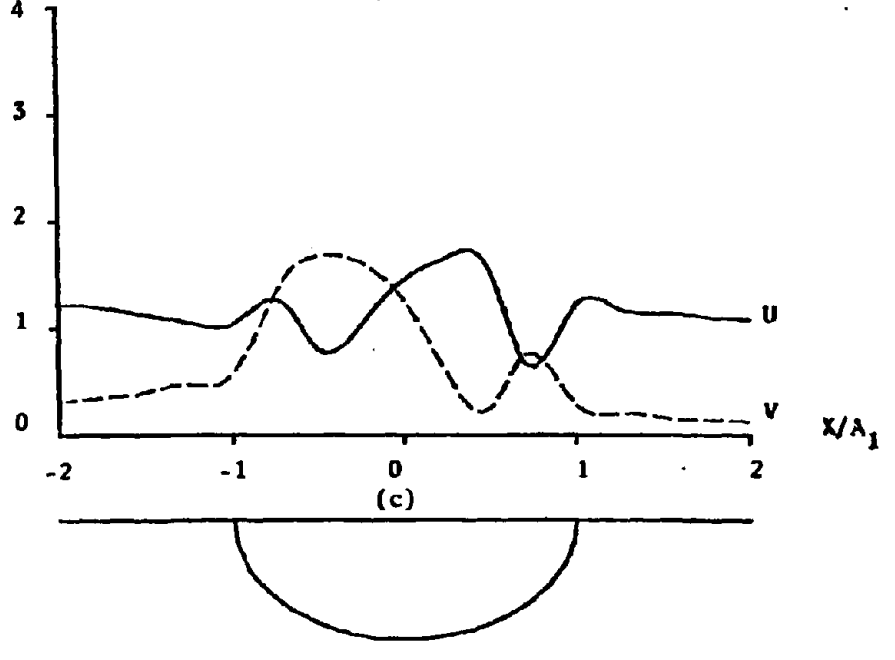

(c)

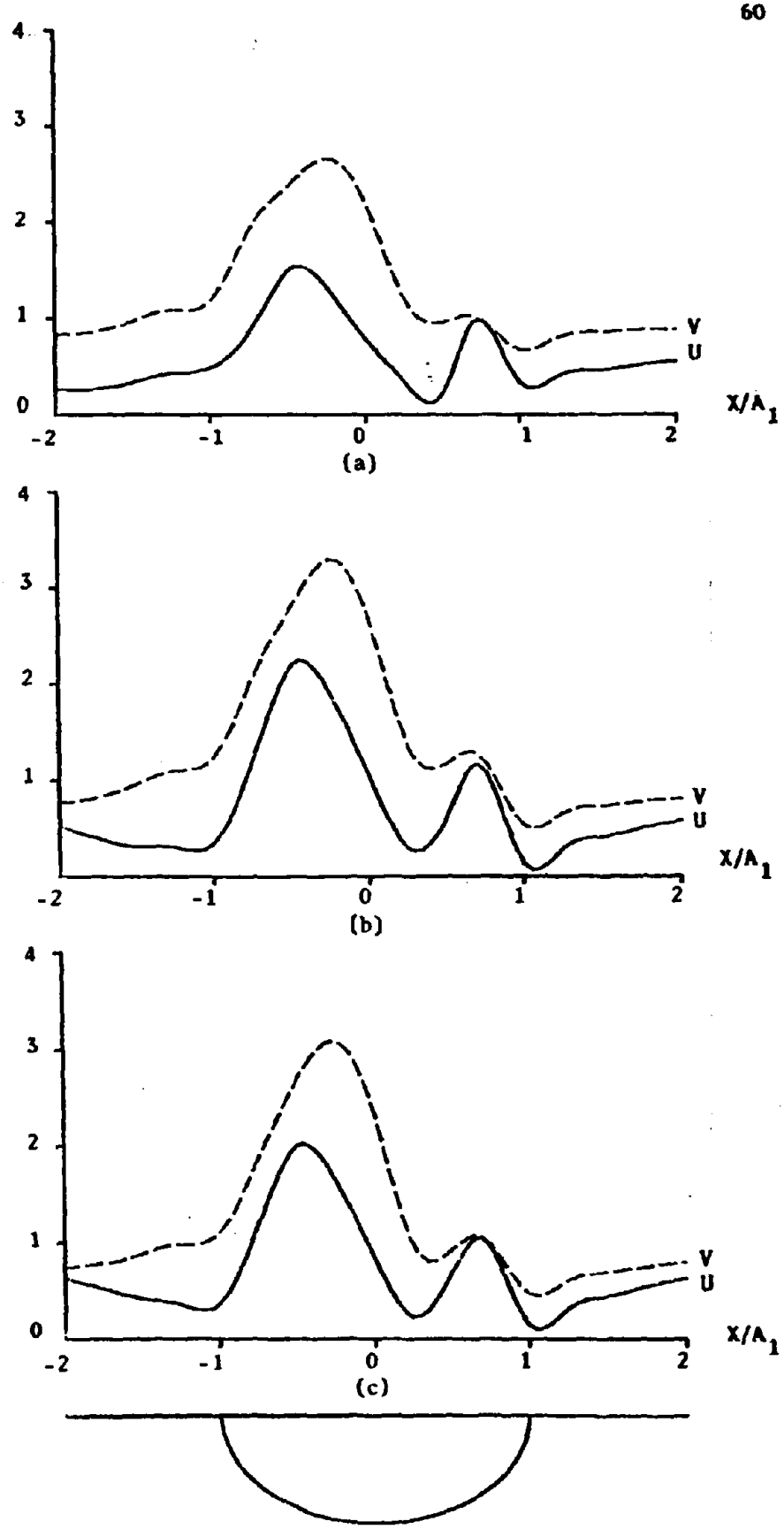
4
3
2
1
0
-2
-1
0
1
2
V
U
X/A1
(a)
4
3
2
1
-2
-1
0
1
2
V
U
X/A1
(b)
4
3
2
1
0
-2
-1
0
1
2
V
U
X/A1
(c)

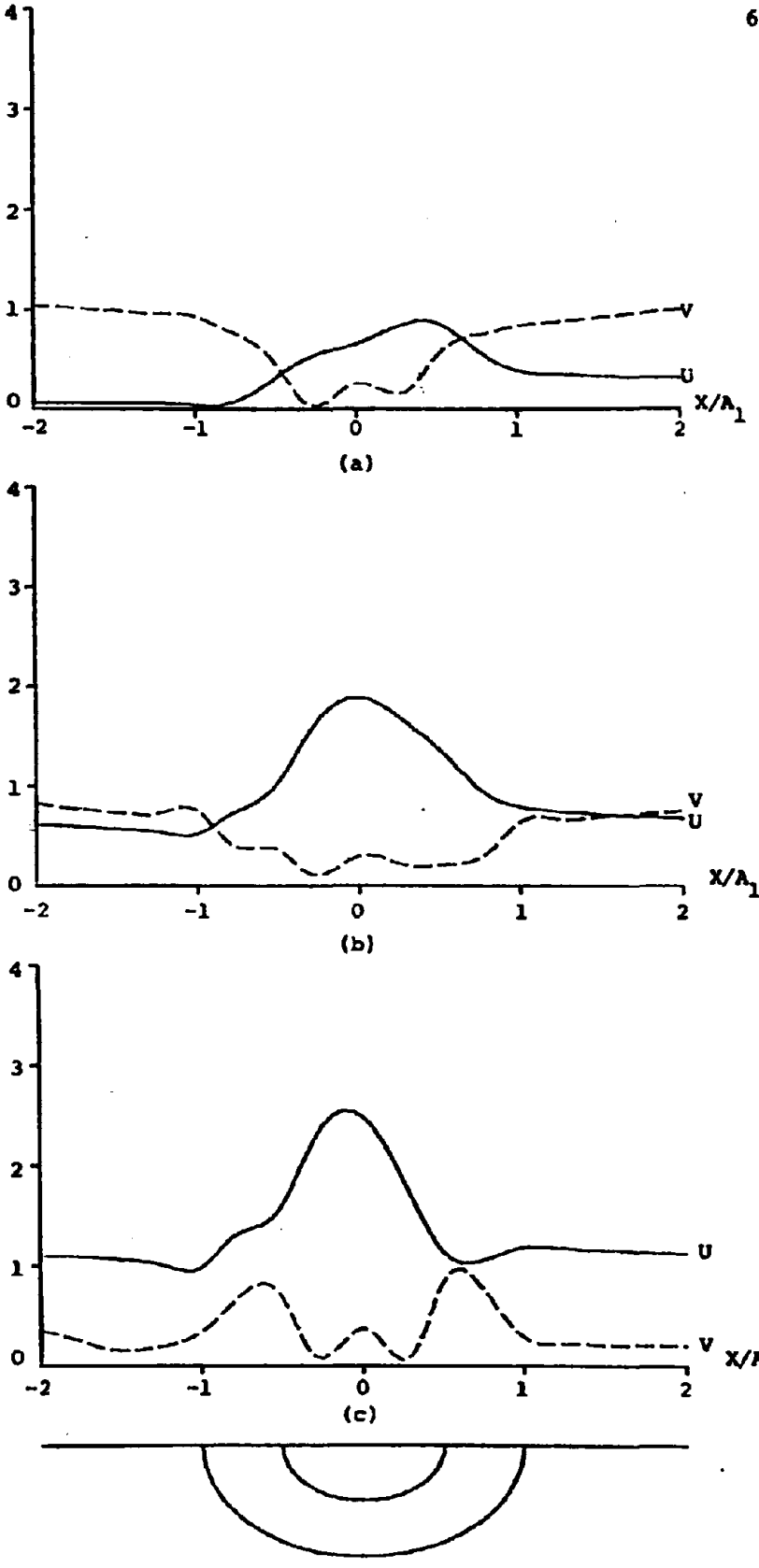
4
3
2
1
0
-2
-1
0
1
2
V
U
X/A1
(a)
4
3
2
1
0
-2
-1
0
1
2
V
U
X/A1
(b)
4
3
2
1
0
-2
-1
0
1
2
U
V
X/A1
(c)

4
3
2
1
0
U
V
X/A1
-2
-1
0
1
2
(a)
4
3
2
1
0
U
V
X/A1
-2
-1
0
1
2
(b)
4
3
2
1
0
U
V
X/A1
-2
-1
0
1
2
(c)

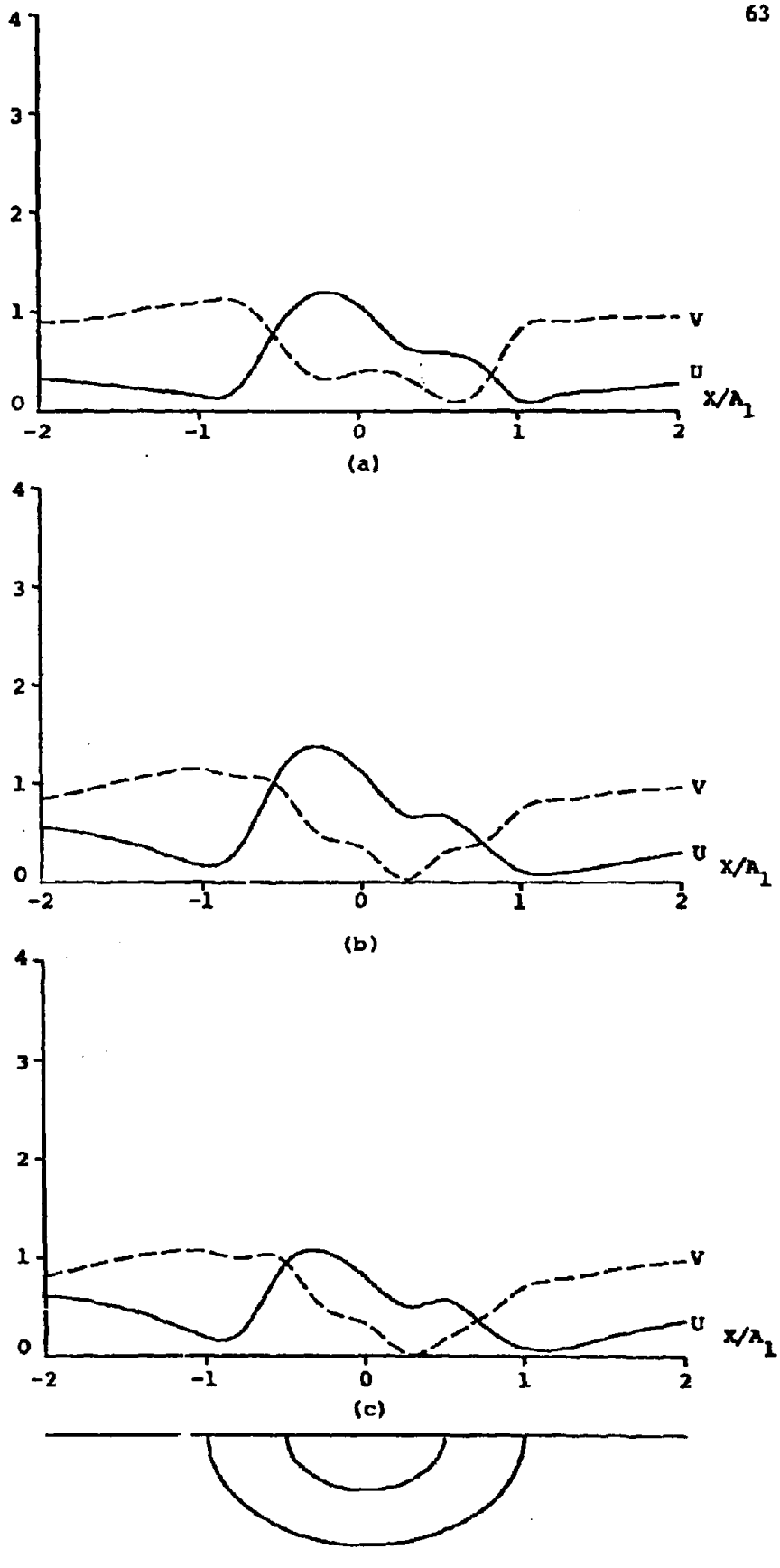
4
3
2
1
0
-2
-1
0
1
2
V
U
X/A1
(a)
4
3
2
1
0
-2
-1
0
1
2
V
U
X/A1
(b)
4
3
2
1
0
-2
-1
0
1
2
V
U
X/A1
(c)

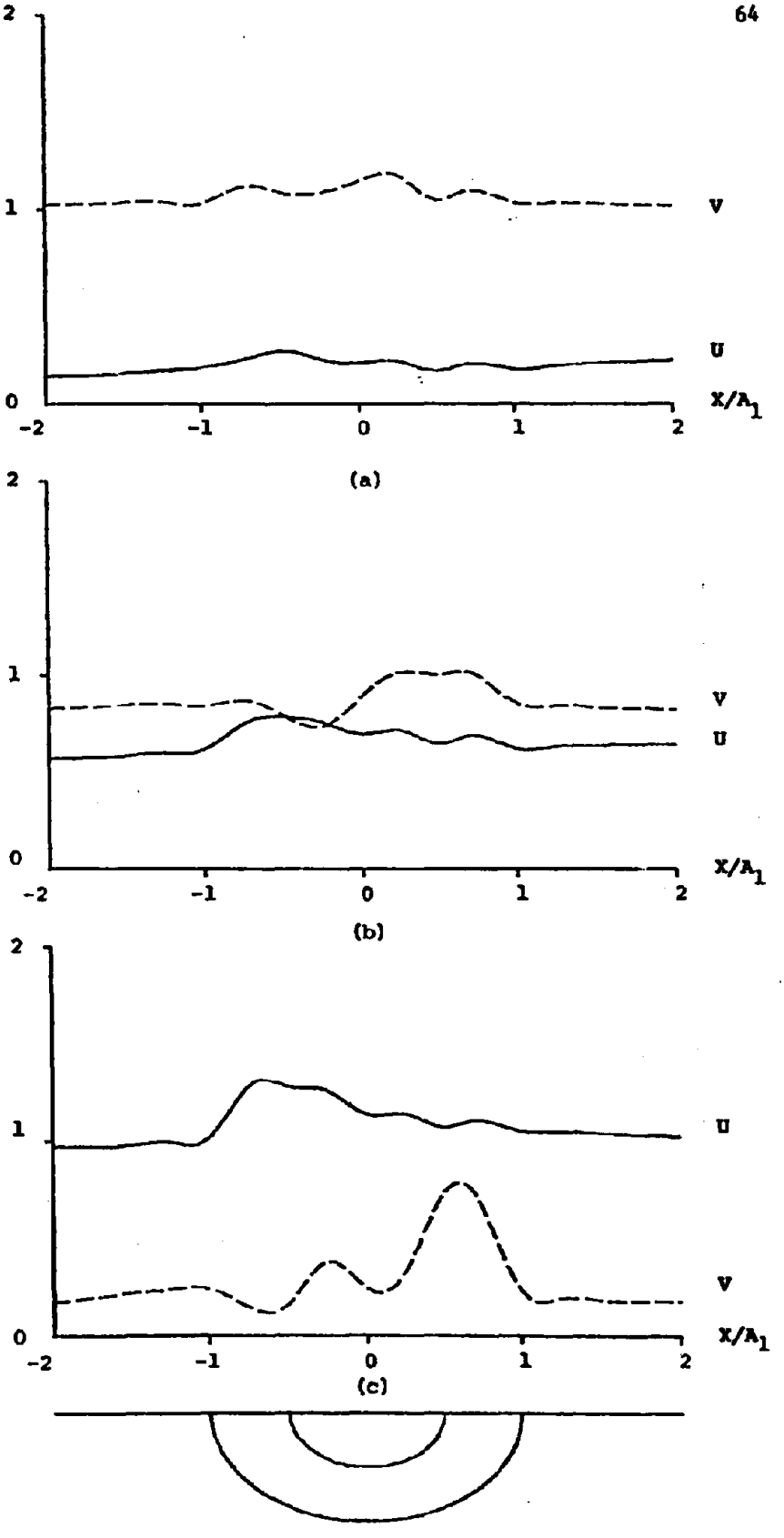
2
1
0
V
U
X/A1
-2
-1
0
1
2
(a)
2
1
0
V
U
X/A1
-2
-1
0
1
2
(b)
2
1
0
U
V
X/A1
-2
-1
0
1
2
(c)

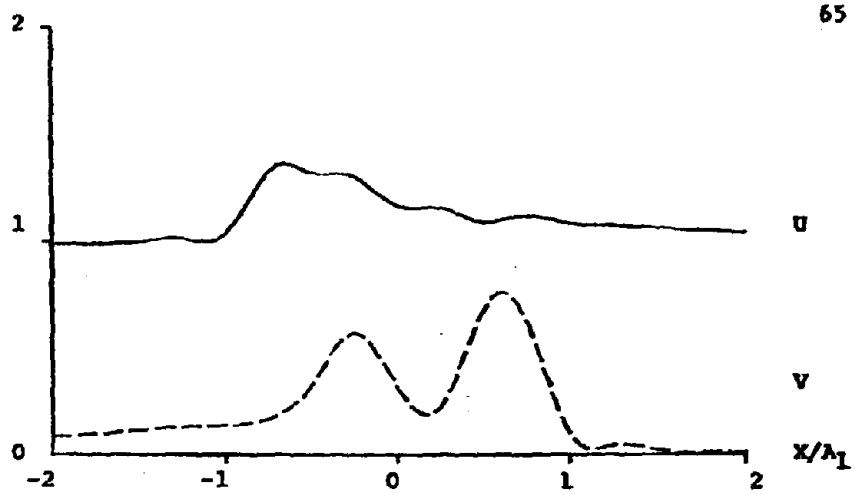

(a)

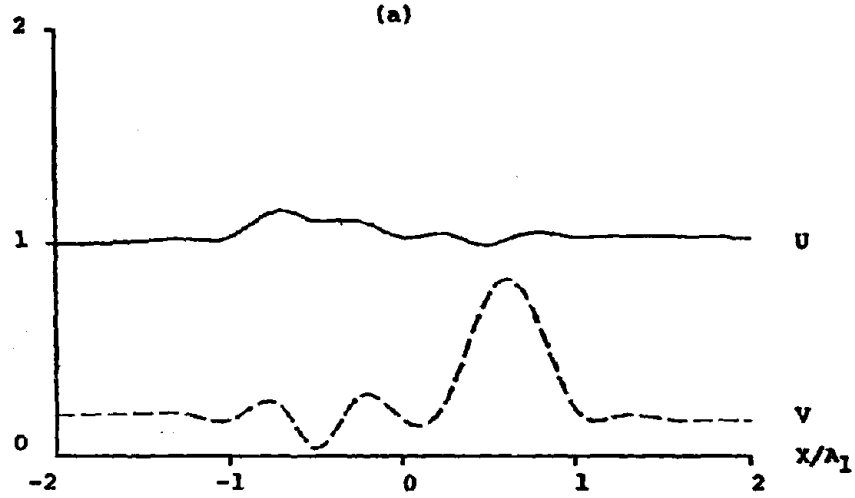

(b)

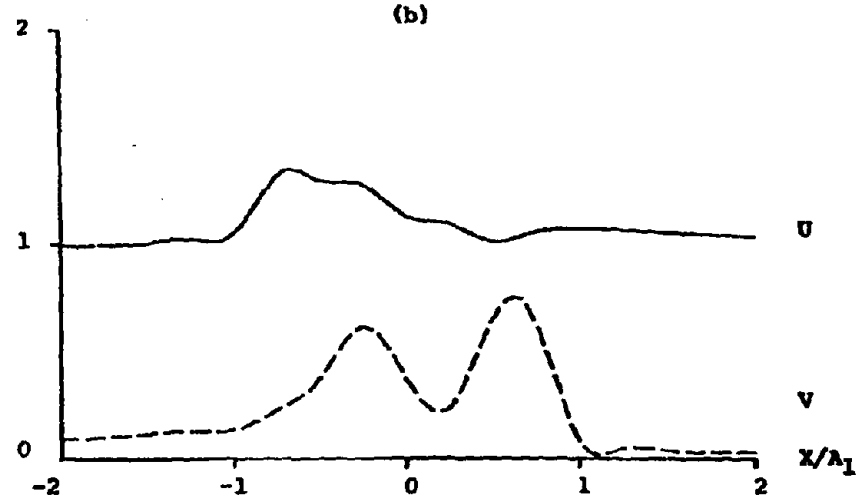

(c)

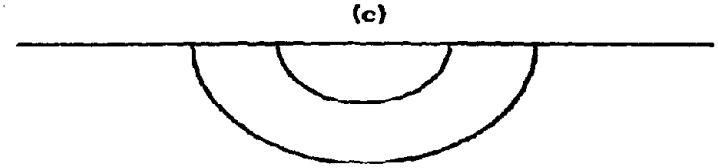

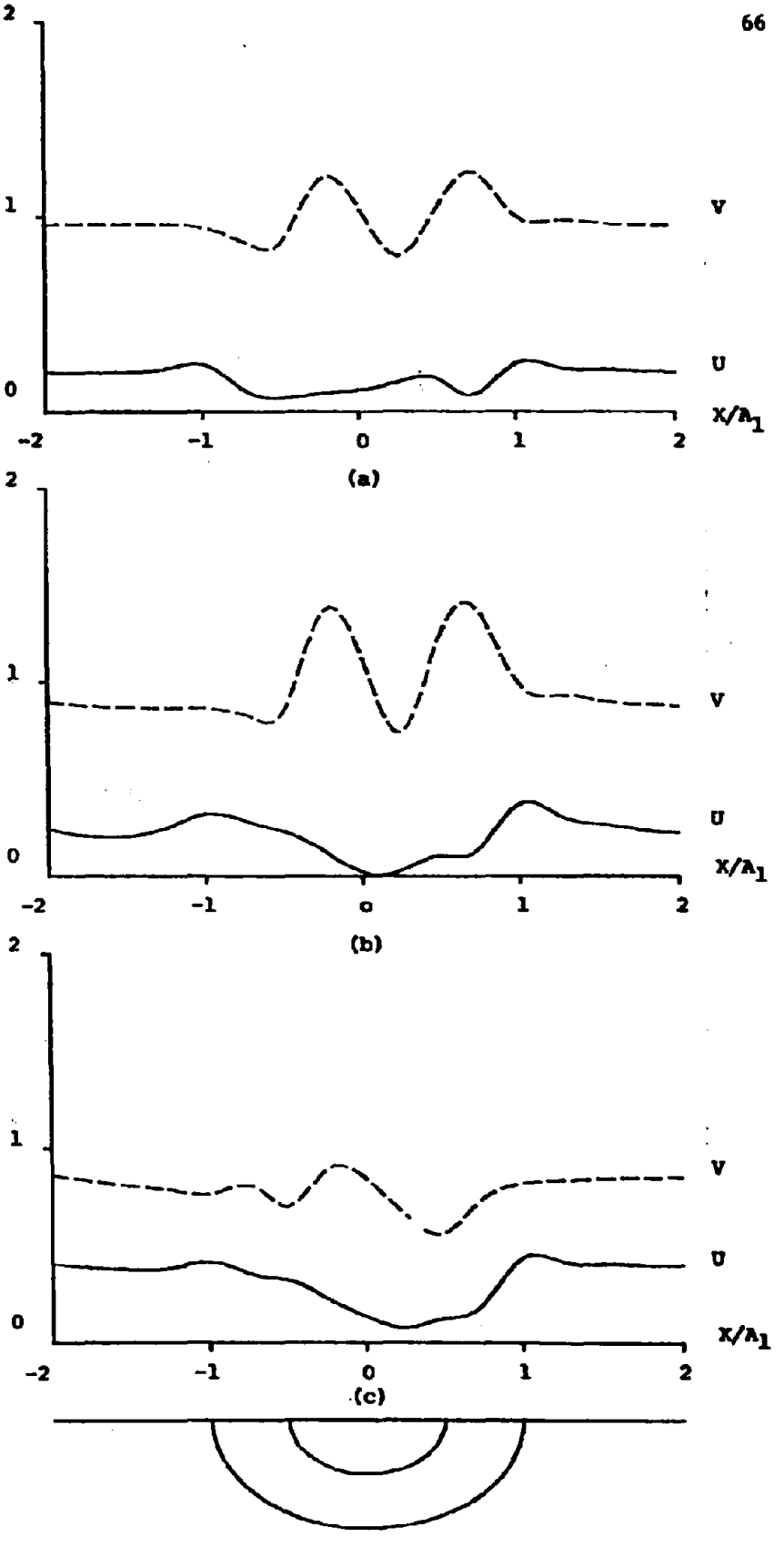
2
1
0
V
U
X/A1
-2
-1
0
1
2
(a)
2
1
0
V
U
X/A1
-2
-1
o
1
2
(b)
2
1
0
V
U
X/A1
-2
-1
0
1
2
(c)

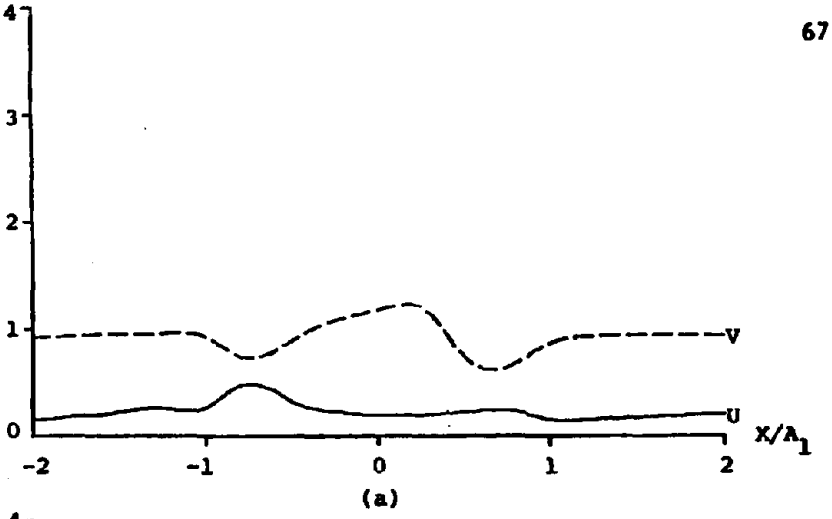

(a)

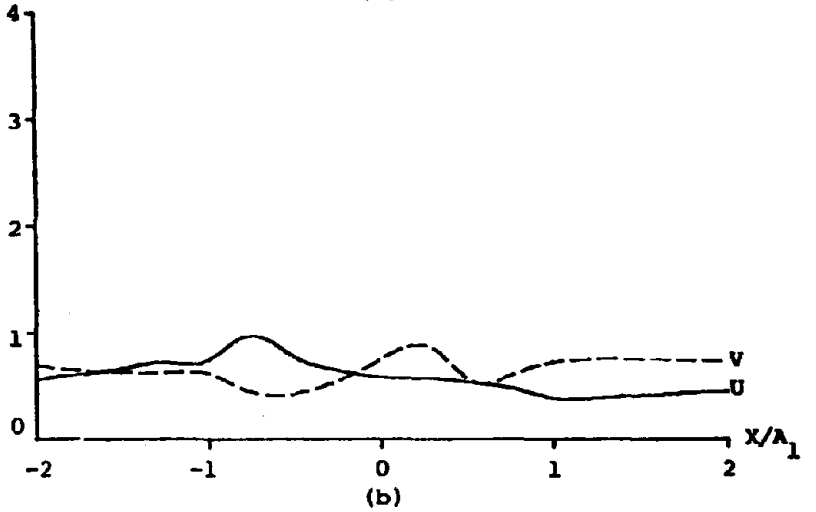

(b)

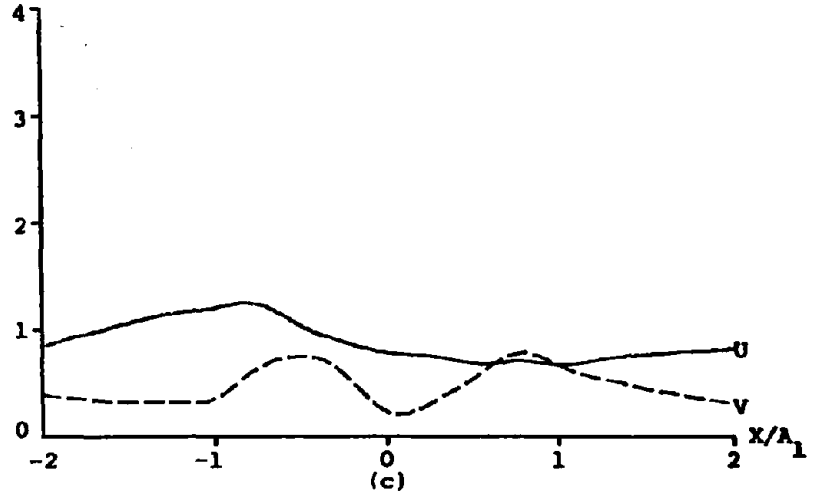

(c)

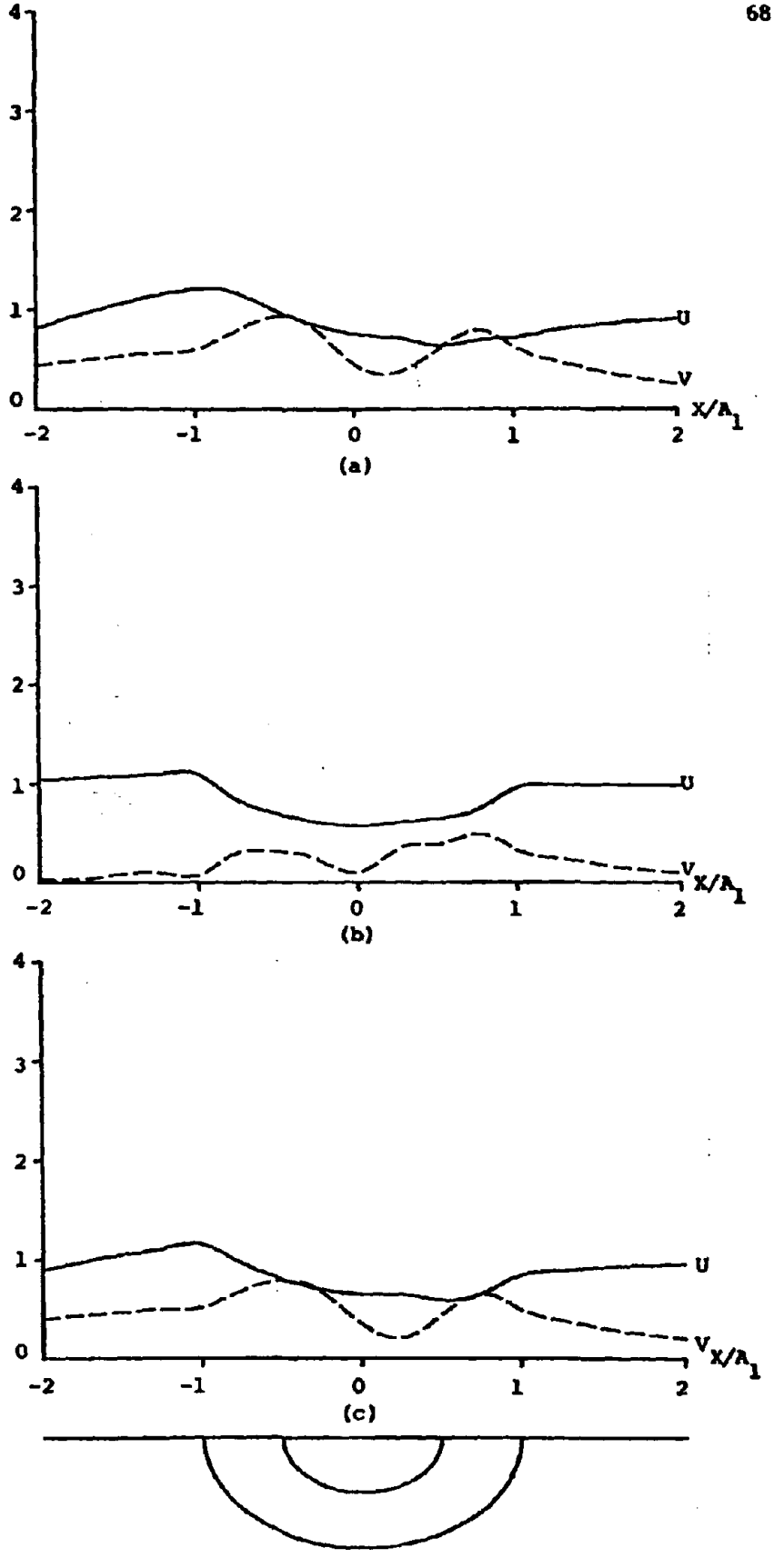
4
3
2
1
0
U
V
X/A1
-2
-1
0
1
2
(a)
4
3
2
1
0
U
V
X/A1
-2
-1
0
1
2
(b)
4
3
2
1
0
U
V
X/A1
-2
-1
0
1
2
(c)

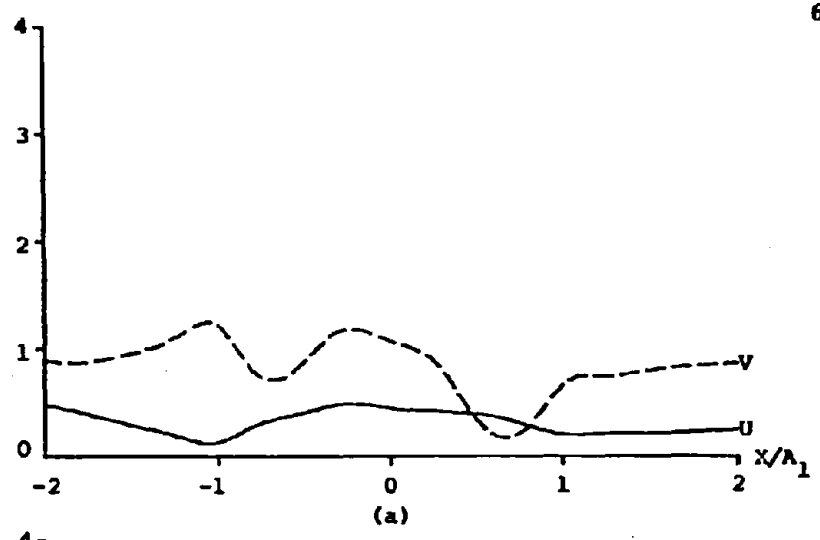

(a)

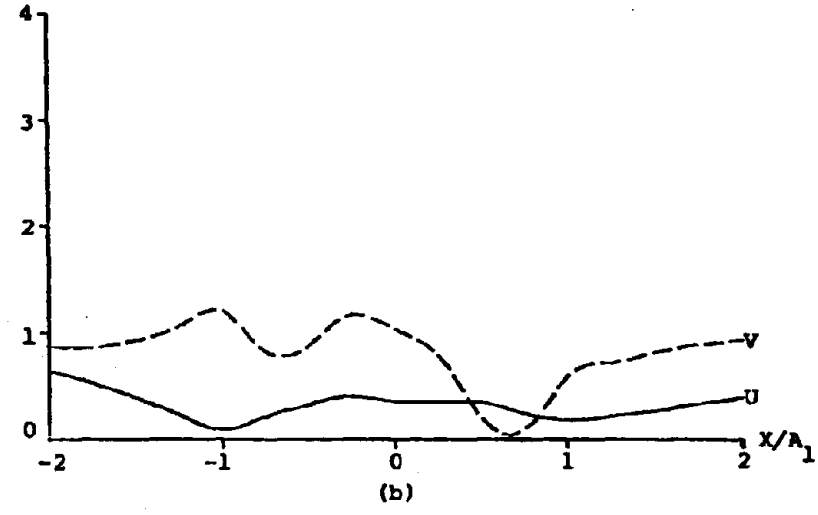

(b)

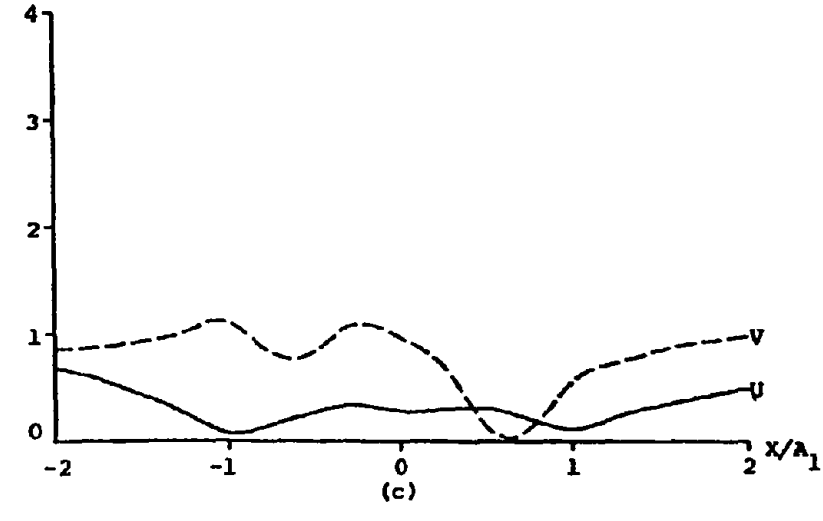

(c)

STRONG GROUND MOTION IN THE LOS ANGELES BASIN: Incident SH Waves*

by

M. Dravinski

Abstract

Amplification of motion caused by diffraction and scattering of a plane harmonic SH-wave by layered medium of the Los Angeles basin is investigated by using an indirect boundary integral equation approach. The basin is modeled as a set of irregular dipping layers embedded into an elastic half-space. The material of the layers is assumed to be homogeneous, isotropic and linearly elastic. Perfect bonding between the layers is understood.

Displacement spectra are evaluated for different cross sections of the basin for a different number of layers and for various incident waves. Numerical results demonstrate that the presence of the dipping layers in the basin may cause very large amplification of the surface ground motion. The motion appears to be very sensitive upon the number and material properties of the layers, frequency and angle of incidence of the incoming wave, and the location of the observation point at the surface of the half-space.

*Submitted for publication.

Introcudtion

The geology of the Los Angeles basin is characterized by great complexity. Still the structure of the basin has been investigated in considerable detail. The study of Yerkes et al. (1965), for example, provided an elaborate account into the thickness of the sediments throughout the basin. The term 'Los Angeles basin' in this paper refers to the structure of the alluvium for Los Angeles and its vicinity, as shown by Fig. 1.

Experimental studies by Hanks (1975) and Wong et al. (1976), for example, established very clearly that the presence of surface and/or subsurface irregularities in the soil medium may have pronounced effect upon the surface strong ground motion. This conclusion is confirmed through further research by Boore (1972), Wong and Jennings (1975), Griffiths and Bollinger (1975), Sanchez-Sesma and Rosenblueth (1979), Sanchez-Sesma and Esquivel (1979), Wong (1982), and Dravinski (1982a).

Study of the seismicity of Southern California by Hileman et al. (1973) indicates that within the area of the Los Angeles basin one should expect about four earthquakes per year of magnitude greater than 3. Since, "there is no evidence to suggest that thus moderate to high seismicity is decreasing" (Anderson et al., 1981) it is of considerable importance a) to develop detailed instrumentation for the monitoring of the seismic activities in the basin and b) to investigate theoretically possible strong ground motion amplification patterns throughout the basin during an earthquake.

The main objective of the present paper is to introduce a rather simple theoretical model for the study of strong ground motion in the Los Angeles basin. This model should be viewed as an introduction to more realistic and thus far more complex models in the future.

Method of Solution

There are basically two methods of analyzing soil amplification problems: 1) Numerical methods and 2) analytical methods, which rely upon the solution of the equations of elastodynamics by analytical means. Complex geology of the Los Angeles basin precludes construction of the closed form analytical solution and one has to analyze the problem by using numerical techniques. Most commonly used numerical methods, finite differences and finite elements require a computational grid to fill the solution domain of the problem model. As a result, these procedures appear to be inefficient for geotechnical problems which involve large dimensions.

Often it is possible to construct a surface integral representation for the solution of the problem. Corresponding integral equations involve only the boundary and initial values. Solution of the integral equations then leads to the solution at any interior point of the problem model under consideration (Cruse and Rizzo, 1968; Cole et al., 1978). Since only the boundary of the model is being discretized, the number of unknowns is significantly reduced where compared to the finite element or finite difference procedures. For a detailed review of these methods, known as the boundary integral equations methods, (BIEM) the reader is referred to a paper by Brebbia (1981).

Indirect BIEM used in the present paper originates in the works of Kupradze (1963), Copley (1967) and Oshaki (1973). Extension of the method to wave propagation problems in geophysics and earthquake engineering is due to Sanchez-Sesma and Rosenblueth (1979), Sanchez-Sesma and Esquivel (1979), Apsel (1979), Dravinski (1982a,b) and Wong (1982). Recently, the author extended the indirect BIEM to the problems involving dipping layers

of arbitrary shape (Dravinski, 1983). Therefore, the present work is an application of the method to the problem of strong ground motion of the Los Angeles basin.

Solution of Problem

For the problem geometry present by Fig. 2 a brief review of the method of solution is presented next. Spatial domain of each layer is denoted by D_j, j=0,1,2,...,R, where subscripts 0,1,2,...,R refer to the half-space, the first layer, ..., and the R-th layer, respectively. Interfaces between the layers are denoted by C_i, i=1,2,..., R.

Since the problem model is assumed to be of the antiplane strain-type the equation of motion for steady state waves is defined by

$$(\nabla^2 + k_j^2)w_j(x,y,\omega) = 0 \quad ; \quad j=0,1,2,\ldots,R \quad ; \quad \nabla^2 \equiv \frac{\partial^2}{\partial x^2} + \frac{\partial^2}{\partial y^2}, \tag{1}$$

where w represents the only non-zero component of the displacement field acting along the z-axis, k is the wave number, and ω denotes the circular frequency. Solution of the problem must satisfy stress free boundary conditions along the surface of the half-space, continuity of stress and displacement field along the interfaces C_i,i=1,2,...,R, and appropriate radiation condition at infinity.

The incident field is assumed of the form

$$w^{inc} = \exp\left[-ik_o(x\sin\theta_o + y\cos\theta_o) + i\omega t\right]; \; i = \sqrt{-1} \tag{2}$$

where θ_o represents the angle of incidence.

The total wave field in the elastic medium can be described as (Dravinski, 1983)

$$w_o = w^{ff} + w_o^s \quad ; \quad \underline{r} \in D_o \tag{3a}$$

$$w_j = w_j^s \quad ; \quad \underline{r} \in D_j \; ; \; j=1,2,\ldots,R, \tag{3b}$$

where superscripts ff and s denote the free and scattered wave field, respectively. The unknown scattered waves are determined to be

$$w_o^s(\underline{r}) = a_{m_1}^o G_o(\underline{r};\underline{r}_{m_1}) \; ; \; \underline{r} \in D_o \; ; \; \underline{r}_{m_1} \in C_1^- \; ; \; m_1=1,2,\ldots,M_1 \; ; \tag{4a}$$

$$w_i^s(\underline{r}) = b_{\ell_i}^i G_i(\underline{r};\underline{r}_{\ell_i}) + a_{m_{i+1}}^i G_i(r;r_{m_{i+1}}) \; ; \tag{4b}$$

$$\underline{r}_i \in D_i \; , \; i=1,2,\ldots,R-1$$
$$\ell_i=1,2,\ldots,L_i$$
$$m_i=1,2,\ldots,M_i$$
$$\underline{r}_{\ell_i} \in C_i^+ \; ; \; \underline{r}_{m_i} \in C_i^-$$

$$w_R^s(\underline{r}) = b_{\ell_R}^R G_R(\underline{r};\underline{r}_{\ell_R}) \; ; \; \underline{r} \in D_R \; ; \; \underline{r}_{\ell_R} \in C_R^+, \tag{4c}$$

where summation over repeated subscripts is assumed. The summation convention is suppressed for repeated indices if one index is a superscript and the other one is a subscript. Subscripted indices, such as ℓ_i and m_i, should be viewed as simple indexes ℓ and m, respectively. In equations (4a-c) G denotes the Green's function for a line load in a half-space and N_i, M_i, and L_i, i=1,...,R denote the orders of approximation of the solution. Therefore, the scattered wave field is represented in terms of the finite number of descrete line sources. The auxiliary surfaces C_i^{+-}, i=1,2,...,R and the location of sources is assumed, while the source intensities a's and b's are calculated in the mean-square-sense from the continuity condition of displacement and stress fields along the interfaces between the layers (Dravinski, 1983).

Evaluation of Results

Surface displacement spectras have been evaluated numerically for two sections of the Los Angeles basin. The sections ABCD and EFG are depicted by Fig. 1. Geology of these sections was investigated in considerable detail by Yerkes et al. (1965). For the sake of simplification it is assumed that each cross-section has been rectified into a straight plane.

For numerical evaluation of the results all variables are presented in dimensionless form. For that purpose the wave velocity β_o and the shear modulus μ_o are chosen to be equal unity. All distances are normalized in such a way that one unit length corresponds to two kilometers of the basin and surface displacement amplitude is normalized with respect to the amplitude of the surface free-field motion. For convenience, a dimensionless frequency Ω is introduced as the ratio of the total length of the first dipping layer and the wavelength of the incident field.

Each interface $C_i, i=1,2,\ldots,R$ is defined by N_i collocation points through which a normalized cubic B-splin approximation is determined.. This procedure permitted construction of an algorithm applicable to a wide range of interface shapes including the ones associated with the sections ABCD and EFG of the Los Angeles basin.

Results depicted by Figs. 3a,b correspond to the amplitude of the surface displacement spectra for cross section ABCD, modeled as a set of three dipping layers embedded into an elastic half-space. Several conclusions are apparent from analysis of the Figs. 3a,b: a) The presence of dipping layers may cause very large strong ground motion amplification effects, b) Surface ground motion amplification may change greatly within a very short distance, and c) Ground motion appears to be very sensitive

upon the angle of incidence of the incoming wave.

Observations from some recent earthquakes (Jennings, 1971) indicate that the areas of damage can be highly localized. It has been noted that the intensity of ground shaking can change significantly within a short distance (Hudson, 1972). The results presented by Figs. 3a,b clearly confirm these field observations.

An increase in the frequency of the incident field resulted in surface ground motion shown by Figs. 4a,b. Comparison of Figs. 3a,b with Figs. 4a,b incidate great sensitivity of the surface ground motion amplification pattern upon the frequency of the incident wave field. If one views the ground motion amplification as a result of interference between the incident and the scattered wave field, it is obvious from the presented results that the frequency of the incident wave affects that interference greatly. The interference may be constructive or destructive thus resulting in amplification or reduction of the surface ground motion. This phenomenon of local amplification (reduction) of the surface motion is very clearly displayed in Figs. 3a,b and 4a,b. The change in material properties of the layers appears to be a very important parameter for resulting surface strong ground motion of the basin. Results of Figs. 5a,b correspond to the same incident wave and geometry of the layers as in the case of results depicted by Figs. 3a,b. The change in material properties of the layers caused a very different surface ground motion amplification pattern. This is an indication that inaccuracy in the material properties of the subsurface irregularities will reflect very strongly upon the resulting surface motion.

For a cross section EFG of the Los Angeles basin (see Fig. 1) the surface strong ground motion is depicted by Figs. 6a,b. As in the

case of the section ABCD the model incorporates three dipping layers embedded into an elastic half-space. Earlier studies of strong ground motion amplification effects due to subsurface irregularities (Dravinski, 1982) demonstrated that the surface motion is sensitive upon the embeddment depth of the irregularity. Consequently, except in one case (Fig. 7), in each cross section of the basin studied in the present paper, the interface C_1 (between the half-space and the first layer) is taken as the deepest one available from the field measurements of the sediment depth (Yerkes et al., 1965). Although the wavelength of the incident field and the material properties of the layers is the same as for the section ABCD (see Figs. 4a,b) different geometry of the dipping layers caused a very different ground motion response. (Note, the dimensionless frequency changed from that in Figs. 4a,b since the width of the layers is different.) Thus, geometry of the dipping layers appears to be very important in the resulting surface motion of the soil medium.

If more detailed modeling of the subsurface geology is required this can be accomplished by incorporating more details into the model. As an illustration of that procedure applied to the section EFG of the Los Angeles basin the surface displacement is evaluated for the substructure shown by Fig. 7. A characteristic of this model is that the second layer contains not one but two dipping layers defined by the interfaces C_{31} and C_{32}. Interfaces C_1 and C_2which define the first dipping layer are of the same character as in the previous models. The scattered wave field in the layers is then specified by

$$w_o^s(\underline{r}) = \sum_{m_1} a_{m_1}^o G_o(\underline{r};\underline{r}_{m_1}) \; ; \; \underline{r} \in D_o \; ; \; \underline{r}_{m_1} \in C_1^- \; ; \; m_1=1,2,\ldots,M_1 \qquad (5a)$$

$$w_1^s(\underline{r}) = b^1_{\ell_1} G_1(\underline{r};\underline{r}_{\ell_1}) + a^1_{m_2} G_1(\underline{r};\underline{r}_{m_2}) \; ; \; \underline{r} \in D_1 \; ; \; \underline{r}_{\ell_1} = C_1^+ \; ; \; \underline{r}_{m_2} \in C_2^- \tag{5b}$$

$$\ell_1=1,2,\ldots,L_1 \; ; \; m_2=1,2,\ldots,M_2$$

$$w_2^s(\underline{r}) = b^2_{\ell_2} G_2(\underline{r};\underline{r}_{\ell_2}) + a^2_{m_{31}} G_2(\underline{r};\underline{r}_{m_{31}}) + a^2_{m_{32}} G_2(\underline{r};\underline{r}_{m_{32}});$$

$$\underline{r} = D_2 \; ; \; \underline{r}_{\ell_2} \in C_2^+ \; ; \; \underline{r}_{m_{31}} \in C_{31}^-$$

$$\underline{r}_{m_{32}} \in C_{32}^- \; ; \; m_{31}=1,2,\ldots,M_{31}$$

$$m_{32}=1,2,\ldots,M_{32} \tag{5c}$$

$$w_{31}^s(\underline{r}) = b^{31}_{\ell_{31}} G_{31}(\underline{r};\underline{r}_{\ell_{31}}) \; ; \; \underline{r} \in D_{31} \; ; \; \underline{r}_{\ell_{31}} \in C_{31}^+ \; ; \; \ell_{31}=1,2,\ldots,L_{31} \tag{5d}$$

$$w_{32}^s(\underline{r}) = b^{32}_{\ell_{32}} G_{32}(\underline{r};\underline{r}_{\ell_{32}}) \; ; \; \underline{r} \in D_{32} \; ; \; \underline{r}_{\ell_{32}} \in C_{32}^+ \; ; \; \ell_{32}=1,2,\ldots,L_{32}, \tag{5e}$$

where the summation convention over repeated indices is understood. Again the auxiliary surfaces C_i^{+-}, i=1,2,31, and 32 and the location of sources are assumed and the unknown source intensities a's and b's are calculated in the mean-square-sense through use of the continuity of the displacement and stress field along each of the interface between the layers.

Although very simple, the method of solution is not without difficulties. Namely, the location of sources along the auxiliary surfaces must be chosen very carefully to obtain accurate results. For this reason, an extensive testing of the indirect BIEM has been done (Dravinski 1982a,b; Wong, 1982). It was found that the auxiliary surfaces C_i^{+-} should not be placed in the immediate vicinity of the corresponding interface C_i. In the present paper the auxiliary surfaces C_i^+ and C_i^- are obtained by scaling the corresponding interface C_i by a factor of 2 and 1/2, respectively. The order of approximation of the solution (N_i,M_i, L_i, i=1,2,...,R in equations (4a-c) and (5a-3)) is chosen in such a way that their increase in value

produced practically no change in the resulting displacement field. Testing of the program codes is done in the following way: The material properties and shape of the layers are assumed so that the problem reduces to ground motion amplification due to a semielliptical alluvial valley. In all cases the exact results of Wong and Trifunac (1974) are recovered.

Comparison of Figs. 6a and 7 indicate similarities in the response for the same section modeled with a different number of layers and subjected to the incident wave of the same wavelength. A very strong reduction of the motion atop the soft layers is observed in both cases. From Fig. 7 one can observe ahead of the illuminated side of the layers a very rapid change from essentially free-field motion to the motion modified locally by the presence of the scattered wave field. However, this is the case for a particular set of physical parameters chosen in the problem. Presented results indicate that a change in the frequency of the incident wave may result in a very different surface displacement amplification pattern.

Summary and Conclusions

Surface displacement spectral amplitude is calculated for two characteristic cross sections of the Los Angeles basin using an indirect boundary integral equation approach. Numerical results indicate that the presence of dipping layers may cause locally very large ground motion amplification effects at the surface of the half-space. The amplification appears to be very sensitive upon frequency and angle of incidence of the incoming wave. The surface ground motion is strongly dependent upon the number, geometry and the material properties of the layers. Thus, detailed information about the subsurface geology of the basin is required in order to evaluate surface motion accurately.

Presented results confirm field observation from some recent earthquakes that the area of intense ground shaking can be highly localized and that it may change significantly within a short distance.

Acknoweledgement

This research has been supported by a grant (CEE-81-19696) from the National Science Foundation.

References

Anderson, J.G., Trifunac, M.D., Teng, T.L., Ancini, A. and Moslem, K. (1981). "Los Angeles Vicinity Strong Motion Accelerograph Network," Report No. CE 81-04, Dept. of Civil Engng., Univ. Southern Calif.

Apsel, R.J. (1979). "Dynamic Green's Functions for Layered Media and Applications to Boundary Value Problems," Ph.D. Thesis, U.C. San Diego.

Boore, D.M. (1972). "A Note on the Effect of Simple Topography on Seismic SH-Waves," Bull. Seism. Soc. Amer., 62, 275-284.

Brebbie, C.A. (1981). "Introductory Remarks," Boundary Element Methods, Proceedings of the Third International Seminar, Irvine, California, July 1981, Editor C.A. Brebbie, CML Publications, Springer-Verlag, New York.

Cole, D.M., Kosloff, D.D. and Minster, J.B. (1978). "A Numerical Boundary Integral Equation Method for Elastodynamics. I," Bull. Seism. Soc. Amer., 68, pp. 1331-1357.

Copley, L.A. (1967). "Integral Equation Method for Radiation from Vibrating Surfaces," J. Acoust. Soc. Amer., 41, pp. 807-816.

Cruise, T.A. and Rizzo, F.J (1968). "A Direct Formulation and Numerical Solution of the General Transient Elastodynamic Problem. I," J. Math. Applic., 22, pp. 224-259.

Dravinski, M. (1982a). "Scattering of SH-Waves by Subsurface Topography," ASCE, J. Eng. Mech. Div., 108, No. EM1, pp. 1-17.

Dravinski, M. (1982b) "Influence of Interface Depth Upon Strong Ground Motion," Bull. Seism. Soc. Amer., 72, No. 2, pp. 597-614.

Dravinski, M. (1983). "Scattering of Plane Harmonic SH-Waves by Dipping Layers of Arbitrary Shape," Bull. Seism. Soc. Amer., 73, pp.

Griffiths, D.W. and Bollinger, G.A. (1979). "The Effect of Appalachian Mountain Topography on Seismic Waves," Bull. Seism. Soc. Amer., 69, 1081.

Hanks, T. (1975). "Strong Ground Motion in the San Fernando, California Earthquake: Ground Displacements," Bull. Seism. Soc. Amer., 65, 193-226.

Hileman, J.A., Allen, C.R. and Nordquist, J.M. (1973). 'Seismicity of the Southern California Region', 1 February 1932 to 31 December 1972, Seismological Laboratory, California Institute of Technology, Pasadena, California.

Hudson, D.E. (1972). "Local Distribution of Strong Earthquake Ground Motions," Bull. Seism. Soc. Amer., 62, pp. 1765-1786.

Jennings, P.C. (ed.) (1971). "San Fernando Earthquake of February 9, 1971," EERL-71-02, Calif. Inst. Tech., Pasadena, California.

Kupradze, V.D. (1963). "Dynamical Problems in Elasticity," Progress in Solid Mechanics, Vol. 3, Editors I.N. Sneddon and R. Hill, North Holland, Amsterdam.

Sanchez-Sesma, F.J. and Esquivel, J.A. (1979). "Ground Motion on Alluvial Valley Under Incident Plane SH Waves," Bull. Seism. Soc. Amer., 69, pp. 1107-1120.

Sanchez-Sesma, F.J. and Rosenblueth, E. (1979). "Ground Motions at Canyons of Arbitrary Shape Under Incident SH-Waves," Earthquake Engng. Struct. Dyn., 7, pp. 441-450.

Wong, H.L., and Trifunac, M.D. (1974). "Surface Motion of a Semi-Elliptical Alluvial Valley for Incident Plane SH Waves," Bull. Seism. Soc. Amer., 64, pp. 1389-1408.

Wong, H.L. and Jennings, P.C. (1975). "Effect of Canyon Topography on Strong Ground Motion," Bull. Seism. Soc. Amer. 65, 1239-1257.

Wong, H.L., Trifunac, M.D. and Westermo, B.D. (1976). "Effects of Surface and Subsurface Irregularities on the Amplitudes of Monochromatic Waves," Bull. Seism. Soc. Amer., 67, No. 2, 353-368.

Wong, H.L. (1982). "Diffraction of P, SV, and Rayleigh Waves by Surface Topographies, "Bull. Seism. Soc. Amer., 72, pp. 1167-1184.

Yerkes, R.F., McCulloh, T.H., Schoellhamer, J.E. and Vedder, J.A. (1965). "Geology of the Los Angeles Basin California - an Introduction," Geological Survey Professional Paper, 420-A.

Figure Captions

Fig. 1 Alluvium thickness in the Los Angeles Basin (after Yerkes et al., 1965)

Fig. 2 Theoretical Model

Fig. 3a,b Normalized surface displacement spectral amplitude: Section A-B-C-D.. (For all the results $\mu_o = \beta_o = 1$. $\Omega = 2.59$, $N_1 = 40$, $N_2 = 33$, $N_3 = 31$, $M_1 = L_1 = 20$, $M_2 = L_2 = M_3 = L_3 = 16$, $\mu_1 = 0.6$, $\beta_1 = 0.8$, $\mu_2 = 0.2$, $\beta_2 = 0.6$, $\mu_3 = 0.1$, $\beta_3 = 0.4$)

Fig. 4a,b Normalized surface displacement spectral amplitude: Section A-B-C-D. ($\Omega = 5.18$, $N_1 = 40$, $N_2 = 33$, $N_3 = 31$, $M_1 = L_1 = 20$; $M_2 = L_2$ $M_3 = L_3 = 16$, $\mu_1 = 0.6$, $\beta_1 = 0.8$, $\mu_2 = 0.2$, $\beta_2 = 0.6$, $\mu_3 = 0.1$, $\beta_3 = 0.4$)

Fig. 5a,b Normalized surface displacement spectral amplitude: Section A-B-C-D. ($\Omega = 2.59$, $N_1 = 40$, $N_2 = 33$, $N_3 = 31$, $M_1 = L_1 = 20$; $M_2 = L_2 = M_3 = L_3 = 16$, $\mu_1 = 0.8$, $\beta_1 = 0.9$; $\mu_2 = 0.6$, $\beta_2 = 0.8$, $\mu_3 = 0.4$, $\beta_3 = 0.7$)

Fig. 6a,b Normalized surface displacement spectral amplitude: Section E-F-G.. ($\Omega = 4.38$, $N_1 = 34$, $N_2 = 23$, $N_3 = 21$, $M_1 = L_1 = 17$, $M_2 = L_2 = 12$, $M_3 = L_3 = 11$, $\mu_1 = 0.6$, $\beta_1 = 0.8$, $\mu_2 = 0.2$, $\beta_2 = 0.6$, $\mu_3 = 0.1$, $\beta_3 = 0.4$)

Fig. 7 Normalized surface displacement spectral amplitude: Section E-F-G. ($\Omega = 2.88$, $N_1 = 23$, $N_2 = 21$, $N_{31} = 11$, $N_{32} = 13$; $M_1 = L_1 = 12$, $M_2 = L_2 = 11$, $M_{31} = L_{31} = 8$, $M_{32} = L_{32} = 7$, $\mu_1 = 0.3$, $\beta_1 = 0.6$, $\mu_2 = 0.1$, $\beta_2 = 0.4$, $\mu_{31} = 0.02$, $\beta_{31} = 0.2$, $\mu_{32} = 0.02$, $\beta_{32} = 0.2$)

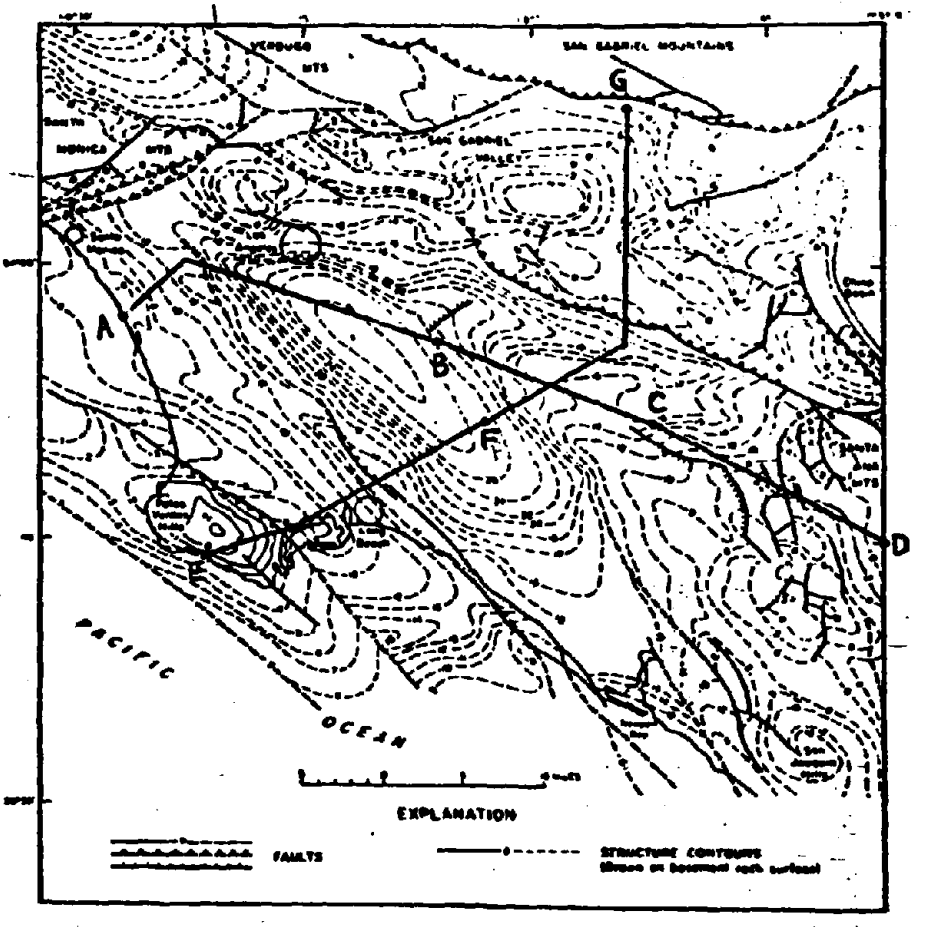
VENTURA
SAN GABRIEL MOUNTAINS
SAN GABRIEL
A
B
C
D
F
G
PACIFIC
OCEAN
EXPLANATION
FAULTS
STRUCTURE CONTOURS

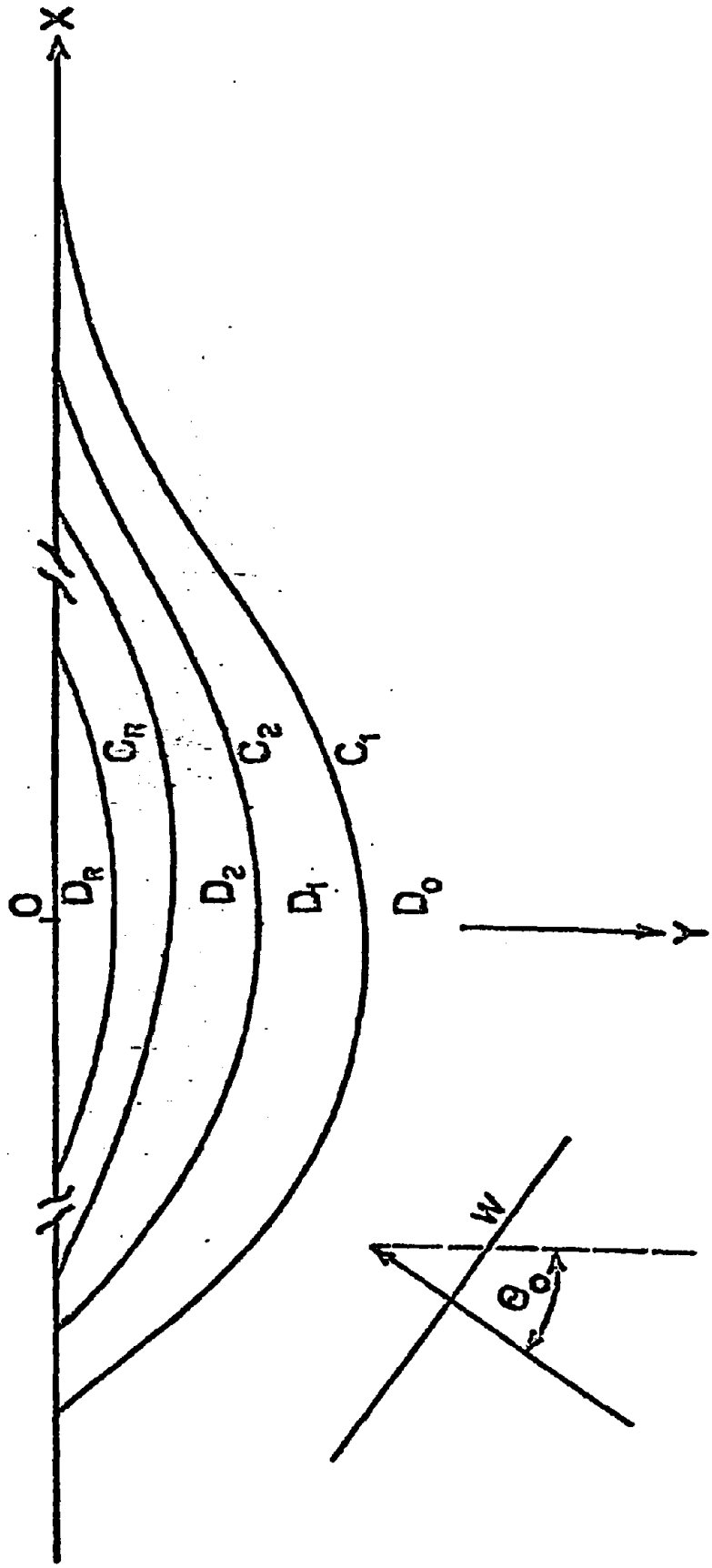
X
O
D_R
D_2
D_1
D_0
C_R
C_2
C_1
Y
W
θ_{0_1}

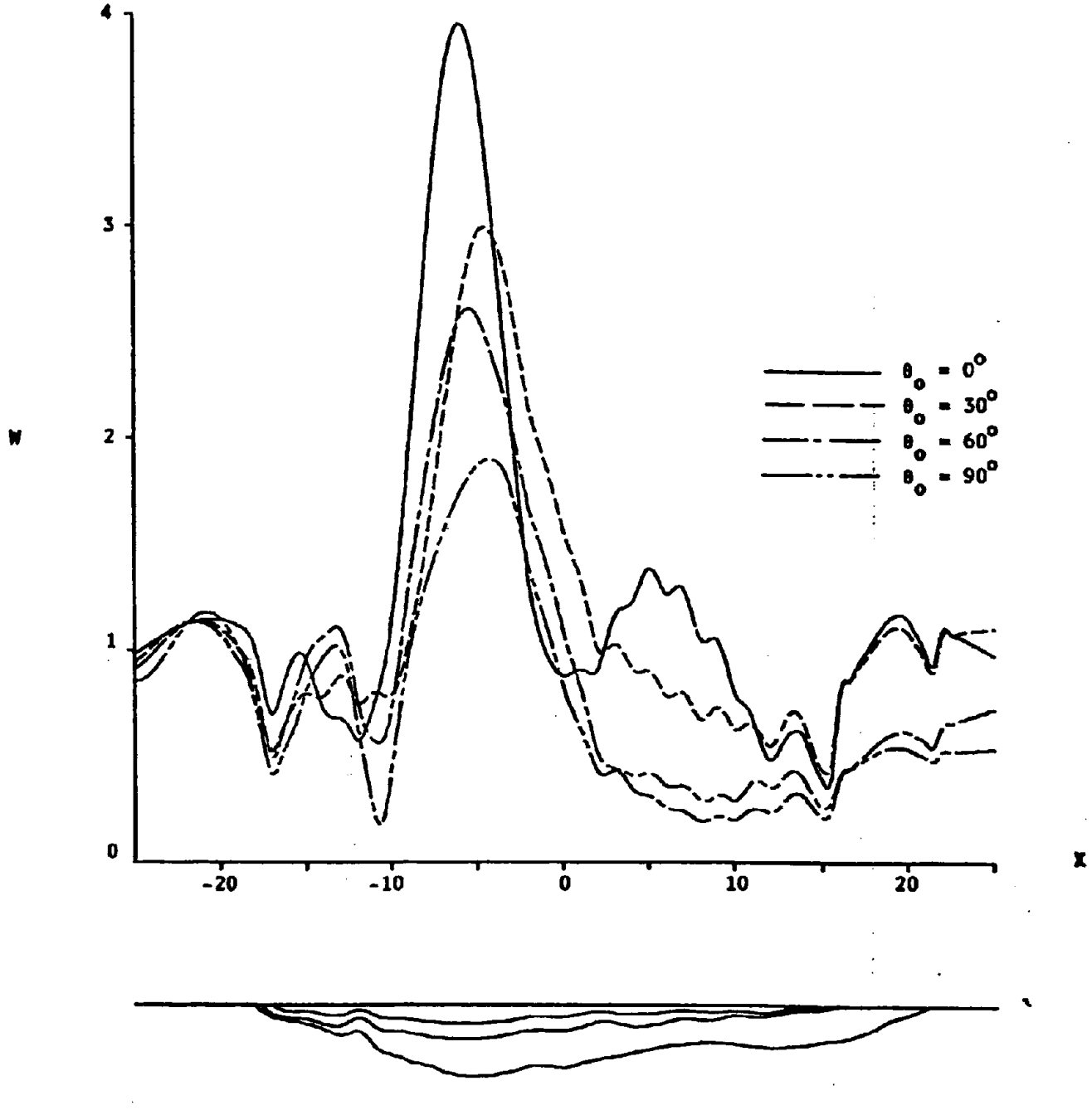
4
3
2
1
0
W
-20
-10
0
10
20
X
θo = 0°
θo = 30°
θo = 60°
θo = 90°

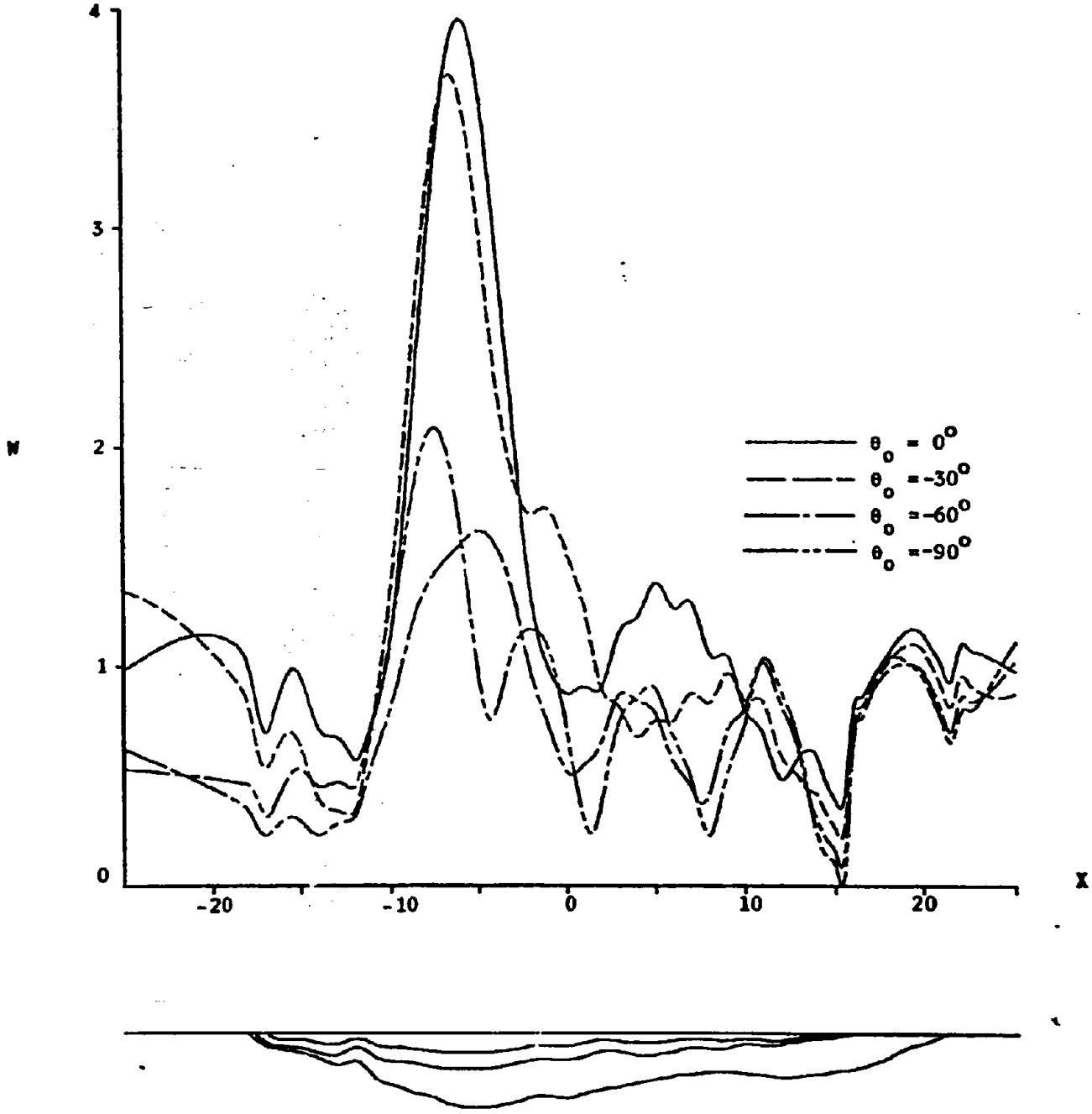
W
X
4
3
2
1
0
-20
-10
0
10
20
θo = 0°
θo = -30°
θo = -60°
θo = -90°

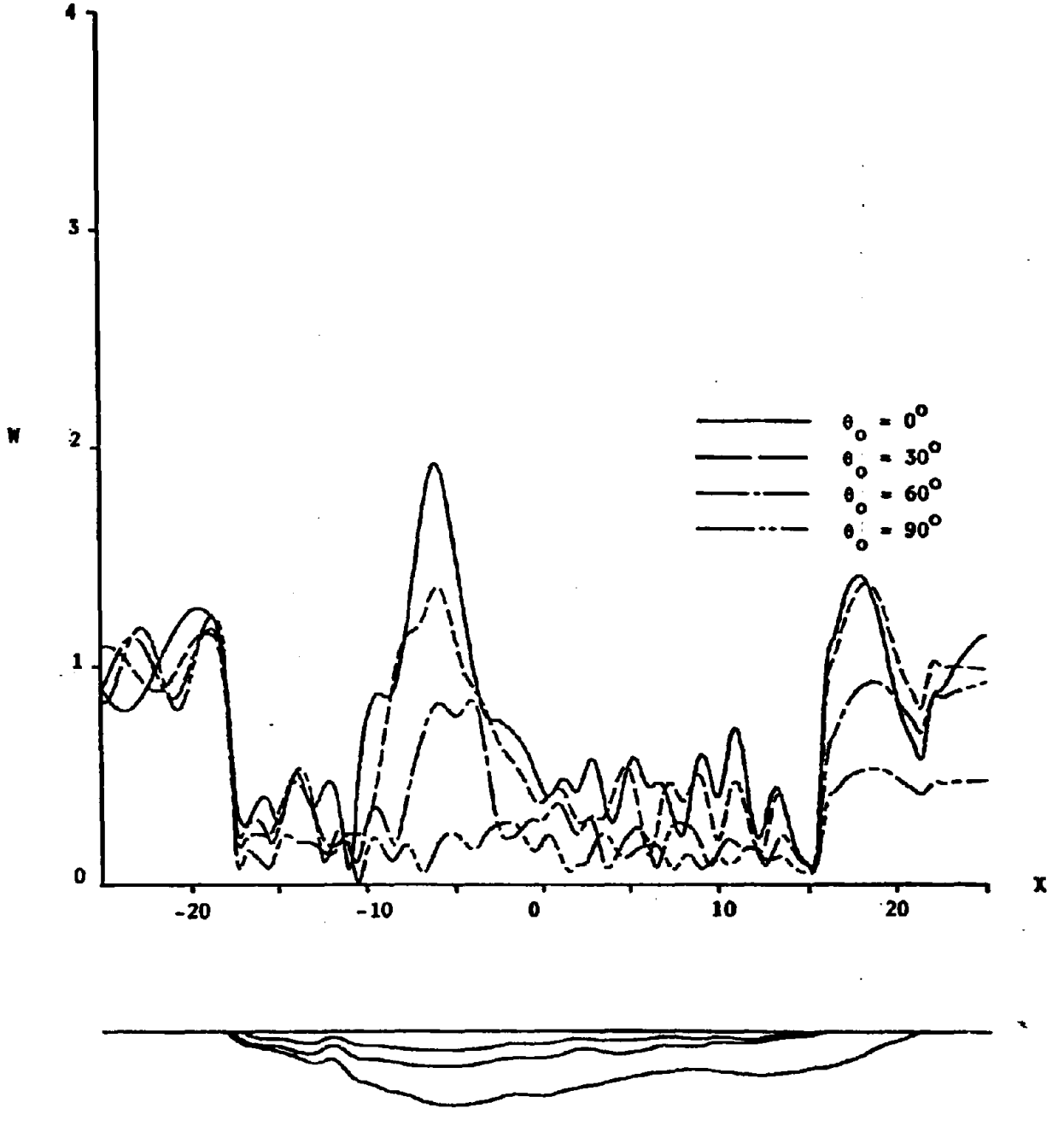
4
3
2
1
0
W
X
-20
-10
0
10
20
$\theta_o = 0^o$
$\theta_o = 30^o$
$\theta_o = 60^o$
$\theta_o = 90^o$

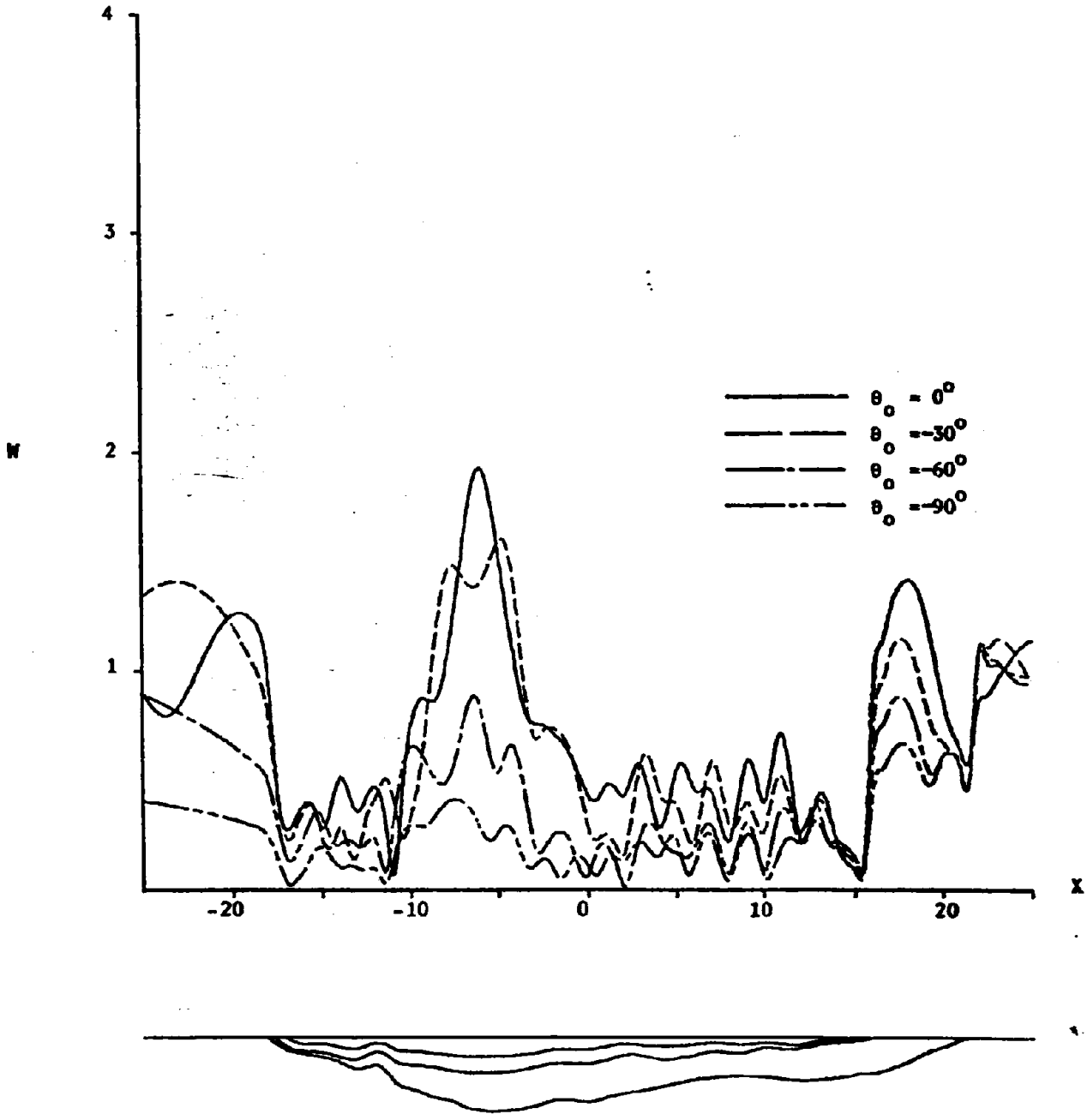
4
3
2
1
W
X
-20
-10
0
10
20
θo = 0°
θo =-30°
θo =-60°
θo =-90°

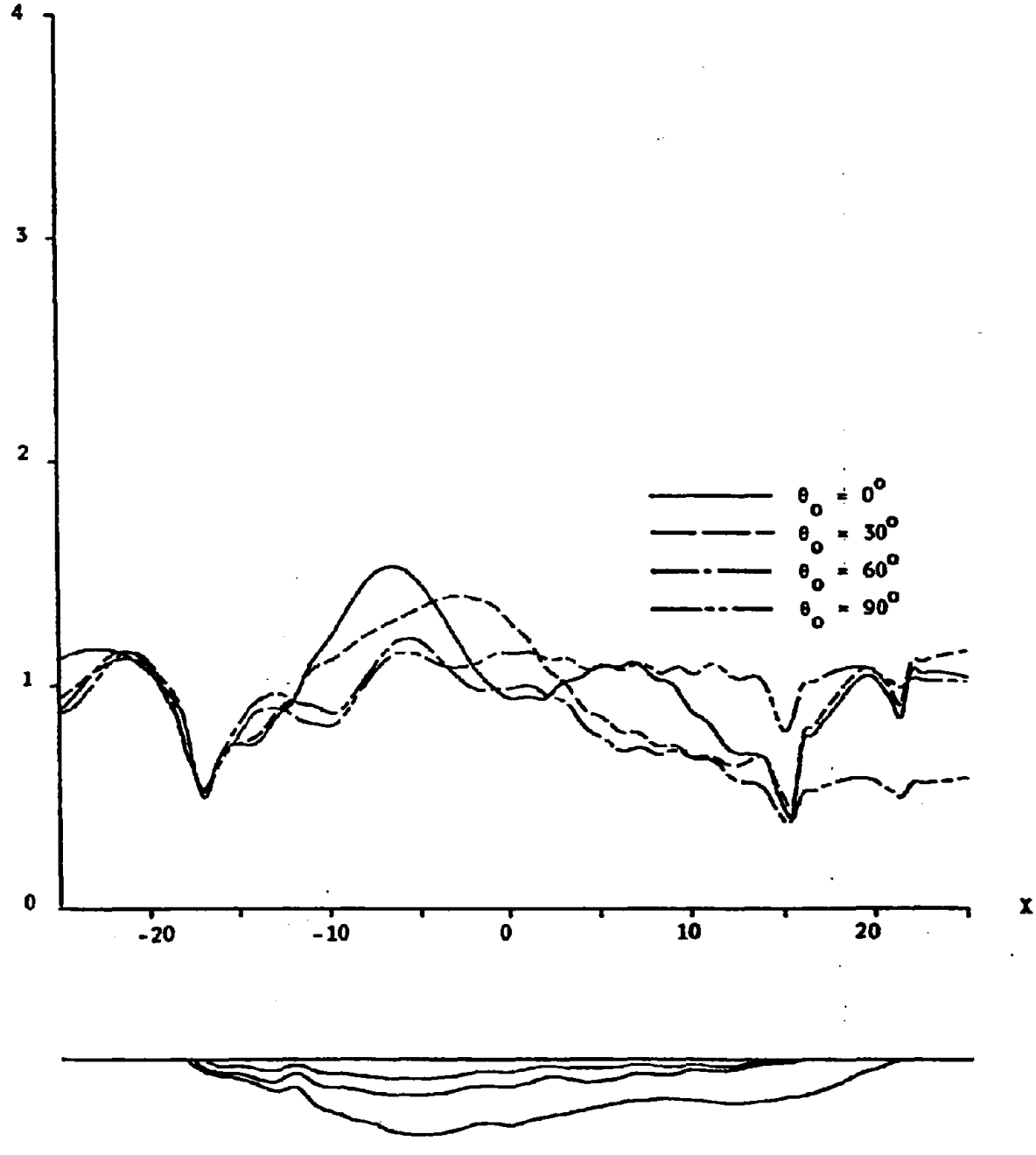
4
3
2
1
0
W
X
-20
-10
0
10
20
θ_o = 0°
θ_o = 30°
θ_o = 60°
θ_o = 90°

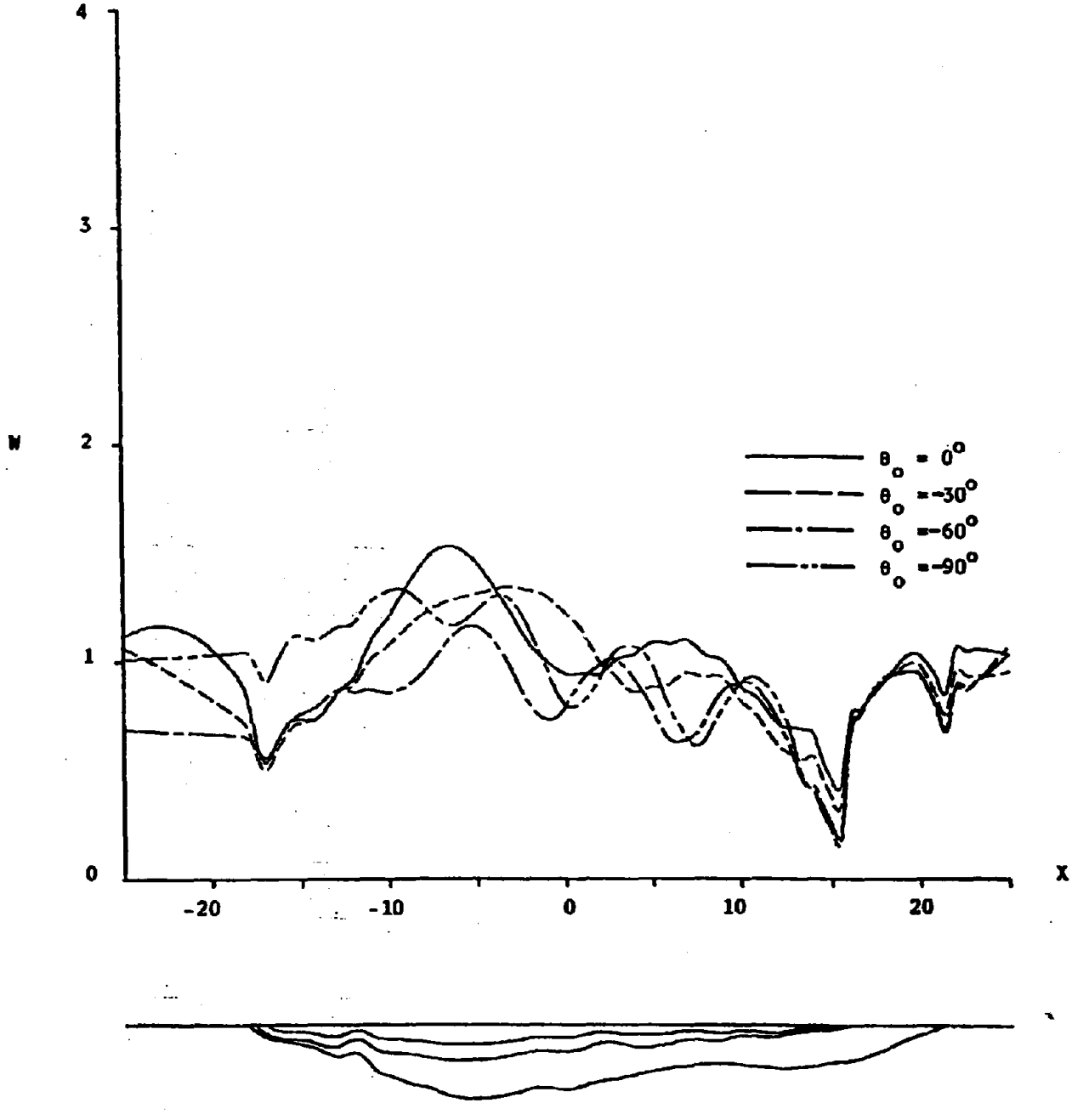
4
3
2
1
0
W
X
-20
-10
0
10
20
θo = 0°
θo =-30°
θo =-60°
θo =-90°

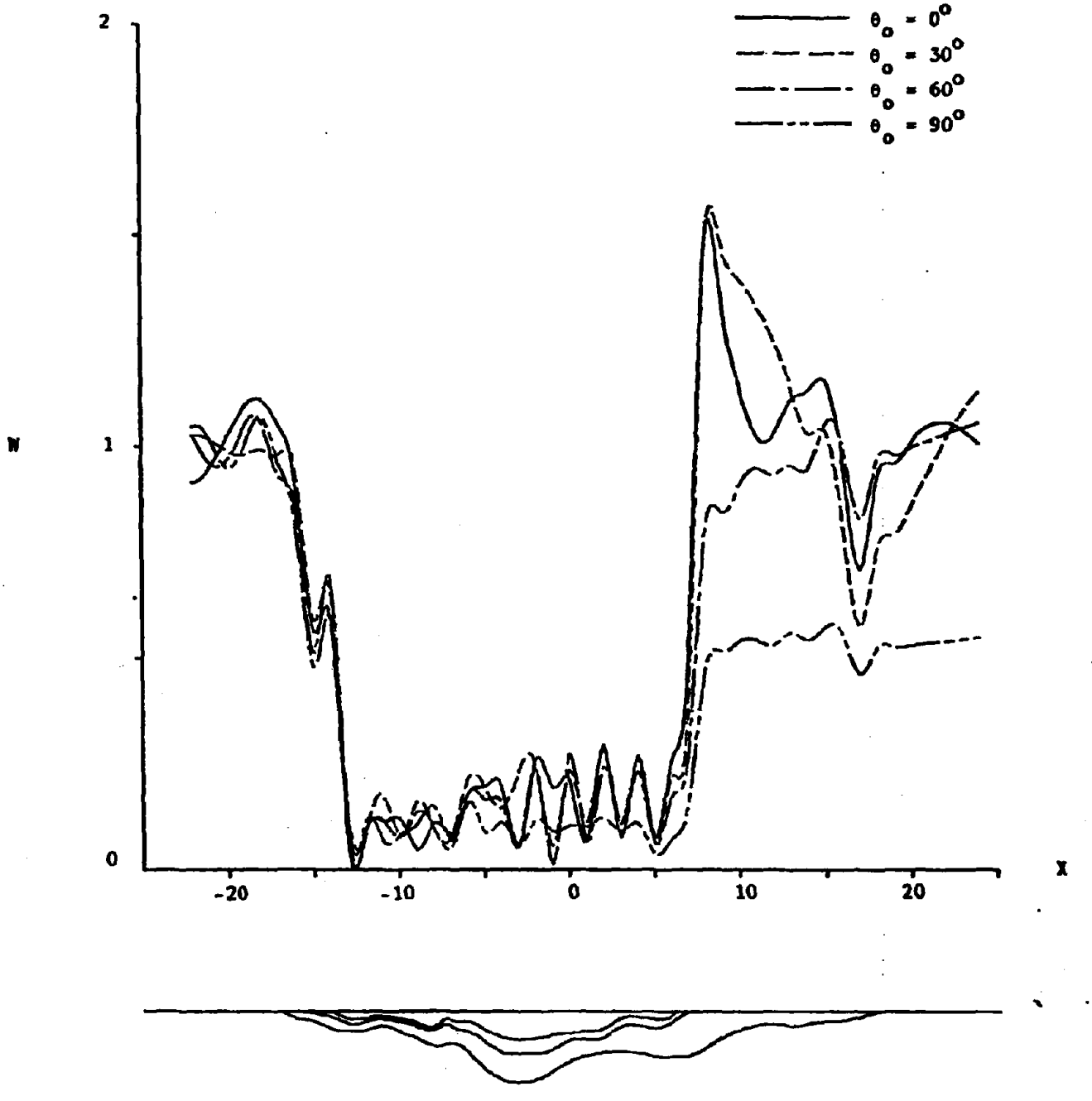
θo = 0°
θo = 30°
θo = 60°
θo = 90°
W
X
2
1
0
-20
-10
0
10
20

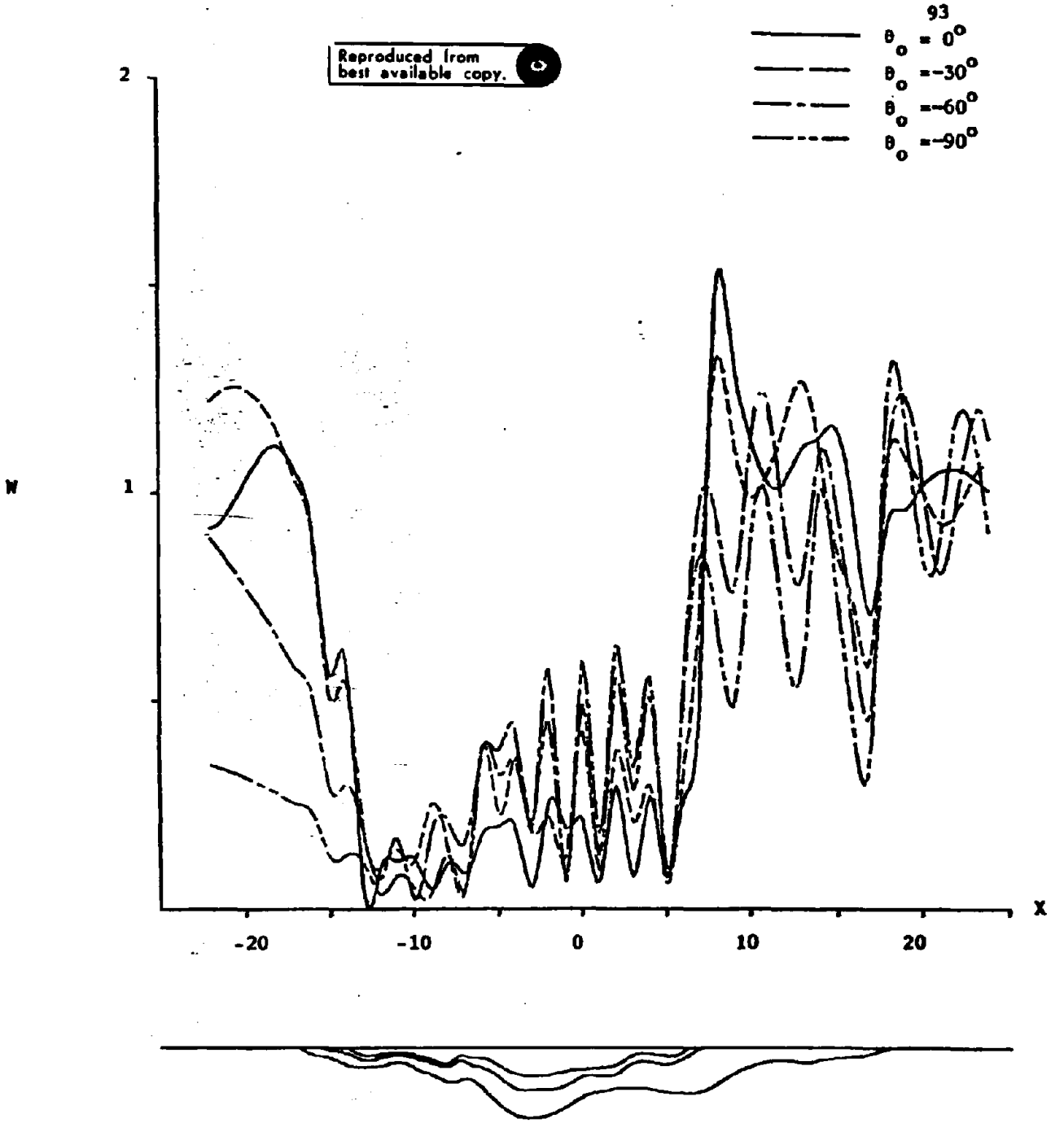

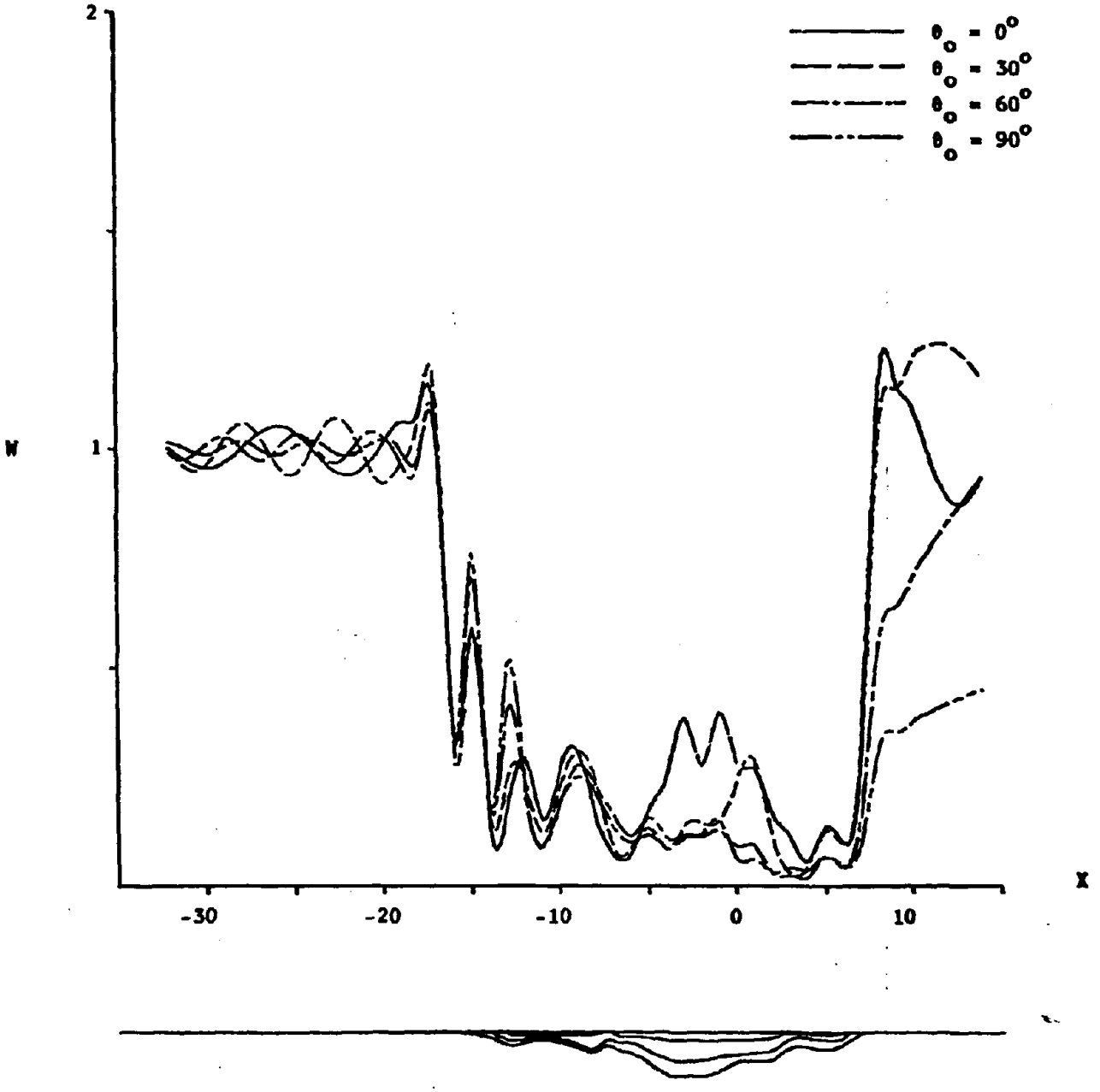
2
1
W
X
-30
-20
-10
0
10
θ_o = 0°
θ_o = 30°
θ_o = 60°
θ_o = 90°

EFFECT OF INCLUSION SHAPE UPON GROUND MOTION*

by Marijan Dravinski[1]

Introduction

Observation from some recent earthquakes (Sozen et al. (17), Jennings (10)) indicated that the area of intense damage can be highly localized. Esteva (9) established that intensity of strong ground motion may change greatly within a short distance. Subsequent investigations (e.g., Boore (2)) reinforced a belief that the inhomogeniety of the soil and surface (subsurface) irregularities are probably the main cause of localized amplification effects. Experimental results by Rogers et al. (14) confirm these results. Simultaneous recording of the Nevada Test Site nuclear events were made at sites underlined by alluvium in the Long Beach area and at sites underlined by rock in the Palos Verdes and Pasadena areas. Those data show peak-ground-velocity alluvium-to-rock ratios as high as 7 and spectral ratios as high as 11 in the period band from 0.2 to 6 sec. These results call for a systematic investigation of the role the shape of an inhomogeniety has in the amplification effects of the surface strong ground motion.

For many problems, it is possible to construct a surface integral representation of the solution. Corresponding integral equations involve only the boundary and initial values (and possibly interior sources) (Cruse and Rizzo (6)). The boundary value problem is thus formulated in terms of boundary values and the solution at interior points need not be

---

[1] Assistant Professor, Department of Mechanical Engineering, University of Southern California, Los Angeles, Calif. 90089-1453

*Accepted for publication.

considered in order to solve the integral equations (4). Once the integral equations are solved, solution at any interior point can be determined through the original representation. Therefore, the main advantage of the boundary integral equation methods (BIEM) lies in fact that only boundary of the body is being discretized, thus reducing the number of unknown variables significantly in comparison to the finite element and finite difference procedures.

Indirect BIEM used in this paper has been used by the author (8) in the study of amplification effects due to an elastic inclusion embedded into an elastic half-space and subjected to different types of moves. The method originates in works by Kupradze (11), Copley (5), and Oshaki (13). Application of the method to the wave propagation problems in geophysics and earthquake engineering is due to Sanchez-Sesma and Rosenblueth (16), Sanches-Sesma and Esquivel (15), Apsel (1), and Wong (19). For detailed literature review pertinent to this BIEM, the reader is refered to a paper by the author (7) and for literature on general BIEM to the paper by Brebbia (3).

Statement of Problem

The problem model consists of an elastic inclusion D_1 completely embedded into an elastic half-space D_o ($-\infty < x < \infty$, $y \geq 0$) subjected to different incident plane harmonic waves. The material of the inclusion and the half-space is assumed to be homogeneous, isotropic, and linearly elastic.

Antiplane Strain Model. The equation of motion for the steady-state waves is specified by

$$(\nabla^2 + k_j^2)w_j(x,y,\omega) = 0 \; ; \; j=0,1 \; ; \; \nabla^2 \equiv \frac{\partial^2}{\partial x^2} + \frac{\partial^2}{\partial y^2} \; , \qquad (1)$$

where subscripts 0 and 1 refer to the half-space and the inclusion,

respectively, k represents the wavenumber, ω denotes the circular frequency and w represents the only nonzero component of displacement field along the z-axis. Throughout the analysis, the factor $e^{+i\omega t}$ is understood and velocity of the shear waves is denoted by β. Boundary conditions are specified by

$$\frac{\partial w}{\partial y} = 0, \text{ at } y = 0. \tag{2}$$

Perfect bonding along the interface C* between the half-space and the inclusion requires

$$w_o = w_1 \tag{3a}$$

$$\underset{\sim}{x} \in C$$

$$\mu_o \frac{\partial w_o}{\partial n} = \mu_1 \frac{\partial w_1}{\partial n}, \tag{3b}$$

where $\underset{\sim}{x}$ represents a position vector, μ is the shear modulus and $\underset{\sim}{n}$ is a unit normal at the interface C. The incident wave is specified by

$$w^{inc} = e^{-ik_1(x \sin\theta_o - y \cos\theta_o)}, \tag{4}$$

where θ_o is the angle of incidence of the incoming wave.

Plane Strain Model. The equation of motion for this model is specified by (Miklowitz (12))

$$\nabla^2\phi_j + h_j^2\phi_j = 0 \tag{5a}$$

$$\nabla^2\psi_j + k_j^2\psi_j = 0 \; ; \; j=0,1, \tag{5b}$$

where ϕ and ψ denote the dilatational and equivoluminal wave potentials, respectively, with corresponding wavenumbers h and k. The velocity of dilatational waves is denoted by α. The boundary conditions at y=0 are given through

$$\sigma_{yyo} = 0 \tag{6a}$$

*Interface C is assumed to be sufficiently smooth with no sharp corners being present.

$$\sigma_{xyo} = 0. \tag{6b}$$

Perfect bonding along the interface C requires

$$u_o = u_1 \tag{7a}$$

$$v_o = v_1 \tag{7b}$$

$$\sigma_{nno} = \sigma_{nn1} \tag{7c}$$

$$\sigma_{nto} = \sigma_{nt1}, \tag{7d}$$

where u and v denote the displacement components along the x and y-axis, respectively. The normal and tangential stress along the interface are denoted by σ_{nn} and σ_{nt}, respectively. Incident wave is assumed to be a plane harmonic P, SV, or Rayleigh wave (8).

Solution of Problem

Antiplane Strain Model. The total wave field in the half space and in the inclusion is found to be (see Ref. 8)

$$w_0(\underline{r}) = w^{ff}(\underline{r}) + \sum_{m=1}^{M} a_m G_0(\underline{r},\underline{r}_m) \quad ; \underline{r} \in D_o \tag{8a}$$

$$w_1(\underline{r}) = \sum_{\ell=1}^{L} b_\ell G_1(\underline{r},\underline{r}_\ell) \quad ; \underline{r} \in D_1, \tag{8b}$$

where $G_{0,1}$ are Green's function for a line load in a half-space, $\underline{r}_m$ and $\underline{r}_\ell$ are assumed, and a_m and b_ℓ are calculated in mean-square-sense for all m and ℓ, respectively (Ref. 8). The superscript ff denotes the free field.

Plane Strain Model. For incident dilatational wave, the total wave field in the half-space and inclusion is specified by

$$\phi_0(\underline{r}) = \phi^{ff}(\underline{r}) + \sum_{m=1}^{M} a_m \phi_0(\underline{r}|\underline{r}_m) \quad ; \underline{r} \in D_o \tag{9a}$$

$$\psi_0(\underline{r}) = \sum_{m=1}^{M} b_m \psi_1(\underline{r}|\underline{r}_m) \quad ; \underline{r} \in D_o, \tag{9b}$$

$$\phi_1(\underline{x}) = \sum_{\ell=1}^{L} c_\ell \phi_1(\underline{x}|\underline{x}_\ell) \; ; \; \underline{x} \in D_1 \tag{9c}$$

$$\psi_1(\underline{x}) = \sum_{\ell=1}^{L} d_\ell \psi_1(\underline{x}|\underline{x}_\ell) \; ; \; \underline{x} \in D_1, \tag{9d}$$

where $\phi(\underline{x}|\underline{x}_{m,\ell})$ and $\psi(\underline{x}|\underline{x}_{m,\ell})$ are Green's functions for dilatational and equivoluminal line loads embedded in a half-space. Locations $\underline{x}_m$ and $\underline{x}_\ell$ are assumed and coefficient a_m, b_m, c_ℓ, and d_ℓ are calculated in mean-square-sense. Similar expressions can be derived for incident SV or Rayleigh waves.

Evaluation of Results

Amplitude of the surface strong ground motion is evaluated for different incident waves and different inclusions with identical cross sectional area. In order to reduce the number of parameters present in the problem, numerical results are presented for fixed embedment depth of the inclusion at single frequency of the incident field.

Incident SH-wave. For four different angles of incidence, the surface strong ground motion corresponding to various inclusions is depicted by Figs. 1-3. Evidently, variation of inclusion produced very little change in the surface response of the half-space for all angles of incidence. The same results were observed by Umek (18) who investigated the influence of rigid foundation shape upon the surface ground motion. Results of Figs. 1-3, on the other hand, demonstrate very clearly that presence of the inclusion may cause significant change of the surface ground motion when compared to motion of the half-space without an inclusion. Motion appears to be very sensitive upon the angle of incidence of the incoming wave. Although not presented here, it can be shown that the contrast in material properties between the half-space and the inclusion and the frequency of the incident wave are of major importance for subsequent

surface ground motion. However, in all these cases change of inclusion shape produced rather small effect upon the resulting strong ground motion. This implies that measurement of the surface displacement field magnitude away from the inclusion would provide very little information about the inclusion shape.

Incident P-wave. For different angles of incidence and various inclusions, surface displacement amplitude for horizontal and vertical displacement components are shown by Figs. 4-9. Results are presented normalized with respect to the amplitude of the surface displacement field, i.e., $(|u^{ff}|^2 + |v^{ff}|^2)^{\frac{1}{2}}$. Comparison of Figs. 4-6 and 7-9 indicate that in the plane strain model surface ground motion is more sensitive upon the inclusion geometry when compared to the antiplane strain model. This may be explained by the fact that for incident SH wave, motion of the media is caused only by the resultant shearing force, which is the zeroth order moment of the shearing stresses. For plane strain model, the resultant force and the resultant moment, i.e., the zeroth and the first order moments of the stresses determine the surface response so one should expect that the effect of the inclusion shape through the scattered wave field would take a stronger influence upon the surface motion (18). The same results can be observed for incident SV and Rayleigh waves.

Summary and Conclusions

Effect of inclusion shape upon surface ground motion is investigated by using an indirect boundary integral equation approach. Results are presented for incident plane harmonic SH and P waves for three elastic inclusions and four angles of incidence. Presented results indicate that surface ground motion is less sensitive upon the change of the inclusion

shape for incident SH waves than for incoming P (SV or Rayleigh) waves. Still, the presence of an elastic inclusion caused locally significant amplification of the surface ground motion for both antiplane and plane strain models. Amplitude of the surface motion appears to be very sensitive upon the number of parameters present in the problem, such as angle of incidence, frequency, material properties of the inclusion and the half-space, and location of the observation point at the ground surface.

Acknowledgement

This research has been supported by a grant CEE-8119696 form the National Science Foundation.

Figure Captions

1. Surface Displacement Amplitude for Incident SH-wave: (For all cases: $\mu_1=\beta_1=1$, $\mu_2=0.17$, $\beta_2=0.5$, $\omega=0.79s^{-1}$, H=3) $R_1=2$, $R_2=1.4$.

2. Surface Displacement Amplitude for Incident SH-wave: $R_1=1.4$, $R_2=2$.

3. Surface Displacement Amplitude for Incident SH-wave: $R_1=R_2=1.67$.

4. Surface Displacement Amplitude for Incident P-wave: Horizontal Component. (For all the cases $\phi^{inc}=i/h_1\cdot\exp[-ih_1(x\sin\theta_0-y\cos\theta_0)]$, $\mu_1=1$, $\mu_2=0.17$, $\beta_1=1$, $\beta_2=0.5$, $\alpha_1=2$, $\alpha_2=1$, $\omega=0.79s^{-1}$, H=3) $R_1=2$, $R_2=1.4$.

5. Surface Displacement Amplitude for Incident P-wave: Horizontal Component $R_1=1.4$, $R_2=2$.

6. Surface Displacement Amplitude for Incident P-wave: Horizontal Component $R_1=R_2=1.67$.

7. Surface Displacement Amplitude for Incident P-wave: Vertical Component $R_1=2$, $R_2=1.4$.

8. Surface Displacement Amplitude for Incident P-wave: Vertical Component $R_1=1.4$, $R_2=2$.

9. Surface Displacement Amplitude for Incident P-wave: Vertical Component $R_1=R_2=1.67$.

1. Apsel, R.J., "Dynamic Green's Functions for Layered Media and Applications to Boundary Value Problems," Ph.D. Thesis, U.C. San Diego, 1979.

2. Boore, D.M., "The Effect of Simple Topography on Seismic Waves: Implications for the Accelerations Recorded at Pacoima Dam, San Fernando Valley, California," Bull. Seism. Soc. Amer., 62, 1608-1619, 1973.

3. Brebbia, C.A., "Introductory Remarks," Boundary Element Methods, Proceedings of the 3rd International Seminar, Irvine, California, July 1981, editor: C.A. Brebbia, Springer-Verlag, New York, 1981.

4. Cole, D.M., Kosloff, D.D. and Minster, J.B., "A Numerical Boundary Integral Equation Method for Elastodynamics I," Bull. Seism. Soc. Amer., 68, pp. 1331-1357, 1978.

5. Copley, L.A., "Integral Equation Method for Radiation from Vibrating Surfaces," J. Acoust. Soc. Amer., 41, pp. 807-816, 1967.

6. Cruse, T.A. and Rizzo, F.J., "A Direct Formulation and Numerical Solution of the General Transient Elastodynamic Problem. I," J. Meth. Analysis and Applications, 22, pp. 244-259, 1968.

7. Dravinski, M., "Scattering of SH Waves by Subsurface Topography, J. Eng. Mech. Div., EN1, pp. 1-16, 1982.

8. Dravinski, M., "Influence of Interface Depth Upon Strong Ground Motion," Bull. Seism. Soc. Amer., 72, pp. 597-614, 1982.

9. Esteva, L. "Microzoning: Models and Reality, Proc. World. Conf. Earthquake Engr.," 6th, New Delhi, 1977.

10. Jennings, P.C. (editor), "San Fernando Earthquake of February 9, 1971," EERL-71-02, California Institute of Technology, Pasadena, 1971.

11. Kupradze, V.D., Dynamical Problems in Elasticity, Progress in Solid Mechanics, Sneddon, I.N. and Hill, R., editors, North Holland, Amsterdam, 1963.

12. Miklowitz, J., The Theory of Elastic Waves and Waveguides, North Holland, Amsterdam, 1978.

13. Oshaki, Y., "On Movements of a Rigid Body in Semi-infinite Elastic Medium," Proc. Japanese Earthquake Engineering Symposium, Tokyo, Japan.

14. Rogers, A.M., Tinsley, J.C., Hayes, W.W. and King, K.W., "Evaluation of the Relation Between Near-Surface Geological Units and Ground Response in the Vicinity of Long Beach, California," Bull. Seism. Soc. Amer., 5, pp. 1603-1622, 1979.

15. Sanchez-Sesma, F.Y., Esquivel, J.A., "Ground Motion on Alluvial Valley Under the Incident Plane SH-waves," Bull. Seism. Soc. Amer., 69, pp. 1107-1120, 1979.

16. Sanchez-Sesma, F.Y., Rosenblueth, E., "Ground Motions at Canyons of Arbitrary Shapes under Incident SH Waves," Earthquake Engn. Struct. Dyn., 7, pp. 441-450, 1979.

17. Sozen, M.A., Jennings, P.C., Matthiesen, R.B., Housner, G.W. and Newmark, N.M., "Engineering Report on the Caracas Earthquake of 29 July, 1967," National Academy of Sciences, Washington, D.C., 1968.

18. Umek, A., "On the Influence of the Geometry of the Foundation on its Impulse Response," J. Appl. Mech., 43, pp. 300-303.

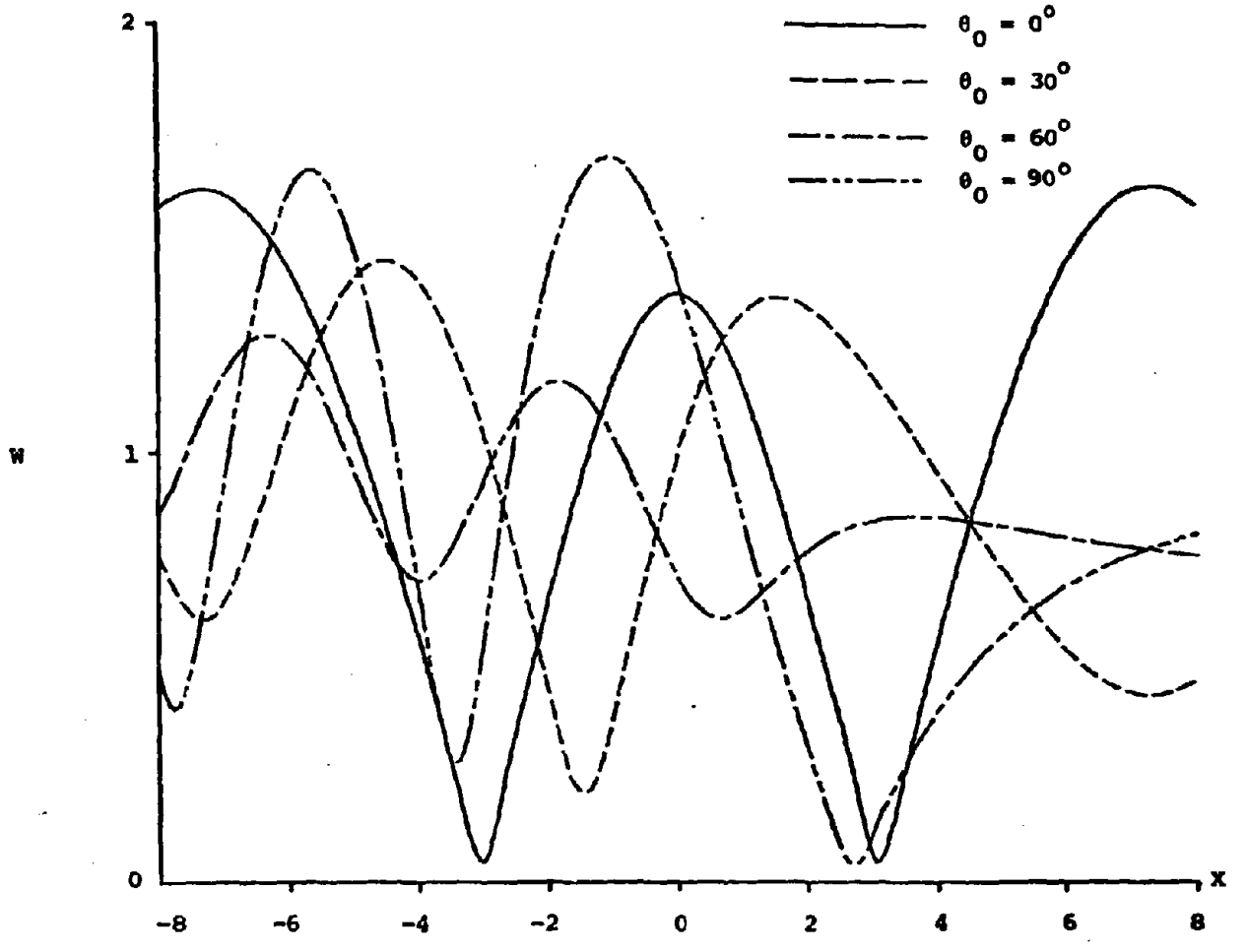
2
1
0
W
X
-8
-6
-4
-2
0
2
4
6
8
$\theta_0 = 0^\circ$
$\theta_0 = 30^\circ$
$\theta_0 = 60^\circ$
$\theta_0 = 90^\circ$

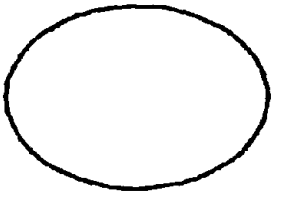

Fig. 1

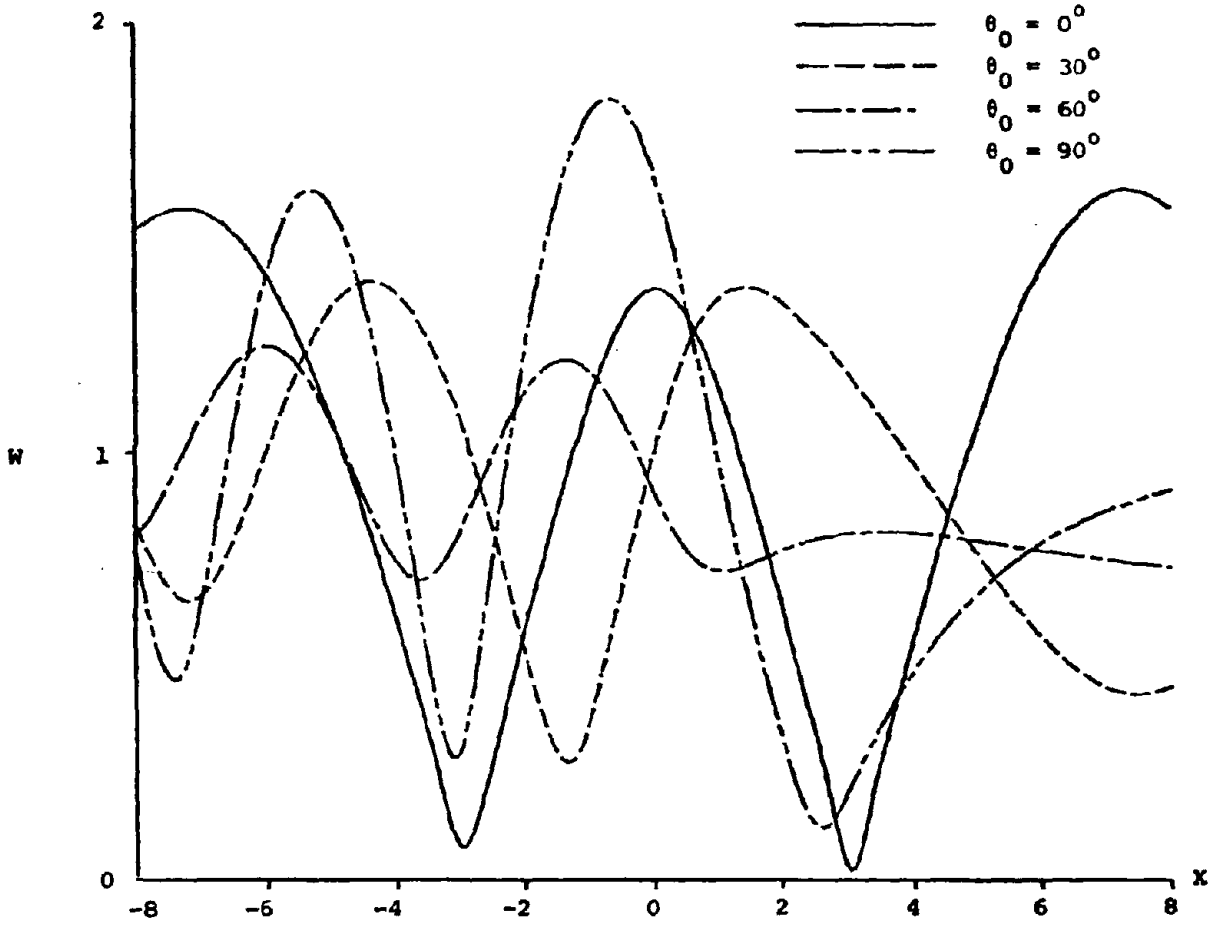
2
1
0
W
X
-8
-6
-4
-2
0
2
4
6
8
$\theta_0 = 0^\circ$
$\theta_0 = 30^\circ$
$\theta_0 = 60^\circ$
$\theta_0 = 90^\circ$

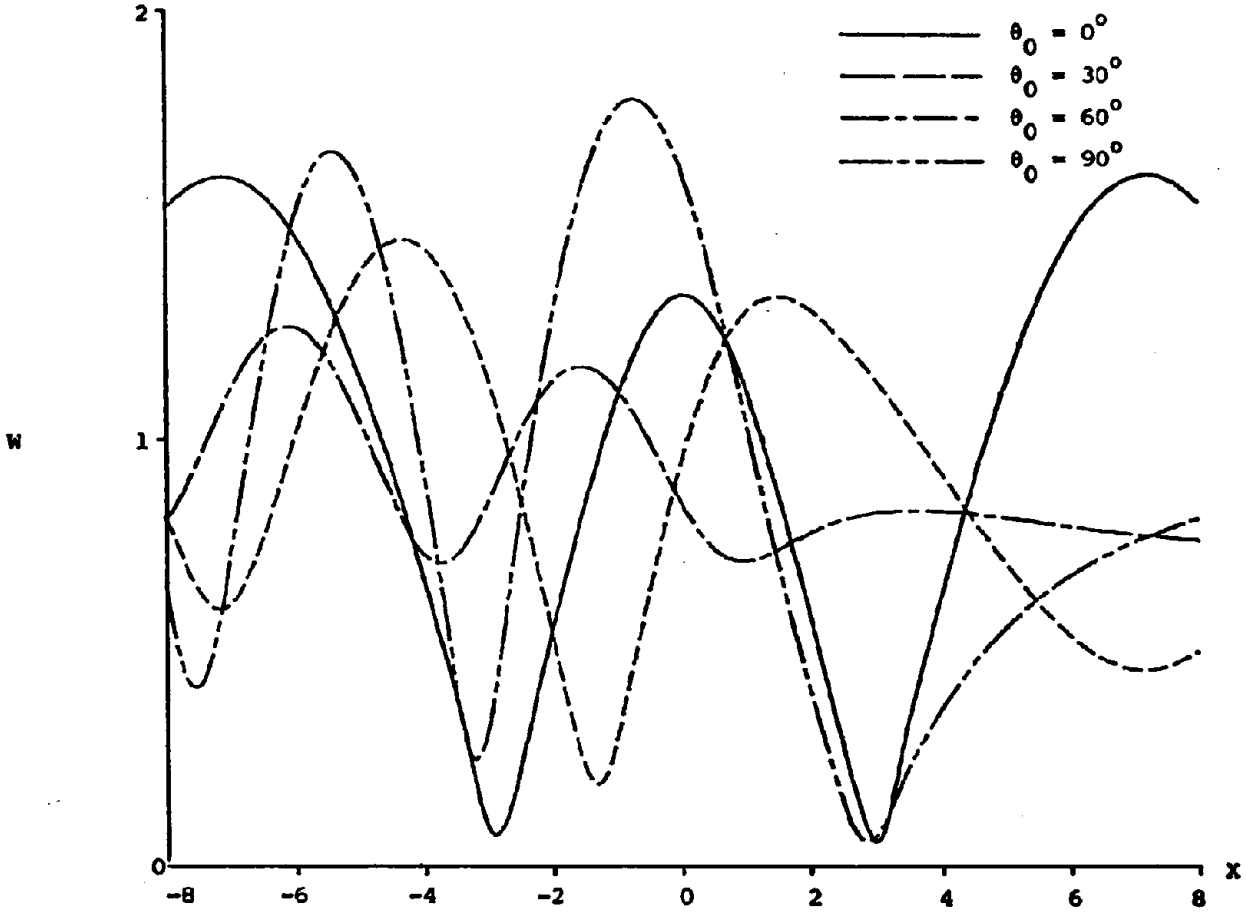

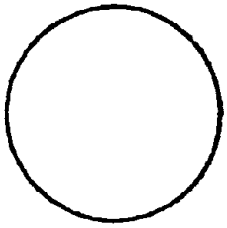

Fig 2

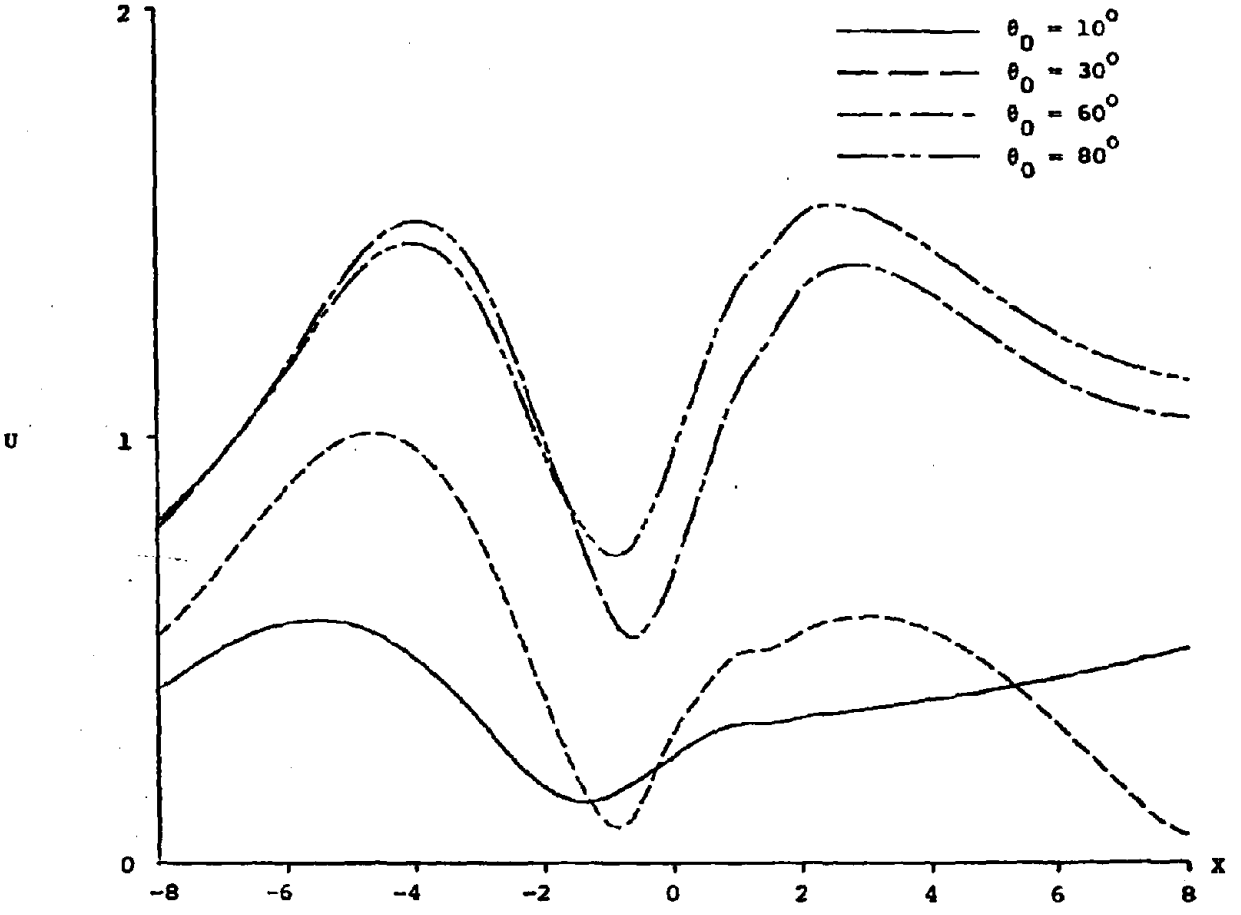
2
1
0
U
X
-8
-6
-4
-2
0
2
4
6
8
θ0 = 10°
θ0 = 30°
θ0 = 60°
θ0 = 80°

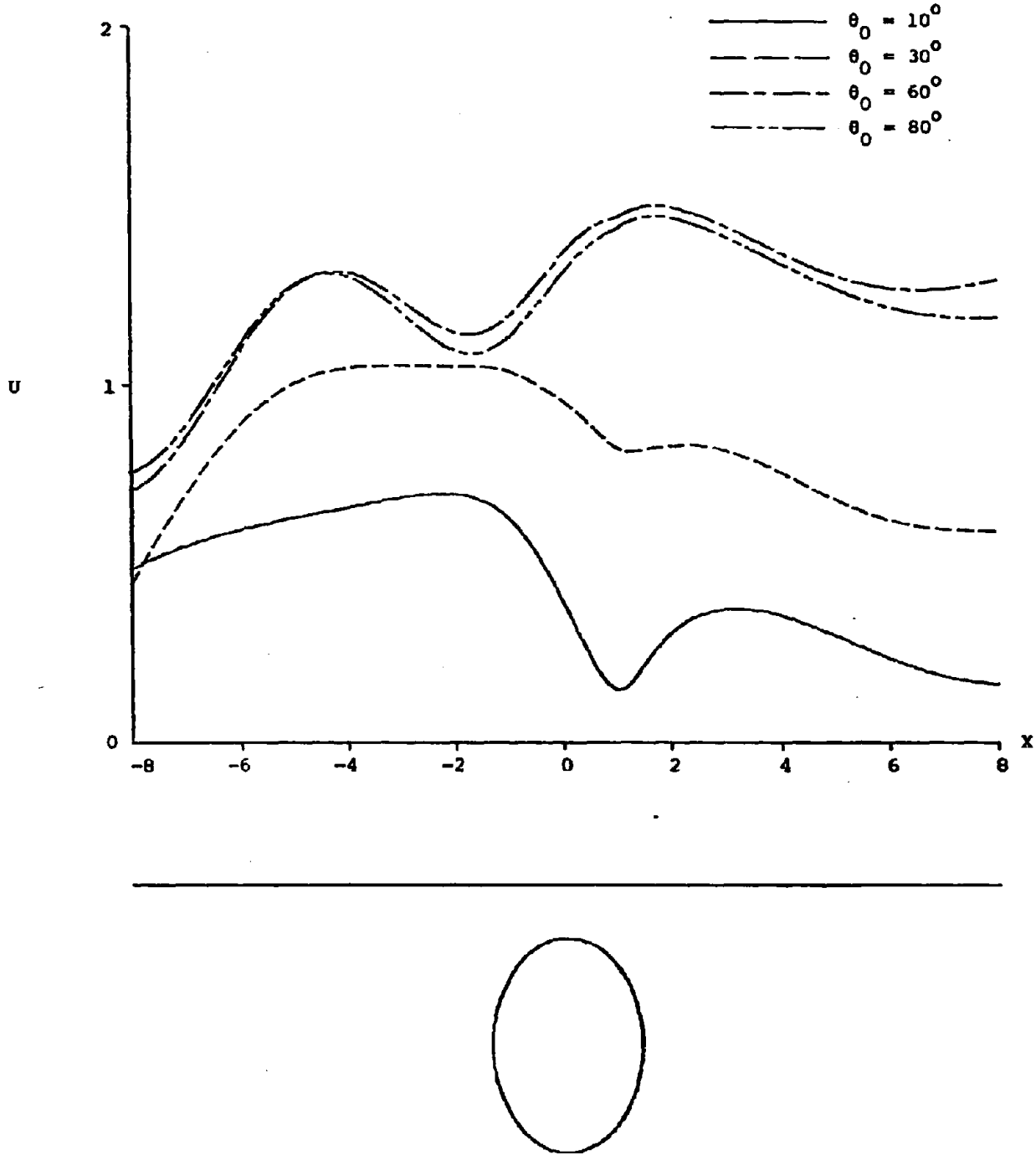

Fig. 5

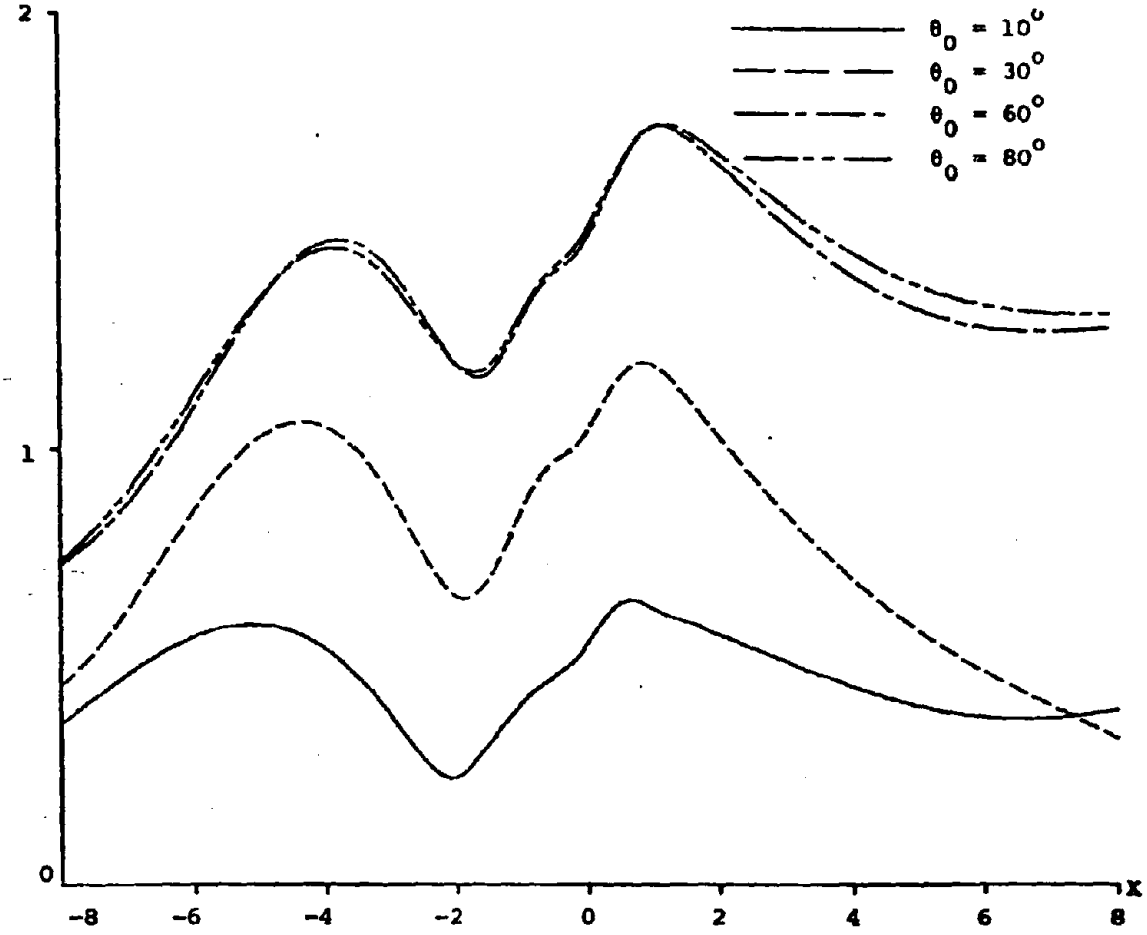
2
1
0
U
X
-8
-6
-4
-2
0
2
4
6
8
θ_0 = 10°
θ_0 = 30°
θ_0 = 60°
θ_0 = 80°

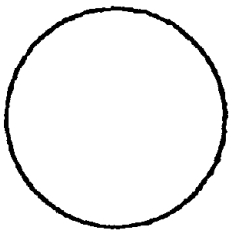

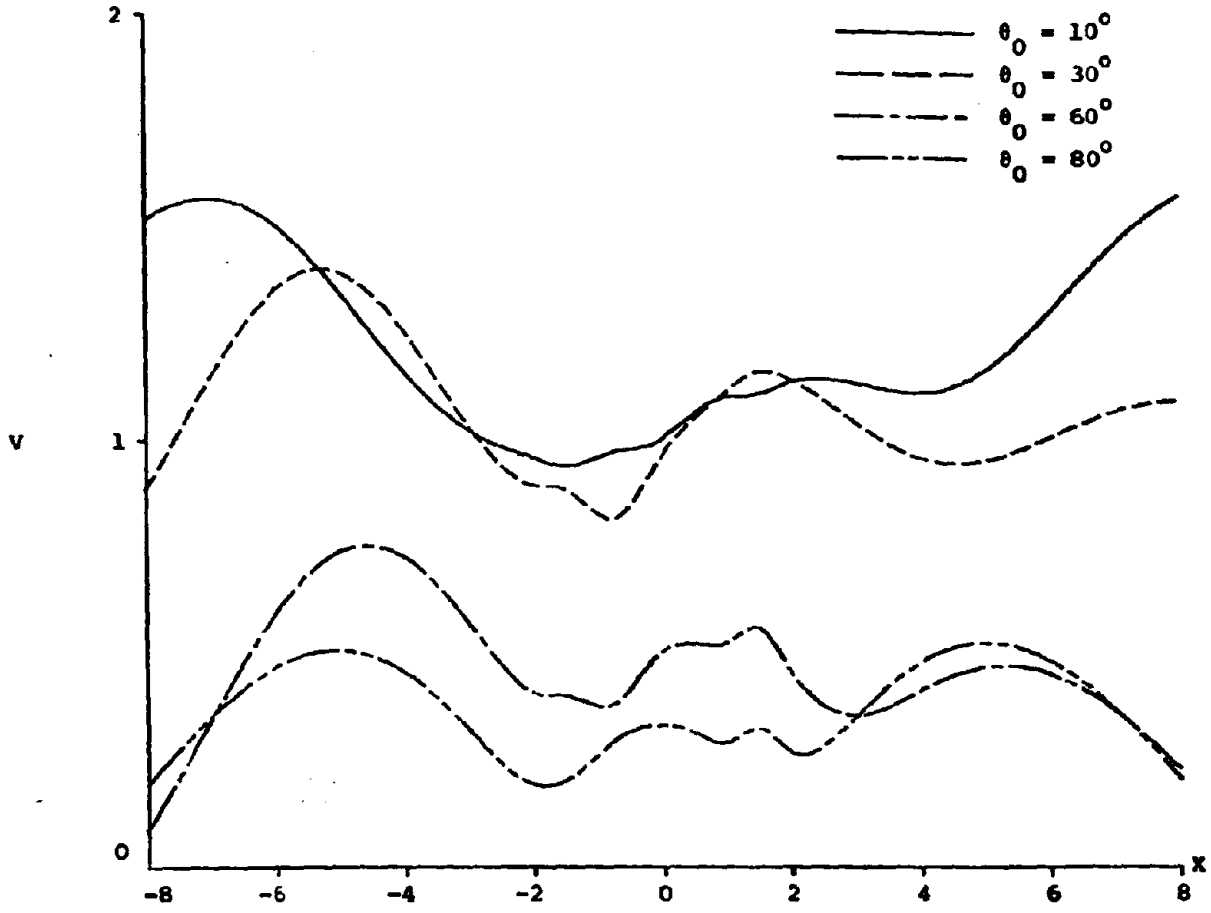
2
1
0
v
x
-8
-6
-4
-2
0
2
4
6
8
$\theta_0 = 10^\circ$
$\theta_0 = 30^\circ$
$\theta_0 = 60^\circ$
$\theta_0 = 80^\circ$

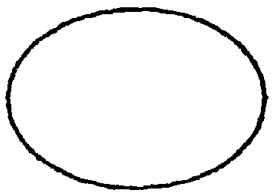

Fig. 7

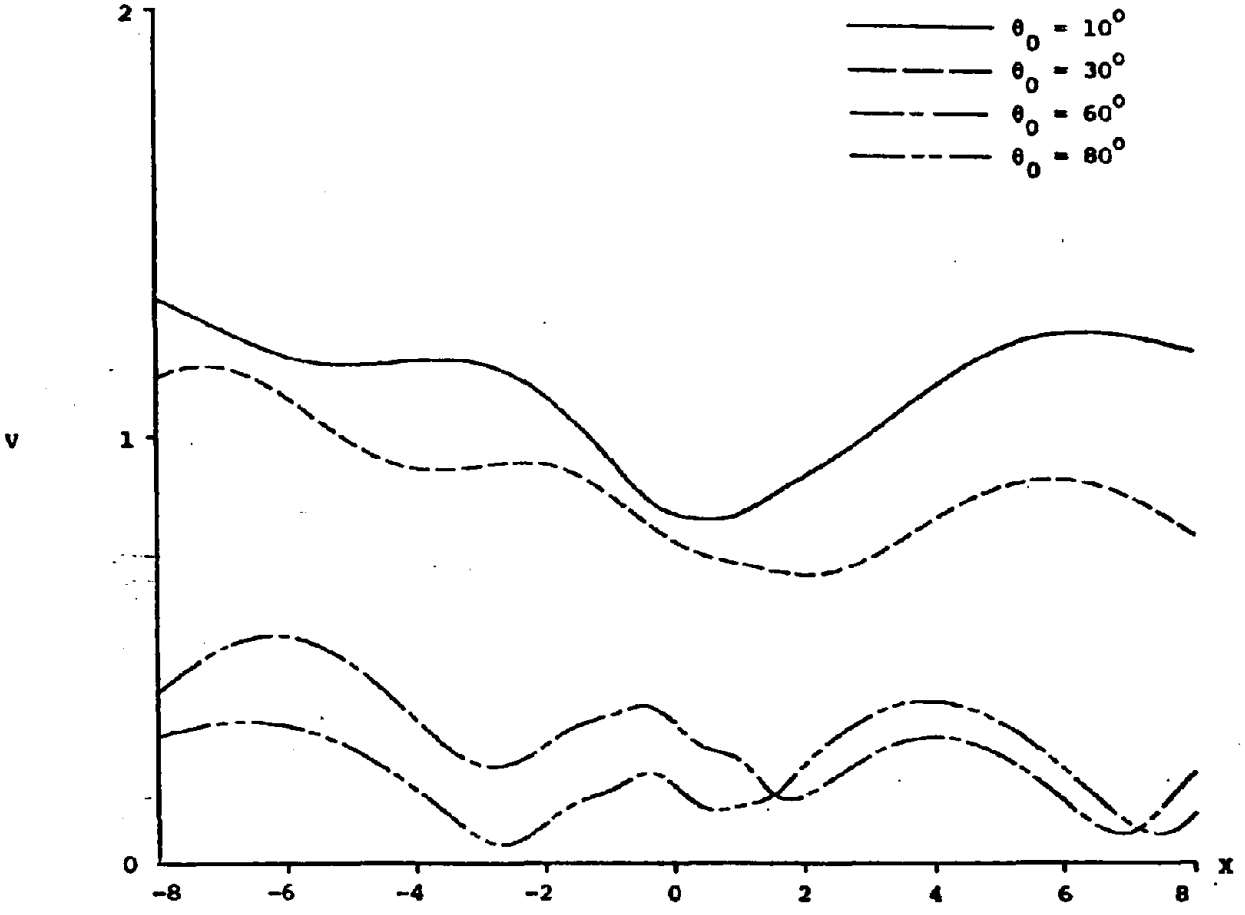
2
1
0
v
x
-8
-6
-4
-2
0
2
4
6
8
$\theta_0 = 10^\circ$
$\theta_0 = 30^\circ$
$\theta_0 = 60^\circ$
$\theta_0 = 80^\circ$

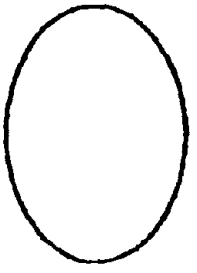

Fig. 8

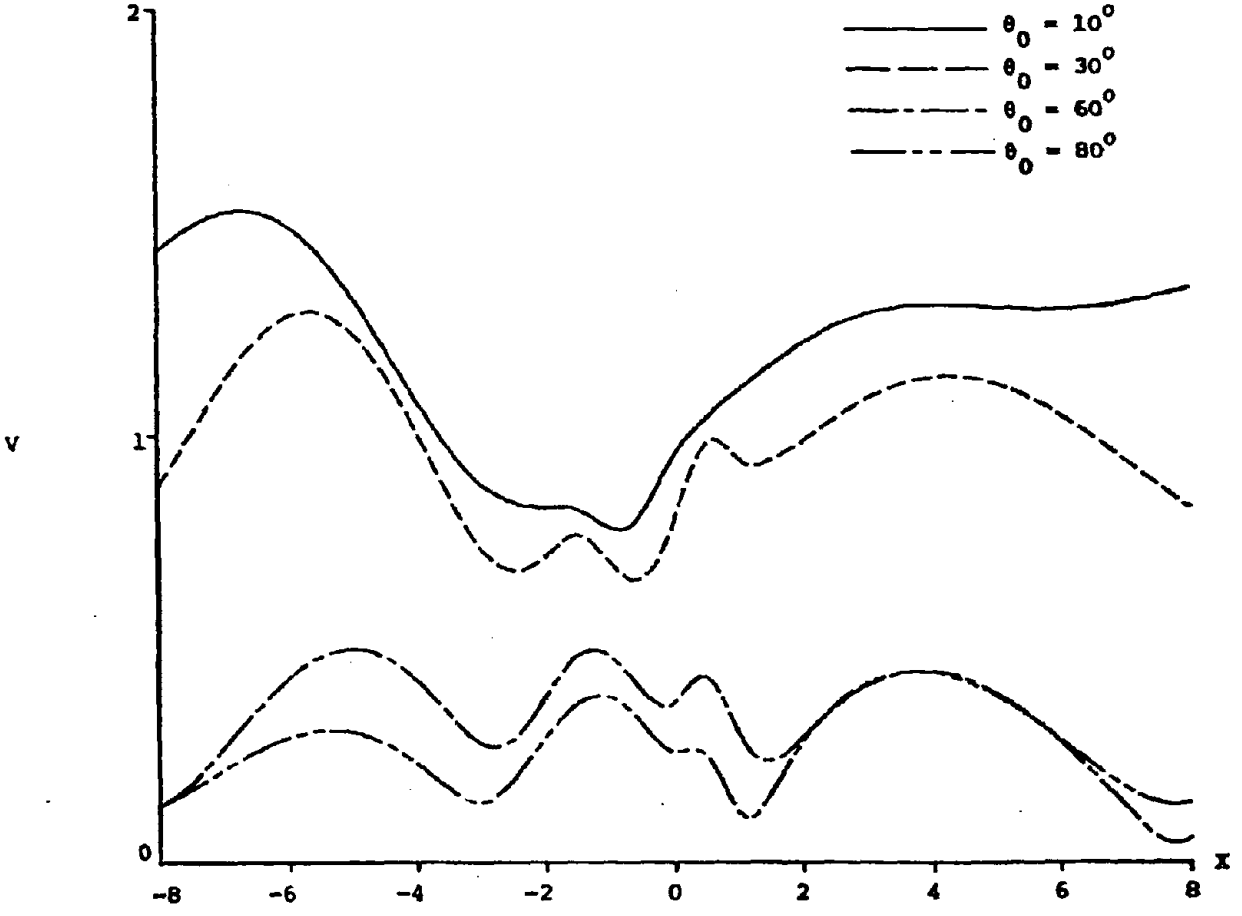
$\theta_0 = 10^\circ$
$\theta_0 = 30^\circ$
$\theta_0 = 60^\circ$
$\theta_0 = 80^\circ$
v
x
2
1
0
-8
-6
-4
-2
0
2
4
6
8

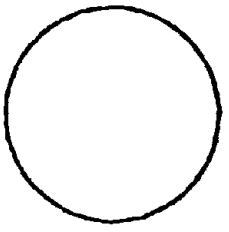

Fig. 9

Ground Motion Amplification due to Elastic Inclusions in a Half-Space *

Marijan Dravinski

Department of Mechanical Engineering

University of Southern California

Los Angeles, California U.S.A.

Summary

Scattering of plane harmonic SH, P, SV and Rayleigh waves by several inclusions of arbitrary shape, completely embedded into an elastic half-space is considered. Perfect bonding between the half-space and the inclusions is assumed. The problem is investigated for linear, isotropic, and homogeneous elastic materials. Displacement field is evaluated throughout the elastic medium so that the continuity conditions between the half-space and the inclusions are satisfied in mean square-sense. Numerical results of the surface displacement field are evaluated for single and two elliptic inclusions. The results show the following: 1. Presence of subsurface inhomogeniety may lead to large amplifications of the surface ground motion; 2. Different surface displacement patterns emerge for different incident waves; 3. Presence of additional inclusion may change significantly the surface displacement response of a single inclusion; 4. The surface motions

*Earthquake Engineering and Structural Dynamics, Vol.11, 313-335 (1983).

extremes strongly depend upon (i) angle of incidence; (ii) frequency of incident field; (iii)embedment depth of the inclusions; (iv) separation distance between the inclusions; (v) material properties of the half-space and the inclusions; and (vi) location of observation point on the surface of the half-space.

INTRODUCTION

The amplification of strong ground motion due to embedded elastic inclusions has not been fully resolved yet. However, it is believed that the subsurface (and/or surface) irregularities are very important factors in localized, amplification effects[1,2]. Observations from some recent earthquakes[3] indicate that the areas of damage can be highly localized. Furthermore, the intensity of ground motion can change substantially within a short distance[4]. Therefore, in order to understand in detail the basic phenomena that occur in soil motion amplification due to local irregularities in the soil, it is necessary to develop methods capable of predicting surface motion at certain sites for a given input.

Diffraction of waves by elastic inclusion embedded into an elastic half-space has been receiving considerable attention lately. For references on this topic, reader is referred to the articles by author[5,6] in which diffraction of elastic waves by an alluvial valley was considered. A boundary integral method was employed to derive displacement field throughout the elastic medium. The method originally proposed by Copley[7] has been applied to problems of strong ground motion seismology by Wong[8], Sanchez-Sesma and Rosenblueth[9], Sanchez-Sesma and Esquivel[10], Apsel[11] and Dravinski[12].

In present paper the boundary integral method is applied to investigate amplification of elastic waves due to elastic inclusions of

arbitrary shape embedded into a half-space.

Statement of Problem

Geometry of the problem is depicted by Fig. 1. Elastic inclusions D_1, D_2, ..., D_R of arbitrary shape* are perfectly bonded to an elastic half-space D_o. Incident plane harmonic SH, P, SV, or Rayleigh wave strikes the inclusions causing deformation throughout the elastic medium. Factor exp ($i\omega t$) is understood. Material of the half-space and the inclusions is assumed to be homogeneous, linearly elastic, and isotropic. Throughout the analysis α, β and μ denote velocity of dilatational waves, velocity of equivoluminal waves, and the shear modulus, respectively.

Anti-Plane Strain Model. Equation of motion for steady-state wave motion is given by[13]

$$\left(\nabla^2 + k_j^2\right) w_j(x,y,\omega) = 0 \quad ; \quad j=0,1,2,\ldots,R; \quad \nabla^2 \equiv \frac{\partial^2}{\partial x^2} + \frac{\partial^2}{\partial y^2} \qquad (1)$$

where the subscript 0 refers to the half-space, and the subscripts 1, 2, ..., R refer to the elastic inclusions. Wave number is denoted by k, ω represents the circular frequency, and w represents the only non-zero component of displacement field acting along the z-axis.

Boundary conditions along the surface of the half-space are given by

*Inclusions are assumed to be sufficiently smooth with no sharp corners being present.

$$\frac{\partial w}{\partial y} = 0 \ , \text{ at } y = 0 \tag{2}$$

For the sake of simplification, an anti-plane strain elastodynamic state $\underset{\sim}{s}^T(\underline{r})$ is introduced along some surface C

$$\underset{\sim}{s}^T(\underline{r}) \equiv [w(\underline{r}), \sigma_{nz}(\underline{r})]; \quad \underline{r} \in C, \tag{3}$$

where T, $\underline{n}$, $\underline{r}$, and σ_{nz} denote the transpose, unit normal vector on C, position vector, and component of a stress tensor, respectively.

Perfect bonding along the interfaces C_j, j=1,2,...,R between the half-space and the inclusions requires continuity of displacement and stress field what in terms of elastodynamic state $\underset{\sim}{s}$ can be written as

$$\underset{\sim}{s}_o(\underline{r}) = \underset{\sim}{s}_j(\underline{r}); \ \underline{r} \in C_j; \ j=1,2,...,R; \ R=1,2,... \ . \tag{4}$$

Incident wave is assumed to be

$$w^{inc} = \exp[-i\, k_o(x \sin\theta_o - y \cos\theta_o)]; \ i \equiv \sqrt{-1}, \tag{5}$$

with θ_o being the angle of incidence (see Fig. 1).

Plane Strain Model. Steady-state motion for this model is governed by[13]

$$\nabla^2 \begin{Bmatrix} \phi_j \\ \psi_j \end{Bmatrix} + \begin{Bmatrix} h_j^2 & \phi_j \\ k_j^2 & \psi_j \end{Bmatrix} = 0 \quad , \quad j=0,1,2,\ldots,R; \; R=1,2,\ldots, \tag{6}$$

where ϕ and ψ represent dilatational and equivoluminal waves, respectively with corresponding wave numbers h and k. Boundary conditions are of the form

$$\left.\begin{aligned} \sigma_{xy0} &= 0 \\ \sigma_{yy0} &= 0 \end{aligned}\right\} \quad \text{for } y = 0 \tag{7a, 7b}$$

Analogously to the anti-plane strain model a plane strain elastodynamic state $\underset{\sim}{q}^T(\underset{\sim}{x})$ is introduced along some surface C

$$q^T(x) \equiv [u(x), v(x), \sigma_{nn}(x), \sigma_{nt}(x)] \quad ; \quad x \in C, \tag{8}$$

where u, v, σ_{nn}, and σ_{nt} denote displacement component along the x and y-axis, and normal and tangential component of a stress tensor, respectively. Consequently, perfect bonding along the interfaces implies

$$\underset{\sim}{q}_o(\underset{\sim}{x}) = \underset{\sim}{q}_j(\underset{\sim}{x}) \; ; \; \underset{\sim}{x} \in C_j \; ; \; j=1,2,\ldots,R \; ; \; R=1,2,\ldots \quad . \tag{9}$$

Incident P-wave is specified by

$$\phi^{inc} = \frac{i}{h_o} \exp[-ih_o(x \sin\theta_o - y \cos\theta_o)] \tag{10}$$

and incident SV-wave is chosen to be

$$\psi^{inc} = -\frac{i}{k_o} \exp[-ik_o(x \sin\theta_o - y \cos\theta_o)]. \tag{11}$$

Incident Rayleigh wave is of the form[14]

$$u^{inc} = \exp(-i\kappa_o x)\left[\exp(-b_L y) - \tfrac{1}{2}\left(2 - \frac{c_o^2}{\beta_o^2}\right)\exp(-b_T y)\right] \tag{12a}$$

$$v^{inc} = i\kappa_o \exp(-i\kappa_o x)\left[-\frac{b_L}{\beta_o^2}\exp(-b_L y) + \frac{1}{2b_T}\left(2 - \frac{c_o^2}{\beta_o^2}\right)\right]^{\frac{1}{2}}, \tag{12b}$$

$$b_L \equiv \kappa_o\left(1 - \frac{c_o^2}{\alpha_1^2}\right)^{\frac{1}{2}} ; \quad b_T \equiv \kappa_o\left(1 - \frac{c_o^2}{\beta_o^2}\right)^{\frac{1}{2}} \tag{12c}$$

where c and κ denote the Rayleigh wave velocity and the wave number, respectively.

Solution of Problem

Anti-Plane Strain Model. Total wave field in the half-space and within the elastic inclusions is specified by

$$w_o = w^{inc} + w_o^s \; ; \; \underset{\sim}{r} \in D_o \tag{13a}$$

$$w_j = w_j^s \; ; \; \underset{\sim}{r} \in D_j \; ; \; j=1,2,\ldots,R \; ; \; R=1,2,\ldots \; , \tag{13b}$$

where the superscript s denotes the scattered wave field. The scattered waves are expressed in terms of single layer potentials[15]

$$w_o^s(\underset{\sim}{r}) = \sum_{j=1}^{R} \int_{C_j^-} g_{oj}(\underset{\sim}{r}_o)\, G_o(\underset{\sim}{r},\underset{\sim}{r}_o)\, d\underset{\sim}{r}_o \; ; \; R=1,2,\ldots; \; \underset{\sim}{r} \in D_o \tag{14a}$$

$$w_j^s(\underset{\sim}{r}) = \int_{C_j^+} g_j(\underset{\sim}{r}_o)\, G_j(\underset{\sim}{r},\underset{\sim}{r}_o)\, d\underset{\sim}{r}_o \; ; \; j=1,2,\ldots,R; \; R=1,2,\ldots, \; \underset{\sim}{r} \in D_j \tag{14b}$$

where surfaces C_j^+ and C_j^-, $j=1,2,\ldots,R$ are defined inside and outside of the corresponding interface C_j, $j=1,2,\ldots,R$[5], and $G_j(\underset{\sim}{r},\underset{\sim}{r}_o)$; $j=0,1,\ldots,R$ are the Green's functions for a line load in the half-space (which are known explicitely[5]). Density functions g_{oj} and g_j, $j=1,2,\ldots,R$ are yet to be determined.

It is obvious from Eqs. 14a,b that the scattered wave field satisfies equations of motion (1) and stress free boundary conditions (2). The unknown density functions g_{oj} and g_j, $j=1,2\ldots,R$ are to be determined through use of the continuity conditions (4). As incident wave strikes the interfaces between the half-space and the inclusions, it is partially reflected back to the half-space and partially transmitted into the inclusions. The interfaces C_j, $j=1,2,\ldots,R$ can be viewed as the location of sources which create reflected and transmitted wave fields. For the sake of simplification, it is proposed to place those sources slightly inside (outside) of the interfaces. Thus, by C_j^- and C_j^+, $j=1,2,\ldots,R$ the inner and outer source surface with respect to interface C_j is understood. For more details on that procedure, the

reader is reffered to a paper by the author[5]. In the present paper it is assumed that the inner (outer) source surface $C_j^-(C_j^+)$, j=1,2,...,R is obtained by simple scaling of the corresponding interface C_j, i.e., by multiplying the coordinates of the interface points by a factor smaller (greater) than unity. If one assumes the density functions in the form of discrete line sources, it follows then

$$g_{oj} = \sum_{m_j=1}^{M_j} a_{m_j}^{o} \, \delta(|\underset{\sim}{r} - \underset{\sim}{r}_{m_j}|); \; \underset{\sim}{r}_{m_j} \in C_j^- \; ; \; j=1,2,\ldots,R; \; R=1,2,\ldots \qquad (15a)$$

$$g_j = \sum_{l_j}^{L_j} b_{l_j}^{j} \, \delta(|\underset{\sim}{r} - \underset{\sim}{r}_{l_j}|) \; ; \; \underset{\sim}{r}_{l_j} \in C_j^+ \; ; \; j=1,2,\ldots,R; \; R=1,2,\ldots, \qquad (15b)$$

where intensities of the sources $a_{m_j}^{o}$ and $b_{l_j}^{j}$ are still to be determined for all j, m_j, and l_j. Substitution of equations (15a,b) into equations (12a,b) provides the scattered wave field in the following form

$$w_o^s(\underset{\sim}{r}) = \sum_{j=1}^{R} \sum_{m_j=1}^{M_j} a_{m_j}^{o} \, G_o(\underset{\sim}{r},\underset{\sim}{r}_{m_j}) \; ; \; \underset{\sim}{r}_{m_j} \in C_j^- \; ; \; \underset{\sim}{r} \in D_o \qquad (16a)$$

$$w_j^s(\underset{\sim}{r}) = \sum_{l_j=1}^{L_j} b_{l_j}^{i} \, G_j(\underset{\sim}{r},\underset{\sim}{r}_{l_j}) \; ; \; \underset{\sim}{r}_{l_j} \in C_j^+ \; ; \; j=1,2,\ldots,R, \; \underset{\sim}{r} \in C_j, \qquad (16b)$$

where M_j and L_j, j=1,2,...,R represent the number of sources along the j-th inner and outer source surface, respectively. Choosing N_j "observation" points along each of the interface C_j, j=1,2,...,R the unknown source intensities are determined through the continuity condition (4) in the least-square-sense[16]

$$[\underset{\sim}{a}_1^T \; \underset{\sim}{a}_2^T \cdots \underset{\sim}{a}_R^T \; \underset{\sim}{b}_1^T \cdots \underset{\sim}{b}_R^T]^T = (\underset{\sim}{A}^* \underset{\sim}{A})^{-1} \underset{\sim}{A}^* \underset{\sim}{f}, \tag{17a}$$

where * denotes the transpose complex conjugate, matrices $\underset{\sim}{A}$ and $\underset{\sim}{f}$ are defined in Appendix A, and intensity coefficient vectors are defined by

$$\underset{\sim}{a}_j \equiv [a^o_{m_j}] \; ; \; m_j = 1,2,\ldots,M_j \; ; \; j=1,2,\ldots,R \; ; \; R=1,2,\ldots \tag{17b}$$

$$\underset{\sim}{b}_j \equiv [b^j_{l_j}] \; ; \; l_j = 1,2,\ldots,L_j. \tag{17c}$$

Once the source intensities are known, total wave field can be determined through equations (16a,b) and (13a,b).

Plane Strain Model. Total displacement field in the half-space and within the inclusions is specified by

$$\underset{\sim}{u}_o = \underset{\sim}{u}^{inc} + \underset{\sim}{u}^s_t \qquad ; \; \underset{\sim}{r} \in D_o \tag{18a}$$

$$\underset{\sim}{u}_j = \underset{\sim}{u}^s_j \quad ; \; \underset{\sim}{r} \in D_j \quad ; \; j=1,2,\ldots,R; \; R=1,2,\ldots, \tag{18b}$$

where displacement vector $\underset{\sim}{u}$ is defined in terms of displacement components by $\underset{\sim}{u}^T = [u,v]$ and superscript s denotes the scattered wave field. Unknown scattered waves are assumed to be expressed in terms of

single layer potentials[15]. Therefore,

$$\phi_o^s(\underline{r}) = \sum_{j=1}^{R} \int_{C_j^-} g_{oj}^{\phi}(\underline{r}_o)\ \phi_o(\underline{r},\underline{r}_o)d\underline{r}_o ;\ \underline{r} \in D_o\ ;\ R=1,2,... \tag{19a}$$

$$\psi_o^s(\underline{r}) = \sum_{j=1}^{R} \int_{C_j^-} g_{oj}^{\psi}\ (\underline{r}_o)\ \psi_o(\underline{r},\underline{r}_o)\ d\underline{r}_o \tag{19b}$$

$$\phi_j^s(\underline{r}) = \int_{C_j^+} g_j^{\phi}(\underline{r})\ \phi_j(\underline{r},\underline{r}_o)\ d\underline{r}_o\ ;\ \underline{r} \in D_j\ ;\ j=1,2,...,R\ ;\ R=1,2,... \tag{19c}$$

$$\psi_j^s(\underline{r}) = \int_{C_j^+} g_j^{\psi}(\underline{r}_o)\ \psi_j(\underline{r},\underline{r}_o)\ d\underline{r}_o\ ;\ \underline{r} \in D_j\ ;\ j=1,2,...,R\ ;\ R=1,2,..., \tag{19d}$$

where the surfaces C_j^{-+}, j=1,2,...,R have been defined in the anti-plane strain model and density functions g_{oj}^{ϕ}, g_{oj}^{ψ}, g_j^{ϕ}, and g_j^{ψ}, j=1,2,...,R are still to be determined. The Green's functions $\phi_j(\underline{r},\underline{r}_o)$ and $\psi_j(\underline{r},\underline{r}_o)$; j=0,1,2,...,R correspond to dilatational and equivoluminal line source in a half-space with stress free boundary, respectively. For explicit solution for the Green's functions the reader is referred to the paper by Lamb[17]. Following the procedure already discussed for the anti-plane strain model, the density functions are assumed of the form

$$g_{oj}^{\phi} = \sum_{m_j=1}^{M_j} a_{m_j}^{o}\ \delta(|\underline{r} - \underline{r}_{m_j}|)\ ;\ \underline{r}_{m_j} \in C_j^-\ ;\ j=1,2,...,R \tag{20a}$$

$$g_{oj}^{\psi} = \sum_{m_j=1}^{M_j} a_{m_j}^{-o}\ \delta(|\underline{r} - \underline{r}_{m_j}|) \tag{20b}$$

$$g_j^{\phi} = \sum_{l_j=1}^{L_j} b_{l_j}^{j} \, \delta(|\underline{r} - \underline{r}_{l_j}|); \; \underline{r}_{l_j} \in C_j^{+} \; ; \; j=1,2,\ldots,R \tag{20c}$$

$$g_j^{\psi} = \sum_{l_j=1}^{L_j} b_{l_j}^{j} \, \delta(|\underline{r} - \underline{r}_{l_j}|). \tag{20d}$$

Substitution of equations (20a-d) into equations (19a-d) leads to the scattered wave field

$$\phi_o^s(\underline{r}) = \sum_{j=1}^{R} \sum_{m_j=1}^{M_j} a_{m_j}^{o} \, \phi_o(\underline{r},\underline{r}_{m_j}) \; ; \; \underline{r}_{m_j} \in C_j^{-} \; ; \; \underline{r} \in D_o \tag{21a}$$

$$\psi_o^s(\underline{r}) = \sum_{j=1}^{R} \sum_{m_j=1}^{M_j} \bar{a}_{m_j}^{o} \, \psi_o(\underline{r},\underline{r}_{m_j}) \tag{21b}$$

$$\phi_j^s(\underline{r}) = \sum_{l_j=1}^{L_j} b_{l_j}^{j} \, \phi_j(\underline{r},\underline{r}_{l_j}) \; ; \; \underline{r}_{l_j} \in C_j^{+} \; ; \; \underline{r} \in D_j \; ; \; j=1,2,\ldots,R \tag{21c}$$

$$\psi_j^s(\underline{r}) = \sum_{l_j=1}^{L_j} \bar{b}_{l_j}^{j} \, \psi_j(\underline{r},\underline{r}_{l_j}), \tag{21d}$$

where M_j and L_j, $j=1,2,\ldots,R$ correspond to the number of sources placed along the source surface C_j^{-} and C_j^{+}, respectively. Choosing M_j observation points along each of the interface C_j the unknown source intensities are determined through the continuity condition (9) in the least-square-sense

$$[\underline{a}_1^T \bar{\underline{a}}_1^T \cdots \underline{a}_R^T \bar{\underline{a}}_R^T \underline{b}_1^T \bar{\underline{b}}_1^T \cdots \underline{b}_R^T \bar{\underline{b}}_R^T] = (\underline{G}^* \underline{G})^{-1} \underline{G}^* \underline{f} \tag{22a}$$

where the coefficient vectors are introduced through

$$\underline{a}_j \equiv [a^o_{m_j}] \; ; \; m_j = 1,2,\ldots,M_j \; ; \; j=1,2,\ldots,R \; ; \; R=1,2,\ldots \tag{22b}$$

$$\bar{\underline{a}}_j \equiv [\bar{a}^o_{m_j}] \tag{22c}$$

$$\underline{b}_j \equiv [b^j_{l_j}] \; ; \; l_j = 1,2,\ldots,L_j \; ; \; j=1,2,\ldots,R \; ; \; R=1,2,\ldots \tag{22d}$$

$$\bar{\underline{b}}_j \equiv [\bar{b}^j_{l_j}]. \tag{22e}$$

Matrix $\underline{G}$ and vector $\underline{f}$ are listed in Appendix A.

The most difficult part in the plane strain model is evaluation of the Green's functions for an equivoluminal and dilatational line load embedded in a half-space. According to the papers by Lamb[17] and Lapwood[18], use of contour integration allowed representation of the Green's functions in a form which is convenient for numerical evaluation[12]. Knowledge of the Green's functions incorporated in equations (21a-d) allows then study of the effects of incident plane P, SV, and Rayleigh waves upon the surface response of the half-space which

contains embedded elastic inclusions of arbitrary shape.

Evaluation of Results

Single Inclusion

In case of single inclusion, the amplitude of the surface displacement field is evaluated for different incident waves and elliptical elastic inclusion, i.e.,

$$C_1: \quad x = R_1 \cos\theta \; ; \; y = R_2 \sin\theta + H \; ; \; 0 \leq \theta \leq 2\pi \qquad (23)$$

where R_1 and R_2 are the principal axes and H is embedment depth of the inclusion. In order to reduce the number of parameters the principal axis are assumed to be fixed ($R_1:R_2 = 2:1$; $R_1 = 4$). For plane-strain-model the results are presented normalized with respect to the surface amplitude of the free-field, i.e., $(|u^{ff}|^2 + |v^{ff}|^2)^{1/2}$.

For convenience, the dimensionless frequency is introduced, $\Omega = 2R_1 / \lambda^{inc}$, as the ratio of the total width of the inclusion and the wavelength of the incident wave.

Incident Plane SH-Wave. According to equations (16a,b) and (13a,b) total displacement field in the half-space and inclusion is specified by

$$w_o(\underline{r}) = w^{inc}(\underline{r}) + \sum_{m_1=1}^{M_1} a^o_{m_1} G_o(\underline{r},\underline{r}_{m_1}) \; ; \; \underline{r} \in D_o \; ; \; \underline{r}_{m_1} \in C_1^- \qquad (23a)$$

$$w_1(\underline{r}) = \sum_{l_1=1}^{L_1} b^1_{l_1} G_1(\underline{r},\underline{r}_{l_1}) \; ; \; \underline{r} \in D_1 \; ; \; \underline{r}_1 \in C_1^+ \, , \qquad (23b)$$

where the source intensities $a^o_{m_1}$ and $b^1_{l_1}$ are evaluated through equation (17a). By increasing the number of observation points N_1 along interface C_1 and number of sources M_1 and L_1 along C_1^- and C_1^+, respectively, one can determine for which M, L, and N the convergence of the results is achieved[5]. This means that further increase in the number of observation and source points will not change the value of the results appreciably.

Surface displacement amplitude depicted by Fig. 2a,b corresponds to frequency $\Omega = 1$ and two embedment depths. It is obvious from Fig. 2a,b that the presence of elastic inclusion results in surface displacement pattern which is different from the free-field response along the surface of the half-space. Furthermore, it appears that embedment depth of the inclusion strongly effects surface ground motion. It is interesting to observe that surface displacement peaks may occur at different locations for different embedment depths. The same phenomenon is observed when the frequency of the incident field changes (as will be shown later).

Incident Plane P-Wave. For single inclusion in the half-space total displacement potentials are specified by

$$\phi_o(\underset{\sim}{r}) = \phi^{inc}(\underset{\sim}{r}) + \sum_{m_1=1}^{M_1} a^o_{m_1} \phi_o(\underset{\sim}{r},\underset{\sim}{r}_{m_1}) \; ; \; \underset{\sim}{r} \in D_o \; ; \; \underset{\sim}{r}_{m_1} \in C_1^- \tag{24a}$$

$$\psi_o(\underset{\sim}{r}) = \sum_{m_1=1}^{M_1} \bar{a}^o_{m_1} \psi_o(\underset{\sim}{r},\underset{\sim}{r}_{m_1}) \tag{24b}$$

$$\phi_1(\underset{\sim}{r}) = \sum_{l_1=1}^{L_1} b^1_{l_1} \phi_1(\underset{\sim}{r},\underset{\sim}{r}_{l_1}) \; ; \; \underset{\sim}{r} \in D_1 \; ; \; \underset{\sim}{r}_{l_1} \in C_1^+ \tag{24c}$$

$$\psi_1(\underset{\sim}{r}) = \sum_{l_1=1}^{L_1} \bar{b}^1_{l_1} \psi_1(\underset{\sim}{r},\underset{\sim}{r}_{l_1}); \tag{24d}$$

where the source intensities are calculated by equation (22a) and incident dilatational wave field is specified by equation (10).

Normalized amplitude of horizontal and vertical component of the surface displacement field for incident P-wave is shown by Fig. 3. For comparison purposes, the angle of incidence, frequency of incoming wave and embedment depths are chosen to be identical to those of the anti-plane strain model (Fig. 2). Results of Fig. 3 indicate that surface displacement field exhibits more complex pattern than in the corresponding anti-plane strain model. Presence of elastic inclusion is "detected" better than in corresponding anti-plane strain model. This difference may be explained as follows: For anti-plane strain model,

the motion of the media is caused only by the resultant shearing force or the zeroth order moment of the shearing stresses. In the case of the plane strain model, the resultant force and the moment, i.e., the zeroth and first order moments of the stresses, determine the surface response. Consequently, one would expect the presence of an inclusion to be more pronounced in the surface response for incident P(SV) waves than in the corresponding case of incoming SH-wave. This is an analog result to the one obtained by Umek[13] in analysis of rigid foundation response embedded in a half-space.

Change of angle of incidence to 80° resulted in the surface displacement fields shown by Fig. 4. It is evident from Figs. 3 and 4 that surface ground motion depends very much upon the angle of incidence.

Incident Plane SV-Wave. Displacement potentials in this case can be obtained from the ones specified by equations (24a-d) if the appropriate change of incident field is done. Surface displacement amplitude field depicted by Figs. 5 and 6 correspond to the same material properties, frequency, angle of incidence and embedment depth as in the case of P-wave results shown by Figs. 3 and 4, respectively. It can be seen from Fig. 6 that presence of elastic inclusion may result locally in very large amplification of surface motion. It is of interest to observe from Figs. 2-6 that the presence of the elastic inclusion does not necessarily result in the so-called "shielding" effect for the part

the surface of the half-space which is in "shade" of the inclusion relative to the incident wave.

Incident Rayleigh Wave. Displacement field in this case is given by the following equations

$$u_o(\underline{r}) = u^{inc}(\underline{r}) + \sum_{m_1=1}^{M_1} \left\{ a^o_{m_1} U^{\phi}_o(\underline{r},\underline{r}_{m_1}) + a^o_{m_1} U^{\psi}_o(\underline{r},\underline{r}_{m_1}) \right\} \tag{25a}$$

$$v_o(\underline{r}) = v^{inc}(\underline{r}) + \sum_{m_1=1}^{M_1} \left\{ a^o_{m_i} v^{\phi}_o(\underline{r},\underline{r}_{m_1}) + \bar{a}^o_{m_1} v^{\psi}_o(\underline{r},\underline{r}_{m_1}) \right\}, \quad \underline{r} \in D_o; \tag{25b}$$

$$\underline{r}_{m_1} \in C_1^-$$

$$u_1(\underline{r}) = \sum_{l_1=1}^{L_1} \left\{ b^1_{l_1} u^{\phi}_1(\underline{r},\underline{r}_{l_1}) + \bar{b}^1_{l_1} u^{\psi}_1(\underline{r},\underline{r}_{l_1}) \right\} ; \underline{r} \in D_i; \ \underline{r}_{l_1} \in C_1^+ \tag{25c}$$

$$v_1(\underline{r}) = \sum_{l_1=1}^{L_1} \left\{ b^1_{l_1} v^{\phi}_1(\underline{r}_1,\underline{r}_{l_1}) + \bar{b}^1_{l_1} v^{\psi}_1(\underline{r},\underline{r}_{l_1}) \right\}, \tag{25d}$$

where u^{inc} and v^{inc} are specified by equations (12a–c) and the source intensities are determined formally by equation (22a). For the Green's functions $u(\underline{r},\underline{r}_o)$ and $v(\underline{r},\underline{r}_o)$ in equations (25a–d) the superscripts ϕ and ψ denote dilatational and equivoluminal line source, respectively.

Normalized surface displacement amplitude for incident Rayleigh waves is shown by Fig. 7. Comparison of Figs. 3–7 indicates that the Rayleigh wave surface response is comparable in amplitude with those of

incident P or SV waves for small embedment depth of the inclusion. In the case of larger embedment depth, surface response is essentially the free-field one since the incident Rayleigh wave decays exponentially with increasing depth. From the results of Fig. 7 it follows that by measuring surface response due to Rayleigh waves, it would be possible to "detect" the presence of the elastic inclusion, provided the embedment depth of the inclusion is not very large.

Therefore, the effect of a single inclusion upon the surface displacement field can be summarized as follows: 1. Displacement field is strongly influenced by the presence of an inclusion provided the embedment depth is not too large; 2. P or SV wave response appears to "detect" better the presence of an inclusion compared to the corresponding SH-wave response.

This concludes the evaluation of results for the single-inclusion-model. The two-inclusion-model is considered next.

Two Inclusions

For two inclusion-model surface displacement amplitude is evaluated numerically for two elliptical inclusions with the first one specified by equation (23) and the second one defined through

$$C_2 : x = R_1 \cos\theta - D \quad ; \quad y = R_2 \sin\theta = H \quad ; \quad 0 \leq \theta \leq 2\pi, \tag{26}$$

where D denotes separation distance between the inclusions. For the sake of reducing the number of parameters in the problem, the inclusions are assumed to be identical in shape with the same embedment depth. In order to examine in more detail the influence of additional inclusion upon the surface motion numerical results for two inclusions are evaluated for incident SH-wave only.

Total displacement field in the half-space and within the two inclusions is specified by

$$w_o(\underline{r}) = w^{inc}(\underline{r}) + \sum_{m_1=1}^{M_1} a^o_{m_1} G_o(\underline{r},\underline{r}_{m_1}) + \sum_{m_2=1}^{M_2} a^o_{m_2} G_o(\underline{r},\underline{r}_{m_2}) \tag{27a}$$

$$\underline{r}_{m_1} \in C_1^- \; ; \; \underline{r}_{m_2} \in C_2^- \; ; \; \underline{r} \in D_o$$

$$w_1(\underline{r}) = \sum_{l_1=1}^{L_1} b^1_{l_1} G_1(\underline{r},\underline{r}_{l_1}) \quad ; \quad \underline{r}_{l_1} \in C_1^+ \quad ; \quad \underline{r} \in D_1 \tag{27b}$$

$$w_2(\underline{r}) = \sum_{l_2=1}^{L_2} b^2_{l_2} G_2(\underline{r},\underline{r}_{l_2}) \quad ; \quad \underline{r}_{l_2} \in C_2^+ \quad ; \quad \underline{r} \in D_2 \tag{27c}$$

where the source intensities are determined formally by equation (17a).

As earlier, the dimensionless frequency ($\Omega = 2R_1/\lambda^{inc}$) is introduced as the ratio of the total width of the inclusion and the wavelength of the incident field. The principal axis (R_1 and R_2) are assumed to be fixed. The embedment depth (H), separation distance (D), frequency (Ω), and angle of incidence (θ_o) are all being varied. Reference frequency for the surface response is chosen to be twice that of the single inclusion model, i.e., $\Omega = 2$.

For comparison purpose, the case of a single inclusion is considered first. Surface displacement amplitude depicted by Fig. 8 corresponds to a single elliptical inclusion width shallow (deep) embedment depth. By increasing the number of "observation" and "source" points until the surface displacement amplitude remained unchanged, it is determined that the convergence of the results is achieved at $N_1 = 45$, and $M_1 = L_1 = 23$ (See Eqs. 16 and 17). In case of two elastic inclusions, number of "observation" and "source" points is chosen to be: $N_1 = N_2 = 45$ and $M_1 = L_1 = M_2 = L_2 = 23$.

Surface displacement field shown by Fig. 9a corresponds to the case of shallow embedment depth. Surface motion atop both inclusions are similar to that of a single-inclusion-response of Fig. 8a. This implies that the mutual interaction between the inclusions is rather small. Increase in embedment depth resulted in surface motion shown by Fig. 9b. Evidently, the response atop illuminated inclusion and inclusion in shade are very different from each other. Strong shielding effect can be observed atop inclusion in shade. (Terms "illuminated" and "in

shade" pertain to inclusions D_1 and D_2, respectively. See Fig. 1 for details). Increase in separation distance (D) between the inclusions produced surface motion shown by Figs. 10a and b. The results of Figs. 10a and b are similar to those of Figs. 9a and b: smaller embedment depth leads to very little interaction between the inclusions while the larger embedment depth results in greater change of the surface motion atop inclusion in shade than atop the illuminated inclusion. As expected, increase in separation distance between inclusions reduced their mutual interaction considerably.

For surface displacement results presented so far, it can be observed that the response atop illuminated inclusion is closer to that atop a single-inclusion-response than the response atop inclusion in shade. This occurs most likely due to scattered wave field from illuminated inclusion which interacts with inclusion in shade together with incident wave field. The wavefield ahead of illuminated inclusion is basically the free-field motion which explains the similarity of the response atop illuminated inclusion and response atop the single-inclusion-model.

Case of more contrasting materials for the half-space and the inclusions is presented by Fig. 11. It is interesting to observe that peak amplitude which occurs in Fig. 9b atop the leading edge of inclusion in shade is observed in Fig. 11 atop the leading edge of illuminated inclusion. Thus, change of material properties of the half-space and the inclusions may result in dramatic change of the

surface displacement pattern. Comparison of Figs. 9b and 11 indicate overall more rapid oscillation with x of the surface response for more contrasting materials of the half-space and the inclusions. Therefore, one has to check the number of "observation" and "source" points needed for convergence. Testing of the boundary integral method used in present work shows[5] that increase of the frequency requires increase of "observation" and "source" points in order to maintain the accuracy of the results. Therefore, in order to describe rapid oscillations of the response with distance accurately, it may be necessary to increase the number of "observation" and "source" points accordingly.

Results presented so far clearly indicate that models involving several scatterers may predict quite different surface displacement patterns when compared to the single-scatterer-models. Special attention should be given to interpretation of the displacement field measured during actual earthquake. Presented results indicate the importance of location of measuring station relative to inhomogenieties below the earth surface. Different instruments geometrically close to each other may record substantially different magnitude of the surface ground motion. During several recent earthquakes[3,4], it was observed that the earthquake damage can be highly localized. As early as 1957 this phenomenon is attributed by Kanai[20] to be caused in part by inhomogenieties of the soil media and in part by surface and/or subsurface topography at the site.

After this brief investigation of the role of the embedment depth

and separation distance upon the surface response, the attention is focused on the sensitivity of the surface motion upon the frequency and angle of incidence of the incoming wave. For this purpose, the embedment depth (H) and the separation distance (D) are assumed to be fixed. The angle of incidence (θ_o) is being changed from vertical incidence (0^o) to grazing incidence (90^o) in increments of 30^o. Eight characteristic stations are chosen at the surface of the half-space for calculation of the displacement amplitude. The stations are specified by the coordinates: $y = 0$, $X/R_1 = -5, -4, -3, -2, -1, 0, 1,$ and 2 and they are labeled one through eight, respectively.

Absolute value of surface displacement at station one for four angles of incidence is depicted by Fig. 12a. (For the sake of clarity, the angle of incidence θ_o is written in the upper right corner of each figure). Station one is chosen to be to the left of the leading edge of the illuminated inclusion, on the surface of the half-space. Calculation of the station-one-response should demonstrate how far the scattered wave field will reach (with appreciable magnitude) ahead of the illuminated inclusion. It can be seen from Fig. 12a that at station one for all four angles of incidence and wide range of frequencies the response is essentially the free-field one. For angles of incidence approaching the grazing incidence, the presence of elastic inclusions is detected at higher frequencies only.

Station two is located atop the leading edge of the illuminated inclusion. Corresponding surface displacement amplitude is shown by

Fig. 12b. For vertical incidence the presence of the scattered waves in the surface response amplitude at station two is felt strongly. For other angles of incidence the deviation from the free-field-results is fairly small with exception of the grazing incidence at higher frequencies, where substantial departure from the free-field pattern can be observed. For observation stations closer to inclusions, one expects intuitively stronger influence of the scattered wave field upon the station response when compared to the stations away from the inclusions. This expectation is verified through results of Fig. 13a which correspond to the station three placed atop the center of the illuminated inclusion. It is evident that the response at the station three is strongly dependent upon the presence of elastic inclusions for wide range of frequencies and all four angles of incidence. In particular, for vertical and near vertical incidence ($\theta_o = 0^o, 30^o$) change in frequency of the incoming wave may produce very different surface displacement amplitude. Similarly, for the same frequency and various angles of incidence the surface motion may be significantly changed (e.g., $\Omega = 2$; $\theta_o = 0^o$ and 90^o).

Station four is located atop the trailing edge of the illuminated inclusion. Corresponding surface displacement pattern is presented by Fig. 13b. Surface response appears to be very sensitive upon the presence of the inclusions and change of angle and frequency of the incoming wave. It is interesting to observe large reduction of surface motion at station four for grazing incidence and moderate frequencies. Comparison of Figs. 12b and 13b indicates different amplification

patterns at the stations atop the leading and trailing edge of the illuminated inclusion for nonvertical angle of incidence. This difference in response at stations two and four is particularly present for grazing incidence. Station atop the trailing edge experiences strong shielding effect compared to the station atop the leading edge where this effect is not detected ($1.8 < \Omega < 2.8$). This is not a surprising result since station four is in the wake of the illuminated inclusion. Consequently, one expects the same phenomenon to be observed at stations five through eight. Indeed, the displacement field results at stations five through eight shown in Figs. 14a,b - 15a,b, respectively, demonstrate occurrence of possible strong shielding effects for different angles of incidence and at different frequencies. Still, at the same stations large amplification of surface ground motion may be possible. The results of Figs. 14a,b - 15a,b clearly indicate that it would be very difficult to characterize the surface strong ground motion at a station by a single parameter of the problem model employed. Rather, a combination of parameters are needed to describe surface ground motion more precisely. For example, at station nine and for grazing incidence, very strong reduction of surface motion can be observed near frequency $\Omega = 3$. For the same station and vertical incidence surface displacement amplitude is essentially the free-field one. On the other hand, for the same station and grazing incidence change of frequency of the incoming wave may result in dramatic change in amplification of the surface ground motion. This can be explained in terms of interaction of incident and scattered waves. The two may interact constructively (destructively) at the observation station thus

resulting in corresponding amplification (reduction) of the surface ground motion. Parameters which effect the two wave fields may influence their interaction and thus effect the surface strong ground motion. Of course, the present model is idealization of the realistic earth media. Still, it provides some insight into coaplex phenomenon of strong ground motion amplification due to subsurface inhomogeneities which may be of use in studies of more realistic models.

On Numerical Evaluation of Results

Extensive testing of the boundary integral method used in the present paper has been done by the author using the known exact solutions available in literature. For example, cases of incident plane SH-waves upon semi-circular and semi-elliptical alluvial valleys were investigated for a wide range of parameters present in the problem. These results can be summarized as follows: a) Boundary integral method provides very good results for a wide range of frequencies; b) For a fixed number of sources the results are more accurate at lower frequencies; c) It was determined that a good choice of source surfaces (C_j^+ and C_j^- in this paper) is the one where they "follow" in shape interface C_j.

Conclusions

Strong ground motion results pertinent to single inclusion model indicate that amplification of surface motion may be strongly influenced by subsurface inhomogeniety, provided the embedment depth is small. The results indicate that surface response is different for different types of incident waves.

Results for the two-inclusion-model indicate that the surface response may be very different from the results in the single-inclusion-model. It is shown that the surface response depends upon several parameters of the problem, such as, angle of incidence, frequency of incoming wave, embedment depth, separation distance of the inclusions, material properties of the half-space and the inclusions, and the location of the observation station at the surface of the half-space. Change in any of the parameters will result in modification of the surface motion amplitude which may be very significant. In particular, the surface motion appears to be very sensitive upon the angle of incidence and frequency of incoming wave.

Although approximate, presented results indicate that the precise characterization of the surface motion amplification effects at a given site may require several parameters which would account for geometry of the model, nature of incident field and material properties of the problem under consideration.

Acknowledgement

This research was supported in part by a grant PFR-8009336 and part by a grant CEE-8119696 from the National Science Foundation.

Constructive criticism by a reviewer and suggestions by the editor R. W. Clough are greatly appreciated.

REFERENCES

1. K. Kanai and T. Tanaka, "On Microtremors, VIII", Bulletin of Earthquake Research Institute, Tokyo University, 39, 97-115 (1961).

2. D. M. Boore, "The Effect of Simple Topography on Seismic Waves: Implications for the Accelerations Recorded at Pacoima Dam, San Fernando Valley, California", Bulletin of Seismological Society of America, 63, No. 5, 1608-1609 (1973).

3. P. C. Jennings (editor), "San Fernando Earthquake of February 9, 1971", EERL-71-02, California Institute of Technology, Pasadena, CA (1971).

4. D. E. Hudson, "Local Distribution of Strong Eqr thquake Ground Motions", Bulletin of Seismological Society of America, 62, No. 6, 1765-1786 (1972).

5. M. Dravinski, "Scattering of SH Waves by Subsurface Topography", Journal of Engineering Mechanics Division, 108, No. 1, (1982).

6. M. Dravinski, "Influence of Interface Depth Upon Strong Ground Motion", Bulletin of Seismological Society of America, Vol. 72, No. 2, pp. 597-614 (1982).

7. L. A. Copley, "Integral Equation Method for Radiation for Radiation from Vibrating Surfaces", Journal of Accoustical Society of america, 41, No. 4, 807-816 (1967).

8. H. L. Wong, "Diffraction of P, SV, and Rayleigh Waves by Surface Topographies", Department of Civil Engineering, Report No. CE 79-05, University of Southern California, Los Angeles, (1979).

9. F. J. Sanchez-Sesma and E. Rosenblueth, "Ground Motions at Canyons of Arbitrary Shapes Under Incident SH waves", Earthquake Engineering and Structural Dynamics, 7, 441-450 (1979).

10. F. J. Sanchez-Sesma and J. A. Esquivel, "Ground Motion on Alluvial Valley Under Incident Plane SH Waves", Bulletin of Seismological Society of america, 69, No. 4, 1107-1120 (1979).

11. R. J. Apsel, Dynamic Green's Functions for Layered Media and Applications to Boundary Value Problems, Ph.D. Thesis, U. C. San Diego (1979).

12. M. Dravinski, "Scattering of Elastic Waves by an Alluvial

Valey of Arbitrary Shape", Department of Civil Engineering, Report No. CE 80-06, University of Southern California, Los Angeles (1980).

13. J. Miklowitz, The Theory of Elastic Waves and Waveguides, North Holland, Amsterdam (1978).

14. Y. C. Fung, Foundations of Solid Mechanics, Prentice Hall, Englewood cliffs, New Jersey, 1965.

15. F. Ursell, "On the Exterior Problem of Acoustics", Proceedings of Cambridge Philosophical Society, 74, 117-125 (1973).

16. B. Noble and J. W. Daniel, Applied Linear Algebra, McGraw-Hill, New York (1969).

17. H. Lamb, "On Propagation of Tremors Over the Surface of an Elastic Solid", Philosophical Transactions of the Royal society of London, Series A, 203, 1-42 (1904).

18. E. R. Lapwood, "The Disturbance Due to a Line Source in a Semi-infinite Elastic Medium", Philosophical Transactions of the Royal society of London, Series A, 247, 63-100 (1948).

19. A. Umek, "On the Influence of the Geometry of the Foundation on its Impulse Response", Journal of Applied Mechanics, 63, No. 2, 300-303 (1976).

20. K. Kanai, "The Requisite Conditions for Predominante Vibrations of Ground", Bulletin of Earthquake Research Institute, Tokyo University, 35, Tokyo, Japan, p. 457 (1957).

Appendix A

Matrix $\underset{\sim}{A}$ in equation (17a) of order $2(N_1 + N_2 + \ldots + N_R) \times (M_1 + M_2 + \ldots + M_R + L_1 + L_2 + \ldots + L_R)$ is defined by

$$\underset{\sim}{A} \equiv \begin{bmatrix} \underset{\sim}{S}^{o}_{N_1 M_1} & \underset{\sim}{S}^{o}_{N_1 M_2} & \cdots & \underset{\sim}{S}^{o}_{N_1 M_R} & -\underset{\sim}{Q}_{N_1 L_2} & \cdots & \underset{\sim}{Q}_{N_1 L_R} \\ \underset{\sim}{S}^{o}_{N_2 M_1} & \underset{\sim}{S}^{o}_{N_1 M_2} & \cdots & \underset{\sim}{S}^{o}_{N_2 M_R} & \underset{\sim}{Q}_{N_2 L_1} & -\underset{\sim}{S}^{2}_{N_2 L_2} & \cdots & \underset{\sim}{Q}_{N_2 L_R} \\ \vdots & & & & & & & \\ \underset{\sim}{S}^{o}_{N_R M_1} & \underset{\sim}{S}^{o}_{N_R M_2} & \cdots & \underset{\sim}{S}^{o}_{N_R M_R} & \underset{\sim}{Q}_{N_R L_1} & \underset{\sim}{Q}_{N_R L_2} & \cdots & -\underset{\sim}{S}^{R}_{N_R L_R} \end{bmatrix}, \tag{A1}$$

where matrix $\underset{\sim}{S}^{j}_{NM}$ of order $2N \times M$ is defined by

$$\underset{\sim}{S}^{i}_{N_j M_l} \equiv [\underset{\sim}{s}_i(\underset{\sim}{r}_{n_j}, \underset{\sim}{r}_{m_l})] \; ; \; n_j = 1,2,\ldots,N_j; \; m_l = 1,2,\ldots,M_l; \; \underset{\sim}{r}_{n_j} \in C_j; \; \underset{\sim}{r}_{m_l} \in C_l^{-}$$
$$i = 0,1,2,\ldots,R; \; R = 1,2,\ldots; \; j = 1,2,\ldots,R; \; l = 1,2,\ldots,R. \tag{A2}$$

The subscript/superscript i refers to domains D_i, $i = 0,1,2,\ldots,R$ (see Fig. 1), $\underset{\sim}{r}_{nj}$ refers to observation points C_j, and $\underset{\sim}{r}_m$ corresponds to source points along C_l^{-}.

Vector $\underset{\sim}{f}$ in equation (17a) of order $2(N_1 + N_2 + \ldots + N_R) \times 1$ is defined by

$$\underset{\sim}{f} \equiv - \begin{bmatrix} \underset{\sim}{s}_{N1} \\ \underset{\sim}{s}_{N2} \\ \vdots \\ \underset{\sim}{s}_{NR} \end{bmatrix} \; ; \; \underset{\sim}{s}_{N_j} \equiv \begin{bmatrix} \underset{\sim}{s}^{inc}(\underset{\sim}{r}_1) \\ \underset{\sim}{s}^{inc}(\underset{\sim}{r}_2) \\ \vdots \\ \underset{\sim}{s}^{inc}(\underset{\sim}{r}_{N_j}) \end{bmatrix} \; ; \; \underset{\sim}{r}_1, \underset{\sim}{r}_2, \ldots, \underset{\sim}{r}_{N_j} \in C_n; \; j = 1,2,\ldots,R. \tag{A3}$$

where $\underset{\sim}{s}$ is an elastodynamic state introduced by equation (3).

Matrix $\underset{\sim}{G}$ in equation (22a) of the order

$4(N_1 + N_2 + \ldots + N_R) \times 2(M_1 + M_2 + \ldots + M_R + L_1 + L_2 + \ldots + L_R)$ is defined by

$$\underset{\sim}{G} \equiv \begin{bmatrix} \underset{\sim}{Q}_{ON_1M_1} & \underset{\sim}{Q}_{ON_1M_2} & \cdots & \underset{\sim}{Q}_{ON_1M_R} & \underset{\sim}{Q}_{1N_1L_1} & \underset{\sim}{Q}_{N_1L_2} & \cdots & \underset{\sim}{Q}_{N_1L_R} \\ \underset{\sim}{Q}_{ON_2M_1} & \underset{\sim}{Q}_{ON_2M_2} & \cdots & \underset{\sim}{Q}_{ON_2M_R} & \underset{\sim}{Q}_{N_2L_1} & \underset{\sim}{Q}_{2N_2L_2} & \cdots & \underset{\sim}{Q}_{N_2L_R} \\ \vdots & & & & & & & \\ \underset{\sim}{Q}_{ON_RM_1} & \underset{\sim}{Q}_{ON_RM_2} & \cdots & \underset{\sim}{Q}_{ON_RM_R} & \underset{\sim}{Q}_{N_RL_1} & \underset{\sim}{Q}_{N_RL_2} & \cdots & \underset{\sim}{Q}_{RN_RL_R} \end{bmatrix} \qquad \text{(A4)}$$

where

$$\underset{\sim}{Q}_{iN_jM_1} \equiv \left[\underset{\sim}{Q}^{\phi}_{iN_jM_1} \; \underset{\sim}{Q}^{\psi}_{iN_jM_1} \right] \qquad \text{(A5)}$$

$$\underset{\sim}{Q}^{\phi}_{iN_jM_1} \equiv \left[q^{\phi}_i \left(\underset{\sim}{r}_{n_j}, \underset{\sim}{r}_{m_1} \right) \right] \; ; \; i=0,1,2,\ldots,R \; ; \; n_j=1,2,\ldots,N_j \quad j=1,2,\ldots,R \quad M_1=1,2,\ldots,M_1 \qquad \text{(A6)}$$

$$\underset{\sim}{Q}^{\psi}_{iN_jM_1} \equiv \left[q^{\psi}_i \left(\underset{\sim}{r}_{n_j}, \underset{\sim}{r}_{n_1} \right) \right] \; ; \; 1=1,2,\ldots,R \quad \underset{\sim}{r}_{n_j} \in C_j \quad \underset{\sim}{r}_{m_1} \in C_1 \qquad \text{(A7)}$$

superscripts ϕ and ψ refer to field quantities associated with Green's functions for dilatational and equivoluminal line source, respectively. Thus $\phi_i(\underset{\sim}{r}_{n_j}, \underset{\sim}{r}_{m_1})$ denotes a plane strain elastodynamic state due to Green's function $\phi_i(\underset{\sim}{r}_{n_j}, \underset{\sim}{r}_{m_1})$, etc. Vector $\underset{\sim}{f}$ in equation (22a) of the order $4(N_1 + N_2 + \ldots + N_R) \times 1$ is specified by

$$\underset{\sim}{f} \equiv \begin{bmatrix} \underset{\sim}{s}_o^{inc}(\underset{\sim}{r}_{1_1}) \\ \underset{\sim}{s}^{inc}(\underset{\sim}{r}_{2_1}) \\ \vdots \\ \underset{\sim}{s}^{inc}(\underset{\sim}{r}_{N_1}) \\ \underset{\sim}{s}^{inc}(\underset{\sim}{r}_{1_2}) \\ \vdots \quad \vdots \\ \underset{\sim}{s}^{inc}(\underset{\sim}{r}_{N_2}) \\ \vdots \quad \vdots \\ \underset{\sim}{s}^{inc}(\underset{\sim}{r}_{1_R}) \\ \vdots \\ \underset{\sim}{s}^{inc}(\underset{\sim}{r}_{N_R}) \end{bmatrix} \qquad \text{(A8)}$$

Figure Captions

Fig. 1 Problem Model

Fig. 2 Surface Displacement Amplitude for Incident SH-Wave.

a) $H/R_1 = 0.75$

b) $H/R_1 = 3$

(If not stated otherwise C-+: $x = \xi^{-+} R_1 \cos\theta$; $y = \xi^{-+} R_2 \sin\theta$ +H; $\xi^- = 0.5$; $\xi^+ = 1.5$; $0 \leq \theta \leq 2\pi$; $M_1 = L_1 = 11$; $N_1 = 23$; sources on observation points equally spaced; $R_1 = 4$; $R_2 = 2$; $\mu_1 = \beta_1 = 1$; $\mu_2 = \beta_2 = 0.8$, $\theta_o = 30^o$, $\Omega = 1$)

Fig. 3 Normalized Surface Displacement Amplitudes for Incident P-Wave: $\theta_o = 30^o$

a) $H/R_1 = 0.75$

b) $H/R_1 = 3$

($M_1 = L_1 = 12$; $N_1 = 24$; -2; $\alpha_2 = 1.6$)

Fig. 4 Normalized Surface Displacement Amplitude for Incident P-Wave: $\theta_o = 80^o$

a) $H/R_1 = 0.75$

b) $H/R_1 = 3$

Fig. 5 Normalized Surface Displacement Amplitudes for Incident SV-Wave: $\theta_o = 30^o$

a) $H/R_1 = 0.75$

b) $H/R_1 = 3$

Fig. 6 Normalized Surface Displacement Amplitude for Incident SV-Wave: $\theta_o = 80^o$

a) $H/R_1 = 0.75$

b) $H/R_1 = 3$

Fig. 7 Normalized Surface Displacement Amplitudes for Incident Rayleigh Wave.

a) $H/R_1 = 0.75$

b) $H/R_1 = 3$

Fig. 8 Surface Displacement amplitude for Incident SH-Waves: Test Case.

a) $H/R_1 = 0.75$

b) $H/R_1 = 3$

(If not stated differently C_1^{-+}: $x = \xi^{-+} R_1 \cos\theta$; $y = \xi^{-+} R_2 \sin\theta + H$; C_2^{-+}: $x = \xi^{-+} R_1 \cos\theta - D$; $y = \xi^{-+} R_2 \sin\theta + H$; $\xi^- = 0.5$; $\xi^+ = 1.2$; $0 \leq \theta \leq 2\pi$; $M_1 = L_1 = 23$; $N_1 = 45$; sources and observation points equally spaced; $R_1 = 4$; $R_2 = 2$; $\mu_1 = \beta_1 = 1$; $\mu_2 = \beta_2 = 0.8$; $\theta_o = 30^o$, $\Omega = 2$)

Fig. 9 Surface Displacement Amplitude for Incident SH-Wave and Two Inclusions.

a) $H/R_1 = 0.75$; $D/R_1 = 3$

b) $H/R_1 = 3$; $D/R_1 = 3$

Fig. 10 Surface Displacement Amplitude for Incident SH-Wave

and Two Inclusions.

a) $H/R_1 = 0.75$; $D/R_1 = 5$

b) $H/R_1 = 3$; $D/R_1 = 5$

Fig. 11 Surface Displacement Amplitude for Incident SH-Wave and Two Inclusions.

a) $H/R_1 = 3$; $D/R_1 = 3$

($\mu_2 = \beta_2 = 0.5$)

Fig. 12 Frequency Surface Response Amplitude for Incident SH-Wave and Two Inclusions.

a) Station One: $x/R_1 = -5$; $y = 0$

b) Station Two: $x/R_1 = -4$; $y = 0$

Fig. 13 Frequency Surface Response Amplitude for Incident SH-Wave and Two Inclusions.

a) Station Three: $x/R_1 = -3$; $y = 0$

b) Station Four : $x/R_1 = -2$; $y = 0$

Fig. 14 Frequency Surface Response Amplitude for Incident SH-Wave and Two Inclusions.

a) Station Five: $x/R_1 = -1$; $y = 0$

b) Station Six : $x/R_1 = 0$; $y = 0$

Fig. 15 Frequency Surface Response Amplitude for Incident SH-Wave and Two Inclusions.

a) Station Seven: $x/R_1 = 1$; $y = 0$

b) Station Eight: $x/R_1 = 2$; $y = 0$

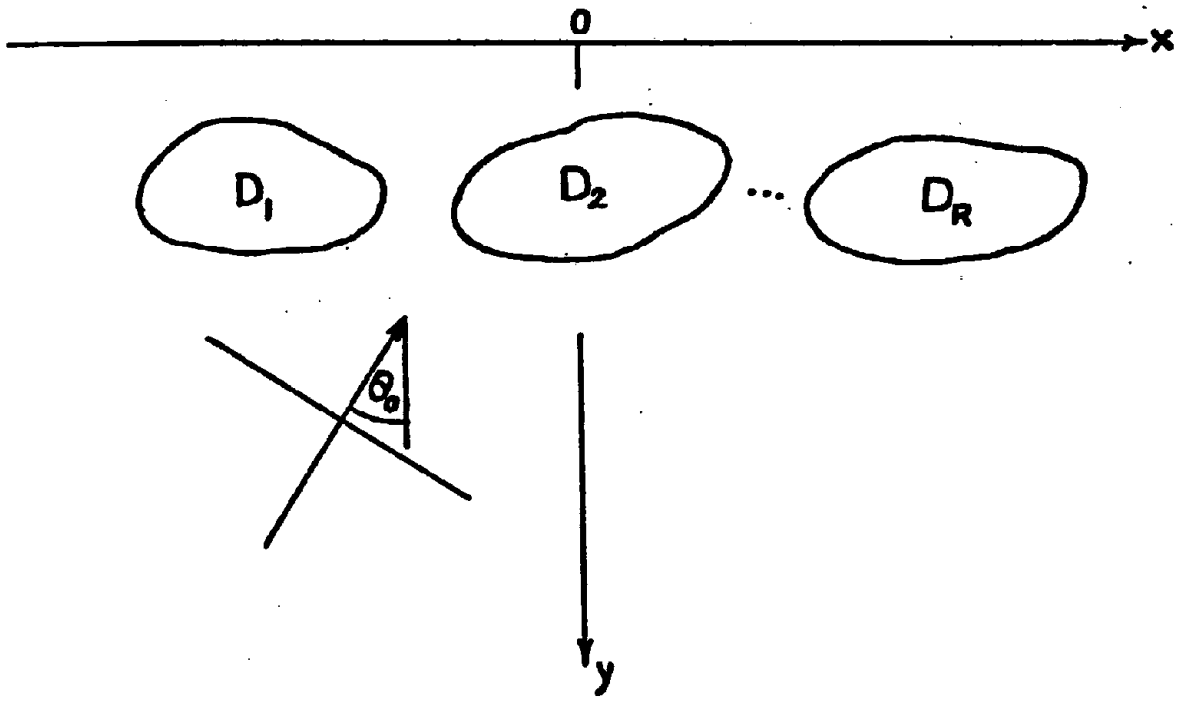

Fig-1

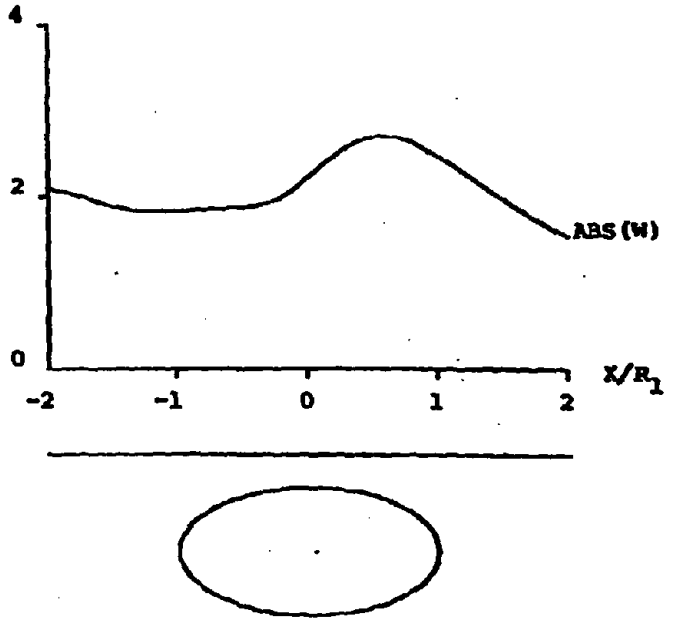

Fig. 2a

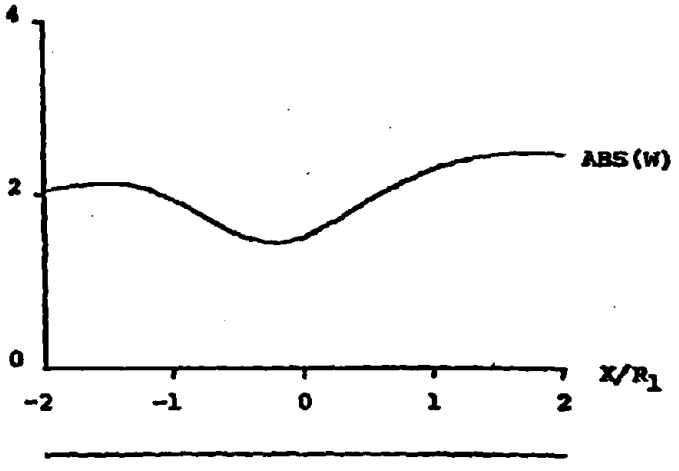

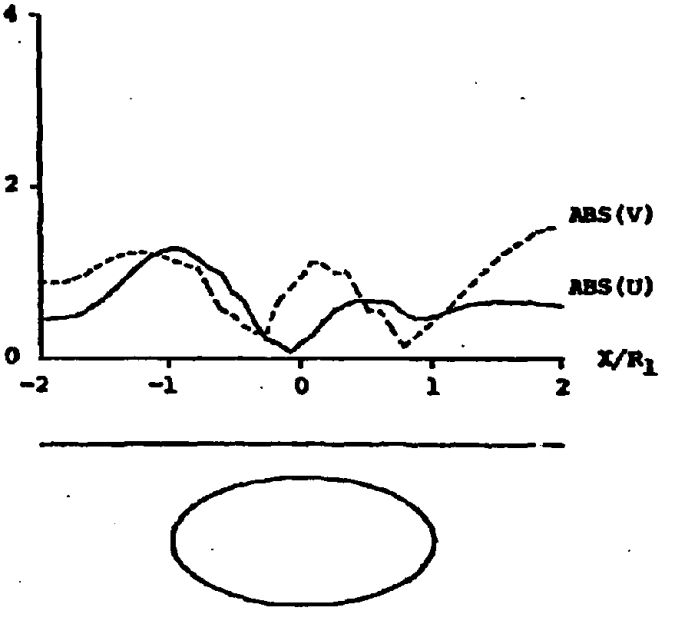

Fig. 3a

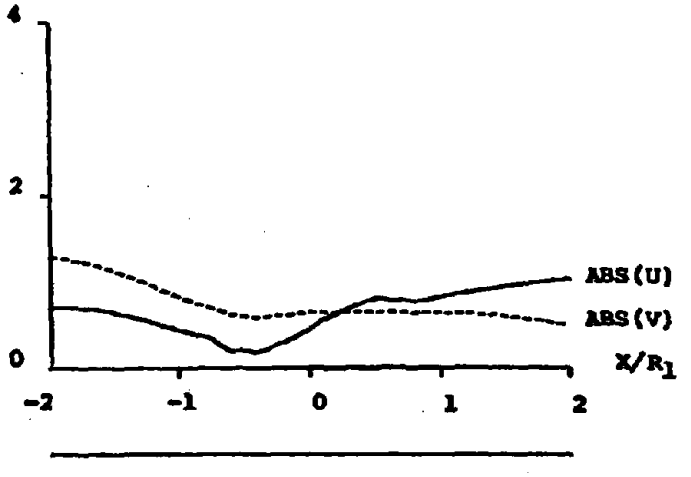

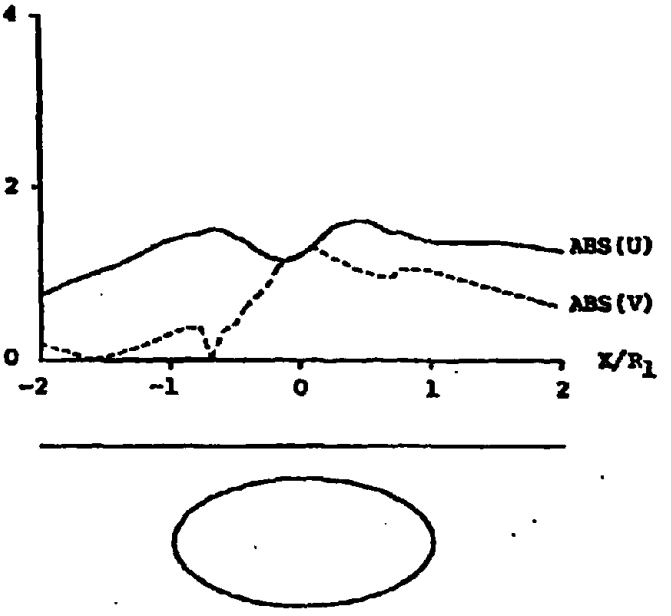

Fig. 4a

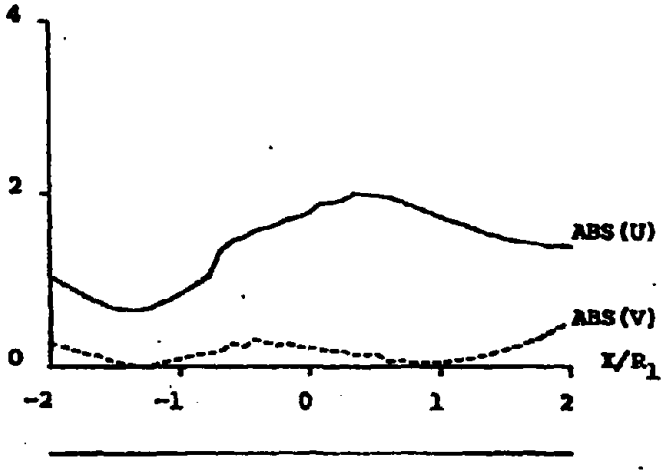

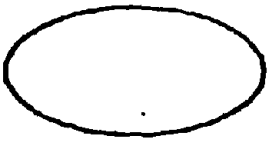

Fig. 4b

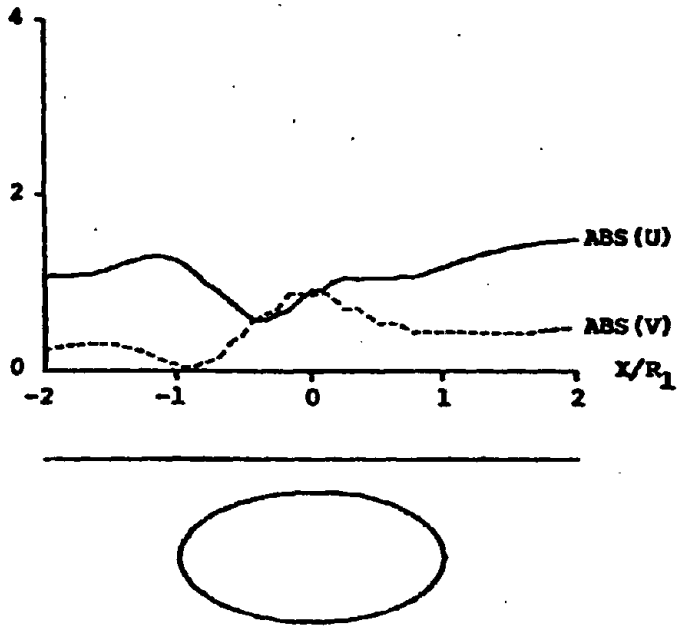

Fig. 5a

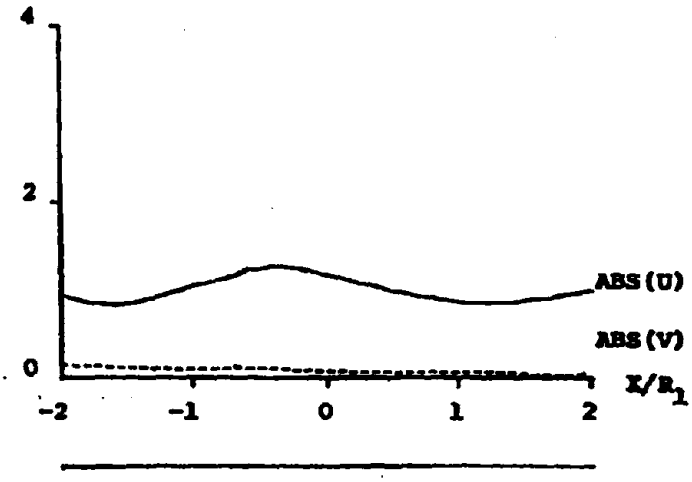

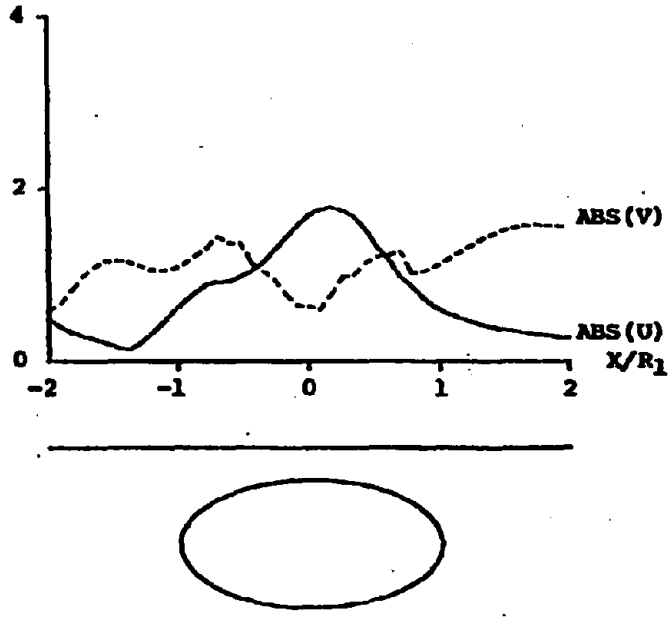

Fig. 6a

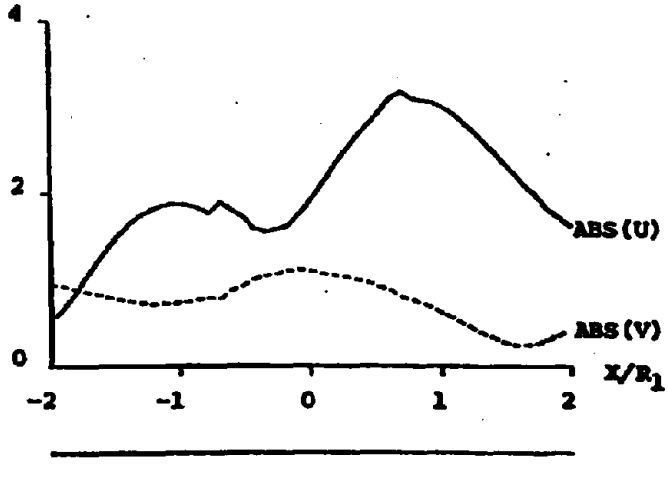

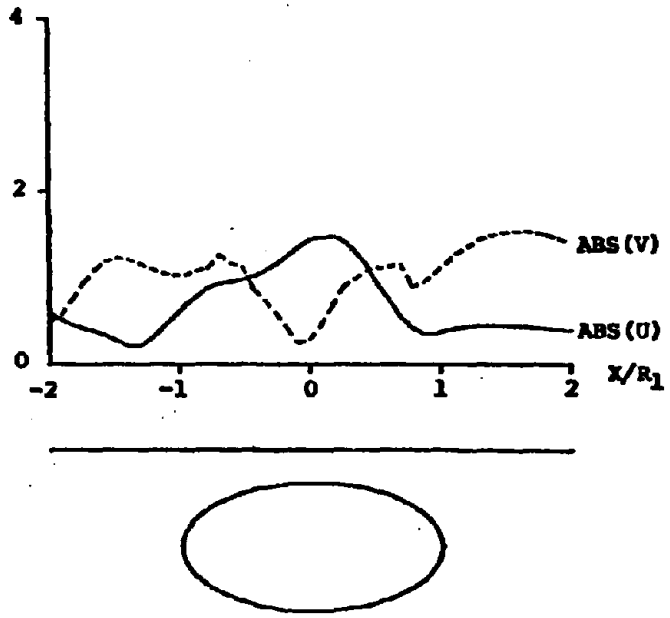

Fig. 7a

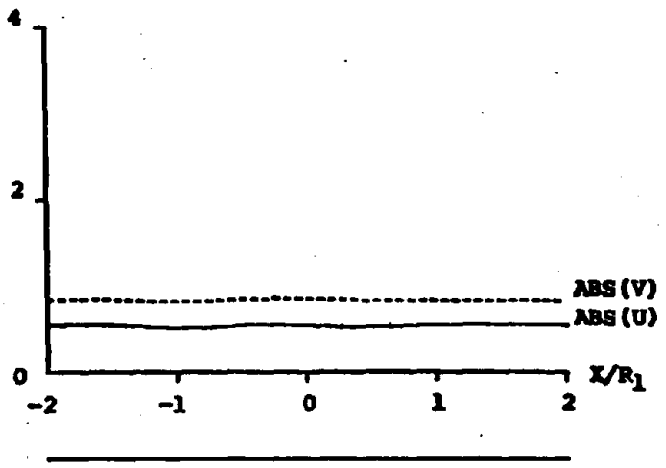

Fig. 7b

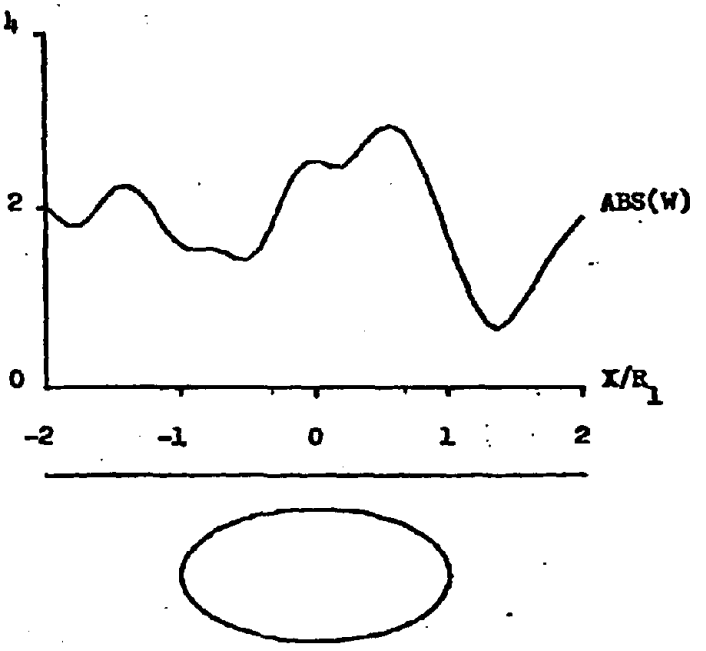

Fig. 8a

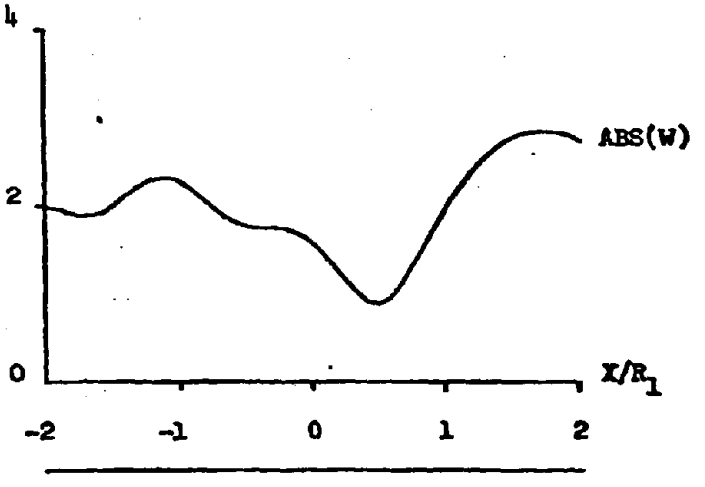

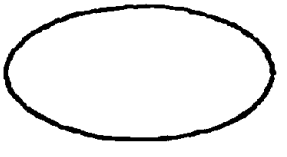

Fig. 8b

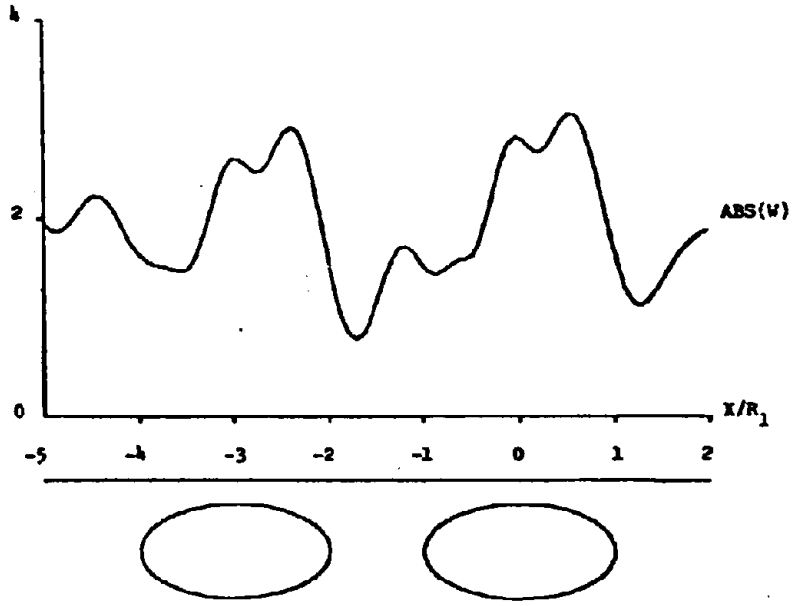

Fig. 9a

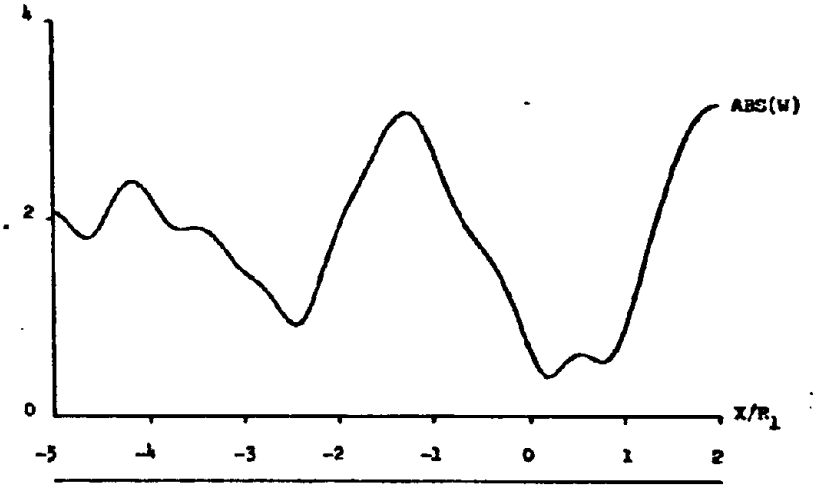

Fig. 9b

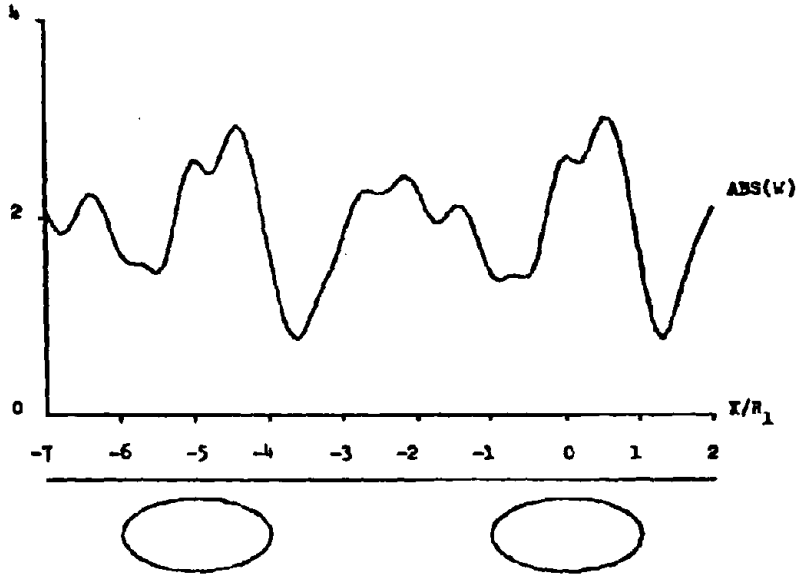

Fig.10a

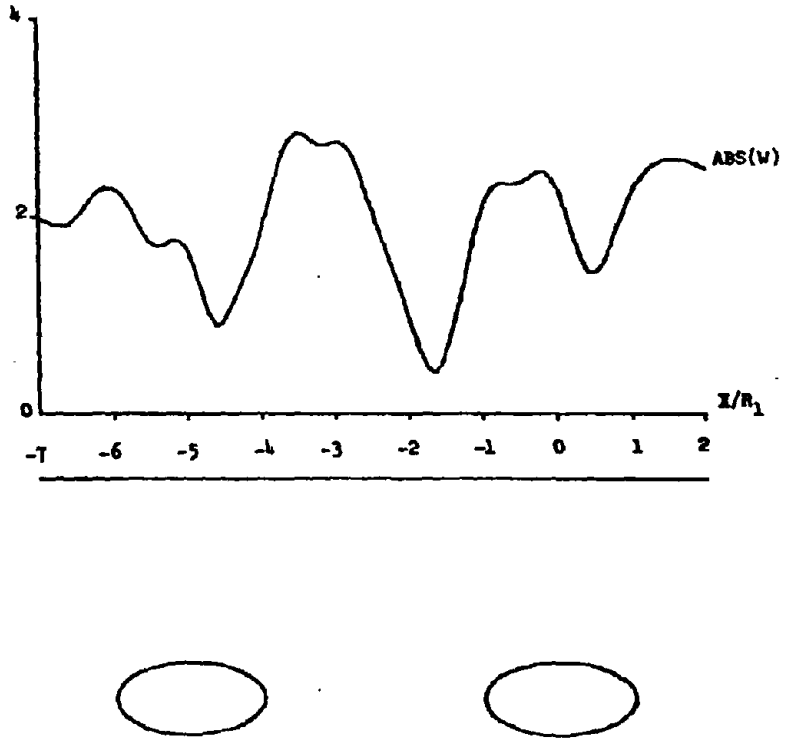

Fig.10b

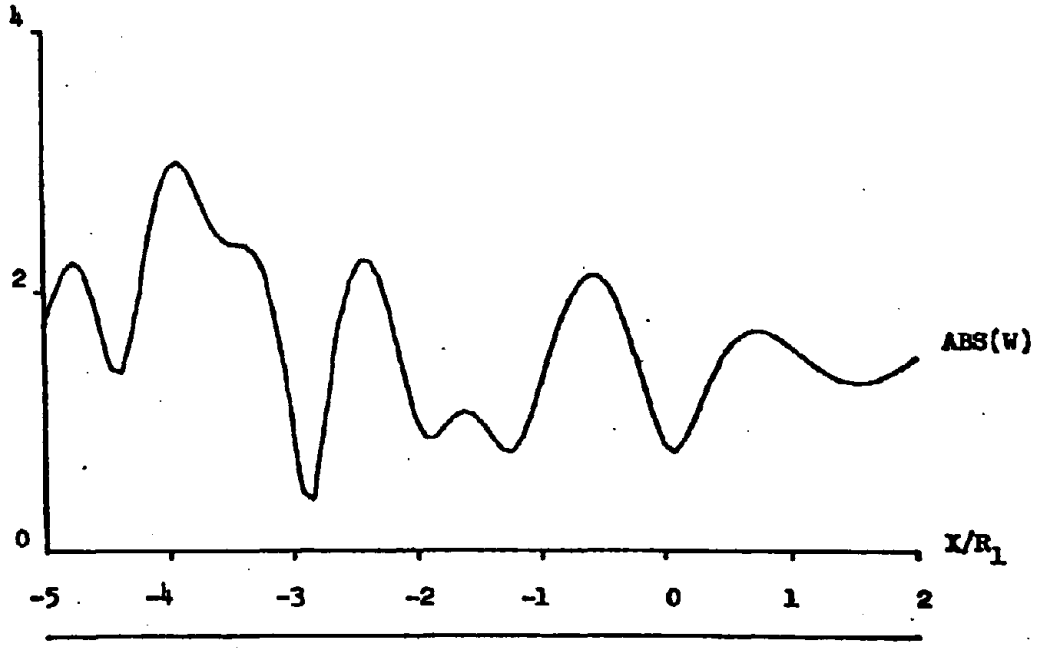

Fig.11

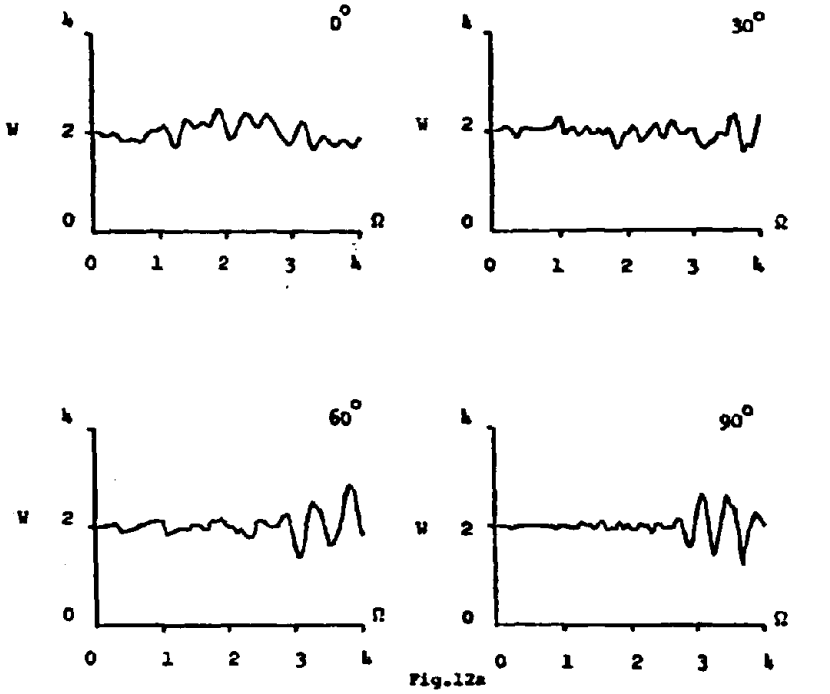

Fig.12a

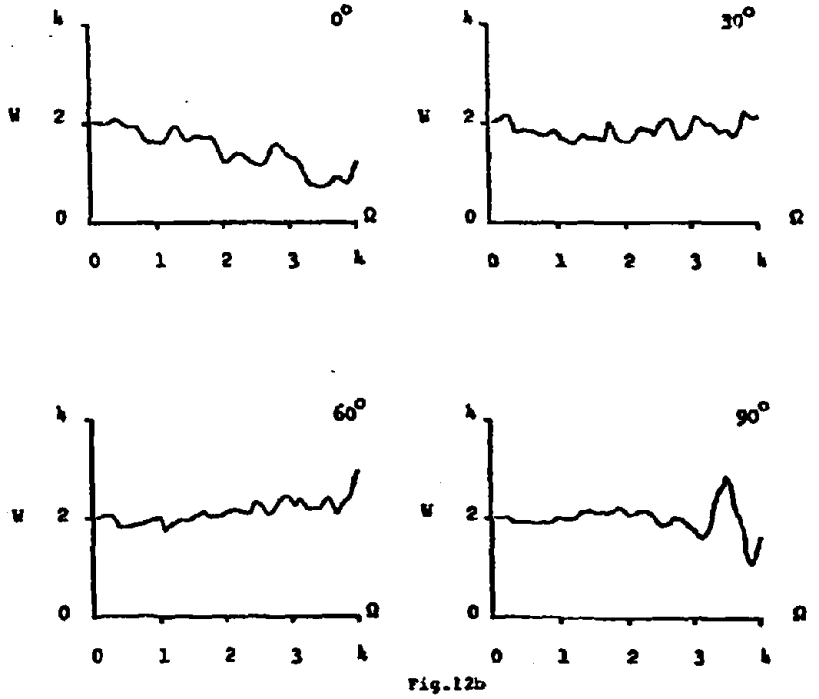

Fig.12b

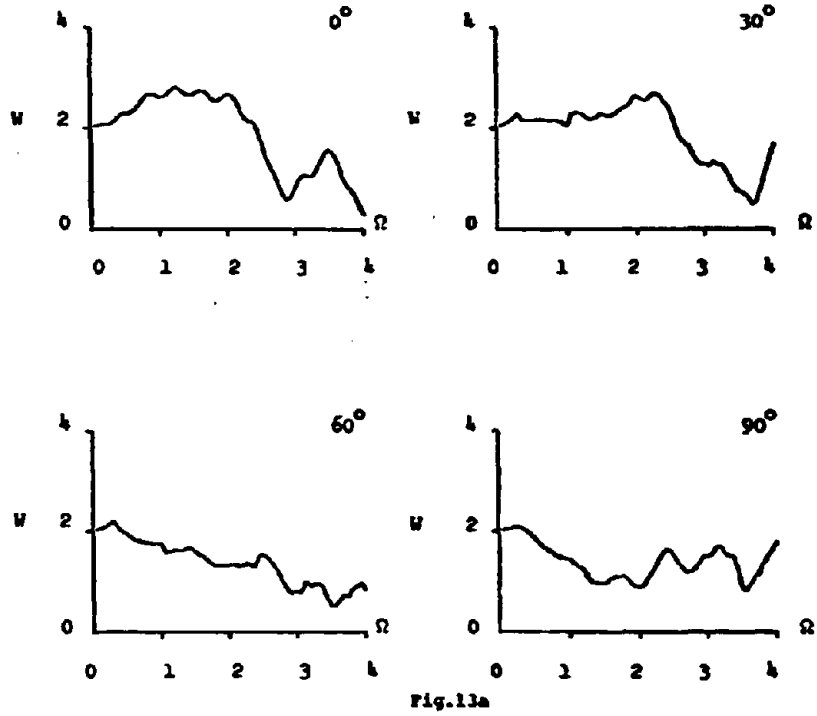

Fig.13a

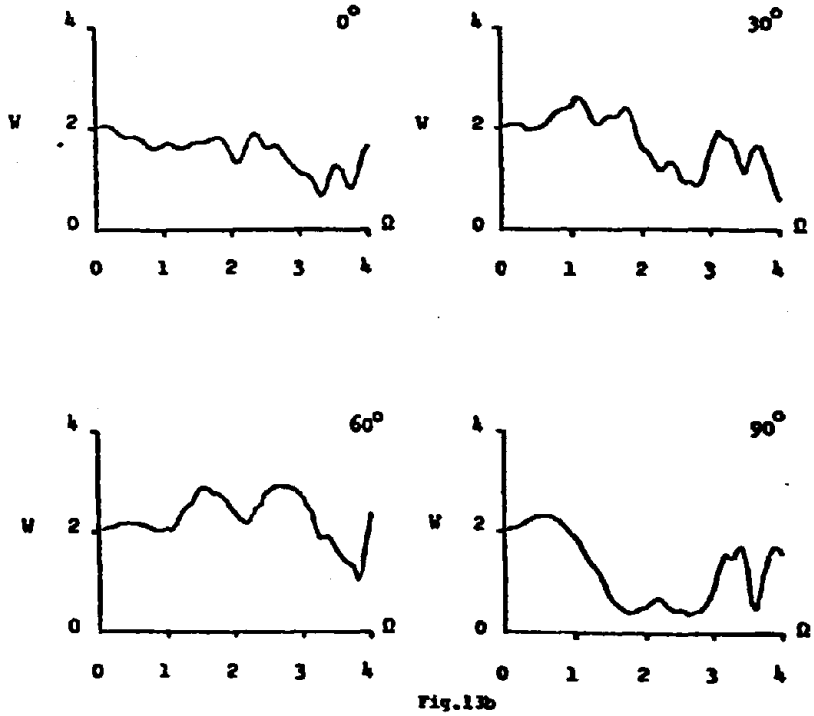

Fig.13b

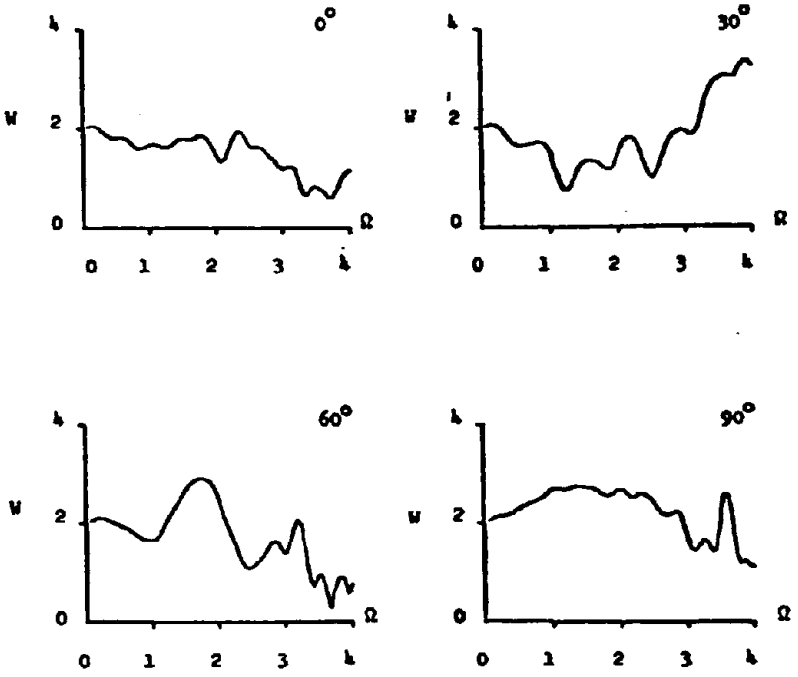

Fig.14a

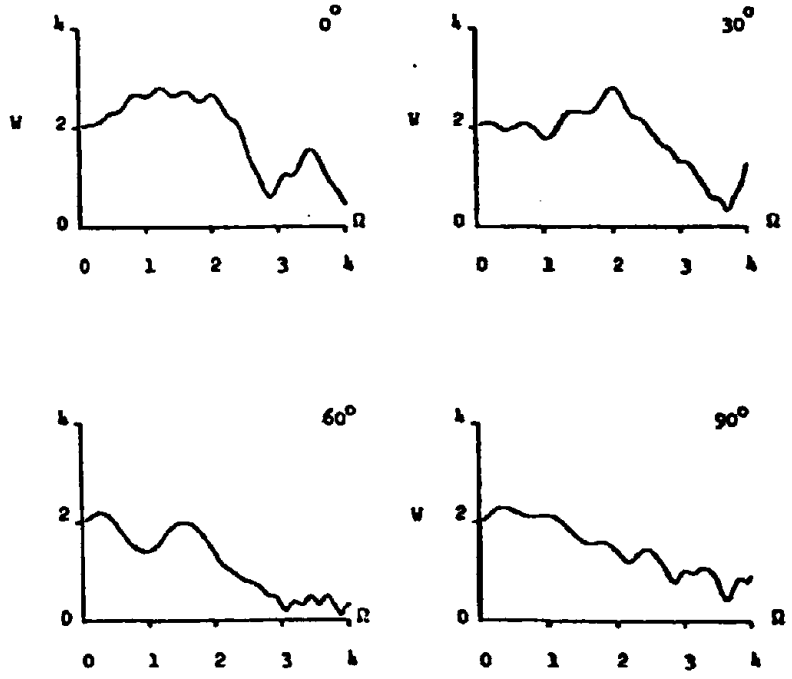

Fig.14b

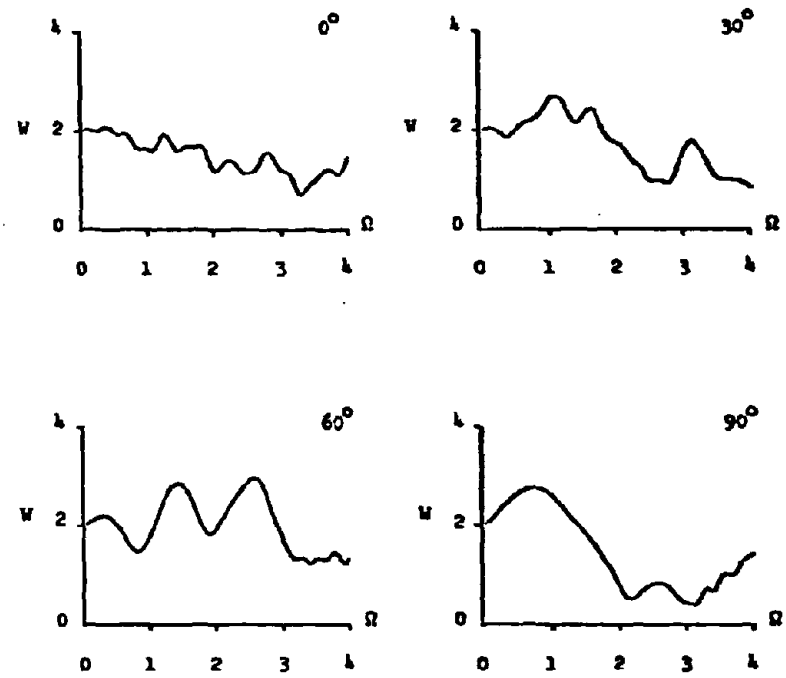

Fig 15a

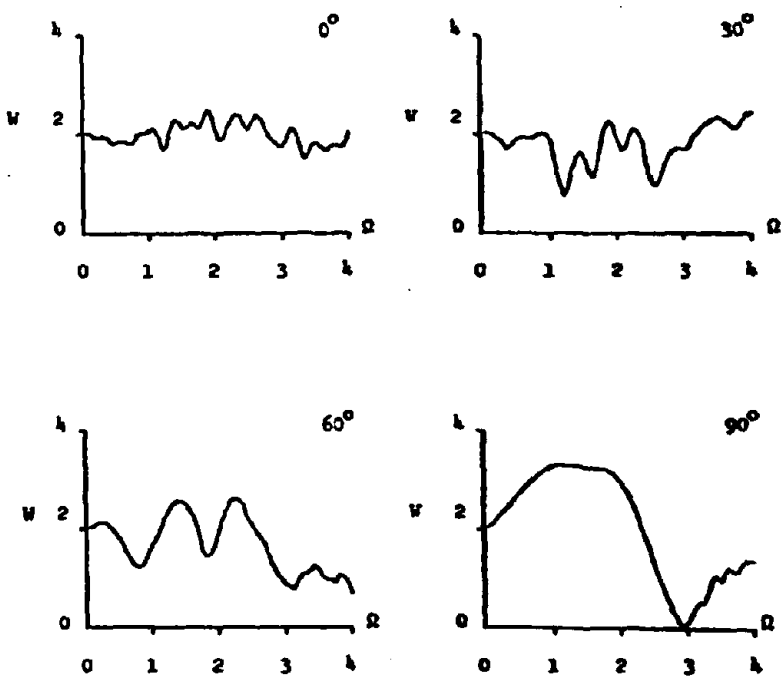

Fig 15b

Amplification of P, SV, and Rayleigh Waves by Two Alluvial Valleys *

by Marijan Dravinski
Department of Mechanical Engineering
University of Southern California, Los Angeles

ABSTRACT

Plane strain model for amplification of harmonic waves by two alluvial valleys of arbitrary shape embedded in a half-space is investigated by using a boundary integral method. Perfect bonding between the valleys and the half-space is assumed. Displacement field is evaluated throughout the elastic medium for linearly elastic, homogeneous and isotropic meterials so that the continuity conditions between the valleys and the half-space are satisfied in mean-square-sense.

Numerical results are presented for two semi-elliptical valleys for incident plane P, SV, and Rayleigh waves for different angles of incidence (for P and SV-waves), frequency of incoming waves, and material properties of the valleys. The results indicate the following: 1. Different incident waves caused different surface displacement amplification; 2. Presence of additional valleys may change the surface motion field significantly; 3. Strong ground motion amplitude appears to be very sensitive upon the frequency of incoming wave and contrast in material properties of the valleys and the half-space.

*Soil Dynamics and Earthquake Engineering,1983,Vol.2,No.2,66-77.

INTRODUCTION

Observations from some recent earthquakes indicate that the areas of intense damage can be highly localized(e.g. Sozen, et. al.,1968;Jennings,1971). Esteva(1977) established that the intensity of strong ground motion may change significantly within a short distance. Investigations by Boore(1973) and Griffiths and Bollinger(1979) confirmed a belief that the inhomogeneity of the soil and surface (subsurface) irregularities are the main cause of localized amplification effects.

Recently,the author (Dravinski,1982a,b) investigated amplification effects due to alluvial valley embedded in a half-space and subjected to incident SH,P,SV, and Rayleigh waves.It was shown that the presence of a subsurface inhomogeneity in the half-space may cause locally very large strong ground motion amplification effects. Variation of the surface ground motion proved to be very sensitive upon a number of parameters present in the problem (such as frequency,angle of incidence,...,etc). However, the question regarding the influence of additional inclusion upon the strong ground motion remained open. By including two alluvial valleys into considerations it is possible to examine critically wheter or not the mutual interaction between the two is of any importance for magnitude of the surface motion and thus determine if it is necessary to incorporate the presence of several scatterers in analysis of strong ground motion in more realistic models.

The results presented in this paper are extension of the work on the corresponding antiplane strain model of the problem (Dravinski,1982d).These results can be summarized as follows:Surface motion amplification strongly depends upon (i) angle of incidence; (ii) frequency of the incident field; and (iii) location of the observation point on the surface of the half-space. Variation in any of the three parameters can produce significant change in the surface motion amplification. It was observed that "illuminated" valley detects very little the presence of additional valley while the response atop the valley "in shade" may be quite different from the single valley-response.Increase in separation distance between the valleys resulted in reduction of interaction between the two.

Comparison of the surface response for the antiplane strain and plane strain model in less general problem models (e.g., Dravinski,1982 c) indicate that the conclusions derived for incident SH-waves do not necesserily apply for incoming P,SV,or Rayleigh waves. Extension of the analysis to the plane strain model allows deeper insight into the basic phenomena of the strong ground motion for the case of multiple inclusions in a soil medium. One expects that the knoweledge acquired through study of the plane strain model would help in extending the analysis to more realistic models,e.g.,three dimensional ones.

Boundary integral method,also known as a source or Oshaki

method,used in this paper, was originally proposed by Copley (1967) and Oshaki(1973). Copley introduced the basic idea of the method to a problem in acoustics, while Oshaki applied similar approach to a problem in elastostatics. Aplication of the method to the wave propagation problems in geophysics and earthquake engineering is due to Sanchez-Sesma and Rosenblueth(1979),Sanchez-Sesma and Esquivel(1979),Wong(1979),Apsel(1979),and Dravinski (1980). At present time the author is not aware of any plane strain model-solutions involving two,or more,alluvial valleys embedded in a half-space which is considered in this paper.

Detailed review of literature pertinent to scattering of elastic waves by surface irregularities and the boundary method in particular was given recently by Dravinski(1982a) and Herrera(1982) and will not be repeated here.

STATEMENT OF PROBLEM

The geometry of the problem is depicted by Fig. 1. Elastic alluvial valleys of arbitrary shape D_1 and D_2,extend uniformly in direction perpendicular to the plane of the drawing. They are perfectly bonded to an elastic half-space of domain D_o. Material of the inclusions and the half-space is assumed to be linearly elastic,homogeneous and isotropic.

Plane motion of the elastic media is described by a dis-

placement vector $u_j=(u_j,v_j)$, j=0,1,2, with

$$u_j=\frac{\partial\phi_j}{\partial x}+\frac{\partial\psi_j}{\partial y}\quad;\quad v_j=\frac{\partial\phi_j}{\partial y}-\frac{\partial\psi_j}{\partial x}\quad;j=0,1,2, \qquad \ldots(1)$$

where ϕ and ψ denote dilatational and equivoluminal displacement potential, respectively. The subscript 0 refers to the half-space, while the subscripts 1 and 2 refer to the elastic inclusions D_1 and D_2, respectively (see Fig.1). The displacement potentials satisfy the equations of motion (Miklowitz,1978)

$$\nabla^2\begin{bmatrix}\phi_j\\ \psi_j\end{bmatrix}+\begin{bmatrix}h_j^2\,\phi_j\\ k_j^2\,\psi_j\end{bmatrix}=\underline{0}\quad;\ j=0,1,2 \qquad \ldots(2)$$

where h and k represent the wave numbers associated with dilatational and equivoluminal waves, respectively. Throughout the derivations factor $\exp(i\omega t)$ is understood. Components of the stress tensor are related to the displacement potentials through (Miklowitz,1978)

$$\sigma_{xx}/\mu=-k^2\phi-2\frac{\partial^2\phi}{\partial y^2}+2\frac{\partial^2\psi}{\partial x\partial y} \qquad \ldots(3a)$$

$$\sigma_{xy}/\mu=-k^2\psi+2\frac{\partial^2\phi}{\partial x\partial y}-2\frac{\partial^2\psi}{\partial x^2} \qquad \ldots(3b)$$

$$\sigma_{yy}/\mu=-k^2\phi-2\frac{\partial^2\phi}{\partial x^2}-2\frac{\partial^2\psi}{\partial x\partial y} \qquad \ldots(3c)$$

where μ denotes the shear modulus. Boundary conditions are specified by

$$\sigma_{xy\ j} = 0 \qquad \text{...(4a)}$$

$$\sigma_{yy\ j} = 0 \qquad y=0 \text{ and } \underset{\sim}{r} \in D_j \ ; \ j=0,1,2 . \qquad \text{...(4b)}$$

Usual radiation conditions are to be satisfied for scattered waves at infinity (Miklowitz,1978). Perfect bonding along the interfaces C_1 and C_2 (see Fig.1) is assumed,i.e.,

$$u_0 = u_1 \qquad \text{...(5a)}$$

$$v_0 = v_1 \qquad \text{...(5b)}$$

$$\sigma_{nn\ 0} = \sigma_{nn\ 1} \qquad \underset{\sim}{r} \in C_1 \qquad \text{...(5c)}$$

$$\sigma_{nt\ 0} = \sigma_{nt\ 1} \qquad \text{...(5d)}$$

$$u_0 = u_2 \qquad \text{...(5e)}$$

$$v_0 = v_2 \qquad \text{...(5f)}$$

$$\sigma_{nn\ 0} = \sigma_{nn\ 2} \qquad \underset{\sim}{r} \in C_2 \qquad \text{...(5g)}$$

$$\sigma_{nt\ 0} = \sigma_{nt\ 2} \qquad \text{...(5h)}$$

where $\underset{\sim}{n}$ denotes unit normal vector along the interface and $\underset{\sim}{r}$ represents position vector. Normal and tangential components of the stress tensor are denoted by σ_{nn} and σ_{nt} ,respectively. Interfaces C_1 and C_2 are chosen to be sufficiently smooth with no sharp corners.

Incident P-wave is specified by

$$\phi^i = \frac{i}{h_1} e^{-ih_1(x \sin\theta_0 - y \cos\theta_0)} \qquad \ldots(6a)$$

where, if not stated differently, the superscript i denotes the incident wave field, $i = \sqrt{-1}$, and θ_o represents the angle of incidence. Incident SV-wave is defined through

$$\psi^i = \frac{-i}{k_1} e^{-ik_1(x \sin\theta_0 - y \cos\theta_0)} \qquad \ldots(6b)$$

and incident Rayleigh wave is chosen in the form

$$u^i = e^{-i\kappa_0 x}[e^{-b_L y} - \frac{1}{2}(2 - \frac{c_0^2}{\beta_0^2})e^{-b_T y}] \qquad \ldots(6c)$$

$$v^i = i\kappa_0 e^{-i\kappa_0 x}[-\frac{b_L}{\kappa_0^2} e^{-b_L y} + \frac{1}{2b_T}(2 - \frac{c_0^2}{\beta_0^2})e^{-b_T y}] \qquad \ldots(6d)$$

$$b_L = \kappa_0(1 - \frac{c_0^2}{\alpha_0^2})^{1/2} \; ; \; b_T = \kappa_0(1 - \frac{c_0^2}{\beta_0^2})^{1/2} \qquad \ldots(6e)$$

where c_0 and κ_0 denote the Rayleigh wave velocity and the corresponding wave number, respectively. Particular forms of the incident field are chosen so that the free-field components of the displacement vector u^{ff} and v^{ff} along the surface of the half-space turn out to be real numbers. All the results of the displacement field are presented normalized with respect to the amplitude $((u^{ff})^2 + (v^{ff})^2)^{1/2}$.

SOLUTION OF PROBLEM

The total wave field in the half-space and the elastic inclusions is specified by

$$u_0 = u^i + u_0^s \qquad \ldots(7a)$$

$$v_0 = v^i + v_0^s \qquad \underset{\sim}{r} \in D_0 \qquad \ldots(7b)$$

$$u_1 = u_1^s \qquad \ldots(7c)$$

$$v_1 = v_1^s \qquad \underset{\sim}{r} \in D_1 \qquad \ldots(7d)$$

$$u_2 = u_2^s \qquad \ldots(7e)$$

$$v_2 = v_2^s \qquad \underset{\sim}{r} \in D_2 \qquad \ldots(7f)$$

where the superscript s denotes the scattered waves. The unknown scatered wave field is assumed to be expressed in terms of single layer potentials (Ursell,1973).Therefore,

$$\phi_0^s(\underset{\sim}{r}) = \int_{C_{1i}} g_{01}^{\phi}(\underset{\sim}{r}_0)\phi_0(\underset{\sim}{r},\underset{\sim}{r}_0)d\underset{\sim}{r}_0 + \int_{C_{2i}} g_{02}^{\phi}(\underset{\sim}{r}_0)\phi_0(\underset{\sim}{r},\underset{\sim}{r}_0)d\underset{\sim}{r}_0 \qquad \ldots(8a)$$

$$\psi_0^s(\underset{\sim}{r}) = \int_{C_{1i}} g_{01}^{\psi}(\underset{\sim}{r}_0)\psi_0(\underset{\sim}{r},\underset{\sim}{r}_0)d\underset{\sim}{r}_0 + \int_{C_{2i}} g_{02}^{\psi}(\underset{\sim}{r}_0)\psi_0(\underset{\sim}{r},\underset{\sim}{r}_0)d\underset{\sim}{r}_0 \qquad \ldots(8b)$$

$$\phi_1^s(\underset{\sim}{r}) = \int_{C_{1o}} g_1^{\phi}(\underset{\sim}{r}_0)\phi_1(\underset{\sim}{r},\underset{\sim}{r}_0)d\underset{\sim}{r}_0 \qquad \ldots(8c)$$

$$\psi_1^s(\underset{\sim}{r}) = \int_{C_{1o}} g_1^{\psi}(\underset{\sim}{r}_0)\psi_1(\underset{\sim}{r},\underset{\sim}{r}_0)d\underset{\sim}{r}_0 \qquad \ldots(8d)$$

$$\phi_2^s(\underset{\sim}{r}) = \int_{C_{2o}} g_2^{\phi}(\underset{\sim}{r}_0)\phi_2(\underset{\sim}{r},\underset{\sim}{r}_0)d\underset{\sim}{r}_0 \qquad \ldots(8e)$$

$$\psi_2^s(\underset{\sim}{r}) = \int_{C_{2o}} g_2^{\psi}(\underset{\sim}{r}_0)\psi_2(\underset{\sim}{r},\underset{\sim}{r}_0)d\underset{\sim}{r}_0 \qquad \ldots(8f)$$

Surfaces C_{1i}, C_{2i}, C_{1o}, and C_{2o} (see Fig.1) are defined in the half-space inside and outside of the interfaces C_1 and C_2 (Dravinski, 1982c) and the density functions g_{01}^{ϕ}, g_{02}^{ϕ}, g_{01}^{ψ}, g_{02}^{ψ}, g_1^{ϕ}, g_1^{ψ}, g_2^{ϕ}, and g_2^{ψ} are yet to be determined. The Green's functions ϕ_j and ψ_j, j=0,1,2 are solutions of the equations

$$\nabla^2\begin{bmatrix}\phi_j(\underset{\sim}{r},\underset{\sim}{r}_0)\\ \psi_j(\underset{\sim}{r},\underset{\sim}{r}_0)\end{bmatrix} + \begin{bmatrix}h_j^2\phi_j(\underset{\sim}{r},\underset{\sim}{r}_0)\\ k_j^2\psi_j(\underset{\sim}{r},\underset{\sim}{r}_0)\end{bmatrix} = -\delta(|\underset{\sim}{r}-\underset{\sim}{r}_0|);j=0,1,2 \qquad \ldots(9a)$$

with appropriate boundary conditions

$$\sigma_{xy\ j}(\underset{\sim}{r},\underset{\sim}{r}_0) = 0 \qquad \ldots(9b)$$

$$\sigma_{yy\ j}(\underset{\sim}{r},\underset{\sim}{r}_0) = 0 \qquad y=0,\text{and } \underset{\sim}{r}\in D_j;j=0,1,2 \qquad \ldots(9c)$$

where $\delta(.)$ denotes the Dirac delta-function. Following the paper by Lamb(1904) explicit forms for the Green's functions in Eqns.(9a-c) were derived by the author (Dravinski,1980). The Green's functions are expressed in terms of improper integrals.

According to Lapwood(1948) application of contour integration allowed representation of the improper integrals in a form convenient for numerical evaluation (Dravinski,1980).

If the density functions are assumed to be of the form

$$\varepsilon_{01}^{\phi}(\underset{\sim}{r}_0) = a_m \delta(|\underset{\sim}{r}_0 - \underset{\sim}{r}_m|) \quad ;\underset{\sim}{r}_m \varepsilon C_{1i};m=1,2,\ldots,M_1 \qquad \ldots(10a)$$

$$\varepsilon_{02}^{\phi}(\underset{\sim}{r}_0) = b_{m'} \delta(|\underset{\sim}{r}_0 - \underset{\sim}{r}_{m'}|) \;;\underset{\sim}{r}_{m'} \varepsilon C_{2i};m'=1,2,\ldots,M_2 \qquad \ldots(10b)$$

$$\varepsilon_{01}^{\psi}(\underset{\sim}{r}_0) = c_m \delta(|\underset{\sim}{r}_0 - \underset{\sim}{r}_m|) \qquad \ldots(10c)$$

$$\varepsilon_{02}^{\psi}(\underset{\sim}{r}_0) = d_{m'} \delta(|\underset{\sim}{r}_0 - \underset{\sim}{r}_{m'}|) \qquad \ldots(10d)$$

$$\varepsilon_{1}^{\phi}(\underset{\sim}{r}_0) = e_\ell \delta(|\underset{\sim}{r}_0 - \underset{\sim}{r}_\ell|) \quad ; \underset{\sim}{r}_\ell \varepsilon C_{1o};\ell=1,2,\ldots,L_1 \qquad \ldots(10e)$$

$$\varepsilon_{1}^{\psi}(\underset{\sim}{r}_0) = f_\ell \delta(|\underset{\sim}{r}_0 - \underset{\sim}{r}_\ell|) \qquad \ldots(10f)$$

$$\varepsilon_{2}^{\phi}(\underset{\sim}{r}_0) = g_{\ell'} \delta(|\underset{\sim}{r}_0 - \underset{\sim}{r}_{\ell'}|) \; ; \underset{\sim}{r}_{\ell'} \varepsilon C_{2o};\ell'=1,2,\ldots,L_2 \qquad \ldots(10g)$$

$$\varepsilon_{2}^{\psi}(\underset{\sim}{r}_0) = h_{\ell'} \delta(|\underset{\sim}{r}_0 - \underset{\sim}{r}_{\ell'}|) \qquad \ldots(10h)$$

the scattered wave field becomes

$$\phi_0^s(\underset{\sim}{r}) = a_m \phi_0(\underset{\sim}{r},\underset{\sim}{r}_m) + b_{m'} \phi_0(\underset{\sim}{r},\underset{\sim}{r}_{m'}) \;;m=1,2,\ldots,M_1 ;m'=1,2,\ldots,M_2 \quad (11a)$$
$$\underset{\sim}{r}_m \varepsilon C_{1i};\ \underset{\sim}{r}_{m'} C_{2i}$$

$$\psi_0^s(\underset{\sim}{r}) = c_m \psi_0(\underset{\sim}{r},\underset{\sim}{r}_m) + d_{m'} \psi_0(\underset{\sim}{r},\underset{\sim}{r}_{m'}) \qquad \ldots (11b)$$

$$\phi_1^s(\underset{\sim}{r}) = e_\ell \phi_1(\underset{\sim}{r},\underset{\sim}{r}_\ell) \quad ;\ell=1,2,\ldots,L_1;\ \underset{\sim}{r}_\ell \in C_{1o} \qquad \ldots (11c)$$

$$\psi_1^s(\underset{\sim}{r}) = f_\ell \psi_1(\underset{\sim}{r},\underset{\sim}{r}_\ell) \qquad \ldots (11d)$$

$$\phi_2^s(\underset{\sim}{r}) = g_{\ell'} \phi_2(\underset{\sim}{r},\underset{\sim}{r}_{\ell'}) \quad ;\ \ell'=1,2,\ldots,L_2;\ \underset{\sim}{r}_{\ell'} \in C_{2o} \qquad \ldots (11e)$$

$$\psi_2^s(\underset{\sim}{r}) = h_{\ell'} \psi_2(\underset{\sim}{r},\underset{\sim}{r}_{\ell'}) \qquad \ldots (11f)$$

where, if not stated differently, summation over repeated indices is understood.

It is interesting to point out physical interpretation of Eqns.(8a-f) and (10a-h). As the incident wave strikes an inclusion it reflects partially back and transmitts partially into the inclusion. Therefore, the interface between the half-space and the inclusion can be viewed as a system of sources which produce the scattered wave fields. This would imply that the integrations indicated in Eqns.(8a-f) should be carried out along the appropriate interface. However, singularity of the Green's functions as the "observation" point ($\underset{\sim}{r}$) approaches the "source" point ($\underset{\sim}{r}_0$) suggests placing the sources slightly away from the original interface (Dravinski,1982a). For the sake of further

simplification, infinite number of sources along the "source" surface is replaced by a finite number which leads to Eqns. (10a-h). Intensities of sources in Eqns.(10a-h) are determined through the continuity conditions (Eqns.(9a-h)) which are to be satisfied in the mean-square-sense (Noble and Daniel,1969),i.e.,

$$[\underset{\sim}{a}\ \underset{\sim}{b}\ \underset{\sim}{c}\ \underset{\sim}{d}\ \underset{\sim}{e}\ \underset{\sim}{f}\ \underset{\sim}{g}\ \underset{\sim}{h}\ ]^T = (\underset{\sim}{A}^*\underset{\sim}{A})^{-1}\underset{\sim}{A}^*\underset{\sim}{f} \qquad \ldots(12)$$

where the matrices in Eqn.(12) are given in Appendix, superscript T denotes the transpose of a matrix,and $\underset{\sim}{A}^*$ is the transpose complex conjugate of $\underset{\sim}{A}$. Coefficient vectors $\underset{\sim}{a}$ through $\underset{\sim}{h}$ contain the unknown intensities of sources introduced by Eqns.(10a-h). Once the source intensities are known, the scattered wave field can be evaluated at any point of elastic media through use of Eqns. (11a-d) for incident P,SV, or Rayleigh wave. This topic is considered next.

EVALUATION OF RESULTS

The amplitude of the surface displacement field is evaluated for incident P,SV, and Rayleigh waves and semi-elliptical alluvial valleys,i.e.,

$$C_1: x = R_1 \cos\theta \ ; \ y = R_2 \sin\theta \qquad \ldots(13a)$$

$$0 < \theta < \pi$$

$$C_2: x = R_1 \cos\theta - D \ ; \ y = R_2 \sin\theta \qquad \ldots(13b)$$

where θ denotes the angle measured positive in CW direction (Fig.1), R_1 and R_2 are the principal axes of an ellipse,and D represents the separation distance between the valleys. In order to reduce the number of parameters and thus simplify the numerical evaluation of the results both alluvial valleys are chosen to be identical in shape and material. Both principal axis R_1 and R_2 are assumed to be fixed. The separation distance D is chosen to be equal to $3R_1$.

Semi-elliptical interface of the valley is chosen for testing purposes. Namely, for scattering of plane SH-wave by a semi-elliptical valley there exists an exact solution of Wong and Trifunac(1974),which permitted detailed testing of the boundary integral method-results for a wide range of parameters present in the problem(Dravinski,1982a). These results can be summarized as follows: 1.The boundary integral method provides very good accuracy of the results for a wide range of frequencies; 2. For fixed number of sources the results are more accurate at lower frequencies; 3.As the number of sources increases, the relative error between the exact and the boundary integral method-solution decreases; 4. Good choice of the source surfaces (C_{11},C_{10},...) is the one in which they "follow" in shape corresponding interface (C_1,...).

For convenience, the dimensioneless frequency ($\Omega = 2R_1/\lambda_1$) is introduced as a ratio of the total width of an alluvial valley and wavelength of the incident wave.

For comparison purposes, single-valley-response is depicted first (Figs. 2-4). For more contrasting material of the valley relative to the half-space, the results are shown by Figs. 5-7. For incoming P and SV-waves, the angle of incidence is assumed to be 10°, 30°, 60°, and 90°. As incidated earlier, surface displacement results at each point are presented normalized with respect to the amplitude of the "free-field" $(|u^{ff}|^2 + |v^{ff}|^2)^{\frac{1}{2}}$ at the same point. Thus, all results appear in dimensionless form.

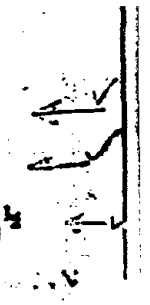

Single-valley-rusults can be summarized briefly as follows: presence of the valley may result in the surface strong ground motion which is very different from the motion that would take place in the half-space if the valley is being absent, i.e., free-field motion; different incident waves caused different amplification patterns at the surface of the half-space; surface motion is strongly dependent upon the angle of incidence; material properties of the valley and the half-space are of great importance for resulting strong ground motion; and surface motion amplification is very sensitive upon the frequency of incoming waves (Dravinski, 1982c).

Since the presence of a subsurface inhomogeniety may influence the strong ground motion in such a complex manner, the following question arises: how does the presence of additional valley effect the surface ground motion atop each of the valleys? This topic is considered next.

Surface displacement amplitude for two alluvial valleys and incident P, SV, and Rayleigh wave of frequency $\Omega = 1$ is shown by Figs. 8-10. It is evident from the results of Figs. 8-10 that the type of wave and angle of incidence influence the surface response significantly. Difference in response atop the two valleys indicates the importance of the interaction between the valleys. Comparison with the single-valley-results (Figs. 2-4) shows that presence of additional valleys may change substantially the

single-valley-response. This should be particularly emphasized for surface response atop the valley in shade. (Terms "illuminated" and "in shade" refer to the valleys D_2 and D_1, respectively.) This is not surprising since to the left of the illuminated valley input motion is caused basically by the free-field only. Ahead of the valley in shade, on the other hand, input field consists of both free-field and scattered waves from the illuminated inclusion. The scattered wave field from illuminated valley is thus causing the response atop the valley in shade to be different from the corresponding single-valley-response. Results of Figs. 8-10 demonstrate that contribution of the scattered waves as an input motion upon the valley in shade may not be neglected. It is interesting to observe from Figs. 8-10 that distribution of local extremes is different for different incoming waves: maximum (minimum) motion for one incident wave may be located at a point on the surface of the half-space which is quite different when compared with location of the maximum (minimum) motion for another incoming wave. In addition, presence of illuminated valley may or may not produce the so called shielding effect atop the valley in shade.

For more contrasting materials of the valleys and the half-space the strong ground motion results are shown by Figs. 11-13. It is obvious from Figs. 8-13 that change in material properties of the valleys causes change in the surface response. For set of parameters chosen in this work, more contrasting materials produced surface displacement field which changes more rapidly with distance than in the case of less contrasting materials. Comparison with Figs. 5-7 leads to the same conclusions as in the case of less contrasting materials: Presence of additional valley may change substantially the single-valley-surface response. This change may be especially large atop the valley in shade.

Results of Figs. 8-13 provide an interesting demonstration of how the angle of incidence influences the strong ground motion. For near vertical incidence and incident P-wave (Figs. 8a and 11a) surface motion is predominantly in vertical direction. Thus, surface displacement field is similar in nature to the incident P-wave which "pulses" soil particles perpendicularly to its wave front, i.e., vertically. For near horizontal incidence of the P-wave (Figs. 9a and 12a) predominant surface motion is taking place in horizontal direction which is again perpendicular to the wave front of the incident wave. For incident SV-wave and near vertical incidence, the horizontal component of the surface motion is prevailing overall (Figs. 9b and 12b), i.e., it behaves similarly as incident wave which moves the soil particles parellel to its wavefront. For near horizontal SV-wave incidence (Figs. 10b and 13b) the strong ground motion pattern is very similar to that of the surface Rayleigh wave (Figs. 10c and 13c). The same conclusions are even more evident from the results of a single-inclusion-model (Figs. 2-7). These results indicate very clearly the importance of the angle of incidence upon the surface amplification pattern in the problem under consideration.

Change of frequency of incident waves to $\Omega = 0.6$ resulted in surface motion shown by Figs. 14-16. Material properties are the same as for the results depicted by Figs. 8-10. Obviously, change in frequency produced marked alteration in displacement field. These results can be summarised as follows: 1) Different incident waves produced different surface displacement patterns; 2) Surface displacement field atop the two valleys are different from each other; 3) Shielding effect atop the valley in shade may or may not occur; and 4) For near vertical (horizontal) incidence of P and SV-waves, the predominant surface motion is of the nature of the incoming wave.

It can be seen from Figs. 10c, 13c, and 16c that the Rayleigh wave response is comparable to those of incident P and SV-waves. This is not surprising since the embedment depth of the valleys is small compared to the wavelength of the incident wave. Since the Rayleigh waves decay exponentially with increase of depth, only part of the elastic media in immediate vicinity of the surface of the half-space contributes substantially to the surface motion. This explains the rather strong contribution of the scattered Rayleigh waves upon the surface motion.

Study by Pekeris and Lifson (1957) indicates that the amplitude of the Rayleigh surface wave is insignificant compared to P and SV-waves for distances that are as much as five times the focal depth of an earthquake. At greater epicentral distances the Rayleigh waves become very prominent (Bolt, 1970). Therefore, the results presented in this paper should be interpreted accordingly.

NUMERICAL EVALUATION OF RESULTS

Extensive testing of boundary integral method (Dravinski, 1982a) suggested a procedure for checking of numerical results. It was observed by comparing the exact and the boundary integral solution that the convergence of the latter can be tested by increasing the number of "observation" points and the "source" points in Eqn. (12) until the results for scattered wave field do not change with their increase. This method has been used in present work to determine the number of sources at which to evaluate the surface displacement field. For simplicity, the same number of sources is chosen inside and outside of the interfaces C_1 and C_2, i.e., $M_1=M_2=L_1=L_2=M$. Number of "observation" points is taken to be the same along the C_1 and C_2, i.e., $N_1=N_2=N$. Ratio of the number of "observation" and "source" points for each of the interface is chosen to be N:M=2:1. "Source" and

"observation" points are chosen to be equally spaced along the corresponding surfaces. The source surfaces C_{1i} and C_{2i} are defined through Eqns. (13a-b) by replacing R_1 and R_2 with R_{1i} and R_{2i}, respectively. Similarly, the source surfaces C_{1o} and C_{2o} are specified by Eqns. (13a-b) provided R_1 and R_2 are replaced by R_{1o} and R_{2o}, respectively. Numerical results are evaluated for $R_{1,2i} = 0.75\ R_{1,2}$ and $R_{1,2o} = 1.25\ R_{1,2}$. Surface displacement amplitude is calculated for different number of "sources" and "observation" points.and then compared. The number of "sources" and the "observation" points is increased, until the difference between the subsequent results is sufficiently small. Earlier studies of the boundary integral method results (e.g., Dravinski, 1982a) indicate that as the frequency of the incident wave increases, the number of "sources" and "observation" points should be increased in order to achieve the same accuracy of the results as in the case of lower frequencies. This is the main reason for relatively low frequency of the input wave for calculations presented in this paper ($\Omega = 0.6$ and $\Omega = 1$). This choice of frequency reduced the cost of calculations substantially.

Through numerical evaluation of the results, it was learned that even for such a simple geometry as chosen in this work the amount of computer memory required for computations is considerable. For more complicated geometry of the interfaces and higher frequency of incident field even more of the memory core is required. However, with present day developments of digital computers, this may not represent any problem in application of the method to more realistic models.

Although approximate, the boundary integral methods provide a way to study a wide class of problems for which no exact solution exists at the present time. Intensive research regarding the existance and uniqueness of the boundary integral solutions (e.g., Herrera, 1982) promises to provide a

through understanding of this powerful method and thus enhance its application to problems of strong ground motion seismology and earthquake engineering.

SUMMARY AND CONCLUSIONS

Strong ground motion amplification is investigated for a half-space with two alluvial valleys of arbitrary shape subjected to plane harmonic P, SV, or Rayleigh waves. The amplitude of surface motion is evaluated using a boundary integral method. It is determined that mutual interaction between the valleys may have a strong influence upon the surface response, particularly atop the alluvial valley in shade. It is observed that surface motion is very sensitive upon the type of incident wave, angle of incidence, material properties of the half-space and the valleys, and frequency of the incoming wave. Shielding effect atop the valley in shade may or may not occur. Motion peeks are observed at different locations for different incident waves.

Although very simple, the model studied in this paper provides results which indicate that in close proximity of several alluvial valleys their mutual interaction may be of great importance in determining the surface response due to an earthquake. Consequently, additional valleys may be required in modeling strong ground motion for some alluvial basins more accurately.

ACKNOWLEDGEMENTS

Special thanks to Prof. I. Herrera for communicating to the author his recent papers dealing with boundary integral methods. Discussion with

Prof. J. E. Luco regarding the boundary integral methods is greatly appreciated.

This paper has been completed through a support by grants PFR-8009336 and CEE-8119696 from the National Science Foundation.

REFERENCES

Apsel,J.R.(1979). Dynamic Green's Functions for Layered Media and Applications to Boundary-Value Problems, Ph. D. Thesis,Univ. of California at San Diego.

Bolt,B.(1970). Elastic Waves in the Vicinity of the Earthquake, Earthquake Engineering,R.L.Wiegel(ed.),Prentice Hall,New York.

Boore,D.M.(1973). The Effect of Simple Topography on Seismic Waves: Implications for Accelerations Recorded at Pacoima Dam,San Fernando Valley,California,Bull. Seism. Soc. Amer.,62,pp.1608-1619.

Copley,L.G.(1967). Integral Equation Method for Radiation from Vibrating Surfaces,J. Acoust. Soc. Amer.,41,pp.807-816.

Dravinski,M.(1980). Scattering of Elastic Waves by an Alluvial Valley of Arbitrary shape,Univ. Southern Calif.,Dpt. Civil Engng., Report No. CE 80-06,Los Angeles,California.

Dravinski,M.(1982a). Scattering of SH-Waves by Subsurface Topography,ASCE,J. Engng. Mech. Div.,108,No.EM1,pp.

Dravinski,M.(1982b). Scattering of Waves by an Alluvial Valley, ASCE,J. Engng. Mech. Div.,108,No.EM1,pp.

Dravinski,M.(1982c). Influence of Interface Depth Upon Strong Ground Motion,Bull. Seism. Sos. Amer.,72,No.2,pp.

Dravinski,M.(1982d). Amplification of SH Waves by Two Alluvial Valleys,submitted for publication.

Esteva,L.(1972). Microzoning:Models and Reality,Proc.World Conf. Earthquake Engr.,6th,New Delhi.

Griffiths,D.W.,and G.A.Bollinger(1979). The Effect of Appalachian Mountain Topography on Seismic Waves, Bull. Seism. Soc. Amer., 69,pp.1081-1105.

Herrera,I.(1982). Boundary Methods for Fluids,Finite Elements for Fluids,Vol.IV,R.H.Gallagher(ed.),John Willey & Sons,New York(to appear).

Jennings,P.C.(editor)(1971). San Fernando Earthquake of February 9,1971,EERL-71-02,Calif. Inst. Tech., Pasadena,California.

Lamb,H.(1904). On Propagation of Tremors Over the Surface of an Elastic Solid,Phil. Trans. Royal Soc. London,A359,203,pp.1-40.

Lapwood,E.R.(1948). The Disturbance due to a Line Source in a Semi-Infinite Elastic Medium,Phil. Trans. Royal Soc. London, A841,242,pp.63-100.

Miklowitz,J.(1978). The Theory of Elastic Waves and Waveguides, North Holland,Amsterdam.

Noble,B., and J.W.Daniel(1969). Applied Linear Algebra,Prentice Hall,New Jersey.

Oshaki,Y.(1973). On movements of a Rigid Body in Semi-Infinite Elastic Medium,Proc. Japanese Earthquake Engng. Symp.,Tokyo, Japan.

Pekiris,C.C., and H. Lifson(1957). Motion of the Surface of a Uniform Elastic Half-Space Produced by a Burried Pulse,J.Acoust. Soc.Amer.,29,p1233.

Sanchez-Sesma,F.J., and J.A.Esquivel(1979). Ground Motion on Alluvial Valleys Under the Incident Plane SH Waves,Bull.Seism. Soc.Amer.,69,pp.1107-1120.

Sanchez-Sesma,F.J.,and E.Rosenblueth(1979). Ground Motion at Canyons of Arbitrary Shapes Under Incident SH-Waves,Earthquake Engng.Struct.Dyn.,7,pp.441-450.

Sozen,M.A.,P.C.Jennings,R.B.Matthiesen,G.W.Housner and N.M.Newmark (1968). Engineering Report on the Caracas Earthquake of July 29, 1967. National Academy of Sciences,Washington,D.C.

Ursel,F.(1973). On the Exterior Problem of Acoustics,Proc. Cambridge Phil.Soc.,74,pp.117-125.

Wong,H.L.(1979). Scattering of P,SV,and Rayleigh Waves by Sub-surface Topographies,Univ.Southern Calif.,Dept.Civil Engng., Report No.CE 7905,Los Angeles,California.

Wong,H.L.,and M.D.Trifunac(1974). Surface Motion of a Semi-Elliptical Alluvial Valley for Incident Plane SH-Waves,Bull. Seism.Soc.Amer.,64,pp.1389-1408.

APPENDIX

Matrix $\underset{\sim}{A}$ in Eqn.(12) is a $4(N_1+N_2)\times 2(M_1+M_2+L_1+L_2)$ matrix defined by

$$\underset{\sim}{A} = \begin{bmatrix} \underset{\sim}{A}_1 & \underset{\sim}{A}_2 \\ \underset{\sim}{A}_3 & \underset{\sim}{A}_4 \end{bmatrix} , \qquad \ldots(A1)$$

where

$$\underset{\sim}{A}_1 = \begin{bmatrix} \phi_0 & \phi_0 & \psi_0 & \psi_0 \\ \underset{\sim}{U}_{N_1M_1} & \underset{\sim}{U}_{N_1M_2} & \underset{\sim}{U}_{N_1M_1} & \underset{\sim}{U}_{N_1M_2} \\ \phi_0 & \phi_0 & \psi_0 & \psi_0 \\ \underset{\sim}{V}_{N_1M_1} & \underset{\sim}{V}_{N_1M_2} & \underset{\sim}{V}_{N_1M_1} & \underset{\sim}{V}_{N_1M_2} \\ \phi_0 & \phi_0 & \psi_0 & \psi_0 \\ \underset{\sim}{\Sigma}_{nnN_1M_1} & \underset{\sim}{\Sigma}_{nnN_1M_2} & \underset{\sim}{\Sigma}_{nnN_1M_1} & \underset{\sim}{\Sigma}_{nnN_1M_2} \\ \phi_0 & \phi_0 & \psi_0 & \psi_0 \\ \underset{\sim}{\Sigma}_{ntN_1M_1} & \underset{\sim}{\Sigma}_{ntN_1M_2} & \underset{\sim}{\Sigma}_{ntN_1M_1} & \underset{\sim}{\Sigma}_{ntN_1M_2} \end{bmatrix} \qquad \ldots(A2)$$

$$\underset{\sim}{A}_2 = \begin{bmatrix} \phi_1 & \psi_1 & & \\ -\underset{\sim}{U}_{N_1L_1} & -\underset{\sim}{U}_{N_1L_1} & \underset{\sim}{0}_{N_1L_2} & \underset{\sim}{0}_{N_1L_2} \\ \phi_1 & \psi_1 & & \\ -\underset{\sim}{V}_{N_1L_1} & -\underset{\sim}{V}_{N_1L_1} & \underset{\sim}{0}_{N_1L_2} & \underset{\sim}{0}_{N_1L_2} \\ \phi_1 & \psi_1 & & \\ -\underset{\sim}{\Sigma}_{nnN_1L_1} & -\underset{\sim}{\Sigma}_{nnN_1L_1} & \underset{\sim}{0}_{N_1L_2} & \underset{\sim}{0}_{N_1L_2} \\ \phi_1 & \psi_1 & & \\ -\underset{\sim}{\Sigma}_{ntN_1L_1} & -\underset{\sim}{\Sigma}_{ntN_1L_1} & \underset{\sim}{0}_{N_1L_2} & \underset{\sim}{0}_{N_1L_2} \end{bmatrix} \qquad \ldots(A3)$$

$$\underset{\sim}{A}_3 = \begin{bmatrix} \underset{\sim}{U}^{\phi_0}_{N_1M_1} & \underset{\sim}{U}^{\phi_0}_{N_2M_2} & \underset{\sim}{U}^{\psi_0}_{N_2M_1} & \underset{\sim}{U}^{\psi_0}_{N_2M_2} \\ \underset{\sim}{V}^{\phi_0}_{N_2M_1} & \underset{\sim}{V}^{\phi_0}_{N_2M_2} & \underset{\sim}{V}^{\psi_0}_{N_2M_1} & \underset{\sim}{V}^{\psi_0}_{N_2M_2} \\ \underset{\sim}{\Sigma}^{\phi_0}_{nnN_2M_1} & \underset{\sim}{\Sigma}^{\phi_0}_{nnN_2M_2} & \underset{\sim}{\Sigma}^{\psi_0}_{nnN_2M_1} & \underset{\sim}{\Sigma}^{\psi_0}_{nnN_2M_2} \\ \underset{\sim}{\Sigma}^{\phi_0}_{ntN_2M_1} & \underset{\sim}{\Sigma}^{\phi_0}_{ntN_2M_2} & \underset{\sim}{\Sigma}^{\psi_0}_{ntN_2M_1} & \underset{\sim}{\Sigma}^{\psi_0}_{ntN_2M_2} \end{bmatrix} \qquad \ldots(A4)$$

$$\underset{\sim}{A}_4 = \begin{bmatrix} \underset{\sim}{0}_{N_2L_1} & \underset{\sim}{0}_{N_2L_1} & -\underset{\sim}{U}^{\phi_2}_{N_2L_2} & -\underset{\sim}{U}^{\psi_2}_{N_2L_2} \\ \underset{\sim}{0}_{N_2L_1} & \underset{\sim}{0}_{N_2L_1} & -\underset{\sim}{V}^{\phi_2}_{N_2L_2} & -\underset{\sim}{V}^{\psi_2}_{N_2L_2} \\ \underset{\sim}{0}_{N_2L_1} & \underset{\sim}{0}_{N_2L_1} & -\underset{\sim}{\Sigma}^{\phi_2}_{nnN_2L_2} & -\underset{\sim}{\Sigma}^{\psi_2}_{nnN_2L_2} \\ \underset{\sim}{0}_{N_2L_1} & \underset{\sim}{0}_{N_2L_1} & -\underset{\sim}{\Sigma}^{\phi_2}_{ntN_2L_2} & -\underset{\sim}{\Sigma}^{\psi_2}_{ntN_2L_2} \end{bmatrix}. \qquad \ldots(A5)$$

For each submatrix in Eqns.(A2-5) the following convention is understood: Superscripts $\phi_0,\phi_1,\ldots,$etc denote the wave potential with which the elements of the particular submatrix are associated with; Subscripts MM and ML determine the size of the matrix and location of the surface where the elements of the matrix are evaluated: N_1,N_2,M_1,M_2,L_1,L_2 are associated with $r\varepsilon C_1,C_2,C_{1i},C_{2i}$, C_{1o},C_{2o},respectively. For example,

$$\underset{\sim}{U}^{\phi_0}_{N_2M_1} = [u^{\phi_0}(\underset{\sim}{r}_i,\underset{\sim}{r}_j)] \; ; \; \underset{\sim}{r}_i\varepsilon C_2 \; ; \; \underset{\sim}{r}_j\varepsilon C_{1i} \; ; \; \begin{matrix} i=1,2,\ldots,N_2 \; ; \\ j=1,2,\ldots,M_1 \; . \end{matrix}$$

Similarly,

$$\underset{\sim}{\Sigma}^{\psi_2}_{ntN_2L_2} = [\sigma^{\psi_2}_{nt}(\underset{\sim}{r}_i,\underset{\sim}{r}_j)] \; ; \; \underset{\sim}{r}_i \epsilon C_2 \; ; \; \underset{\sim}{r}_j \epsilon C_{2o} \; ; \; \begin{matrix} i=1,2,\ldots,N_2 \; ; \\ j=1,2,\ldots,L_2 \; , \end{matrix}$$

etc. Vector f in Eqn.(12) is of the size $4(N_1+N_2)x1$ defined by

$$\underset{\sim}{f}^T = [-\underset{\sim}{U}^{ff}_{N_1} \; -\underset{\sim}{V}^{ff}_{N_1} \; -\underset{\sim}{\Sigma}^{ff}_{nnN_1} \; -\underset{\sim}{\Sigma}^{ff}_{ntN_1} \; -\underset{\sim}{U}^{ff}_{N_2} \; -\underset{\sim}{V}^{ff}_{N_2} \; -\underset{\sim}{\Sigma}^{ff}_{nnN_2} \; -\underset{\sim}{\Sigma}^{ff}_{ntN_2}], \quad \ldots(A6)$$

where

$$\underset{\sim}{U}^{ff}_{N_1} = [u^{ff}(\underset{\sim}{r}_i)] \; ; \; \underset{\sim}{V}^{ff}_{N_1} = [v^{ff}(\underset{\sim}{r}_i)] \; ; \; \underset{\sim}{r}_i \epsilon C_1 ; i=1,2,\ldots,N_1 \quad \ldots(A7)$$

$$\underset{\sim}{\Sigma}^{ff}_{nnN_1} = [\sigma^{ff}_{nn}(\underset{\sim}{r}_i)]; \; \underset{\sim}{\Sigma}^{ff}_{ntN_1} = [\sigma^{ff}_{nt}(\underset{\sim}{r}_i)] \quad \ldots(A8)$$

$$\underset{\sim}{U}^{ff}_{N_2} = [u^{ff}(\underset{\sim}{r}_j)] \; ; \; \underset{\sim}{V}^{ff}_{N_2} = [v^{ff}(\underset{\sim}{r}_j)] \; ; \; \underset{\sim}{r}_j \epsilon C_2 ; j=1,2,\ldots,N_2 \quad \ldots(A9)$$

$$\underset{\sim}{\Sigma}^{ff}_{nnN_2} = [\sigma^{ff}_{nn}(\underset{\sim}{r}_j)]; \; \underset{\sim}{\Sigma}^{ff}_{ntN_2} = [\sigma^{ff}_{nt}(\underset{\sim}{r}_j)] \quad \ldots(A10)$$

and the superscript ff denotes the free field.

FIGURE CAPTIONS

Fig. 1 Problem Geometry

Fig. 2 Surface Displacement Amplitude: Single Alluvial Valley
(If not stated differently: $\Omega = 1$, $R_1 = 4$, $R_2 = 1$, $N = 24$, $M = L = 12$, $\mu_o = \beta_o = 1$, $\mu_1 = \beta_1 = 0.8$, $\alpha_o = 2$, $\alpha_1 = 1.6$)

a) - Incident P-Wave: $\theta_o = 10^\circ$
b) - Incident P-Wave: $\theta_o = 30^\circ$
c) - Incident P-Wave: $\theta_o = 60^\circ$

Fig. 3 Surface Displacement Amplitude: Single Alluvial Valley

a) - Incident P-Wave: $\theta_o = 80^\circ$
b) - Incident SV-Wave: $\theta_o = 10^\circ$
c) - Incident SV-Wave: $\theta_o = 30^\circ$

Fig. 4 Surface Displacement Amplitude: Single Alluvial Valley

a) - Incident SV-Wave: $\theta_o = 60^\circ$
b) - Incident SV-Wave: $\theta_o = 80^\circ$
c) - Incident Rayleigh Wave

Fig. 5 Surface Displacement Amplitude: Single Alluvial Valley
($\mu_1 = \beta_1 = 0.6$, $\alpha_1 = 1.2$)

a) - Incident P-Wave: $\theta_o = 10^\circ$
b) - Incident P-Wave: $\theta_o = 30^\circ$
c) - Incident P-Wave: $\theta_o = 60^\circ$

Fig. 6 Surface Displacement Amplitude: Single Alluvial Valley
($\mu_1 = \beta_1 = 0.6$, $\alpha_1 = 1.2$)

a) - Incident P-Wave: $\theta_o = 80^\circ$
b) - Incident SV-Wave: $\theta_o = 10^\circ$
c) - Incident SV-Wave: $\theta_o = 30^\circ$

Fig. 7 Surface Displacement Amplitude: Single Alluvial Valley
($\mu_1 = \beta_1 = 0.6$, $\alpha_1 = 1.2$)

a) - Incident SV-Wave: $\theta_o = 60^\circ$
b) - Incident SV-Wave: $\theta_o = 80^\circ$
c) - Incident Rayleigh Waves

Fig. 8 Surface Displacement Amplitude: Two Alluvial Valleys
(If not stated differently: $\Omega = 1$, $R_1 = 4$, $R_2 = 1$, $N = 24$, $M = L = 12$, $\mu_o = \beta_o = 1$, $\mu_1 = \beta_1 = \mu_2 = \beta_2 = 0.8$, $\alpha_o = 2$,

$\alpha_1 = \alpha_2 = 1.6$, D = 12)

a) - Incident P-Wave: $\theta_o = 10^o$

b) - Incident P-Wave: $\theta_o = 30^o$

c) - Incident P-Wave: $\theta_o = 60^o$

Fig. 9 Surface Displacement Amplitude: Two Alluvial Valleys

a) - Incident P-Wave: $\theta_o = 80^o$

b) - Incident SV-Wave: $\theta_o = 10^o$

c) - Incident SV-Wave: $\theta_o = 30^o$

Fig. 10 Surface Displacement Amplitude: Two Alluvial Valleys

a) - Incident SV-Wave: $\theta_o = 60^o$

b) - Incident SV-Wave: $\theta_o = 80^o$

c) - Incident Rayleigh Wave

Fig. 11 Surface Displacement Amplitude: Two Alluvial Valleys
($\mu_1 = \beta_1 = \mu_2 = \beta_2 = 0.6$, $\alpha_1 = \alpha_2 = 1.2$)

a) - Incident P-Wave: $\theta_o = 10^o$

b) - Incident P-Wave: $\theta_o = 30^o$

c) - Incident p-Wave: $\theta_o = 60^o$

Fig. 12 Surface Displacement Amplitude: Two Alluvial Valleys
($\mu_1 = \beta_1 = \mu_2 = \beta_2 = 0.6$, $\alpha_1 = \alpha_2 = 1.2$)

a) - Incident P-Wave: $\theta_o = 80^o$

b) - Incident SV-Wave: $\theta_o = 10^o$

c) - Incident SV-Wave: $\theta_o = 30^o$

Fig. 13 Surface Displacement Amplitude: Two Alluvial Valleys
($\mu_1 = \beta_1 = \mu_2 = \beta_2 = 0.6$, $\alpha_1 = \alpha_2 = 1.2$)

a) - Incident SV-Wave: $\theta_o = 60^o$

b) - Incident SV-Wave: $\theta_o = 80^o$

c) - Incident Rayleigh Wave

Fig. 14 Surface Displacement Amplitude: Two Alluvial Valleys
($\Omega = 0.6$, $\mu_1 = \beta_1 = \mu_2 = \beta_2 = 0.8$, $\alpha_1 = \alpha_2 = 1.6$)

a) - Incident P-Wave: $\theta_o = 10^o$

b) - Incident P-Wave: $\theta_o = 30^o$

c) - Incident P-Wave: $\theta_o = 60^o$

Fig. 15 Surface Displacement Amplitude: Two Alluvial Valleys
($\Omega = 0.6$, $\mu_1 = \beta_1 = \mu_2 = \beta_2 = 0.8$, $\alpha_1 = \alpha_2 = 1.6$)

a) - Incident P-Wave: $\theta_o = 80^o$

b) - Incident SV-Wave: $\theta_o = 10^o$

c) - Incident SV-Wave: $\theta_o = 30^o$

Fig. 16 Surface Displacement Amplitude: Two Alluvial Valleys
($\Omega = 0.6$, $\mu_1 = \beta_1 = \mu_2 = \beta_2 = 0.8$, $\alpha_1 = \alpha_2 = 1.6$)

a) - Incident SV-Wave: $\theta_o = 60^o$

b) - Incident SV-Wave: $\theta_o = 80^o$

c) - Incident Rayleigh Wave

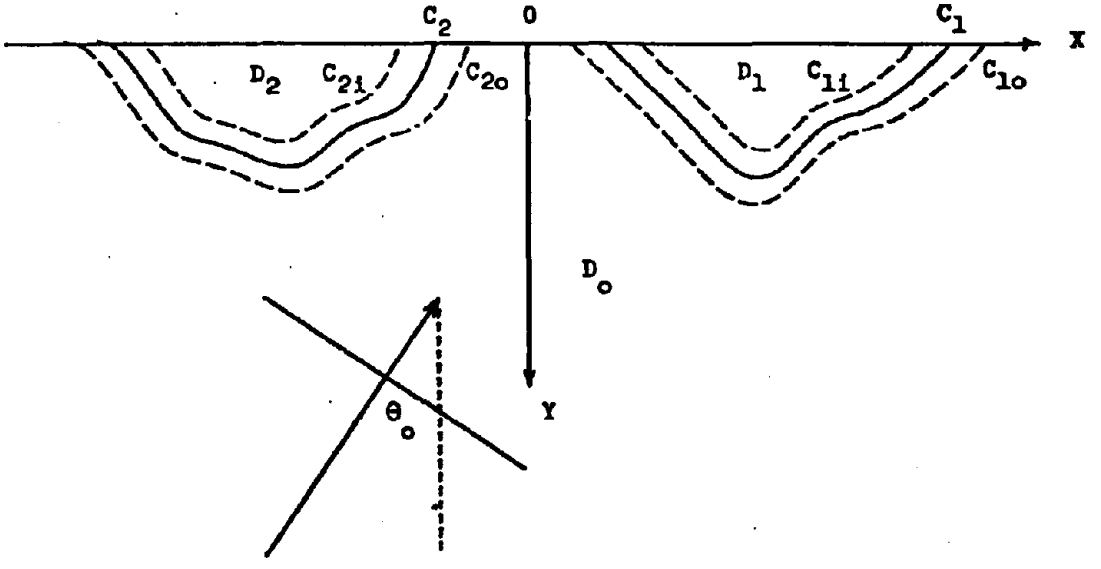

Fig. 1

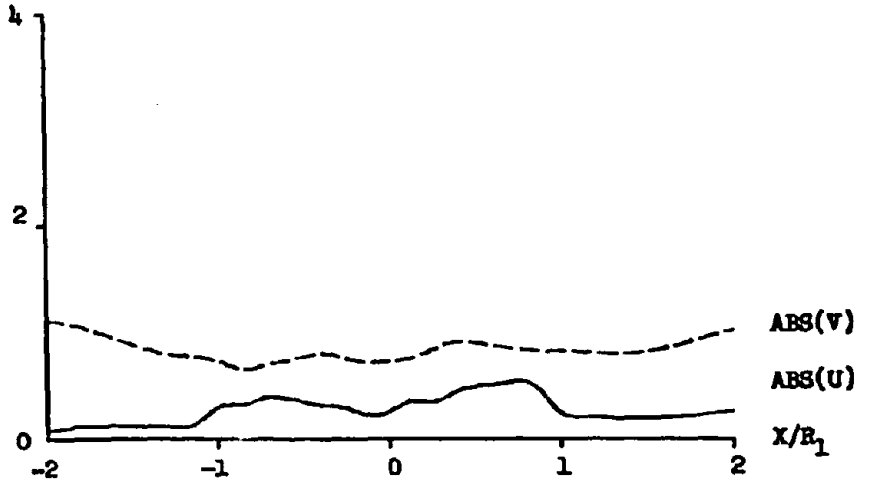

Fig. 2a

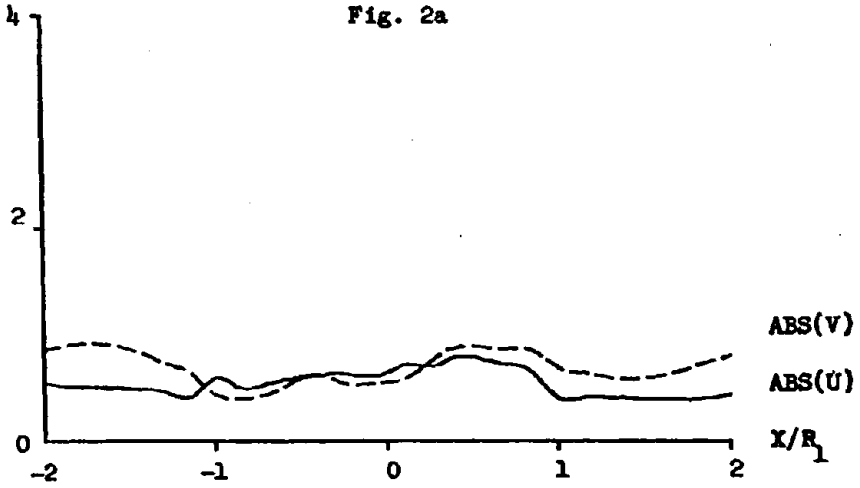

Fig. 2b

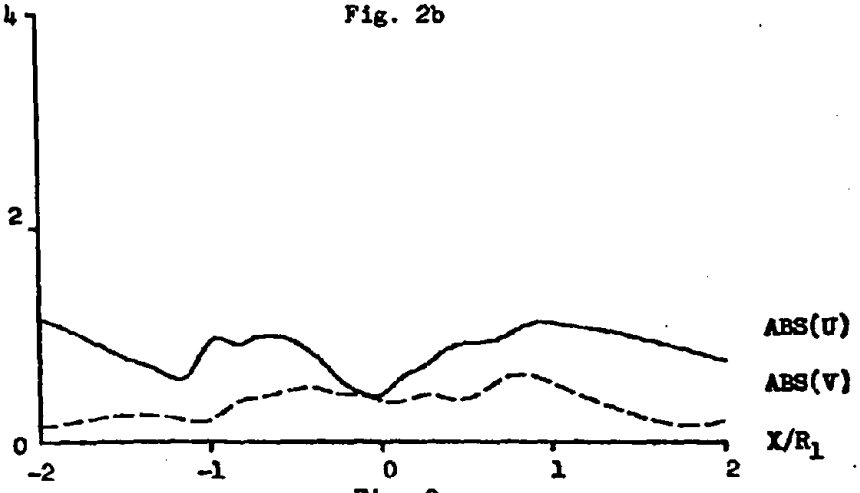

Fig. 2c

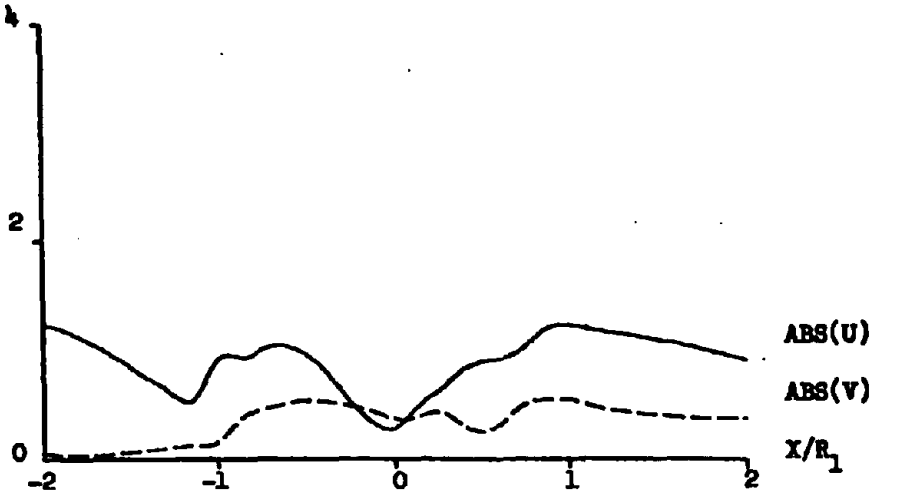

Fig.3a

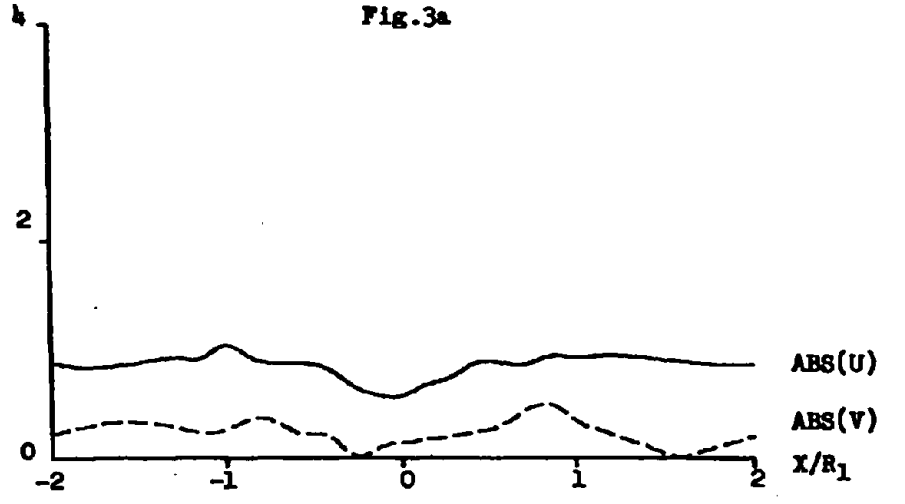

Fig. 3b

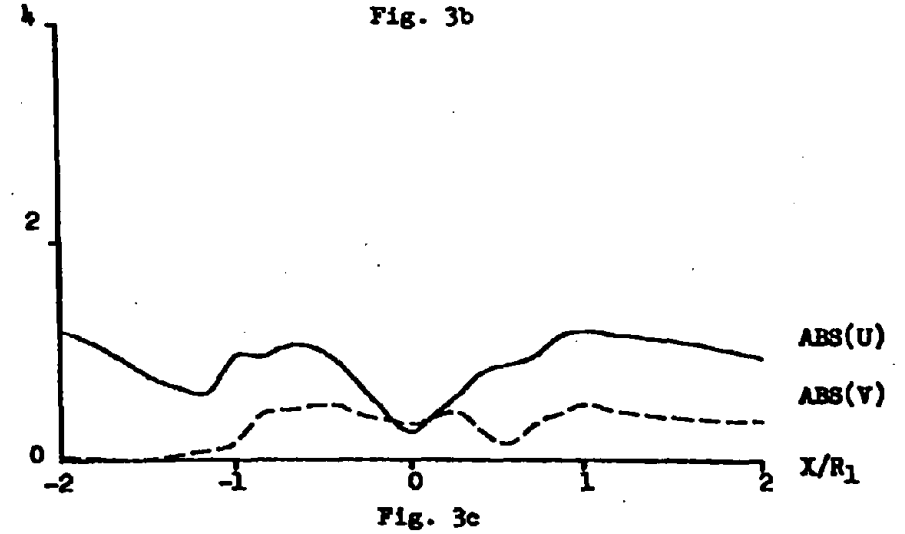

Fig. 3c

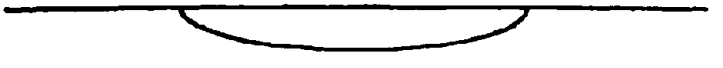

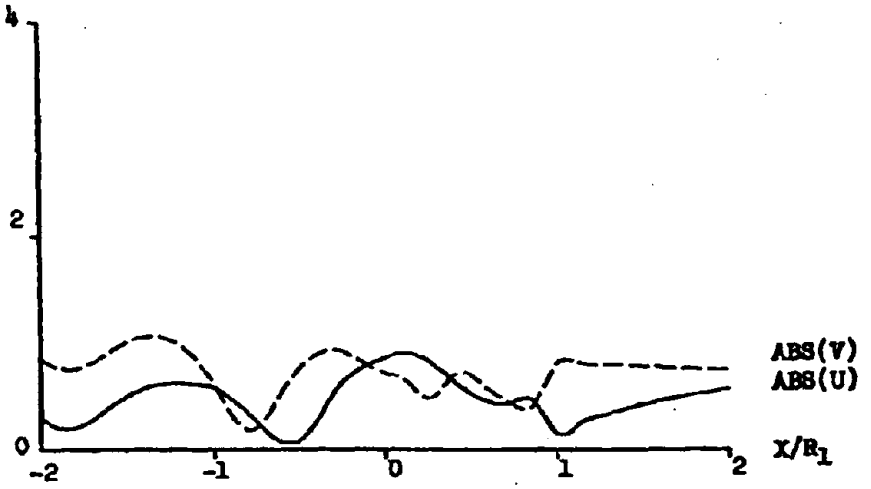

Fig. 4a

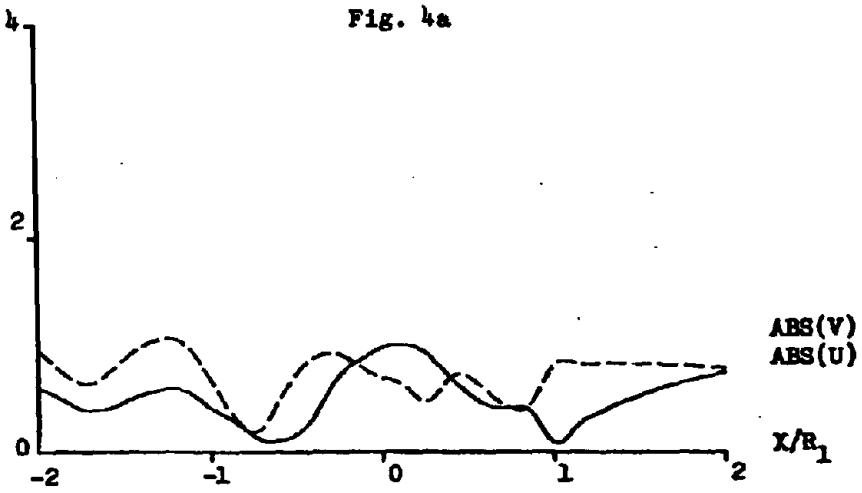

Fig. 4b

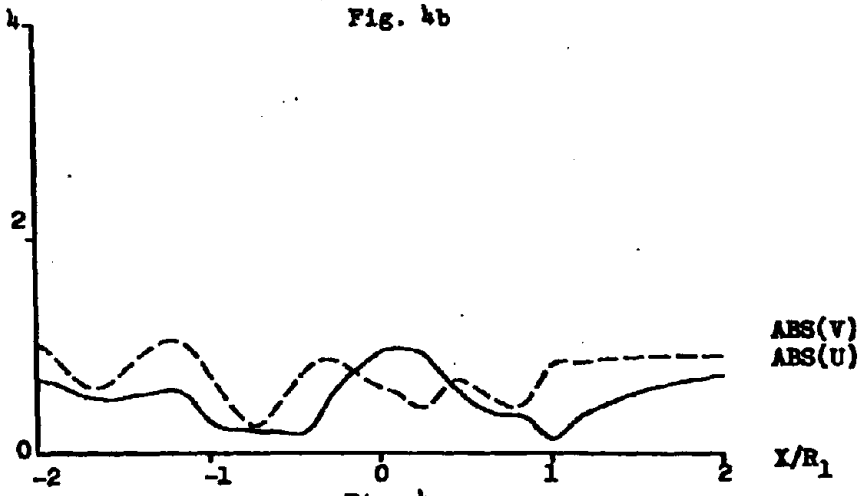

Fig. 4c

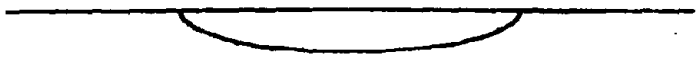

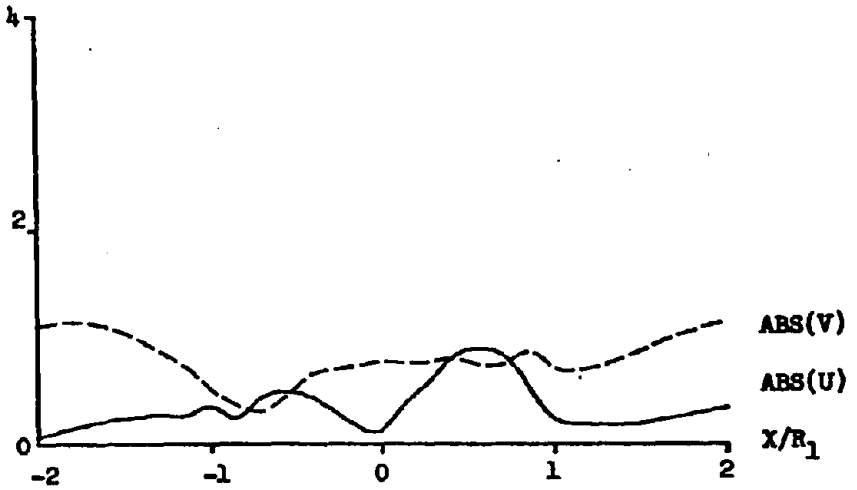

Fig. 5a

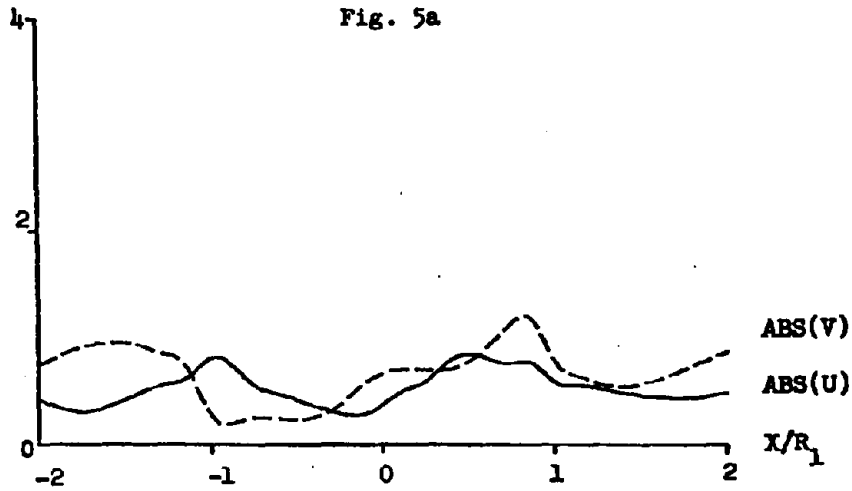

Fig. 5b

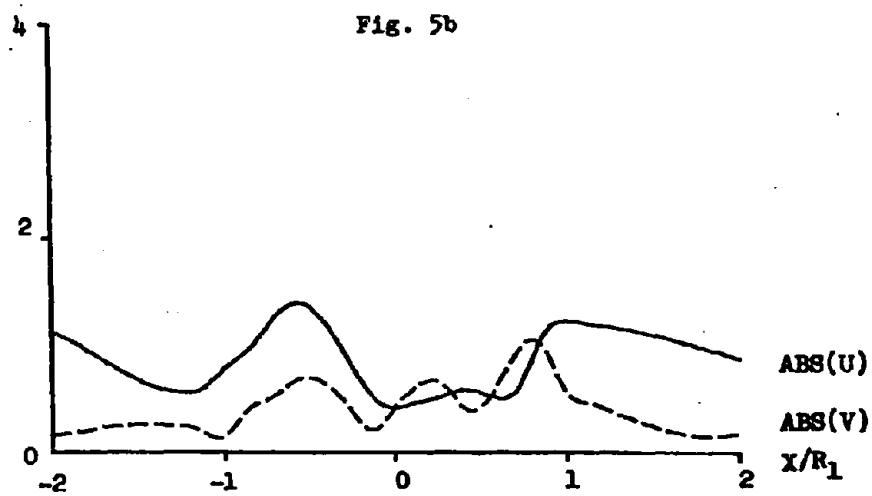

Fig. 5c

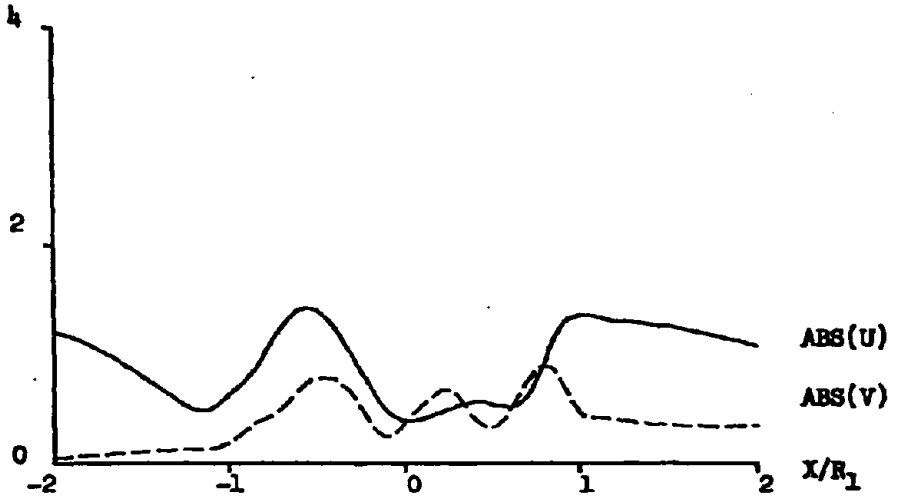

Fig. 6a

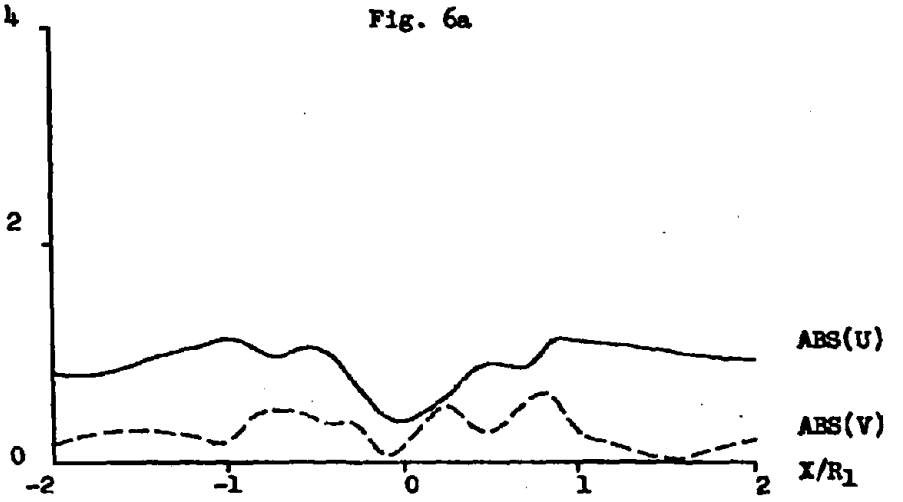

Fig. 6b

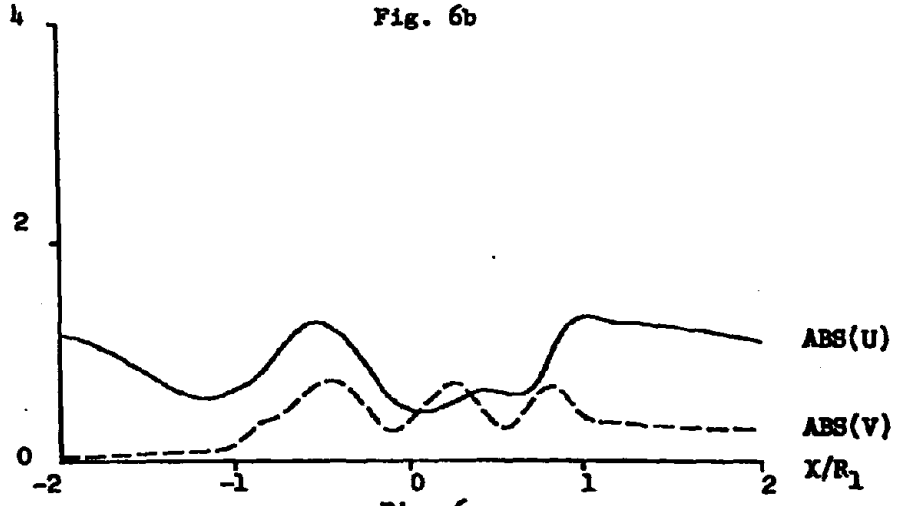

Fig. 6c

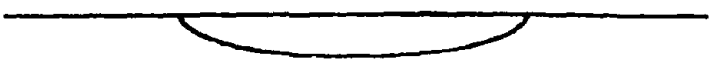

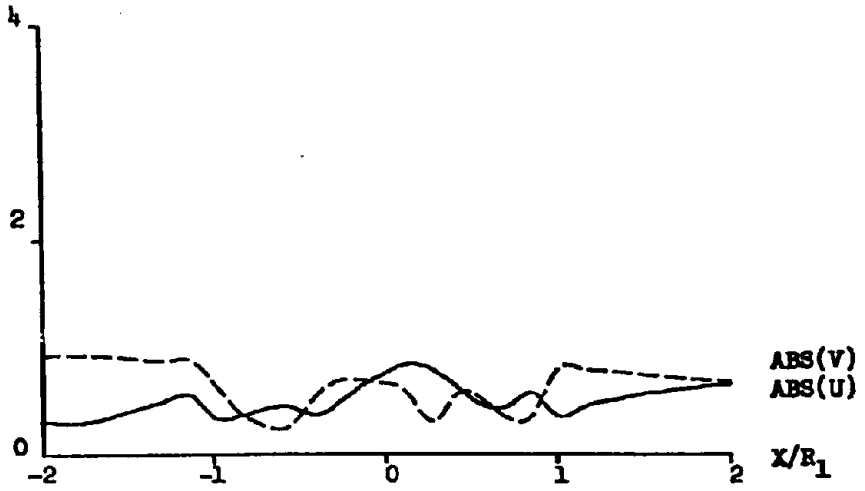

Fig. 7a

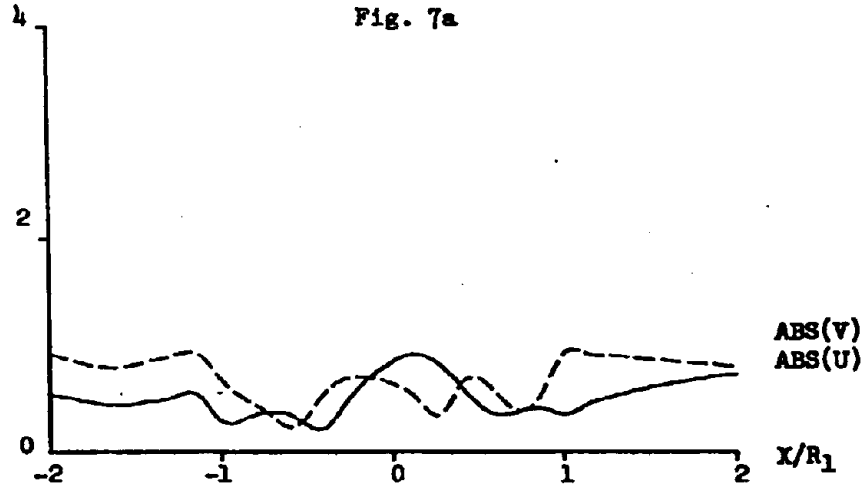

Fig. 7b

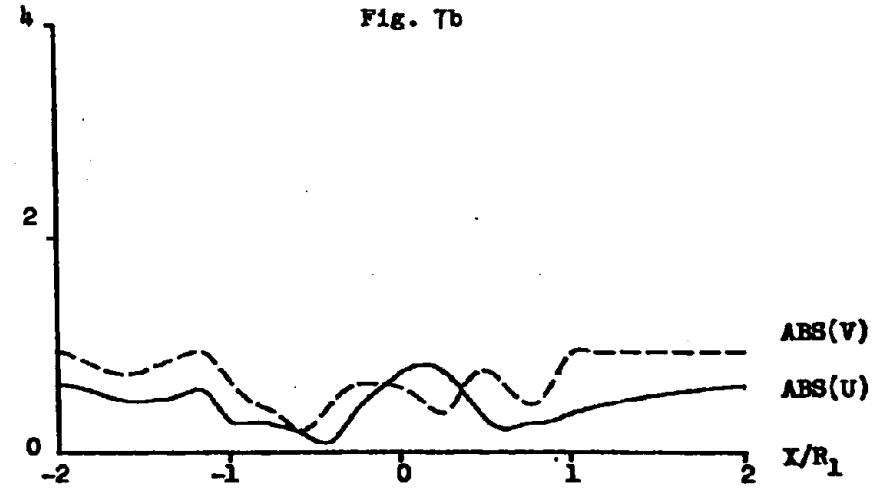

Fig. 7c

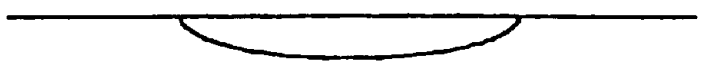

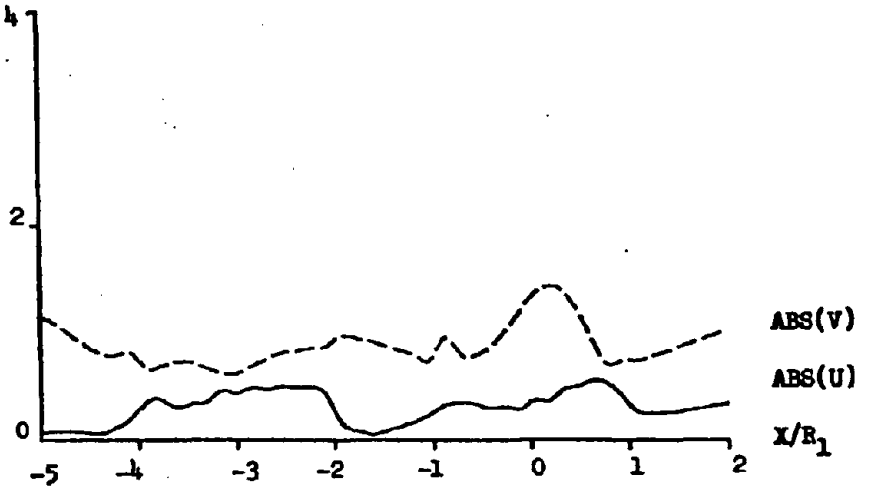

Fig. 8a

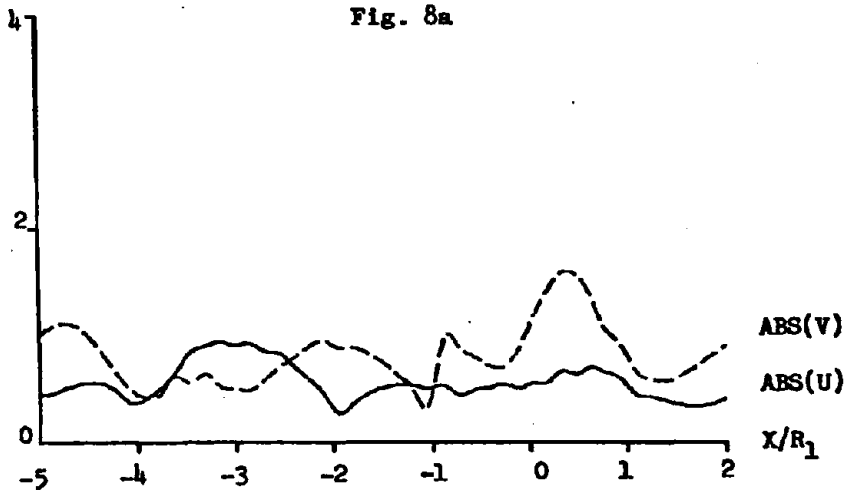

Fig. 8b

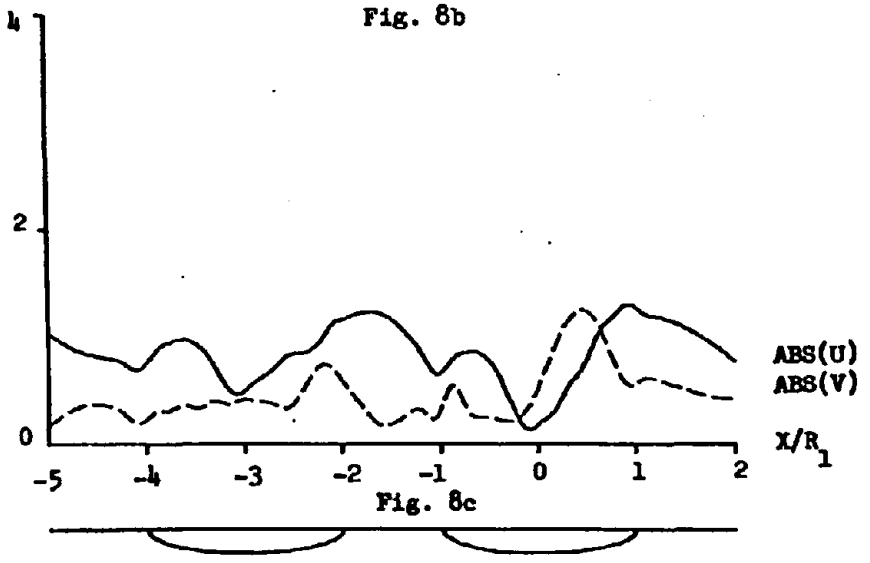

Fig. 8c

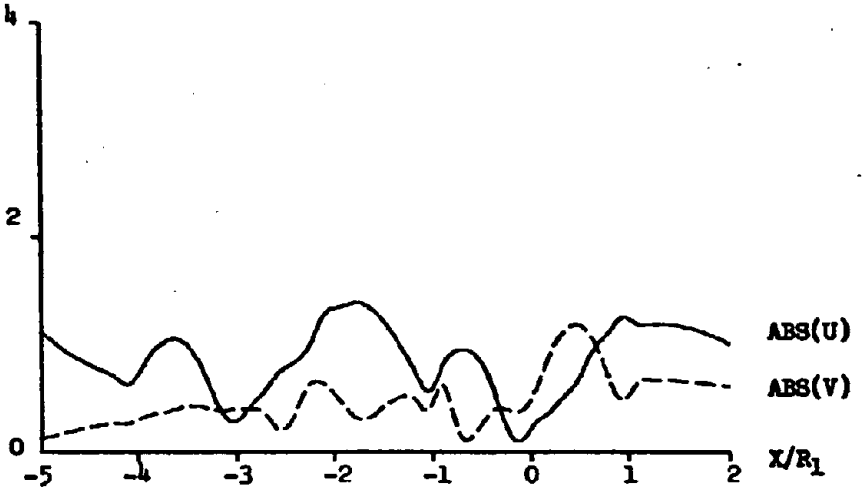

Fig. 9a

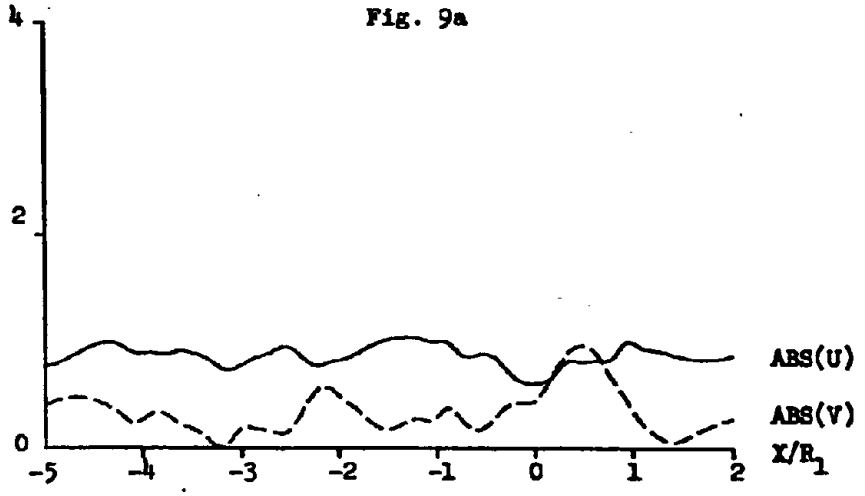

Fig. 9b

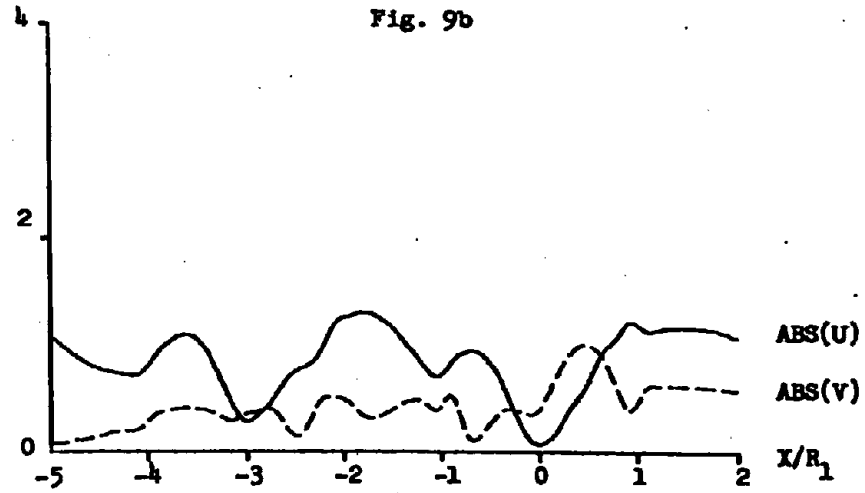

Fig. 9c

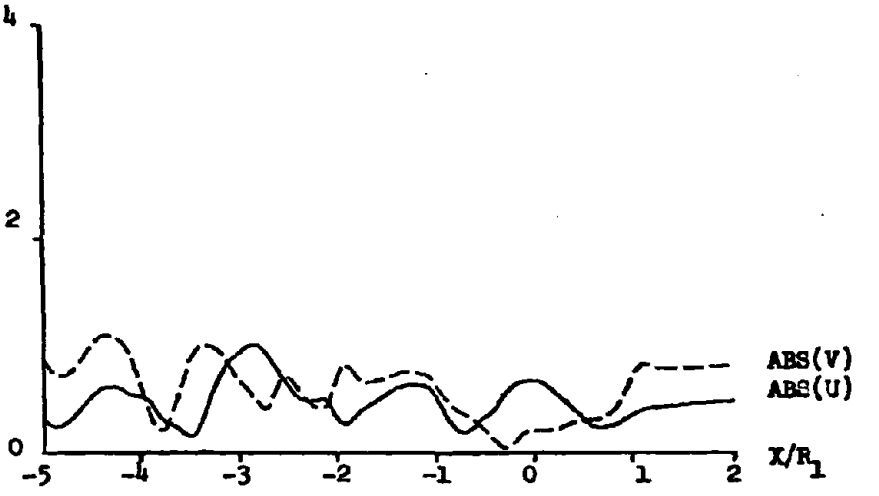

Fig.10a

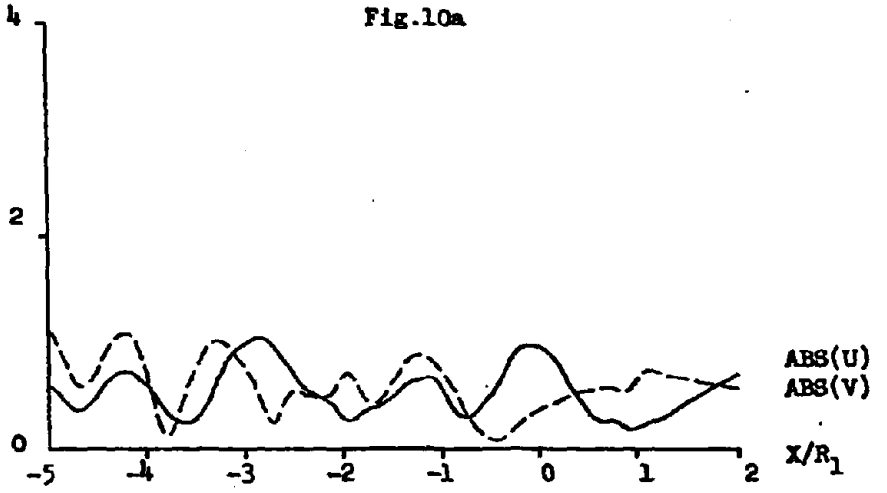

Fig.10b

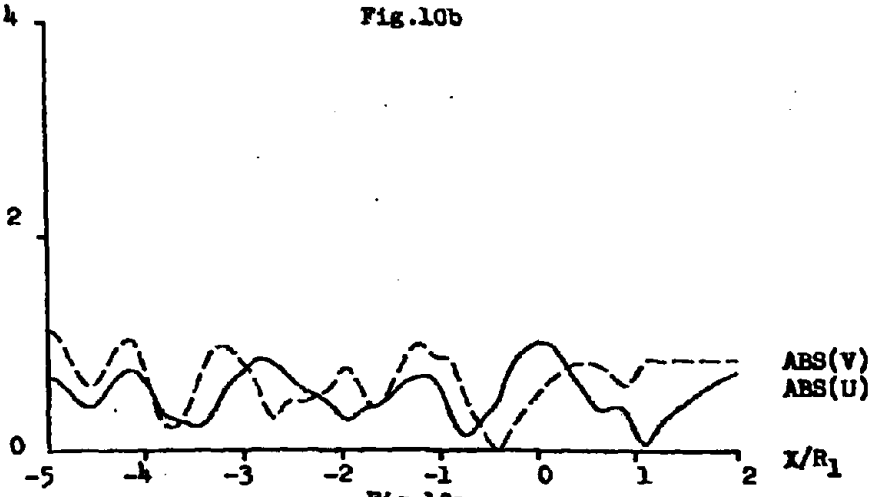

Fig.10c

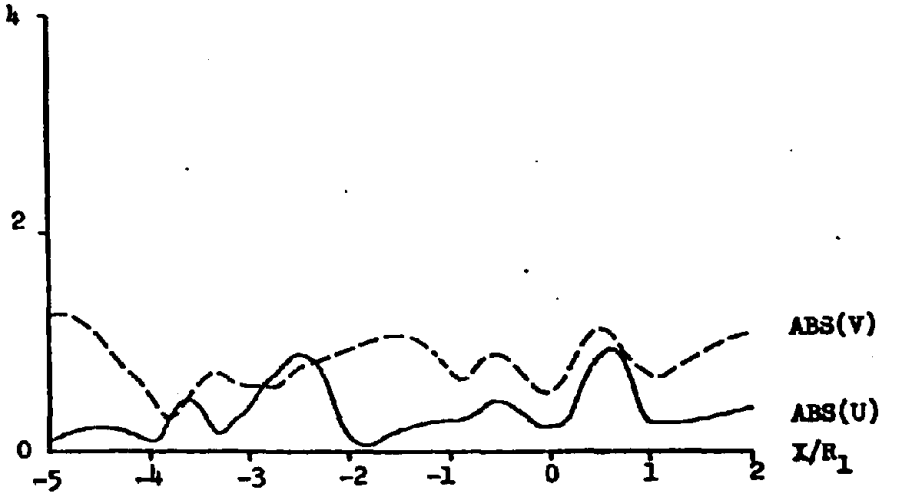

Fig.11a

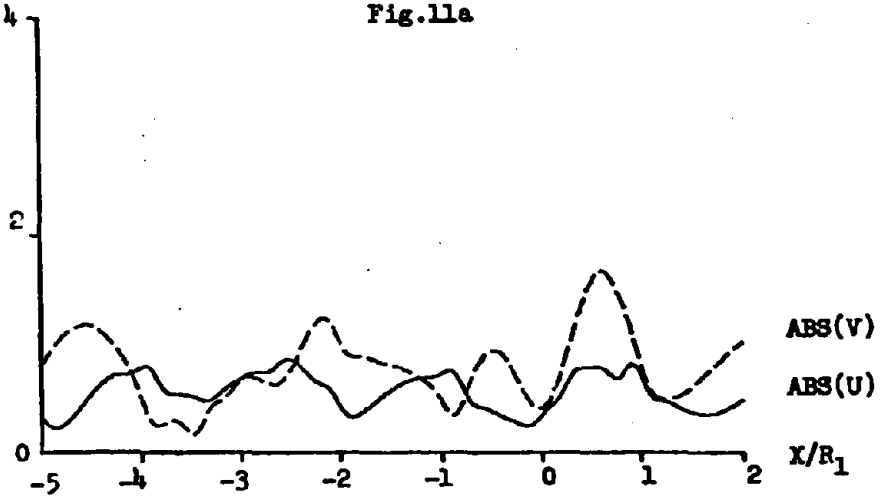

Fig.11b

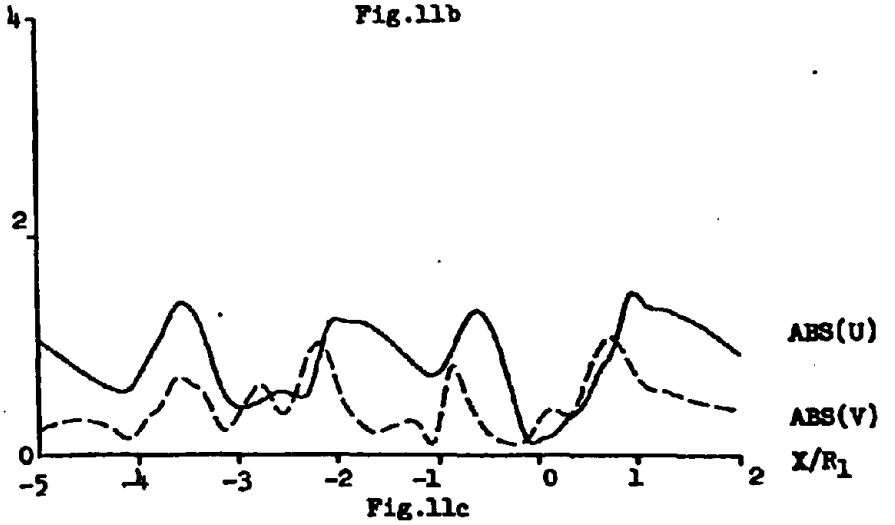

Fig.11c

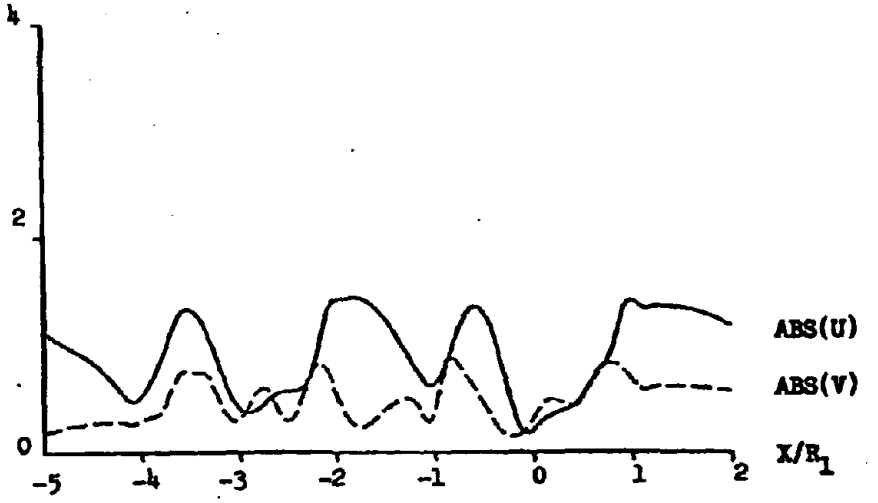

Fig.12a

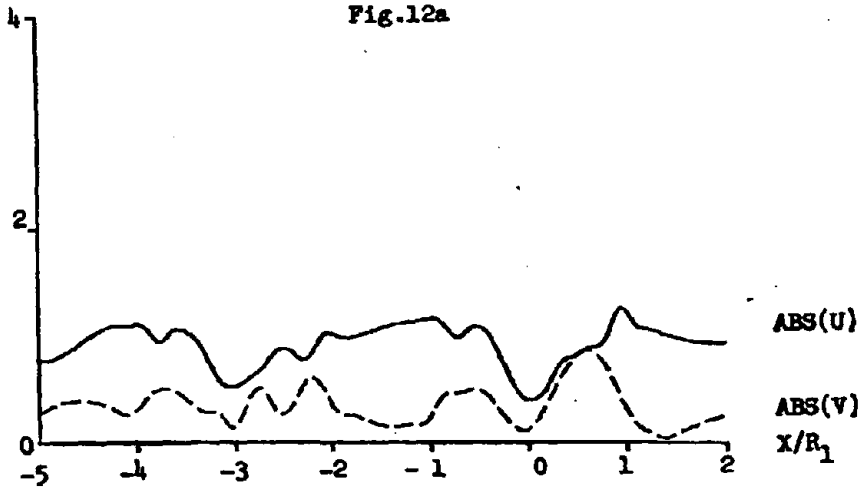

Fig.12b

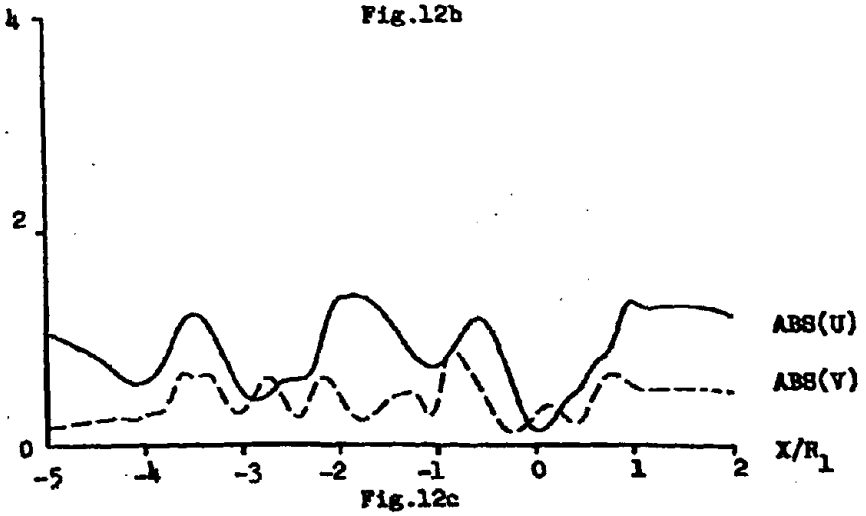

Fig.12c

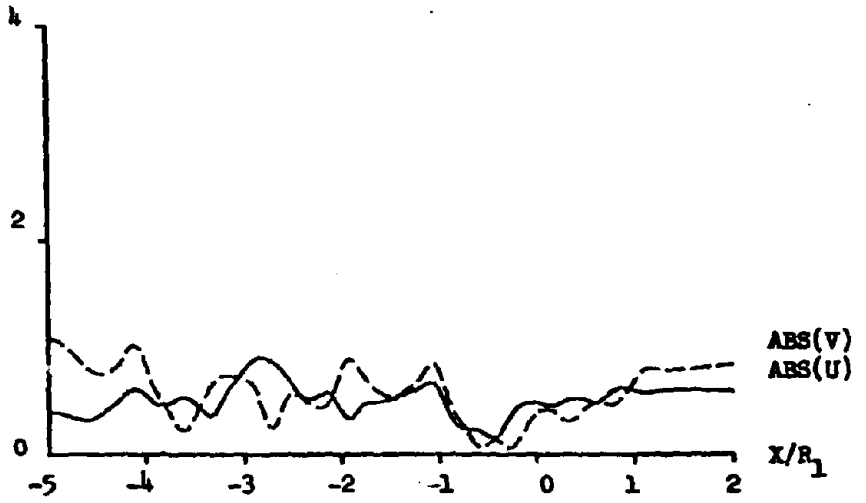

Fig.13a

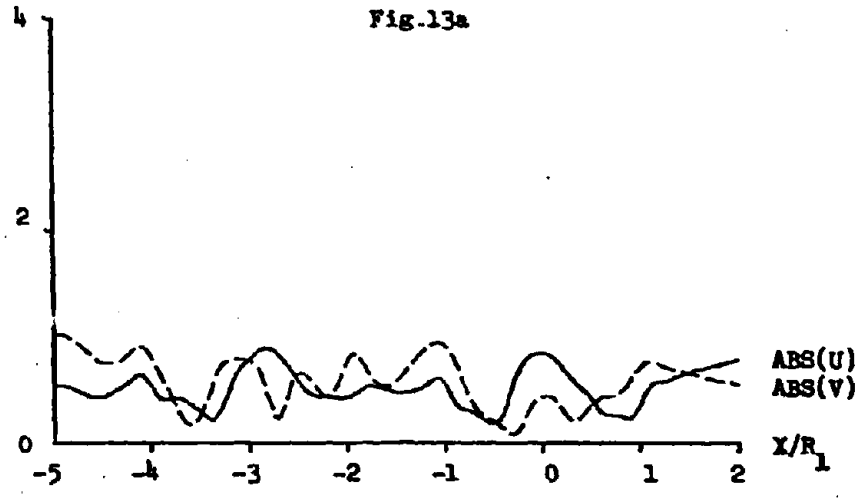

Fig.13b

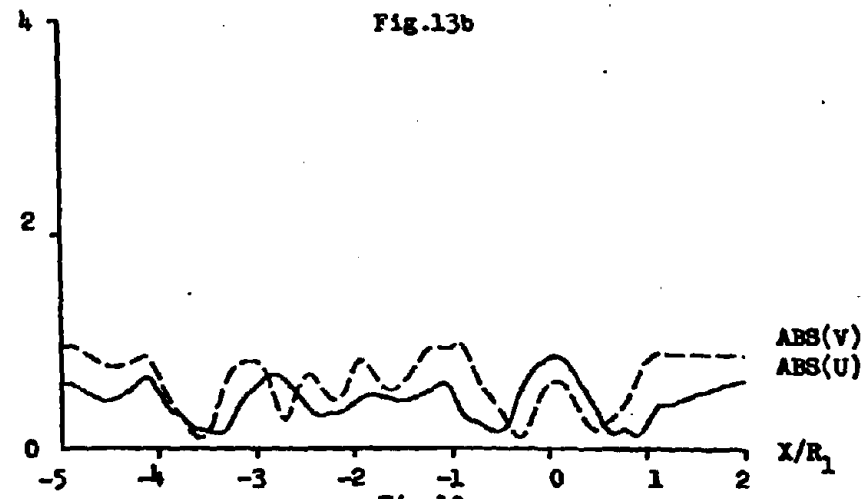

Fig.13c

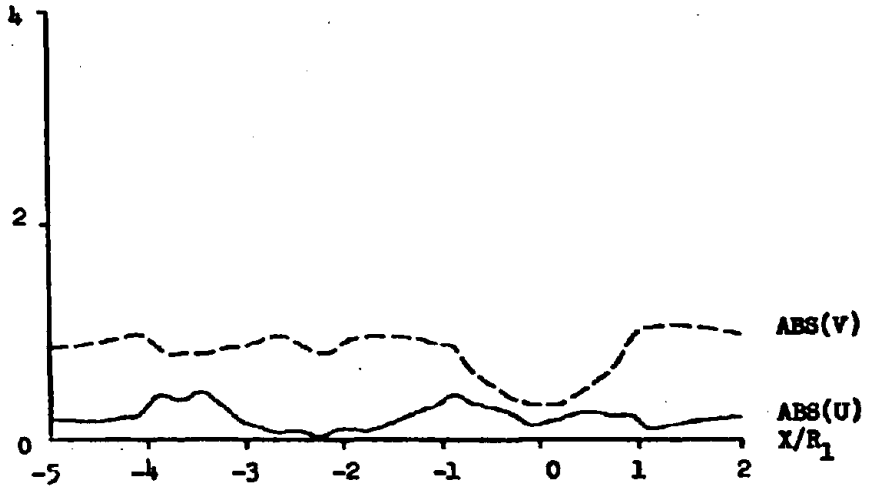

Fig.14a

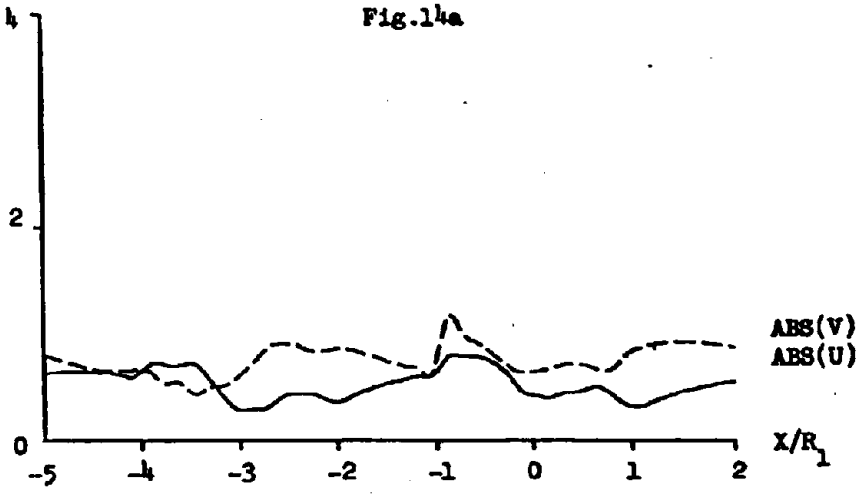

Fig.14b

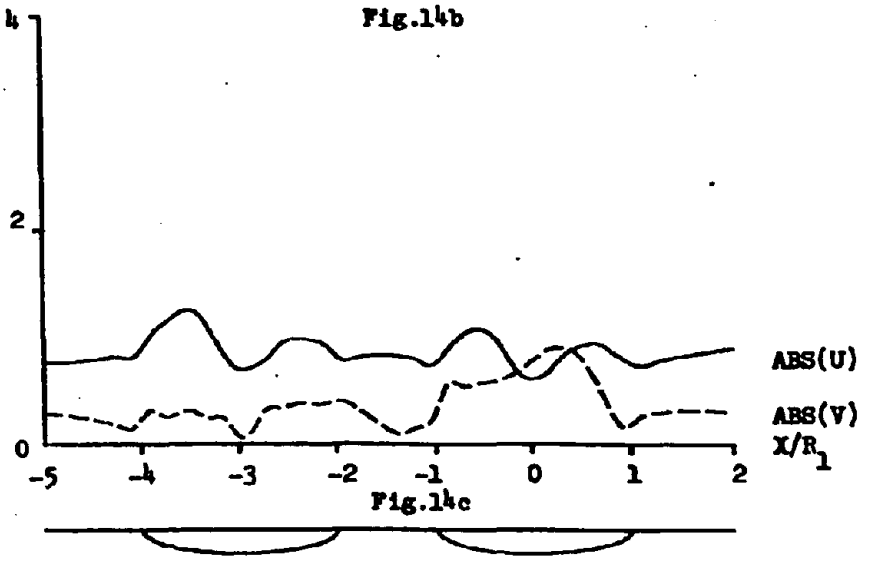

Fig.14c

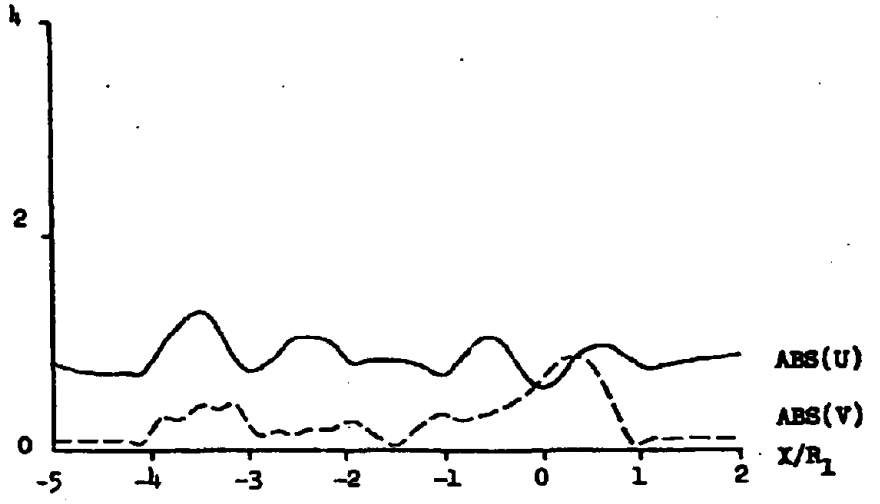

Fig.15a

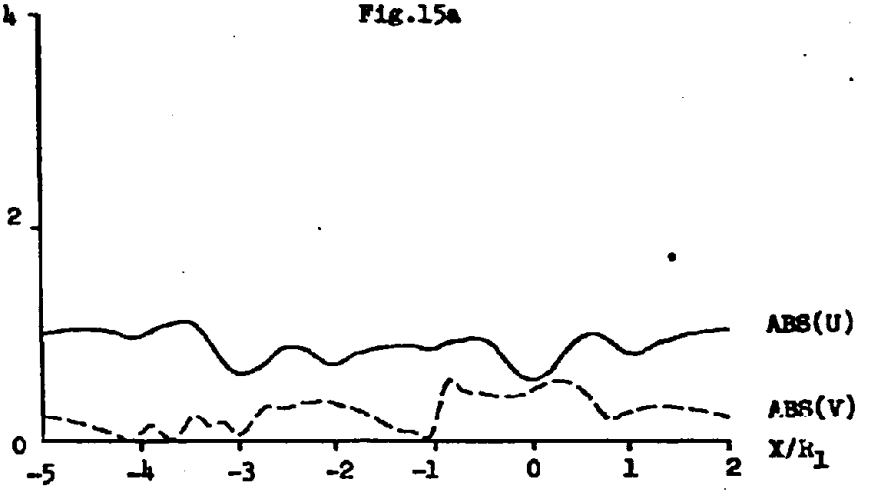

Fig.15b

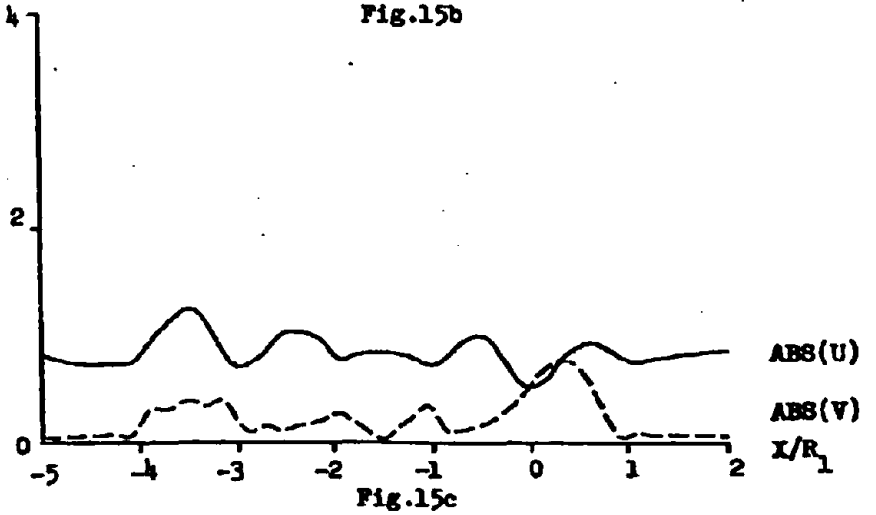

Fig.15c

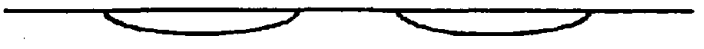

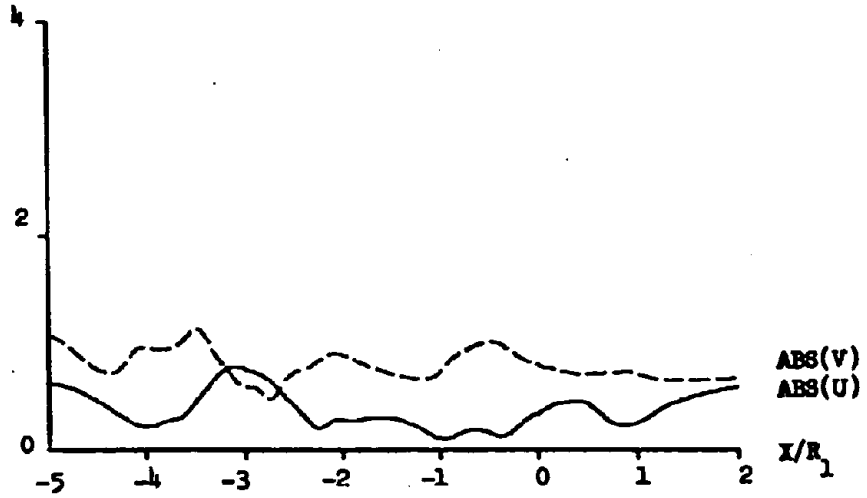

Fig.16a

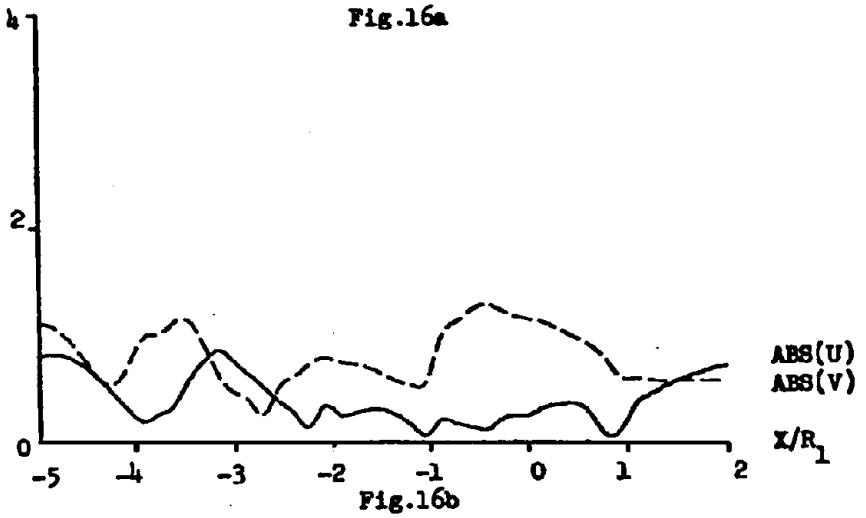

Fig.16b

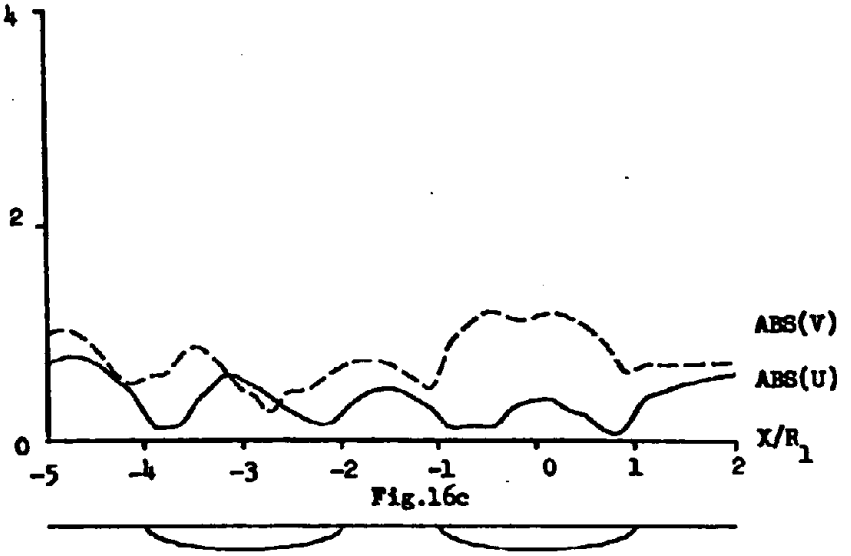

Fig.16c